

ISOLATION AND CHARACTERIZATION OF NITROGENOUS  
METABOLITES FROM THE ASCIDIANS *CYSTODYTES* SP.,  
*LISSOCLINUM PATELLA*, AND *BOTRYLLUS* SP.

by

Leonard A. McDonald

A dissertation submitted to the faculty of  
The University of Utah  
in partial fulfillment of the requirements for the degree of

Doctor of Philosophy

Department of Medicinal Chemistry

The University of Utah

August 1994

Copyright © Leonard A. McDonald 1994

All Rights Reserved

THE UNIVERSITY OF UTAH GRADUATE SCHOOL

## SUPERVISORY COMMITTEE APPROVAL

of a dissertation submitted by

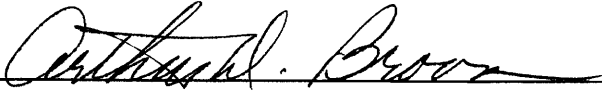
Leonard A. McDonald

This dissertation has been read by each member of the following supervisory committee and by majority vote has been found to be satisfactory.


7/28/94

  
Chair: Chris M. Ireland

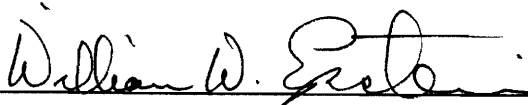
7/28/94

  
Arthur D. Broom

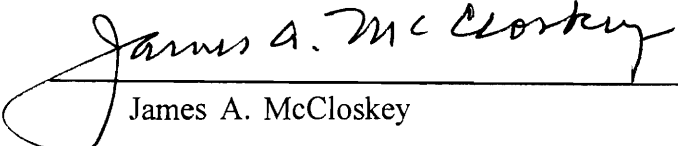
7/28/94

  
Darrell R. Davis

July 28, 1994

  
William W. Epstein

July 28, 1994

  
James A. McCloskey

THE UNIVERSITY OF UTAH GRADUATE SCHOOL

**FINAL READING APPROVAL**

To the Graduate Council of the University of Utah:

I have read the dissertation of Leonard A. McDonald in its final form and have found that (1) its format, citations and bibliographic style are consistent and acceptable; (2) its illustrative materials including figures, tables, and charts are in place; and (3) the final manuscript is satisfactory to the supervisory committee and is ready for submission to The Graduate School.

Date

8/2/07

Chris M. Ireland

Chris M. Ireland  
Chair, Supervisory Committee

Approved for the Major Department

Arthur D. Broom

Arthur D. Broom  
Chair/Dean

Approved for the Graduate Council

Ann W. Hart

Ann W. Hart  
Dean of The Graduate School

## ABSTRACT

This dissertation describes the isolation, characterization, and biological evaluation of several nitrogenous metabolites from ascidians. The first chapter reviews marine natural products that have shown promising biological activities or have been instrumental in enhancing our understanding of certain cellular processes. Since the research described is largely based on bioassay guidance to fractionate extracts of marine ascidians into bioactive secondary metabolites, the second chapter covers general approaches used to find bioactive natural products. The subsequent chapters detail the isolation and characterization of several new nitrogenous metabolites using a variety of spectroscopic techniques.


The active extract of a Fijian *Cystodytes* sp. ascidian was fractionated to yield a series of pyridoacridine alkaloids with topoisomerase II (topoII) activity. The structures of these alkaloids were elucidated primarily using nuclear magnetic resonance (NMR) spectroscopic techniques. The pyridoacridine alkaloids were cytotoxic towards the cultured mammalian cell line HCT116; acting by intercalating into deoxyribonucleic acid (DNA) and inhibiting the catalytic activity of topoII. Chapter 3 details the structure elucidation of these alkaloids and the mechanistic and biological experiments undertaken to support this conclusion.

A new cyclic peptide, patellamide E, was isolated from the ascidian *Lissoclinum patella* collected at Pulau Salu, Singapore. Its structure was determined by NMR spectroscopy, and its absolute configuration by acid hydrolysis and analysis of the derivatized constituent amino acids by high performance liquid chromatography (HPLC). The first part of the fourth chapter describes the structure elucidation of patellamide E.

The second part of Chapter 4 describes the new cytotoxic cyclic peptides, tawicyclamides A and B, which were isolated from the ascidian *Lissoclinum patella*

collected in the Philippines. The structures of these peptides were determined by NMR spectroscopy, oxidation studies, and tandem mass spectrometry (MS/MS). Their absolute configurations were again determined by HPLC analysis of derivatized constituent amino acids obtained from acid hydrolysis. X-ray crystallography confirmed the structure of tawicyclamide B and showed that the compound assumes an unusual three-dimensional conformation, which was facilitated by a *cis*-valine-proline amide bond and stabilized by an intramolecular hydrogen bond. Tawicyclamides A and B represent a new family of cyclic octapeptides, possessing thiazole and thiazoline amino acids but lacking the oxazoline ring characteristic of previously reported cyclic peptides from *L. patella*. NMR data supported the hypothesis that isomerization of the valine-proline amide bond occurred on oxidation of the thiazoline ring to a thiazole. Molecular modeling studies, undertaken to establish the solution structures of tawicyclamide B and dehydrotawicyclamide B, supported the isomerization conjecture.

The new bromotyrosine derivatives, botryllamides A-D, which were isolated from a Philippine *Botryllus* sp. ascidian are discussed in Chapter 5. The structures of these compounds were deduced from NMR and mass spectrometric data.

For  Mollie

To my family for all their  
love, support, and understanding

## TABLE OF CONTENTS

ABSTRACT .....	iv
LIST OF FIGURES .....	ix
LIST OF TABLES .....	xi
LIST OF ABBREVIATIONS.....	xii
ACKNOWLEDGMENTS.....	xv
1. INTRODUCTION AND BACKGROUND.....	1
Rationale for Studying Marine Organisms .....	1
Marine Natural Products Chemistry: Evolution from "Phytochemical" to Biomedical Discipline .....	2
Summary .....	20
2. STRATEGIES FOR DISCOVERING POTENTIAL ANTICANCER AGENTS: BIOASSAY GUIDED FRACTIONATION .....	22
In Vitro Assays .....	23
Mechanistic Assays .....	26
In Vivo Assays .....	29
3. THE CHEMISTRY AND BIOLOGY OF THE ASCIDIAN <i>CYSTODYTES</i> SP.....	30
Chemistry .....	31
Biology .....	42
Mechanistic Studies .....	43
Summary .....	45
Review of Pyridoacridines .....	48
4. THE CHEMISTRY OF THE ASCIDIAN <i>LISSOCLINUM PATELLA</i> .....	49
<i>L. patella</i> from Singapore .....	49
<i>L. patella</i> from the Philippines.....	55
Review of Cyclic Peptides .....	80
5. THE CHEMISTRY OF THE ASCIDIAN <i>BOTRYLLUS</i> SP.....	84
Isolation of the Botryllamides.....	84
Structure Determination of Botryllamide D.....	84
Structure Determination of Botryllamides B, C, and A.....	91



Biology .....	91
Review of Linear Peptide Alkaloids from Ascidians.....	94
6. EXPERIMENTAL .....	95
Chemicals, Reagents, and Organisms .....	95
General Experimental Procedures .....	95
The Chemistry of <i>Cystodytes</i> sp. ....	96
The Chemistry of <i>Lissoclinum patella</i> (Singapore).....	99
The Chemistry of <i>Lissoclinum patella</i> (Philippines) .....	100
The Chemistry of <i>Botryllus</i> sp.....	104
APPENDICES	
A. NMR SPECTRA OF COMPOUNDS FROM <i>CYSTODYTES</i> SP.....	107
B. NMR SPECTRA OF COMPOUNDS FROM <i>LISSOCLINUM</i> <i>PATELLA</i> .....	120
C. CID SPECTRA OF TAWICYCLAMIDE A.....	141
D. NMR SPECTRA OF COMPOUNDS FROM <i>BOTRYLLUS</i> SP.....	155
E. ISOLATION FLOW DIAGRAMS .....	170
REFERENCES.....	175

## LIST OF FIGURES

2.1.	Chemistry involved in the biochemical induction assay .....	27
3.1.	Region of a 300 ms ROESY spectrum of dehydrokuanoniamine B showing the H3-H4 crosspeak .....	34
3.2.	Dehydrokuanoniamine B with HMBC correlations used in assigning the quaternary carbon atoms.....	34
3.3.	Structure of shermilamine C with HMBC correlations used in assigning the quaternary carbon atoms.....	37
3.4.	HMBC correlations used in assigning the quaternary carbon atoms in cystodytin J .....	39
3.5.	Fluorescence spectra of ethidium bromide in PBS solution with various concentrations of diplamine .....	40
3.6.	Normalized fluorescence for ethidium bromide in PBS solution with calf thymus DNA and increasing concentrations of pyridoacridines .....	41
3.7.	Fluorescence spectra of eilatin in PBS solution with various concentrations of calf thymus DNA.....	42
3.8.	Agarose gel showing inhibitory effects of etoposide and diplamine on topoII catalyzed decatenation of kDNA.....	44
4.1.	Proton and COSY derived amino acid spin networks for patellamide E.....	53
4.2.	Partial structures and HMBC correlations for patellamide E .....	54
4.3.	Nickel peroxide oxidation of tawicyclamide A.....	57
4.4.	Proton and COSY derived amino acid spin networks for tawicyclamide A .....	58
4.5.	HMBC correlations for tawicyclamide A.....	59
4.6.	Linear acylium ion of tawicyclamide A .....	62
4.7.	High mass region ( $m/z$ 825-370) from the CID spectrum of the (M+H) <sup>+</sup> ion of tawicyclamide A.....	63
4.8.	Low mass region ( $m/z$ 625-80) from the CID spectrum of the (M+H) <sup>+</sup> ion of tawicyclamide A.....	64

4.9.	CID spectrum and structure of the <i>m/z</i> 682 ion of tawicyclamide A .....	65
4.10.	Partial structure of tawicyclamide B showing five bond correlation between leucine and thiazoline .....	69
4.11.	X-ray model of tawicyclamide B .....	70
4.12.	Stereo drawing of the solution structure of tawicyclamide B .....	71
4.13.	Region of a 300 ms ROESY spectrum of tawicyclamide B showing the H10-H15 crosspeak.....	73
4.14.	Region of a 300 ms ROESY spectrum of tawicyclamide B showing the H3-H27 crosspeak.....	74
4.15.	Stereo drawing of the solution structure of dehydrotawicyclamide B.....	76
4.16.	Region of a 300 ms ROESY spectrum of dehydrotawicyclamide B showing the H13-H15 crosspeak .....	78
4.17.	Region of a 300 ms ROESY spectrum of dehydrotawicyclamide B showing the NH1-H10 crosspeak.....	79
5.1.	EI mass spectrum and fragmentation of botryllamide D.....	86
5.2.	Select HMBC correlations for Botryllamide D.....	89
5.3.	Botryllamide D ROESY correlations and slice through 400 ms ROESY spectrum.....	89
5.4.	Slices from 400 ms ROESY spectra used to establish the configuration about the C5-C6 olefinic bond in botryllamides B, C, and A.....	93

## LIST OF TABLES

2.1.	Human Cell Lines used in Natural Products Screening.....	23
2.2.	Multidrug Resistant Cell Lines used in Evaluating Pure Compounds.....	24
2.3.	CHO Cell Lines used in Screening and Mechanistic Studies.....	25
3.1.	NMR Assignments for the TFA Salt of Dehydrokuanoniamine B .....	33
3.2.	NMR Assignments for the TFA Salt of Shermilamine C.....	36
3.3.	NMR Assignments for Cystodytin J.....	38
3.4.	Cytotoxicity, Differential Toxicity, Topoisomerase Inhibition and Intercalation of the Pyridoacridines Alkaloids .....	41
4.1.	NMR Assignments for Patellamide E.....	51
4.2.	NMR Assignments for Tawicyclamide A .....	60
4.3.	NMR Assignments for Dehydrotawicyclamide A.....	61
4.4.	NMR Assignments for Tawicyclamide B .....	67
4.5.	NMR Assignments for Dehydrotawicyclamide B.....	68
5.1.	NMR Assignments for Botryllamide D.....	87
5.2.	Proton NMR Assignments for Botryllamides D, B, C, and A.....	92

## LIST OF ABBREVIATIONS

ABNR	Adopted Basis-set Newton-Raphson
BCNU	1,3-bis(chloroethyl)-1-nitrosourea
BIA	biochemical induction assay
BNG	6-bromo-2-naphthyl- $\beta$ -D-galactopyranoside
cAMP	cyclic adenosine monophosphate
CHO	Chinese hamster ovary
CID	collision induced dissociation
COLOC	correlation by long range coupling
COSY	correlated spectroscopy
CT	calf thymus
DC	differential cytotoxicity
DEPT	distortionless enhancement by polarization transfer
DMSO	dimethyl sulfoxide
DNA	deoxyribonucleic acid
ds	double stranded
ED <sub>50</sub>	effective dose 50%
EI	electron impact
FAB	fast atom bombardment
FDAA	1-fluoro-2,4-dinitrophenyl-5-L-alanineamide
HCT	human colon tumor
HIV	human immunodeficiency virus
HMBC	heteronuclear multiple bond correlation

HMQC	heteronuclear multiple quantum coherence
HPLC	high performance liquid chromatography
HR	high resolution
IC <sub>50</sub>	inhibitory concentration 50%
ID <sub>50</sub>	inhibitory dose 50%
INEPT	insensitive nuclei enhancement by polarization transfer
IR	infrared
kDNA	kinetoplast deoxyribonucleic acid
LR	low resolution
MD	molecular dynamics
MDR	multidrug resistance
MS	mass spectrometry
MS/MS	tandem mass spectrometry
MTT	3-[4,5-dimethylthiazoyl-2-yl]-2,5-diphenyltetrazolium bromide
NCDDG	National Cooperative Drug Discovery Group
NCI	National Cancer Institute
NMR	nuclear magnetic resonance
nOe	nuclear Overhauser enhancement
NOESY	nuclear Overhauser enhancement spectroscopy
PBS	phosphate buffered saline
PKC	protein kinase C
PS-DQF	phase sensitive double quantum filtered
RNA	ribonucleic acid
ROESY	rotating frame Overhauser enhancement spectroscopy
SDS	sodium dodecylsulfate
ss	single stranded
T/C	treated/control

TFA	trifluoroacetic acid/trifluoroacetate
TLC	thin-layer chromatography
TOCSY	total correlation spectroscopy
topoI	topoisomerase I
topoII	topoisomerase II
TPA	12-O-tetradecanoylphorbol-13-acetate
UV	ultraviolet

## ACKNOWLEDGMENTS

I would like to thank Prof. Chris M. Ireland for his inspiration, guidance, support, and most importantly, for allowing me the freedom to grow as a scientist. His foresight and trust enabled me to pursue my dreams and facilitated my development as a natural products scientist. I am indebted to Prof. Darrell R. Davis for his help and advise, especially for posing questions such as "Have you thought about...?" when I am desperately attempting to solve an NMR problem. I am equally indebted to Mr. Jay Olsen for countless hours of help and prayers to the NMR gods. I would like to thank Prof. Louis R. Barrows for the fruitful collaboration on the pyridoacridines and for his encouragement. I am grateful to Dr. Mark P. Foster for his help, advice, collaboration, and especially for his friendship. I would like to thank Drs. Dennis R. Phillips, Elliot Rachlin, and John Peltier for acquiring my mass spectral data. I am thankful to all of the Medicinal Chemistry faculty for always taking the time to answer questions or give useful advice, and to my colleagues in the Ireland Research Group (past and present) for their help, friendship and understanding. Thanks Swersey, I didn't let them give me any crap.

I am grateful to Bristol-Myers Squibb and Lederle Laboratories for providing biological test results. The National Institutes of Health (NIH) provided financial support through a Minority Graduate Fellowship for which I am very grateful. The research described in this dissertation was supported in part by NIH grants CA 36622 and CA 50750, awarded to Prof. Chris M. Ireland.

My deepest gratitude goes to my family (present and future) for their love, support, and understanding throughout the years. Thanks Mom, I love you too. You taught me the value of hard work and persistence, which were crucial to my success in graduate school.



Uncle B., Aunt G., and Anthony, I appreciate all of the help that you and the rest of the family have given me over the years. Finally, a very special thanks to Mollie for your love, friendship, support, understanding, patience, trips to the desert, etc. I could not have done it without you. You are largely responsible for my success in Utah.

## CHAPTER 1

### INTRODUCTION AND BACKGROUND

#### Rationale for Studying Marine Organisms

Oceans occupy more than 70% of the earth's surface and, in terms of volume, over 95% of the earth's biosphere.<sup>1</sup> More than 95% of the animal species on earth are invertebrates and marine organisms make up the majority of invertebrate phyla.<sup>2</sup> The commercial availability of the self-contained underwater breathing apparatus (SCUBA) has made the top layer of the marine environment (~50 m) more accessible to scientists while the depths at which marine organisms could be collected have been greatly extended by submersibles such as the Johnson-Sea-Link II.<sup>3</sup>

Marine natural products have contributed significantly to our understanding of important molecular processes such as tumor promotion<sup>4</sup> and phosphorylation-dephosphorylation in malignancy.<sup>5</sup> Marine organisms have provided a variety of bioactive compounds with therapeutic potential.<sup>6</sup> Many of these bioactive marine natural products have novel and varied molecular structures that are without terrestrial precedence,<sup>7-14</sup> and may therefore serve as pharmacophores, which can be chemically elaborated to yield more specific and efficacious therapeutic agents. Chemical modifications of pharmacophores can widen their therapeutic window by either increasing their efficacy or decreasing their toxicity.

Ecology also provides a rationale for focusing on marine organisms.<sup>15</sup> Because the sessile, soft bodied, shell-less marine organisms have no physical means of protection, it has been proposed that some of these organisms use chemicals (secondary metabolites) in defense against predation.<sup>16,17</sup> Further arguments have been made suggesting that marine

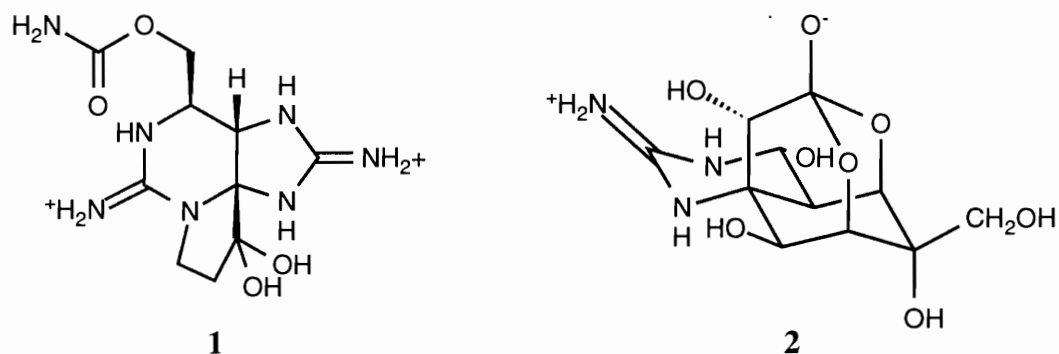
invertebrates have developed in a fairly stable environment and can therefore divert a large amount of their biosynthetic resources to developing secondary metabolites for survival.<sup>18</sup> Some scientists have looked at the competitive interplay among various marine organisms in their natural environment and have inferred biomedical potential to the compounds used in this interaction.<sup>17</sup> The biomedical potential of compounds derived from marine animals has inspired the research undertaken and presented in the upcoming chapters.

### Marine Natural Products Chemistry: Evolution from "Phytochemical" to Biomedical Discipline

Research focusing on marine natural products has undergone an evolution over the past three decades from a "phytochemical" based to a biomedically oriented discipline. The phytochemical approach, following the same strategy applied to plants, generally involves the isolation and characterization of compounds with little consideration of biological activity. The biomedical importance of marine natural products has been recognized and mechanism based approaches are increasingly being used to guide the isolation of novel compounds. The evolution came about because of the fruitful interaction between scientists from various disciplines such as chemistry, biochemistry, pharmacology, and molecular biology and this interdisciplinary approach has led to increasingly sophisticated methods for targeting, isolating, and characterizing novel marine natural products with biomedical potential. The advancements in the field of marine natural products chemistry are at the same time both the result of and the impetus for increasing sophistication in allied fields such as pharmacology and molecular biology. In fact, the novel structures and wide ranging pharmacological activities of marine natural products have helped to fuel this evolution and have kept scientists focused on marine organisms as a source of potential pharmaceuticals.

Some early biomedical efforts in marine natural products chemistry focused on secondary metabolites such as toxins that posed significant threats to humans.<sup>19</sup> Examples include the effort to isolate and characterize saxitoxin (**1**), the agent responsible for

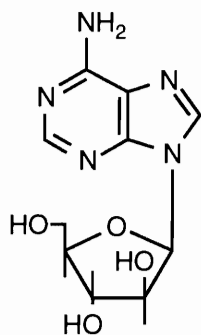
paralytic shellfish poisoning and tetrodotoxin (**2**), which is responsible for the fatalities caused by the puffer fish.<sup>20</sup> Studies using these toxins as molecular probes have subsequently made significant contributions to our understanding of the sodium channel.<sup>21</sup> Much research today still focuses on compounds and organisms that are human poisons, and additional interesting compounds, mostly derived from dinoflagellates or microalgae, have been uncovered and are also used as molecular probes.<sup>22</sup>



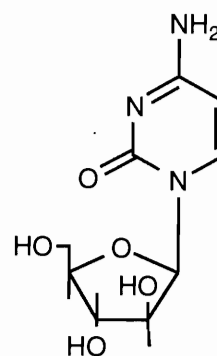
Most early researchers, however, looked primarily at the novel chemistry that could be found by thoroughly examining new organisms, a method paralleling the phytochemical approach used in studying plants. Although the phytochemical method tended to focus on compounds that were abundant and easy to isolate, it has fortuitously led to the discovery of some biologically active secondary metabolites, as well as compounds that served as molecular prototypes in the development of biomedically useful agents. Examples of such agents include the clinically useful antiviral/anticancer compounds vidarabine (ara-A) (**3**),<sup>23</sup> and cytarabine (ara-C) (**4**),<sup>24</sup> which were inspired by the novel structures of arabinosyl nucleosides from sponges,<sup>25,26</sup> and the insecticide cartap HCl (**5**), which was inspired by nereistoxin (**6**) from the annelid *Lumbriconereis heteropoda*.<sup>27</sup>

Regardless of the initial impetus for isolating a compound, intensive pharmacological investigations often follow isolation to establish its molecular mechanism of action. The mechanism in turn forms the basis for developing additional assays capable of detecting other similarly acting compounds.

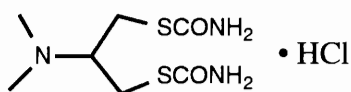
Bioactivity results from interaction between a compound and macromolecular



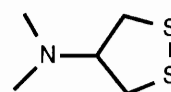
3



4



5



6

receptor(s). Pharmacological studies using “toxins” often lead to the conclusion that these compounds are too toxic for therapeutic use. Though therapeutically limited, these bioactive substances may still be used as probes to provide information about a specific receptor, and knowledge gained in such receptor studies may be used in designing compounds that are highly specific to that receptor. The use of compounds as probes can ultimately advance the biomedical sciences. In the case where mechanistic studies have yielded sufficient information about specific receptors involved in aberrant processes, this knowledge can also be instrumental in designing compounds to be used in therapy. The use of compounds as probes to better understand biological processes at the molecular level fills the literature and has played significant roles in the advancement of the field of marine natural products chemistry.

The vastness of the marine environment, the abundance of its resources, and the potential for yielding bioactive compounds continue to attract researchers to the field of marine natural products chemistry. The need and desire to find more therapeutically useful compounds have spurred many of the advances in this field. Other factors contributing to

the progression towards biomedically oriented research in marine natural products chemistry include fundamental advances in physics, chemistry, biochemistry, pharmacology, and molecular biology. These advances have led to the development of new bioassays that exploit a variety of organisms, cell types, cellular processes, or molecular targets to detect bioactive compounds. Some marine natural products have played significant roles in defining new receptor targets as noted earlier. The desire to achieve the commercial successes enjoyed by microbial natural products has led scientists to use increasingly sophisticated bioassay guidance to increase the probability of finding a therapeutically useful compound.

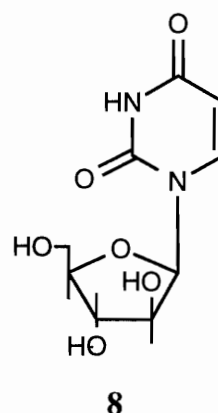
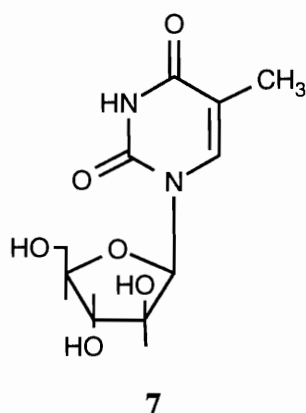
#### Discovering Biomedically Significant Marine Natural Products: An Assay Based Approach

Research groups looking for biomedically significant natural products from marine organisms often use a disease oriented approach, with focus on one or more therapeutic areas. Examples in the area of anticancer drug discovery will be used to chronicle the developments in natural products chemistry. Since the results from bioassays are the main determinant of which compounds will be isolated, this section has been organized in terms of the assays of increasing sophistication and specificity. A clear evolution in drug screening strategies from “compound-oriented” (or chemistry driven) to “disease-oriented” (or biology driven) can be seen as paralleling the revolutionary changes in direction undertaken by the National Cancer Institute (NCI).<sup>28</sup>

In reviewing compounds that are significant in the history of marine natural products chemistry, emphasis will be placed on those derived mainly, but not exclusively, from marine invertebrate animals. Many compounds show activities in multiple assays, and these will be discussed in the appropriate sections according to where they have made the most significant contributions.

### No Assays: The Search for New Chemistry

The arabinosyl nucleosides spongothymidine (**7**) and spongouridine (**8**) from the Caribbean sponge *Cryptotethia crypta* were of interest because they contained the rare sugar arabinose.<sup>25,26</sup> These arabinosyl nucleosides inspired the syntheses of ara-C (**4**),<sup>24</sup> a widely used antileukemic chemotherapeutic agent<sup>29</sup> and ara-A (**3**),<sup>23</sup> a clinically effective antiviral drug.<sup>30,31</sup> The arabinosyl nucleosides have been credited with propelling the field of marine natural products chemistry towards biomedical significance. The discovery of **7** and **8** are examples where isolation was empirical and based solely on thin layer chromatographic (TLC) detection of a compound. This method, using no biological or mechanistic assay for directing isolation, has serendipitously led to important compounds in several therapeutic areas.



### Biological Assays

Since anticancer agents are expected to act *in vivo*, some biological measure of effectiveness is necessary when targeting these compounds. Many of the approaches to finding potential anticancer agents use some biological assay as the endpoint; however, the majority of them are *in vitro* assays. Many compounds are capable of exerting multiple biological activities and some may be detected by *in vitro* assays while others produce responses only in *in vivo* assays. In some cases *in vitro* or *in vivo* activity is a good predictor of anticancer activity whereas in other instances this is not true.

## Antimicrobial Assays

The loose correlation between *in vitro* antimicrobial and *in vivo* antitumor activities has been used to justify the use of antimicrobial assays for targeting potential anticancer compounds. A multitude of marine natural products have been isolated using antimicrobial screens because testing against bacterial strains is simple and inexpensive.<sup>32</sup> However, since none of these compounds have progressed to the clinic as anticancer agent (or an antibiotic), it appears that antimicrobial activity is not predictive of anticancer activity.

## Cytostatic or Growth Inhibitory Assays

The failure of antimicrobial assays to correlate with anticancer activity led some researchers to turn to the more specific cytostatic assays, which were expected to be better predictors of anticancer activity. The fertilized sea urchin egg assay or the fertilized starfish egg assay were used to detect compounds that can act as DNA, RNA, or protein synthesis inhibitors, or as antimetabolic agents.<sup>33</sup>

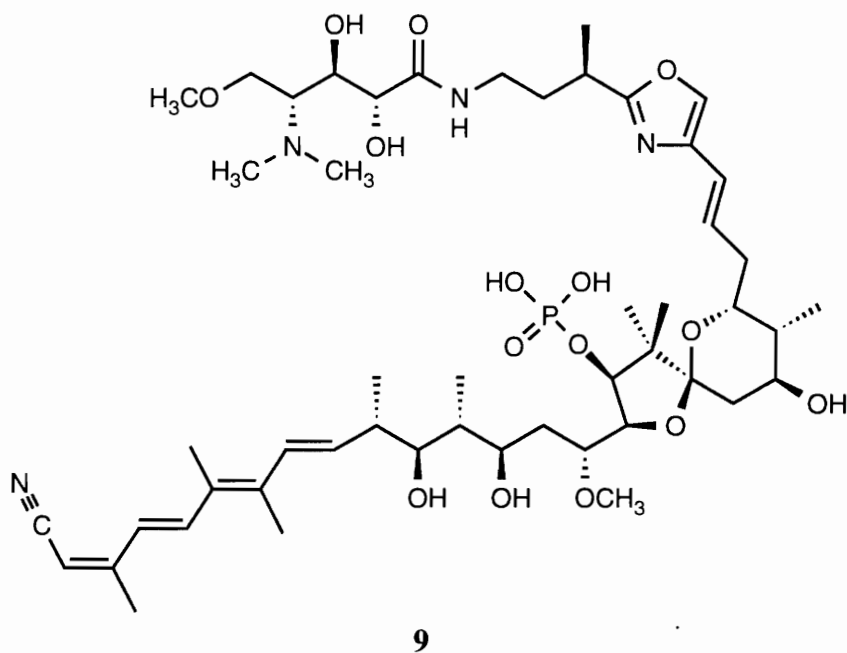
One of the most potent compounds in the cytostatic assay, calyculin A (**9**), was isolated from the marine sponge *Discodermia calyx*.<sup>34</sup> The compound inhibited the first division of fertilized starfish eggs at 0.001  $\mu\text{g}/\text{mL}$  and also caused fragmentation of the DNA in fertilized sea urchin eggs.<sup>33</sup> Calyculin A, also a potent tumor promoter, was reported to be a more potent inhibitor of protein phosphatases 1 and 2A than okadaic acid (see below) and thus, has contributed to our understanding of tumor promotion and phosphorylation-dephosphorylation in cell growth.<sup>35,36</sup> Calyculin A was also active *in vivo* in the P388 and Erlich tumor models (T/C = 144 and 245, respectively).

## Ichthyotoxicity Assays

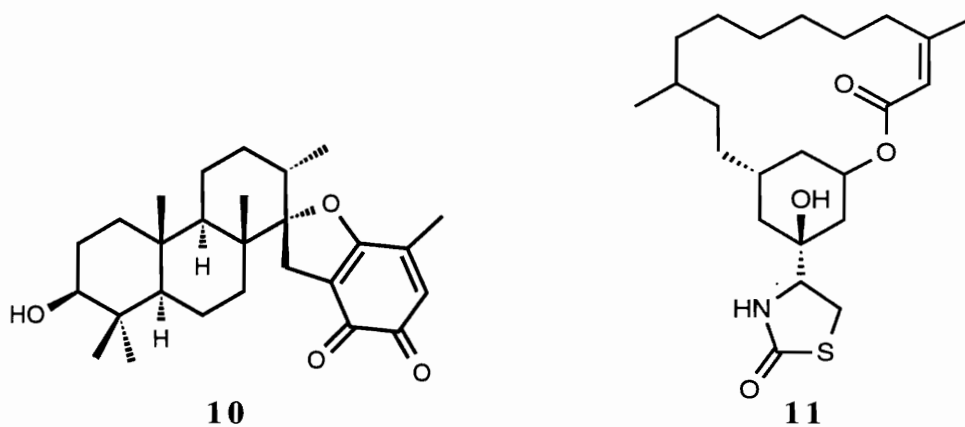
Some compounds that are isolated as a result of their toxicity to fish appear to act by inhibiting microfilament organization. Ichthyotoxicity assays may be considered *in vivo* assays and appear to be a good predictors of anticancer activity.

Stypoldione (**10**), an *ortho*-quinone isolated from the Caribbean brown alga





*Styopodium zonale*,<sup>37,38</sup> proved to be a potent inhibitor of cell division in the fertilized sea urchin egg assay ( $ED_{50} = 1.1 \mu\text{g/mL}$ ). Stypoldione was initially identified as one of the ichthyotoxic constituents of the alga and was subsequently shown to inhibit microtubule polymerization by binding to tubulin.<sup>39</sup> Compound **10** is thought to poison sulfhydryl-dependent proteins by adding to their sulfhydryl groups.<sup>40</sup>



Latrunculin A (**11**), a 2-thiazolidinone containing macrocyclic diterpene initially isolated from the sponge *Latrunculia magnifica*,<sup>41</sup> showed in vivo activity in the A549 subcutaneous-implanted lung tumor xenograft model in mice (T/C of 146% at 0.3

mg/kg).<sup>42</sup> The compound was initially targeted because of its toxicity to fish. Latrunculin A binds to actin in a 1:1 molar ratio,<sup>43</sup> is able to alter cell shape, disrupt microfilament organization without affecting microtubules in cultured neuroblastoma and fibroblast mouse cells,<sup>44,45</sup> and inhibits several microfilament mediated processes.<sup>46</sup>

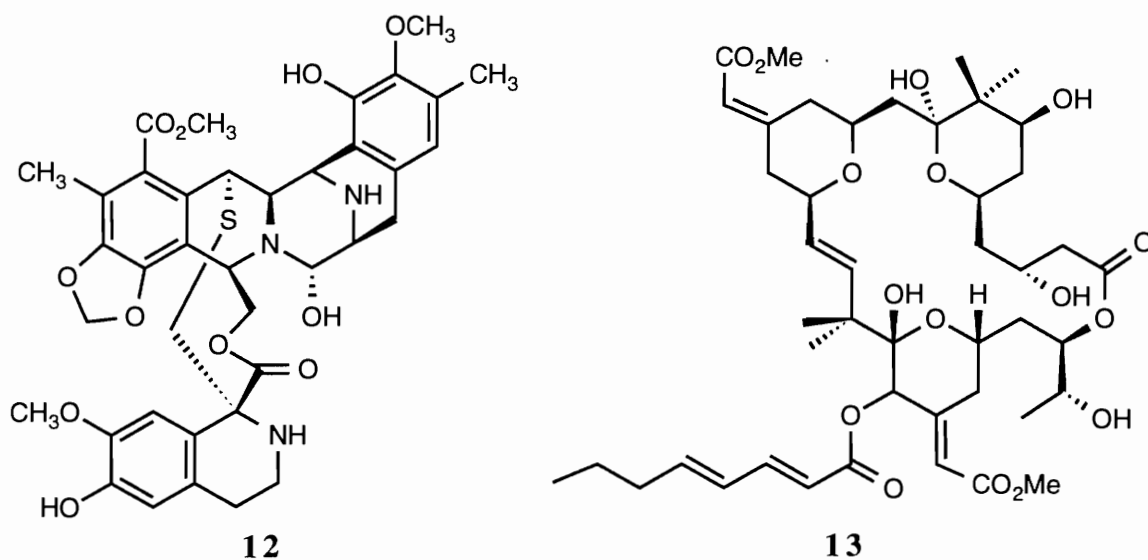
#### Other In vivo Assays

In an effort to improve the correlation between bioassays and antitumor activity, researchers established various in vivo tumor models, using experimental animals as the initial screening step. For example, until 1985 the NCI used a leukemia mouse model (L1210 or P388) for initial prescreening.<sup>28</sup> Although in vivo assay methods are expensive and time consuming,<sup>47</sup> there have been some significant successes, particularly in finding compounds that are active against leukemias and lymphomas.

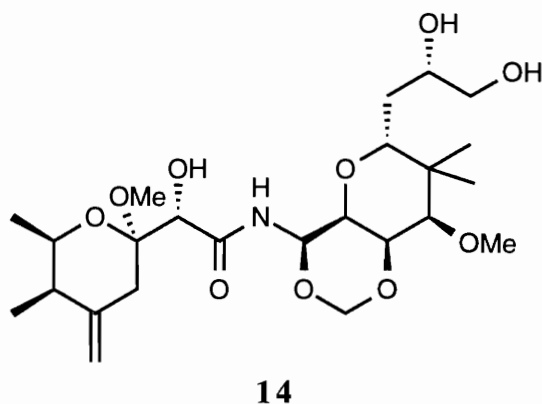
The outstanding in vivo activity associated with extracts of the Caribbean ascidian *Ecteinascidea turbinata* was ultimately traced to the ecteinascidins.<sup>48-51</sup> These compounds exhibited impressive cytotoxic and antitumor activities. The most potent, ecteinascidin 729 (**12**) was extremely cytotoxic (ID<sub>50</sub> of 0.0004 µg/mL) towards L1210 leukemia cells<sup>52</sup> and showed T/C of 214% at 3.8 µg/kg against P388 murine leukemia and 246% at 10 µg/kg against B16 melanoma.<sup>50</sup> These compounds are undoubtedly excellent candidates for anticancer agents.

The initial claim that the bryozoan *Bugula neritina* may contain anticancer constituents<sup>53</sup> was strengthened by the isolation of bryostatin 1 (**13**) from this organism.<sup>54</sup> This macrocyclic lactone was quite cytotoxic towards P388 cells in vitro (ED<sub>50</sub> of 0.89 µg/mL) and exhibited excellent activity in the P388 lymphocytic leukemia model in mice (T/C of 152-196 at 10-70 µg/kg).<sup>54</sup> Bryostatin 1 has shown protein kinase C (PKC) activating and antitumor promoting activities,<sup>55</sup> and is now undergoing clinical trials as an anticancer agent.

The crude extract of a *Mycale* sp. sponge showed 83% life extension of P388



leukemia bearing mice relative to the control group. This in vivo activity was ultimately traced to the tricyclic amide mycalamide A (**14**), which showed activity in a variety of tumor models (T/C = 233, 175, and 156% against M5076, B16, and P388, respectively at the optimal dosages).<sup>56</sup>

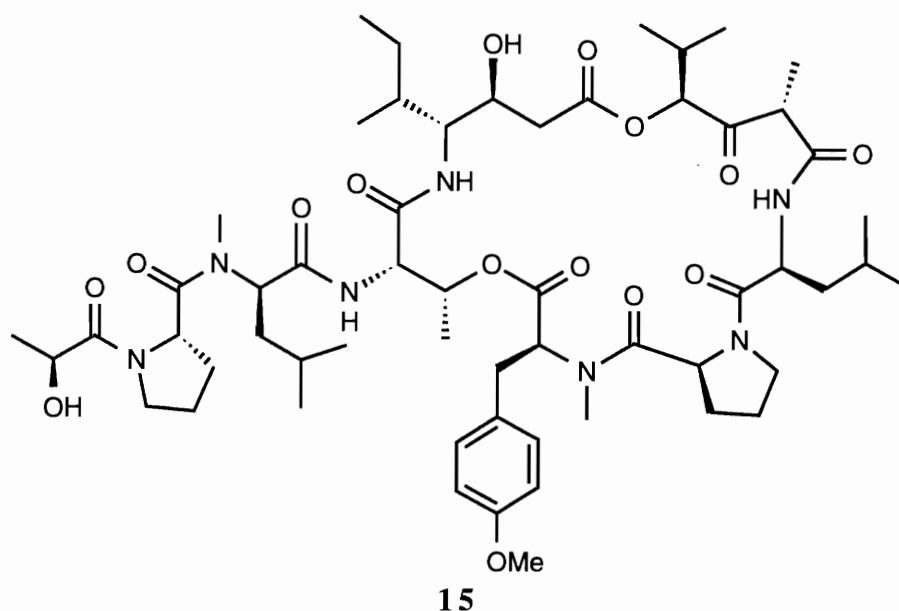


### Cytotoxicity Assays

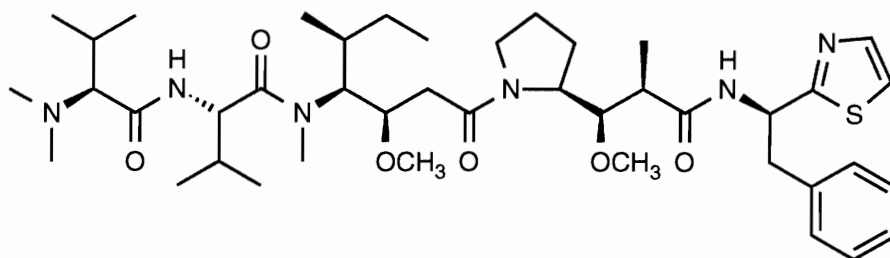
Cytotoxicity assays using established tumor cells in culture have been used for many years to identify novel compounds with antitumor potential. There are many compounds that are classified as cytotoxic and these have been the subject of many recent reviews.<sup>12-14,57</sup> Compounds that have shown exceptional cytotoxicity and have subsequently

demonstrated in vivo activity or have been utilized to probe specific receptors will be recounted here.

Didemnin B (**15**), a depsipeptide isolated from the colonial ascidian *Trididemnum solidum*, was initially targeted by shipboard assays screening for a variety of activities including cytotoxicity.<sup>58-60</sup> Didemnin B showed promising in vivo antileukemic and antitumor activities<sup>60</sup> and has become the first marine natural product to be evaluated in clinical trials in the United States as an anticancer agent.<sup>61-64</sup> Didemnin B also shows promising antiviral<sup>58,60,65</sup> and immunosuppressive activities.<sup>66,67</sup>

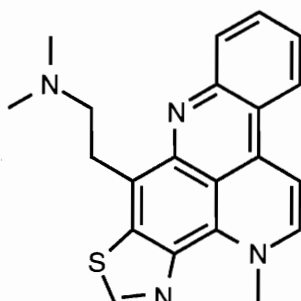


The cytotoxic peptide dolastatin 10 (**16**) obtained, by bioassay-directed fractionation, from the opisthobranch mollusc *Dolabella auricularia* exhibited exceptional in vivo activity in the PS leukemia (T/C of 169-202% at 1-4  $\mu\text{g}/\text{kg}$ ) and B16 melanoma (T/C of 142-238% at 1.44-11.1  $\mu\text{g}/\text{kg}$ ) models.<sup>68</sup> Dolastatin 10 was cytotoxic towards L1210 murine leukemia cells with an  $\text{IC}_{50}$  value of 0.3-0.9 nM and resulted in mitotic arrest of the leukemic cells.<sup>69,70</sup> Mechanistic studies showed that dolastatin 10 inhibited tubulin polymerization and microtubule assembly.<sup>69</sup> The compound also reportedly inhibits tubulin dependent GTP hydrolysis and binds noncompetitively to the vincristine binding site on tubulin, thus adding to the small number of tubulin inhibitors binding at this site.<sup>71</sup>

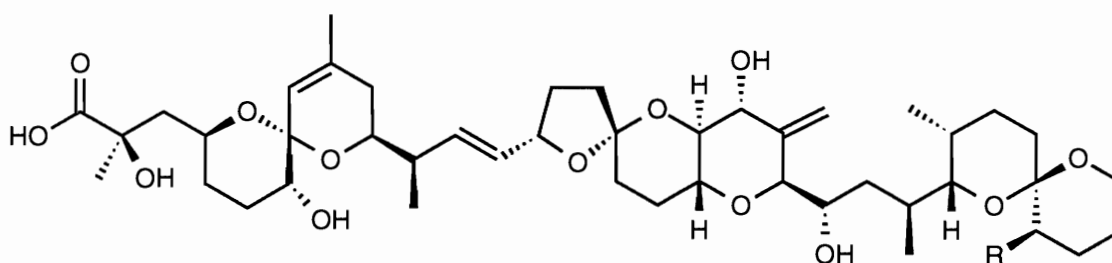


16

The pyridoacridine alkaloid, dercitin (**17**), from a Bahamian *Dercitus* sp. sponge,<sup>72</sup> showed in vitro (P388 IC<sub>50</sub>: 0.05 µg/mL) and in vivo activity in the P388 mouse leukemia model (T/C of 170 at 5 mg/kg). Additionally, the compound was shown to disrupt DNA and RNA synthesis and intercalate into DNA.<sup>73</sup> Dercitin is among a large group of cytotoxic pyridoacridine alkaloids (Chapter 3) thought to exert their cytotoxicity by intercalating into DNA and inhibiting the function of nucleic acid specific enzymes.<sup>74</sup>



17



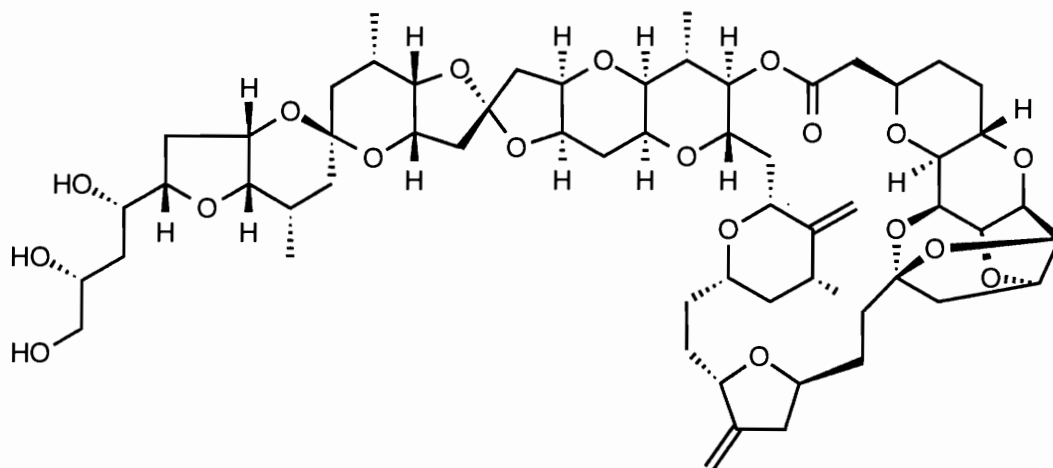
18

Okadaic acid (**18**), initially isolated from the marine sponges *Halichondria okadai* and *H. melanodocia*,<sup>75</sup> was toxic towards P388 and L1210 cells with ED<sub>50</sub>'s of 1.7 x 10<sup>-3</sup>, and 1.7 x 10<sup>-2</sup> µg/mL, respectively. Okadaic acid was subsequently isolated from the marine dinoflagellate *Prorocentrum lima*.<sup>76</sup> Although the cytotoxicity of this metabolite

initially attracted attention, this compound, by virtue of its tumor promoting and phosphatase inhibitory activities, has made vast contributions to our understanding of cell regulation (see below).

### Selective Cytotoxicity

The approaches using single cell lines or in vivo tumor models (e.g., murine leukemias and lymphomas) have yielded several potential antileukemic agents, but the majority of the compounds found using these methods are also cytotoxic towards normal cells. The past decade has seen a tremendous emphasis placed on assays capable of detecting compounds that are selectively cytotoxic towards certain solid tumors.<sup>28</sup> These efforts resulted in batteries of human tumor cell lines such as NCI's panel of over 60 tumor cell lines, representing more than 10 different cancer types. Compounds demonstrating selectivity in this assay are tested against the sensitive human tumor xenografts in nude mice. It is also expected that this approach will give rise to patterns of cytotoxicity that could correlate with specific mechanism(s) of action.<sup>28,47</sup>

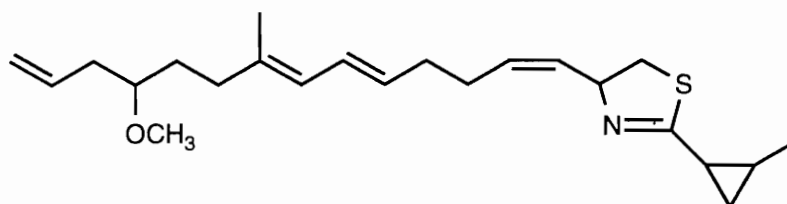


19

The polyether macrolide halichondrin B (**19**), initially isolated from the marine sponge *Halichondria okadai*, showed remarkable in vivo activity in the P388 lymphocytic leukemia (T/C of 323% at 10  $\mu\text{g}/\text{kg}$ ) and B16 melanoma (T/C of 244% at 5  $\mu\text{g}/\text{kg}$ )

models.<sup>77</sup> Renewed interest in this compound stemmed from analysis of its differential cytotoxicity pattern in the NCI panel of cell lines which predicted that **19** would be an antimetabolic agent.<sup>78</sup> Confirmation of this prediction came when halichondrin B was shown to inhibit glutamate-induced tubulin polymerization. Halichondrin B caused accumulation of L1210 cells arrested in mitosis at the cytotoxic concentration of 0.3 nM.<sup>78</sup> Halichondrin B thus confirms the importance of the differential cytotoxicity assay as a predictor of potential anticancer agents.

The antimetabolic agent, curacin A (**20**), from the cyanobacterium *Lyngbya majuscula*, was initially detected because of its toxicity to brine shrimp and antiproliferative activity. Curacin A, when tested in the NCI panel of tumor lines, revealed a cytotoxicity pattern consistent with an antimetabolic agent and was subsequently shown to be a colchicine class tubulin inhibitor.<sup>79</sup>



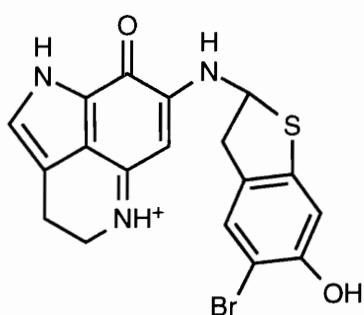
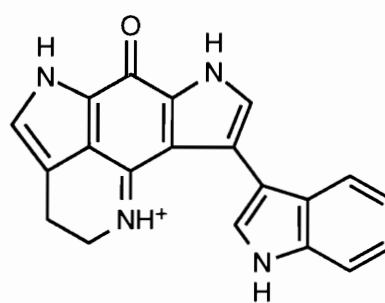
20

#### Cytotoxicity Assays with Molecular Target Defined (DNA Damage Repair Assays)

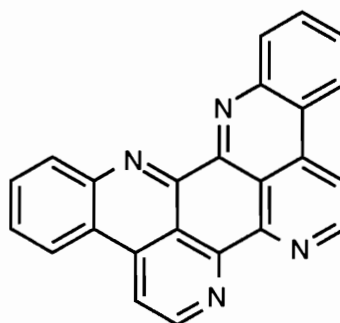
Toxicity towards cells in which the molecular target is known can be considered as a demonstration of selective cytotoxicity. Enhanced toxicity towards DNA repair deficient Chinese hamster ovary (CHO) cells, relative to the repair proficient variants, is an example of differential or selective cytotoxicity. Compounds showing activity in some molecular-target-defined assays are believed to interact with nucleic acids or may have topoisomerase (topo) inhibiting activity. Examples of marine natural products that are active in the differential cytotoxicity assay include the makaluvamines and wakayin.

The makaluvamines, from the Fijian sponge *Zyzya* sp., showed enhanced toxicity

towards DNA double strand break repair deficient *xrs-6* CHO cells relative to the repair competent BR1 strain and are (topoisomerase II) topoII inhibitors.<sup>80,81</sup> For example, makaluvamine F (**21**) showed sixfold enhanced toxicity toward *xrs-6* relative to BR1 and an IC<sub>90</sub> of 25  $\mu$ M in the topoII decatenation inhibition assay.<sup>80</sup> Wakayin (**22**), a pyrroloiminoquinone alkaloid, isolated from a *Clavalina* sp. ascidian,<sup>82</sup> showed 9.8-fold enhanced toxicity towards *xrs-6* relative to BR1 CHO lines and inhibited topoII catalyzed decatenation of kDNA at 250  $\mu$ M.<sup>83</sup>

**21****22**

Another cell line used to detect compounds acting by a specific mechanism is the *E. coli* BR513 strain that is specifically engineered to detect DNA damaging compounds in the biochemical induction assay (BIA). Eilatin (**23**) is the only reported example of a marine natural product active in this assay (Chapter III). Eilatin causes induction of  $\beta$ -galactosidase at 2  $\mu$ g/disk in the BIA.<sup>74</sup>

**23**



### Mechanism-Based Assays

Mechanism-based approaches are increasingly being employed in the search for novel, potential chemotherapeutic agents. Very specific biochemical assays are used to find cytotoxic compounds that work by mechanisms that are similar to those of established drugs. Many compounds have affinity for certain cellular receptors in mammalian cells and most of them ultimately exert their activity via interaction with one or more of these receptors. In fact, it is believed that all secondary metabolites evolved under selective pressure from some receptor.<sup>84</sup>

It is anticipated that greater efficacy and cell type selectivity may be achieved by employing mechanism-based approaches for discovering compounds that target receptors or enzymes involved in the pathogenesis of neoplastic diseases. The use of these assays stems from advances in the understanding of tumor biology and biochemistry made over the past decades. The assays are inherently more specific than those using whole cells or animals.

Although this section focuses on the use of mechanism-based assays, it also includes compounds discovered using more traditional approaches but later shown to have some effect at a specific receptor. Studies using these compounds have either demonstrated the importance of the receptor or have helped to initially identify it.

### Topoisomerase Inhibition Assays

Recently, much attention has been focused on topoisomerase inhibitors since many clinically useful drugs have been shown to act by inhibiting topoII, an enzyme crucial to cell proliferation. Marine natural products that inhibit topoII include the makaluvamines,<sup>80,81</sup> pyridoacridines (Chapter 3),<sup>74,85</sup> and wakayin.<sup>83</sup>

There are many topoII inhibitors known, but there are relatively few topoisomerase I (topoI) inhibitors.<sup>86</sup> Since topoI was shown to be the target of the antitumor plant alkaloid camptothecin and its derivatives,<sup>87</sup> intensive efforts are also underway to find new

inhibitors of this enzyme.

#### Antimitotic Agents (Microtubule Assembly-Tubulin Polymerization Inhibition Assays)

Antimitotic agents that bind to tubulin and interfere with microtubule assembly often result in mitotic arrest.<sup>88</sup> Some of the more promising antitumor agents acting by this mechanism include dolastatin 10 (**16**)<sup>68</sup> and halichondrin B (**19**)<sup>77</sup> discussed earlier.

#### Nucleotide Biosynthesis Inhibition Assays

Marine natural products that affect de novo nucleotide biosynthesis or their incorporation into DNA are not common. However, the previously discussed arabinonucleosides (**7-8**), credited with propelling the field of marine natural products chemistry towards prominence in the 1950s and synthetic analogs, act by this mechanism.<sup>31</sup>

#### Signal Transduction Inhibition Assays

Macromolecules involved in signal transduction during cell growth provide excellent targets for inhibition. One of the most intensively studied molecules in the signal transduction pathway, protein kinase C (PKC), has become an important target in the effort to stem malignant transformation. Mechanism-based assays designed to detect compounds that perturb signal transduction pathways are being employed in marine natural products chemistry.

For example, latrunculin A (**11**) showed activity in an EL-4.IL-2 cell adhesion assay that correlates with PKC agonism or antagonism. Latrunculin A reduces EL-4.IL-2 cell adhesion presumably by antagonizing the activity of PKC and showed enhanced cytotoxicity towards the A549 non-small cell lung carcinoma line, relative to the P388 leukemic line.<sup>42</sup>

Some pyridoacridine alkaloids (e.g., eilatin (**23**)) from a *Eudistoma* sp. ascidian were recently reported to exhibit growth regulatory properties (inhibition of proliferation and

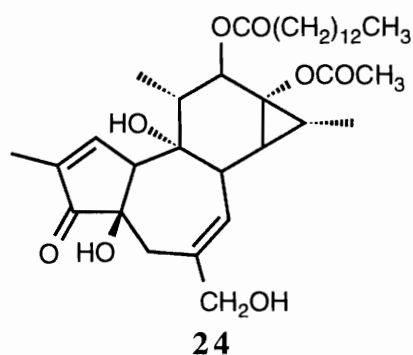
induction of differentiation and reverse transformation of transformed cells), presumably by acting on the cyclic adenosine monophosphate (cAMP) signaling system.<sup>89</sup>

### DNA Interactive Agents

Compounds that interact with DNA are among the most useful anticancer compounds in the clinic. These compounds interact with DNA in a variety of ways including intercalation, alkylation, and noncovalent binding. Many marine natural products are screened for their ability to intercalate into DNA as part of routine evaluation of their mode of action. Members of the pyridoacridine class (e.g., dercitin (**17**) and eilatin (**23**))<sup>73,74,90</sup> and the makaluvamines<sup>80</sup> are examples of marine natural product intercalating agents.

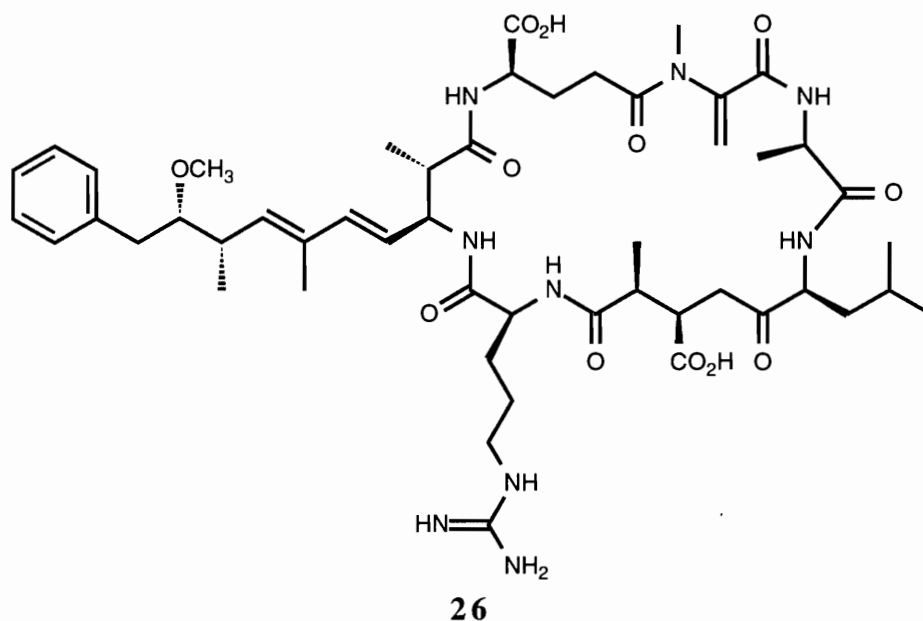
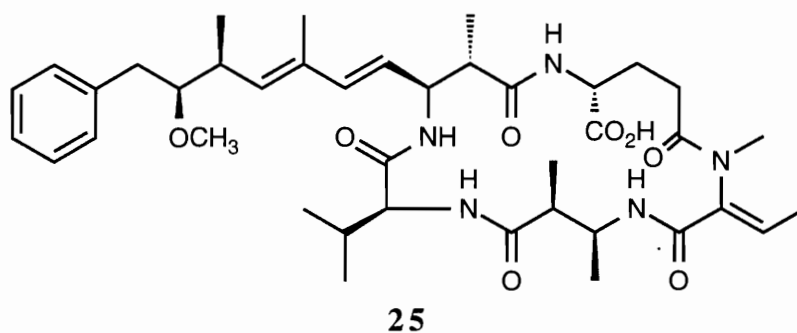
### Protein Phosphatases and Tumor Promotion

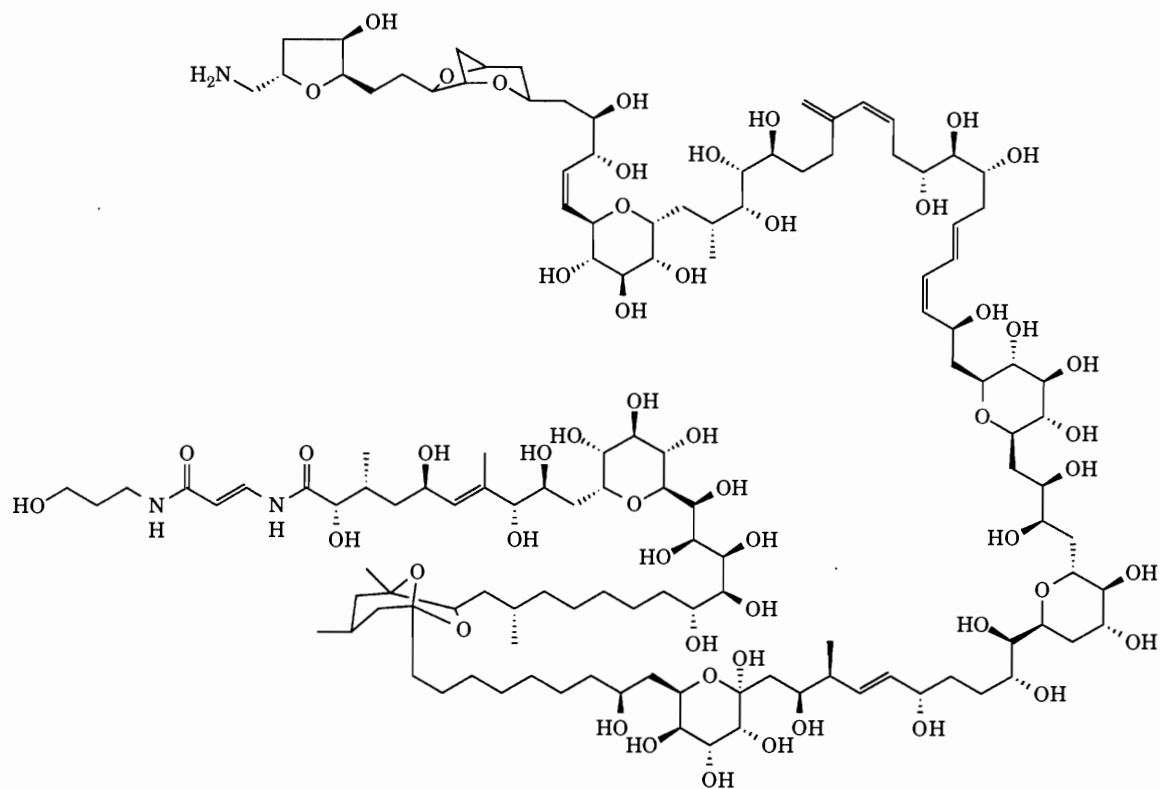
Protein phosphatases have been shown to be important in malignant transformations, and apparently act as tumor suppressors in vivo by maintaining the proper level of protein phosphorylation.<sup>5</sup> Although okadaic acid (**18**), one of the toxins responsible for diarrhetic shellfish poisoning,<sup>22</sup> has not shown much potential for clinical utility, it has proven to be a valuable probe in defining the role of phosphorylation–dephosphorylation in malignant transformations, and as a probe for specific protein phosphatases.<sup>91</sup> The phorbol ester TPA<sup>92</sup> (**24**) promotes tumors in animals exposed to carcinogens by activating PKC,



whereas okadaic acid, a non-TPA type tumor promoter, acts by a mechanism not involving activation of PKC.<sup>4</sup> The toxin **18** hinders dephosphorylation by inhibiting protein

phosphatase activity.<sup>93</sup> Although not a TPA-type tumor promoter, okadaic acid, by inhibiting protein dephosphorylation, causes accumulation of the same phosphorylated proteins believed to be involved in tumor promotion.<sup>94</sup> Okadaic acid is routinely used as a probe for classifying serine-threonine protein phosphatases as either type 1, 2A, or 2B, based on the concentration of compound required for inhibition of phosphatase activity.<sup>91</sup> Other compounds such as motuporin (**25**),<sup>95</sup> microstatin-LR (**26**),<sup>96</sup> calyculin A (**9**),<sup>35</sup> and palytoxin (**27**)<sup>22</sup> have also shown phosphatase inhibitory activity.





27

### Summary

Although marine derived natural products have been intensively studied by chemists over the past 35 years, their biomedical potential was not fully recognized until recently. The early "phytochemical" approach to discovering biomedical marine natural products have yielded several important leads; however, it has been largely supplanted by a more targeted approach which relies heavily on the use of increasingly sophisticated biological and mechanism-based assays. The success of the biological assay guided approach is evidenced by the increased number of potentially useful marine natural products discovered through the use of such assays.<sup>7-14</sup> Although the use of mechanism-based assays for compound screening is on the rise, these types of assays are, at present, unlikely to replace the more traditional biological assays such as *in vitro* cytotoxicity and *in vivo* tumor models, which remain the primary tools for the discovery of potential antineoplastic compounds. This is because mechanism-based screens are, by design, expected to detect

only a very narrow range of compounds, while biological assays are broad based screens.

There are several advantages to using whole cell or animal assays over mechanism-based assays. First, a compound showing activity in a cell based assay has exerted its effects by presumably binding to some receptor. Since the desired effect has been obtained in the form of activity, it is not necessary to isolate or characterize that receptor. Second, activity in such assays tends to indicate that the compound is capable of crossing the cell membrane. Third, since the cell contains a multitude of receptors against which a compound can potentially act, it is not necessary to use a bank of different enzymes for screening. It is therefore important to use a combination of approaches in the search for novel, potentially useful therapeutic agents from marine organisms.

Although there has been a tremendous increase in our understanding of the etiology of cancer from a molecular perspective during the past decade, effective treatment for many solid tumors remains elusive. Thus, many research groups have active programs directed towards finding useful anticancer chemotherapeutic agents. A variety of approaches using a multitude of assay methods are undertaken. The efforts of the Ireland Research Group are directed toward the goal of finding potential anticancer agents and the approaches used are described in the next chapter. The projects described in this dissertation are aimed at finding active or novel compounds with anticancer potential, or those that are potentially useful as molecular probes.

## CHAPTER 2

### STRATEGIES FOR DISCOVERING POTENTIAL

#### ANTICANCER AGENTS: BIOASSAY

#### GUIDED FRACTIONATION

The goals of my research are to identify and characterize new biologically active compounds from marine organisms; and in some instances, to establish the mechanism of action of these compounds. The research strategy begins with the choice of organism. In the Ireland Research Group, there is a bias towards the phylum Chordata (subphylum: Urochordata (= Tunicata), class: Ascidiacea (= ascidians or sea squirts)) consisting of invertebrate animals that are exclusively marine and predominantly sessile.

The strategy for discovering active compounds involves the use of a variety of biological assays ("bioassays") to initially identify and subsequently guide the fractionation of active extracts. Bioassay guidance ultimately leads to the component(s) of the crude extract that initially gave rise to the activity. This research is oriented towards the isolation of potential anticancer agents; consequently, the assays used are designed to detect compounds that kill or retard the growth of tumor cells. These assays range from relatively simple antimicrobial assays to assays for cytotoxicity, selective cytotoxicity, *in vivo* activity, and enzyme inhibition. By its very nature, the research conducted in the Ireland Research Group is interdisciplinary and therefore involves several collaborators. This chapter discusses the various approaches used in our group for identifying potential anticancer agents.

## In Vitro Assays

### Antimicrobial Assays

Antimicrobial assays determine if a crude extract or pure compound has antibiotic activity against a given organism. Organisms such as the yeasts *Candida albicans* and *Saccharomyces cerevisiae* and the bacteria *Bacillus subtilis* and *Pseudomonas aeruginosa* have been used in our laboratory. Antimicrobial activity against a specific strain of *Escherichia coli* used in the BIA may also be assessed in addition to induction (see below). These assays are performed using the disk diffusion method. Due to poor correlation between antimicrobial and antitumor activities, these assays are considered of limited utility. However, when a clear correlation exists between antimicrobial and in vivo activity, the antimicrobial assay may be used to guide fractionation.

### Cytotoxicity Assays

The ability of a compound to inhibit the replication of various cell lines is evaluated using the MTT assay.<sup>97-99</sup> This work is done in the laboratory of Prof. Louis R. Barrows of the Department of Pharmacology and Toxicology. Several human tumor cell lines derived from various tissues and one leukemic line are used (Table 2.1). Selective cytotoxicity may be assessed using this panel of cell lines.

Table 2.1

Human Cell Lines used in Natural Products Screening	
Cell Line	Type
HCT116	Colon cancer
A498	Kidney carcinoma
MCF-7	Breast adenocarcinoma
PC-3	Prostate adenocarcinoma
SK-MEL-1	Skin (malignant melanoma)
A549	Lung adenocarcinoma
HL-60	Blood (promyelocytic leukemia)



Via collaboration with Prof. Graydon Harker, a number of mitoxantrone resistant human cell lines are also available to evaluate pure compounds that have shown selective cytotoxicity or enhanced toxicity towards xrs-6 CHO mutants discussed below. Table 2.2 contains a description of these multidrug resistant (MDR) cell lines.

### Cell Lines Sensitive to DNA Damaging Agents

Our interest on anticancer compounds has led to specifically focusing those agents that interact with DNA. A mechanism based screening protocol to discover cytotoxic compounds that act by mediating topoisomerase activity or DNA strand breaks has been employed. These assays are often used as secondary screens to test compounds or extracts showing antimicrobial or cytotoxic activity.

#### CHO Differential Cytotoxicity Assays

Single strand (ss) break repair-deficient EM9 CHO cells are sensitive to topoI inhibitors (e.g., camptothecin). This cell line lacks a functional *XRCC1* gene and is deficient in its ability to repair DNA single strand breaks.<sup>100</sup> Double strand (ds) break repair-deficient xrs-6 CHO cell lines are sensitive to compounds that cause ds breaks either directly or by inhibiting topoII. By stabilizing cleavable complexes and inhibiting the

Table 2.2

Multidrug Resistant Cell Lines used in Evaluating Pure Compounds

Cell Line (origin)	Genetic Alteration	Characteristics
MX1 (from CEM)	Reduced levels of nuclear topoII and absence of the $\beta$ isoform.	Mitoxantrone resistant and reduced sensitivity to topoII poisons.
MX2 (from HL-60)	Reduced levels of topoII due to absence of the $\beta$ isoform and attenuated topoII activity.	Mitoxantrone resistant and reduced sensitivity to topoII poisons.
LK2/10 (from LK2)	Increased p-glycoprotein levels.	Mitoxantrone resistant. General MDR resistant.

rejoining reaction catalyzed by the enzyme, topoII poisons result in ds breaks.<sup>101,102</sup> The UV20 CHO line is deficient in its ability to repair bulky DNA adducts or crosslinks.

Since many clinically useful compounds damage DNA or interfere with its replication, compounds isolated in our laboratory are tested for their ability to exert enhanced toxicity towards the ss-break repair deficient EM9, the excision repair deficient UV20, or the ds-break repair-deficient *xrs-6*<sup>103</sup> CHO mutant line relative to the repair-proficient BR1<sup>100</sup> cell line. Toxicity is measured using a modification of the MTT tetrazolium salt colorimetric assay used to determine HCT cytotoxicity.<sup>97-99</sup> This work is also conducted in the laboratory of Prof. Barrows and a number of drugs acting by known mechanisms have been used to validate this assay.<sup>83</sup> Table 2.3 summarizes the genetic alterations and characteristics of the CHO cell lines used in screening crude extracts or to evaluate pure DNA active compounds.

*Escherichia coli* responds to various adverse conditions by inducing SOS functions.<sup>105</sup> Agents responsible for this induction include genotoxic agents, mutagens or compounds that inhibit DNA replication. The mechanism that appears to mediate the induction response involves the activation of the *recA* protease by binding to single strand DNA (or DNA-degradation products). The *recA* protease then cleaves a repressor molecule, the *lexA* product, which in turn causes the cell to make more *recA* protein and other enzymes involved in DNA repair.<sup>106</sup>

Table 2.3

CHO Cell Lines used in Screening and Mechanistic Studies.

Cell Line	Genetic Alteration	Characteristics
EM9	Reduced <i>XRCC1</i> gene expression.	Sensitive to topoI poisons
<i>xrs-6</i>	DNA ds break repair deficient.	Sensitive to topoII poisons and agents that cause ds-DNA breaks.
UV20	Lacking DNA excision repair gene.	Sensitive to DNA alkylation (bulky adducts and DNA crosslinks).
BR1	Elevated levels of O <sup>6</sup> -alkylguanine-DNA-alkyltransferase.	DNA repair proficient (BCNU <sup>104</sup> resistant)

### Biochemical Induction Assay (BIA)

The repressors of lytic growth of some bacteriophages, such as  $\lambda$  phage, are also cleaved by the *recA* protease, thereby inducing lytic growth under adverse conditions such as assault to the host's DNA. The BIA uses a  $\lambda$ -*lacZ* lysogenic *E. coli* strain. *E. coli* that are lysogenic for a  $\lambda$ -*lacZ* fusion phage produce  $\beta$ -galactosidase, a product of the *lacZ* gene, on induction of the prophage by DNA damaging agents.<sup>107</sup> Since many useful anticancer agents act by interacting with DNA, the BIA is expected to detect such agents when used to screen crude extracts. The BIA is carried out by Leonard A. McDonald.

Induced levels of  $\beta$ -galactosidase are a direct response to SOS-induced  $\lambda$  gene expression. Quantification of  $\beta$ -galactosidase is accomplished colorimetrically by detecting the cleavage product of the 6-bromo-2-naphthyl- $\beta$ -D-galactopyranoside (**28**) substrate using fast blue RR salt (4-benzoylamino-2,5-dimethoxybenzenediazonium chloride hemi[zinc chloride] salt, (**29**)).<sup>108</sup>  $\beta$ -Galactosidase is essential in lactose metabolism. The normal function of  $\beta$ -galactosidase is to metabolize the disaccharide lactose to galactose (**30**) and glucose. *E. coli* uses galactose as its sole carbon source under normal conditions. The cleavage of the substrate **28** is a  $\beta$ -galactosidase catalyzed hydrolysis of the  $\beta$ -glycosidic bond (Figure 2.1). Coupling between the bromonaphthol (**31**) cleavage product and the diazonium salt, **29**, produces the highly colored azo dye (**32**), which may be quantified.

Aromatic rings that couple to diazonium salts must contain good electron releasing "activating" groups such as -OH, -NH<sub>2</sub>, -NHR or -NR<sub>2</sub> since diazoniums are only weakly electrophilic. The substitution generally occurs ortho to the activating group as in Figure 2.1.

### Mechanistic Assays

#### Topoisomerase Assays

The topoisomerase enzymes are common targets for many compounds that ultimately affect DNA replication.<sup>109-112</sup> DNA topological transformations such as catenation-

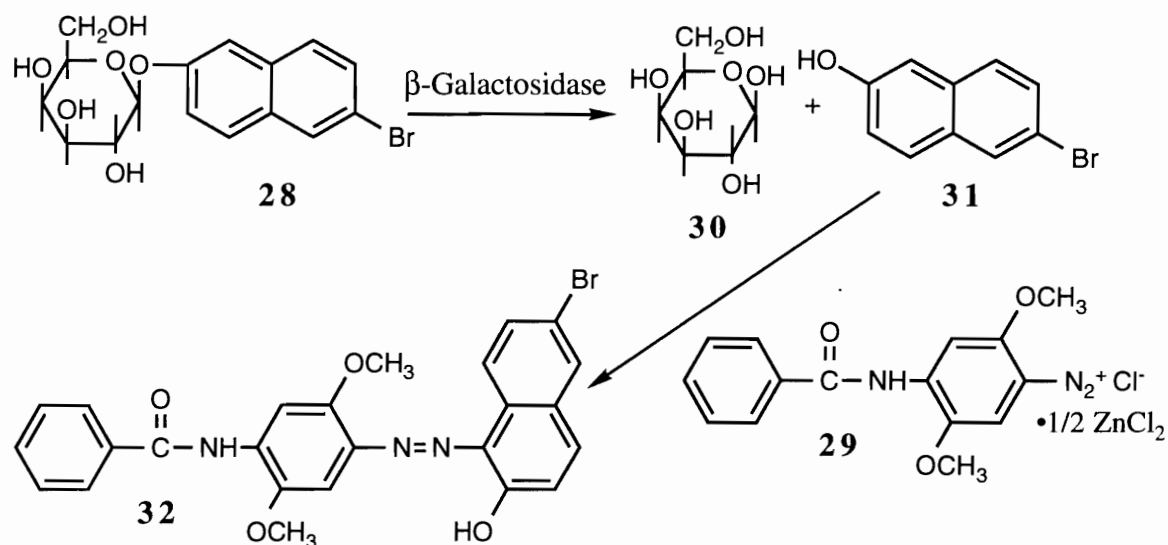


Figure 2.1. Chemistry involved in the biochemical induction assay.

decatenation and unwinding are controlled by topoisomerases.<sup>113</sup> The three-dimensional structure of DNA regulates many of its functions within the cell. Topoisomerases are ultimately involved in regulating the tertiary structure of DNA and are instrumental in maintaining chromosome structure and separating daughter chromatids during mitosis.<sup>113,114</sup> TopoII acts by transiently breaking both strands of double helix DNA, thereby allowing the topological transformations that are necessary for DNA replication.<sup>114</sup>

The high levels of topoII that exist in proliferating cells versus the lower levels present in nonreplicating cells result in some topoII inhibitors preferentially killing cancer cells,<sup>112</sup> presumably because of the greater need for cell replication machinery in the former. Drugs that interact with nucleic acids are therefore among the most useful cancer chemotherapeutic agents.<sup>115</sup> Intercalating compounds such as acridines, ellipticines, anthracyclines, actinomycins, and anthracenediones are known to induce topoII-mediated double strand breaks in DNA.<sup>109-112</sup> Many intercalators are thought to stabilize the covalent enzyme-DNA “cleavable” complex by interfering with the DNA rejoining step catalyzed by topoII.<sup>116,117</sup>

The anticancer activity and mode of action of the camptothecin analog topotecan, a

topoI inhibiting drug, have increased interest in designing assays to find other topoI poisons.<sup>87</sup> TopoI is thought to be involved in gene transcription and DNA replication in normal cells. The enzyme acts by breaking and religating only a single DNA strand.

The topoisomerase assays are carried out in the laboratory of Prof. Barrows.

#### Decatenation Inhibition and DNA Relaxation Assays

The decatenation inhibition assay measures a compound's ability to inhibit the topoII-catalyzed release of linear and circular DNA monomers from high molecular weight kDNA.<sup>118</sup> The released DNA monomers can be resolved and quantitated on a 1% agarose gel while the fully catenated kDNA is too large to penetrate into the gel. Enzyme inhibition is measured by monitoring the disappearance of the monomer-length DNA bands as a function of increasing compound concentration.

A DNA relaxation assay is used to detect topoI poisons. This assay measures the ability of a compound to inhibit the topoI catalyzed relaxation (unwinding) of supercoiled pBR322 DNA.<sup>119</sup>

The decatenation inhibition and DNA relaxation assays are carried out in the laboratory of Prof. Barrows.

#### Cleavable Complex Assay

The K<sup>+</sup>-SDS precipitation assay (performed in Prof. Barrow's laboratory) is used to assess the involvement of cleavable complex formation in topoII inhibition. The assay is used to measure covalent DNA-protein complexes in whole cells by measuring precipitable radioactivity.

#### Intercalation Assay

The intercalation assay is designed to provide information about the mechanism of action of a compound. Compounds that bind DNA often do so by intercalation. The ethidium bromide displacement assay shows the ability of a compound to intercalate into DNA. When intercalated into DNA, ethidium bromide exhibits dramatically enhanced

fluorescence along with a shift of its emission maximum.<sup>120</sup> When a competing intercalator displaces ethidium bromide from DNA, the fluorescence of ethidium bromide decreases. The fluorescence of ethidium bromide determined in the presence of DNA as a function of compound concentration provides a measure of intercalative ability of the compound.

### Inhibition of Macromolecular Synthesis

In an effort to establish molecular mechanism of action, compounds that are good intercalators or topoII inhibitors are often tested for their effects on the rates of DNA, RNA, and protein synthesis. These tests are done in the laboratory of Prof. Barrows. The inhibition of incorporation of the radiolabelled precursors [<sup>3</sup>H]leucine (protein), [<sup>3</sup>H]uridine (RNA), and [<sup>3</sup>H]thymidine (DNA) into HCT or BR1 cells is used to assess the effects of these compounds on macromolecular synthesis.

### In Vivo Assays

In vitro active compounds are tested for antileukemic or antitumor activities in the P388 leukemia or ovarian carcinoma (Ovcar3) tumor models at Lederle Laboratories (Pearl River, NY).

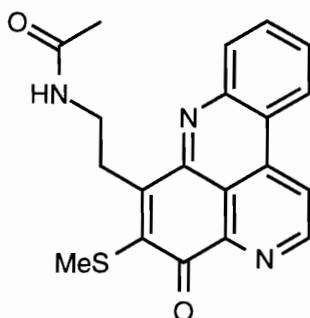
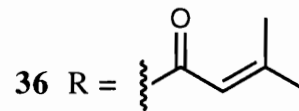
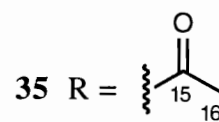
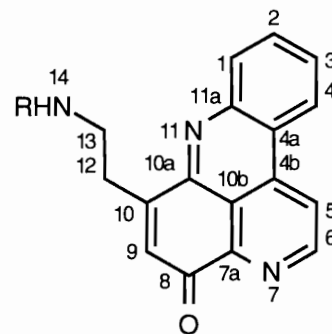
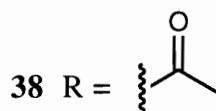
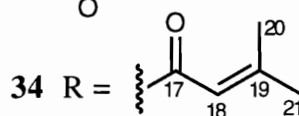
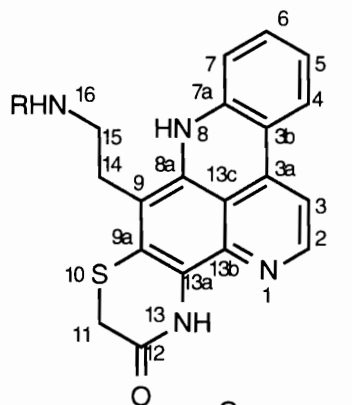
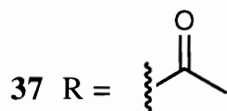
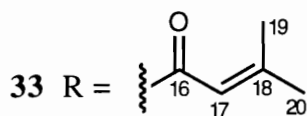
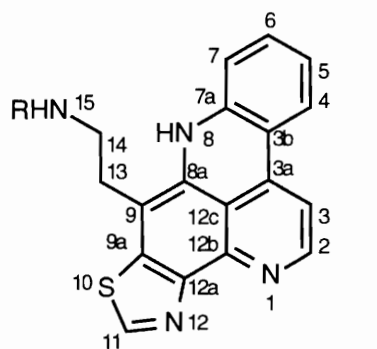
## CHAPTER 3

### THE CHEMISTRY AND BIOLOGY OF THE ASCIDIAN

#### *CYSTODYTES* SP.

This chapter describes the isolation and characterization of a series of pyridoacridine alkaloids from a Fijian *Cystodytes* sp. (Order: Aplousobranchia, Family: Polycitoridae (colonial)) ascidian: dehydrokuanoniamine B (**33**), shermilamine C (**34**), cystodytin J (**35**), and the known compounds cystodytin A<sup>121</sup> (**36**), kuanoniamine D<sup>122</sup> (**37**), shermilamine B<sup>123</sup> (**38**), and eilatin<sup>90</sup> (**23**). These compounds and the previously reported diplamine<sup>124</sup> (**39**) were evaluated in order to establish their mechanism of action.

Initial interest in this organism stemmed from activity noted in the biochemical induction assay (BIA)<sup>108</sup> and from the observed cytotoxicity of the crude extract against the human colon tumor cell line HCT116. Pyridoacridine alkaloids derived from ascidians and sponges are reported to exhibit a variety of interesting properties including DNA intercalation,<sup>73,125</sup> topoII inhibition,<sup>85</sup> calcium release,<sup>121</sup> anti HIV,<sup>126</sup> and in vivo antitumor<sup>73</sup> activities. The pyridoacridines discussed herein exhibited varying degrees of cytotoxicity towards HCT cells and were subsequently shown to inhibit the function of topoII and to intercalate into DNA. The ability of the pyridoacridines to inhibit topoII correlated with their ability to intercalate and inhibit the growth of HCT cells. Their capacity to bind DNA, inhibit topoII, disrupt DNA and RNA synthesis, and inhibit replication of HCT cells is consistent with a cytotoxicity mechanism involving intercalation and prevention of topoII from binding to its DNA substrate. This proposed mechanism for pyridoacridine-induced inhibition of HCT cell replication is examined in this chapter.



39

## Chemistry

### Isolation of the Pyridoacridine Alkaloids

Shipboard screening using the BIA<sup>108</sup> showed that the MeOH extract from a purple fleshy *Cystodytes* sp. ascidian<sup>127,128</sup> was capable of interacting with DNA.<sup>105</sup>

Subsequent bioassay guided fractionation of the MeOH extract of the frozen animal led to the isolation of a bright yellow alkaloid which was solely responsible for the BIA activity of the crude extract. This compound was spectroscopically identical to eilatin (**23**), a dibenzotetraazaperylene pyridoacridine previously isolated from a Red Sea *Eudistoma* sp. ascidian.<sup>90</sup> Further examination of the extract led to the isolation of several additional



pyridoacridines (**23**, **33-38**) which were inactive in the BIA, but showed significant cytotoxicity toward HCT cells in vitro.

The numbering scheme for compounds **33**, **34**, and **35** parallels those published for compounds **37**, **38**, and **36** respectively.

### Structure Elucidation of Dehydrokuanoniamine B

Compound **33** was obtained as an orange amorphous solid. High resolution FAB mass measurement provided the molecular formula  $C_{23}H_{21}N_4OS$ . Due to its limited solubility in several deuterated solvents, **33** was converted to its TFA salt for subsequent NMR studies. The proton, carbon, and COSY spectra of **33** are shown in Appendix A. The extensive conjugation and heteroaromatic nature of **33** was evident from its UV spectrum and blue shift upon addition of acid. Analysis of the NMR data (Table 3.1) revealed four isolated spin systems, two exchangeable signals and one downfield aromatic singlet.

The signals at 8.27 (H4, d,  $J = 8.2$  Hz), 7.27 (H5, ddd,  $J = 8.2, 5.3, 2.1$  Hz), and 7.72 ppm (H6 & H7, m) in the  $^1H$  NMR spectrum ( $DMSO-d_6$ ) were assigned to a 1,2-disubstituted benzene ring. Another spin system consisting of signals at 8.46 (H2, d,  $J = 6.5$  Hz) and 7.87 ppm (H3, d,  $J = 6.5$  Hz) was indicative of a trisubstituted pyridine ring. A very strong nuclear Overhauser enhancement (nOe) correlation between 7.87 (H3) and 8.27 ppm (H4) in the ROESY<sup>129,130</sup> spectrum of **33** facilitated assignment of these proton signals to adjacent rings (Figure 3.1).

The proton detected heteronuclear multiple bond correlation (HMBC)<sup>131</sup> experiment showed correlations between the quaternary carbon signal at 114.13 ppm (C3b) and the exchangeable proton signal at 11.71 ppm (H8) and also to the aromatic signals at 7.27 ppm (H5) and 7.87 ppm (H3) (Figure 3.2). Additional HMBC correlations between the 118.25 ppm (C12c) quaternary carbon and H8 as well as H3 were indicative of a pyridoacridine. Signals at 3.31 (H14, dt,  $J = 5.3, 7, 3$  Hz) and 3.12 ppm (H13, t,  $J = 7.3$  Hz) indicated a pair of coupled methylene groups, whereas those at 5.63 (H17, septet,  $J = 1.1$  Hz), 2.15

Table 3.1

NMR<sup>a</sup> Assignments for the TFA Salt of Dehydrokuanoniamine  
B in DMSO-*d*<sub>6</sub>

Atom no.	$\delta$ <sup>13</sup> C	$\delta$ <sup>1</sup> H	(mult., <i>J</i> (Hz))	HMBC <sup>b</sup> correlations
2	142.72	8.46	(d, 6.5)	C3, C3a, C12b
3	107.57	7.87	(d, 6.5)	C2, C3b, C12c
3a	148.50			
3b	114.13			
4	125.53	8.27	(d, 8.2)	C3a, C6, C7a
5	122.98	7.27	(ddd, 8.2, 5.3, 2.1)	C3b, C6, C7
6	135.30	7.72	(m)	C4, C7a
7	117.51	7.72	(m)	C3b, C5
7a	140.48			
8	—	11.71	(bs)	C3b, C12c
8a	132.80 <sup>c</sup>			
9	108.44			
9a	143.15			
11	153.83	9.43	(s)	C9a, <sup>d</sup> C12a
12a	132.74 <sup>c</sup>			
12b	131.80			
12c	118.25			
13	30.98	3.12	(t, 7.3)	C8a, C9, C9a, C14
14	36.19	3.31	(td, 7.3, 5.3)	C9, C16
15	—	8.35	(t, 5.3)	C14, C16
16	167.84			
17	118.08	5.63	(septet, 1.1)	C16, C18, C19, C20
18	150.30			
19	19.50	2.15	(d, 1.1)	C17, C18, C20
20	26.84	1.79	(d, 1.1)	C17, C18, C19

<sup>a</sup> Proton and carbon data were acquired at 500 and 125 MHz, respectively.

<sup>b</sup> The HMBC experiment was optimized to observe <sup>n</sup>*J*<sub>CH</sub> couplings of 8.5 Hz.

<sup>c</sup> Interchangeable assignments.

<sup>d</sup> Seen only when the HMBC experiment was optimized to observe 5 Hz <sup>n</sup>*J*<sub>CH</sub> couplings.

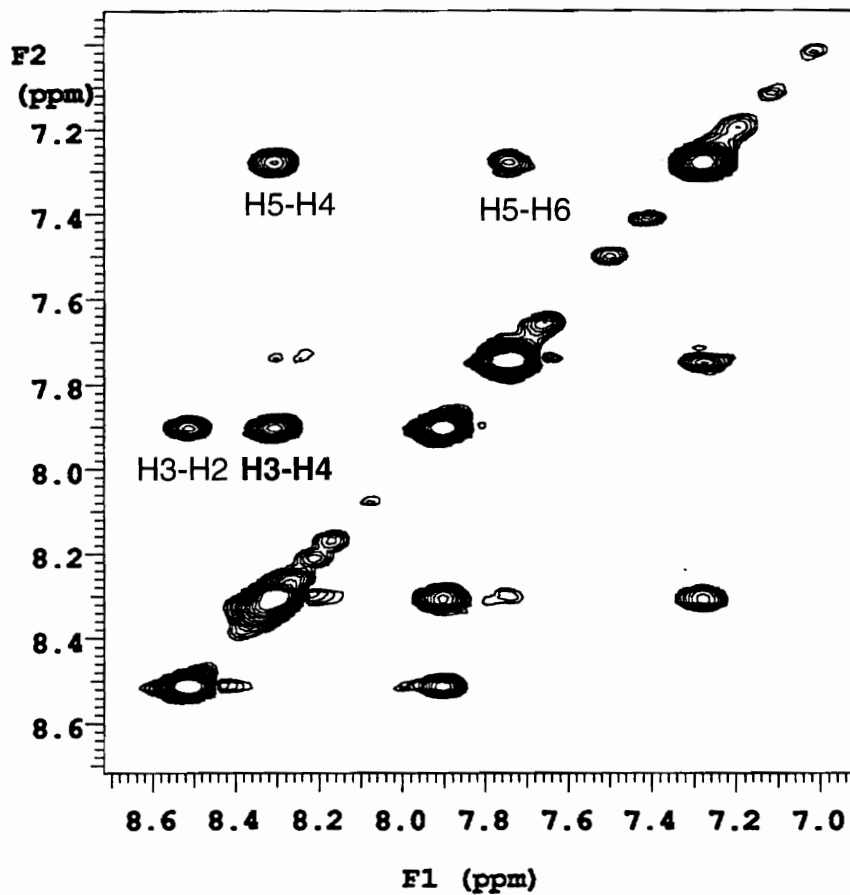


Figure 3.1. Region of a 300 ms ROESY spectrum of dehydrokuanoniamine B showing the H3-H4 crosspeak.

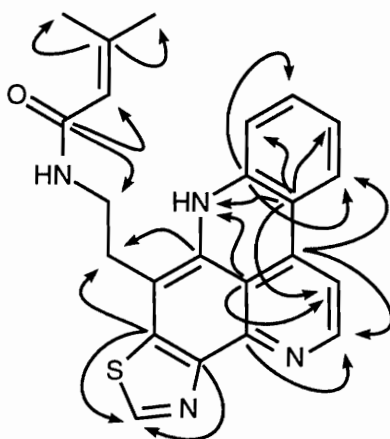


Figure 3.2. Dehydrokuanoniamine B with HMBC correlations used in assigning the quaternary carbon atoms.

(H19, d,  $J = 1.1$  Hz), and 1.79 ppm (H20, d,  $J = 1.1$  Hz) suggested an isobutenyl group. In addition to the downfield shift of C20,<sup>121</sup> the presence of a significant ROESY correlation between H17 and H20 established that they were *cis* relative to each other. These data, plus a singlet at 9.43 ppm (H11), suggested that the compound belonged to the kuanoniamine class<sup>122,125</sup> and was in fact dehydrokuanoniamine B. Assignments of C9a and C12a were based on HMBC correlations to H11 and chemical shift comparisons with literature values for these carbons.<sup>122</sup> The regiochemistry of the nitrogen and the sulfur of the thiazole ring and the correct assignments of the adjacent carbons have been firmly established for the kuanoniamine class.<sup>72,122,125</sup> Carroll and Scheuer used the benzothiazole model to show that electron delocalization and conjugation across the *H11*-C11-N12-*C12a* bonds facilitated a large long range proton-carbon coupling between the highlighted atoms ( $^3J_{C12a-H11} = 13.8$  Hz) (see structure **33** for numbering scheme). The long range proton-carbon correlation across the *H11*-C11-S10-*C9a* bonds is less ( $^3J_{C9a-H11} < 5$  Hz).<sup>122</sup> Although only the C12a-H11 correlation is observed when the HMBC experiment was optimized for observing  $^nJ_{CH}$  of 8.5 Hz, both the C12a-H11 and C9a-H11 correlations were observed when the experiment was optimized to observe  $^nJ_{CH}$  of 5 Hz.

### Structure Elucidation of Shermilamine C

The NMR data for shermilamine C (**34**), contained in Table 3.2, were almost identical to those reported for shermilamine B (**38**),<sup>123,132</sup> with the greatest differences occurring in the regions of the spectrum corresponding to the side chain. The proton, carbon, and COSY spectra of **34** are shown in Appendix A. Thorough examination of these data revealed that **34** possessed the same isobutenyl side chain found in **33**.

The HMBC correlations instrumental in assigning the quaternary carbon atoms of shermilamine C are shown in Figure 3.3.

Table 3.2

NMR<sup>a</sup> Assignments for the TFA Salt of Shermilamine C in  
DMSO-*d*<sub>6</sub>

Atom no.	$\delta$ <sup>13</sup> C	$\delta$ <sup>1</sup> H	(mult., <i>J</i> (Hz))	HMBC <sup>b</sup> correlations
2	146.06	8.35	(d, 5.9)	C3, C3a, C13b
3	105.92	7.45	(d, 5.9)	C2, C3b, C13c
3a	144.48			
3b	114.74			
4	124.78	8.04	(d, 7.9)	C3a, C6, C7a
5	122.22	7.11	(dd, 7.9, 7.9)	C3b, C7
6	133.78	7.55	(dd, 7.9, 7.9)	C4, C7a
7	116.97	7.51	(d, 7.9)	C3b, C5
7a	140.09			
8	—	11.37	(bs)	
8a	131.45			
9	111.46			
9a	127.97			
11	29.49	3.58	(s)	C9a, C12
12	164.27			
13	—	9.64	(bs)	C9a, C11
13a	117.86 <sup>c</sup>			
13b	130.56			
13c	117.14			
14	27.97	2.89	(t, 7.2)	C8a, C9, C9a, C15
15	36.61	3.08	(m)	C17
16	—	8.56	(t, 5.7)	C15, C17
17	168.31			
18	117.92 <sup>c</sup>	5.70	(t, 1.1)	C17, C20, C21
19	150.81			
20	19.60	2.22	(s)	C18, C19, C21
21	26.95	1.84	(s)	C18, C19, C20

<sup>a</sup> Proton and carbon data were acquired at 500 and 125 MHz, respectively.

<sup>b</sup> The HMBC experiment was optimized to observe <sup>n</sup>*J*<sub>CH</sub> couplings of 8.5 Hz.

<sup>c</sup> Interchangeable assignments.

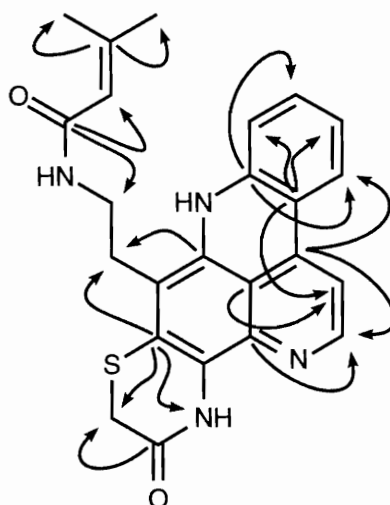


Figure 3.3. Structure of shermilamine C with HMBC correlations used in assigning the quaternary carbon atoms.

#### Structure Elucidation of Cystodytin J

The iminoquinone nature of **35** was initially revealed by its behavior during FAB mass spectrometry. FAB mass spectrometry in a reducing matrix such as glycerol produced an ion at  $m/z$  320 corresponding to the reduced molecular ion  $((M+2)+H)^+$ . A similar experiment in 3-nitrobenzyl alcohol, a less reducing matrix, produced ions predominantly at  $m/z$  318  $(M+H)^+$  but also some at  $m/z$  320. This behavior has been reported for the iminoquinone cystodytins by Kobayashi et al.<sup>121</sup> HR FAB MS provided the molecular formula  $C_{19}H_{18}N_3O_2$  for the reduced form of **35**.

The proton, carbon and COSY spectra of **35** are shown in Appendix A. The  $^{13}C$  spectrum showed 18 distinct resonances. The HMBC experiment later revealed that C1 and C2 were degenerate, both resonating at 131.87 ppm. Examination of the NMR data (Table 3.3) revealed the presence of a 1,2-disubstituted aromatic ring, a polarized  $\pi$  bond in a six membered aromatic ring, an isolated olefinic proton, two coupled methylene groups—one of which was further coupled to an exchangeable proton, and a methyl singlet.

A strong NOESY correlation between H4 and H5 placed the H1-H2-H3-H4 spin system of the 1,2-disubstituted aromatic ring adjacent to the H5-H6 polarized  $\pi$  bond.

Table 3.3

NMR<sup>a</sup> Assignments for Cystodytin J in CDCl<sub>3</sub>

Atom no.	$\delta$ <sup>13</sup> C	$\delta$ <sup>1</sup> H	(mult., <i>J</i> (Hz))	HMBC <sup>b</sup> correlations
1	131.87	8.29	(d, 8.1)	C3, C4a, C11a
2	131.87	7.94	(ddd, 8.1, 7.1, 1.4)	C4, C11a
3	129.83	7.83	(ddd, 8.1, 7.1, 1.4)	C1/C2, C4a
4	122.84	8.42	(d, 8.1)	C2, C4b, C11a
4a	121.78			
4b	136.92			
5	118.99	8.18	(d, 5.5)	C4a, C10b
6	149.76	8.94	(d, 5.5)	C4b, C5, C7a
7a	146.48			
8	183.31			
9	132.82	6.85	(s)	C7a, C10a, C12
10	152.17			
10a	150.33			
10b	117.84			
11a	145.32			
12	31.72	3.25	(t, 6.4)	C9, C10, C10a, C13
13	39.28	3.79	(dt, 5.9, 6.4)	C10, C12, C15
14	—	6.59	(br)	C13, C15
15	170.43			
16	23.30	2.02	(s)	C15

<sup>a</sup> Proton and carbon data were acquired at 500 and 125 MHz, respectively.

<sup>b</sup> The HMBC experiment was optimized to observe <sup>n</sup>*J*<sub>CH</sub> couplings of 8.5 Hz.

HMBC correlations (C4a-H3, C4b-H4, C4a-H5, and C4b-H6) assigned the intervening quaternary carbons C4a and C4b. The isolated olefinic proton H9 was determined to be a part of the iminoquinone ring and was positioned relative to the methylene side chain via HMBC correlations as indicated in Table 3.3 and Figure 3.4. HMBC correlations between H12 and C10 established the connection between the methylene side chain and the iminoquinone ring.

The spectral data for **35** were virtually identical to those reported for **36**.<sup>121,133</sup> The acetyl side chain by which **35** differed from other cystodytins (e.g., **36**) was evident from the three proton singlet at 2.02 ppm (H16). Both H16 and H13 showed HMBC correlations to the C15 carbonyl group confirming the acetyl side chain. Figure 3.4 summarizes the HMBC correlations relevant in establishing the structure of **35** and assigning the quaternary carbon atoms.

#### Structures of Known Pyridoacridines

The additional pyridoacridines **36**, **37**, **38**, and **23** showed spectroscopic properties matching those reported in the literature.<sup>90,121-123</sup> Pyridoacridine **39**, isolated from a *Diplosoma* sp. ascidian, was previously reported by Charyulu et. al.<sup>124</sup>

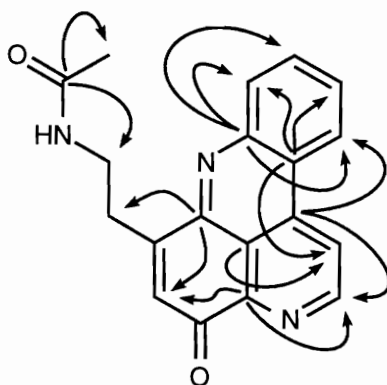


Figure 3.4. HMBC correlations used in assigning the quaternary carbon atoms in cystodytin J.



## DNA Intercalation Studies

An ethidium bromide displacement assay was used to evaluate the relative ability of the pyridoacridines to interact with DNA.<sup>134</sup> Figure 3.5 shows a series of fluorescence emission spectra for ethidium bromide measured in the presence of calf thymus (CT) DNA and various concentrations of **39**. It is apparent that upon increasing the concentration of **39**, there was a decrease in the fluorescence of ethidium bromide due to its displacement from DNA. For example, 69  $\mu\text{M}$  **39** was sufficient to displace nearly all the ethidium bromide (2.5  $\mu\text{M}$ ) from DNA, bringing its fluorescence to a level approaching that of the non-intercalated molecule.

Figure 3.6 and Table 3.4 show the relative ability of the pyridoacridines to intercalate into DNA. The ethidium bromide displacement constants ( $K$ , Table 3.4) are measures of intercalation. Compounds **35** and **39** were the most efficient intercalators and were also the most cytotoxic of the series as shown in Table 3.4. Equally important is that the less active compounds did not intercalate well into DNA. For example, **34** was the poorest intercalator and the least cytotoxic pyridoacridine, followed by **38** which was the second to last in terms of cytotoxicity and intercalative ability.

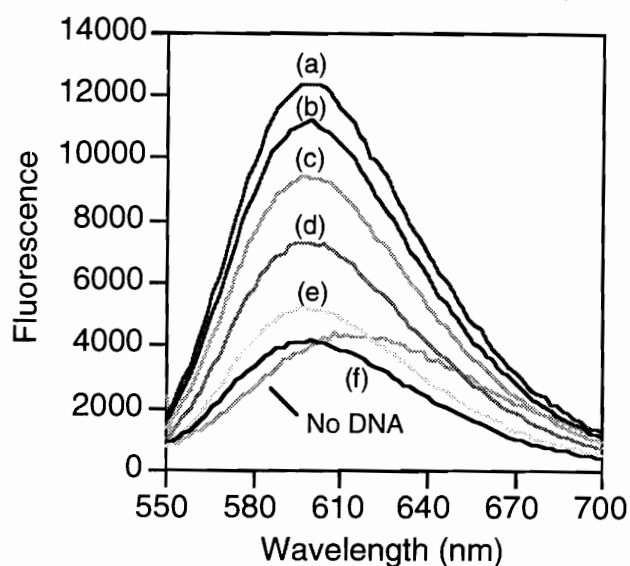


Figure 3.5. Fluorescence spectra of ethidium bromide in PBS solution (2.5  $\mu\text{M}$ ) with 50  $\mu\text{g}$  CT DNA and 0.0 (a), 3.4 (b), 6.8 (c), 13.7 (d), 27.4 (e), and 68.5 (f)  $\mu\text{M}$  diplamine (**39**). Excitation at 530 nm.

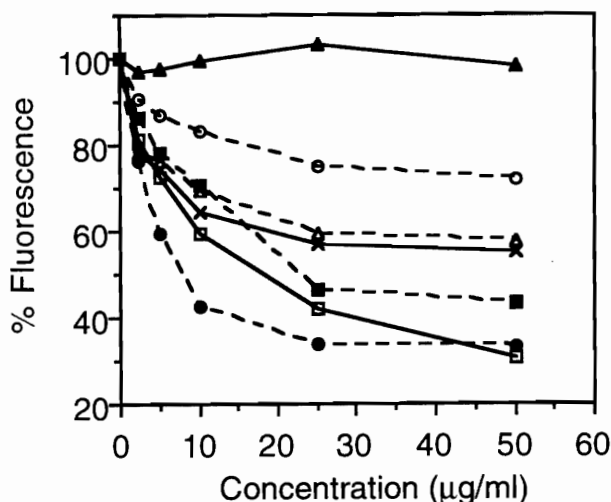


Figure 3.6. Normalized fluorescence for ethidium bromide (1.27  $\mu\text{M}$ ) in PBS solution with calf thymus DNA and increasing concentrations of pyridoacridines **33** (--- $\Delta$ ---), **34** (— $\blacktriangle$ —), **35** (— $\square$ —), **37** (--- $\blacksquare$ ---), **38** (--- $\circ$ ---), **23** (— $\times$ —), and **39** (--- $\bullet$ ---). Excitation at 530 nm, emission at 600 nm. The fluorescence in the presence of DNA and absence of compound represents 100%.

Table 3.4

Cytotoxicity, Differential Toxicity, Topoisomerase Inhibition and Intercalation of the Pyridoacridines Alkaloids and Control Compounds.

Compound	HCT Inhibition $\text{IC}_{50}$ , $\mu\text{M}$	xrs-6 Inhibition $\text{IC}_{50}$ , $\mu\text{M}$	DC ratio <sup>a</sup>	TopoII Inhibition $\text{IC}_{90}$ , <sup>b</sup> $\mu\text{M}$	Intercalation $K$ , <sup>c</sup> $\mu\text{M}$
<b>33</b>	8.3	80.0	1	115	>100
<b>34</b>	16.3	8.1	1	138	>100
<b>35</b>	1.6	135.6	1	8.4	54
<b>37</b>	7.8	88.9	2	127	62
<b>38</b>	13.8	14.9	1	118	>100
<b>23</b>	5.3	ND <sup>d</sup>	ND <sup>d</sup>	ND <sup>d</sup>	>100
<b>39</b>	<1.4	71.2	1	9.2	21
Etoposide	2.5	.14	7	68	ND <sup>d</sup>
m-AMSA	6.3	0.24	4	33	ND <sup>d</sup>
Mitoxantrone	ND <sup>d</sup>	.001	9	1.1	ND <sup>d</sup>

<sup>a</sup> Differential Cytotoxicity (DC) ratio = BR1  $\text{IC}_{50}$  / xrs-6  $\text{IC}_{50}$ .

<sup>b</sup> Concentration at which 90% of monomer-length kDNA production is apparently inhibited.

<sup>c</sup> Concentration of compound required to reduce ethidium bromide fluorescence to 50% of control (see results and discussion).

<sup>d</sup> ND = Not determined.

Eilatin (**23**) is fluorescent and produces an emission peak at 514 nm when irradiated at 520 nm. Figure 3.7 shows the increase in the fluorescence intensity of **23** at the emission maximum upon addition of CT DNA. For example, addition of 50  $\mu\text{g}$  CT DNA caused a 484% increase in the fluorescence of a 2.8  $\mu\text{M}$  solution of **23**. The fluorescence of **23** continued to increase as more DNA was added, similar to the intercalator ethidium bromide.<sup>120</sup> The increase in fluorescence intensity upon the addition of DNA provided additional evidence for intercalative binding.

### Biology

#### HCT Cytotoxicity

The cytotoxicity assay provided a relative measure of the pyridoacridines toxic potencies against HCT cells in vitro. The results in Table 3.4 show that all compounds are cytotoxic to varying degrees. Compounds **35** and **39** are the most potent; both inhibiting HCT replication with  $\text{IC}_{50}$  values of less than 2  $\mu\text{M}$ .

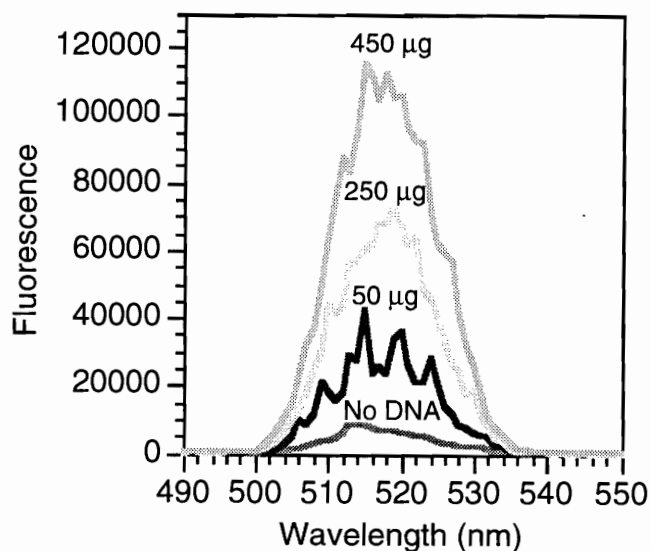


Figure 3.7. Fluorescence spectra of eilatin in PBS solution (2.8  $\mu\text{M}$ ) with 50 (a), 250 (b), and 450 (c)  $\mu\text{g}$  calf thymus DNA. Excitation at 520 nm.

## Biochemical Induction

Eilatin (**23**) was active in the BIA at greater than 2  $\mu\text{g}/\text{disk}$ , suggesting that it was capable of inducing an SOS response in *E. coli* cells.<sup>108</sup> The remaining compounds were inactive in this assay. Compound **23** is a 1,10-phenanthroline derivative and has two sets of nitrogen atoms capable of chelating Ni(II) ions.<sup>90</sup> 1,10-Phenanthrolines with the nitrogen atoms correctly situated for bidentate coordination are excellent ligands for chelating metal ions.<sup>135</sup> 1,10-Phenanthroline metal complexes have been reported to cleave ds-DNA in an oxygen dependent reaction yielding products that are inhibitors of DNA polymerase I.<sup>136</sup> It has been shown that metal complexes of 1,10-phenanthroline bind to DNA by intercalation.<sup>137</sup> It is therefore not surprising that **23** showed activity in the BIA since the compound also intercalates into DNA (Figures 3.6 and 3.7). However, these data suggest that intercalation alone is not sufficient for the induction of SOS response since other pyridoacridines which are inactive in the BIA are better DNA intercalators than **23** (Figure 3.6).

## Differential Cytotoxicity

Enhanced toxicity towards the DNA ds-break repair-deficient CHO xrs-6 cell line versus the repair-competent BR1 line indicates “cleavable complex” mediated cytotoxicity; BR1/xrs-6 IC<sub>50</sub> ratios greater than 3 are considered significant in this assay.<sup>80,81,83</sup> None of the pyridoacridines show significant BR1/xrs-6 differential (Table 3.4), suggesting that no cleavable complex formation has occurred and that the compounds do not cause ds-breaks in DNA.<sup>101,102</sup>

## Mechanistic Studies

### Decatenation Inhibition

The relative ability of the pyridoacridines to inhibit topoII was measured in vitro using the decatenation inhibition assay. Figure 3.8 shows the abilities of etoposide and **39** to effect dose dependent inhibition of topoII-catalyzed kDNA decatenation in vitro. In this

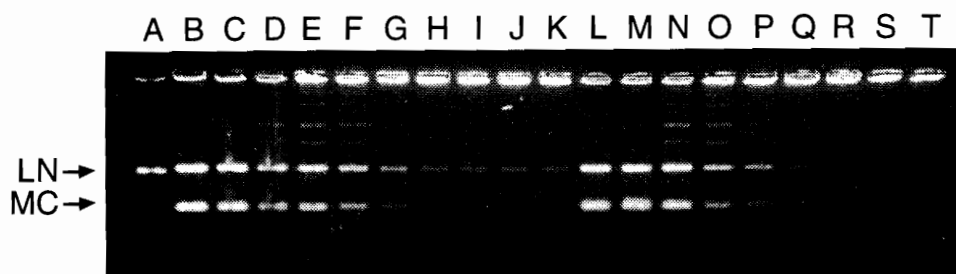


Figure 3.8. Agarose gel showing inhibitory effects of etoposide and diplamine on topoII catalyzed decatenation of kDNA. Lane A, linear monomer-length 2.5 kb DNA marker; Lane B, control reaction (kDNA + topoII); Lanes C-K, 8.5, 28.3, 42.5, 56.6, 84.9, 283.2, 424.7, 566.3, and 849.5  $\mu\text{M}$  etoposide, respectively; Lanes L-T, 1.4, 4.6, 6.8, 9.1, 13.8, 45.8, 68.5, 91.3, and 137.0  $\mu\text{M}$  **39**, respectively. LN, Linear DNA; MC, Monomer Circle DNA.

assay, **39** ( $\text{IC}_{90} = 9.2 \mu\text{M}$ )<sup>138</sup> is a more potent inhibitor of topoII catalytic activity than the classic cleavable complex stabilizing etoposide ( $\text{IC}_{90} = 68 \mu\text{M}$ ). A relative ranking of the pyridoacridines' ability to inhibit topoII catalyzed decatenation is provided in Table 3.4. The table gives the concentrations at which topoII inhibition was apparent (approximately 90% inhibition). Although all compounds are capable of inhibiting decatenation, **35** and **39** are the most potent ( $\text{IC}_{90} = 8.4$  and  $9.2 \mu\text{M}$ , respectively) inhibitors whereas **34** and **38** are among the least potent ( $\text{IC}_{90} = 138$  and  $118 \mu\text{M}$ , respectively). This is consistent with their relative cytotoxicity and intercalative abilities.

The concentrations of compound required for enzyme inhibition are greater than those needed to inhibit HCT cell growth. This may be due to the large amount of DNA required for visualization and quantification, and consequently the large amount of enzyme used for DNA cleavage in this assay.

#### Cleavable Complex Formation

The involvement of cleavable complex formation in cell death was not supported by the results from the BR1/xrs-6 assay. However, the  $\text{K}^+$ -SDS assay was carried out to definitively determine if inhibition of topoII-mediated kDNA decatenation was associated

with cleavable complex formation. Compound **39** produced no detectable protein-DNA complex above 1.4  $\mu\text{M}$ , the concentration at which it caused 50% inhibition of HCT cells. Lower concentrations of **39** were used to exclude the possibility of self inhibition<sup>116</sup> due to disruption of the enzyme-substrate interaction; however, cleavable complex formation was not demonstrated at any level. Although it is not clear exactly how these compounds kill cells, protein-DNA covalent links or lesions resulting from disintegration of “cleavable complexes” are evidently not responsible for cytotoxicity. This and other results suggest that DNA, not the protein-DNA complex, is the target of the pyridoacridines.

#### Pyridoacridines Effect on DNA, RNA, and Protein Synthesis

Assays to determine the effects of compounds **35** and **39** on cellular macromolecule synthesis were performed using 90-95% lethal drug concentrations ( $\text{IC}_{90}$ ). These assays were performed in Prof. Barrows laboratory. Dramatic effects on RNA and DNA synthesis were observed. RNA synthesis fell to approximately 50% of control levels in the first hour and continued to fall to approximately 10% of control levels by 9 h, while DNA synthesis fell from 100% of control levels in the first hour to below 50% by the third hour and to approximately 10% by h 6 and 9 of drug treatment. No effect was observed on protein synthesis during the 9 h exposure period. These effects are similar to those observed for other DNA or topoisomerase-targeting drugs (e.g., actinomycin D, mitoxantrone and camptothecin) and are consistent with effects expected of topoisomerase inhibition.

#### Summary

Based on the observed correlations between HCT cytotoxicity, topoII inhibition, and DNA intercalation, it is hypothesized that the pyridoacridines bring about cell death by inhibiting DNA interactive proteins (e.g., topoII) following intercalation. The studies indicate that the pyridoacridines inhibit proliferation of HCT cells by interfering with DNA synthesis. This interference is likely due to disruption of topoII enzyme function. It is

hypothesized that, by intercalating into DNA, the pyridoacridines disrupt the interaction between topoII and its DNA substrate; consequently, the enzyme cannot carry out its normal functions during replication. The strong correlations between DNA intercalation, topoII inhibition and cytotoxicity, in addition to the ability of these compounds to disrupt DNA synthesis, strongly support this hypothesis.

The hypothesis suggests one possible cytotoxicity mechanism for the pyridoacridine alkaloids and provides a reasonable explanation for our observations and those of others,<sup>85</sup> that these compounds inhibit the enzyme topoII. These findings are consistent with the report that the pyridoacridine alkaloid dercitin (**17**), does not significantly stabilize cleavable complexes.<sup>72</sup> The fact that these compounds showed neither enhanced toxicity towards DNA ds-break repair-deficient CHO cell lines nor produced cleavable complexes, suggests that they inhibit topoII catalytic activity not by producing a cleavable complex, but by binding to DNA itself. Since the pyridoacridines intercalate into DNA with high affinity and may change the topology of the molecule, it is likely that they inhibit other DNA binding enzymes necessary for replication. Therefore, other enzymes such as polymerases or topoI may be unable to bind or function properly due to the presence of intercalator molecules in the DNA.

The relative cytotoxic, intercalative, and topoII inhibitory activities of the pyridoacridines give some indication of the effects of structural variation within this class. Inspection of the pyridoacridine structures reveals that **35** and **39** have only four rings and are iminoquinones. They are the best intercalators, topoII inhibitors and the most potent cytotoxins of the series. The diminished potencies of the other pyridoacridines may result in part from steric effects of the additional ring(s), although the electronic effect of the iminoquinone may also be important. Since intercalation appears to be crucial for cytotoxicity, it is understandable why **34** and **38** are among the least active compounds in all the assays.

Although the topoII-DNA complex is considered the primary target of a number of

DNA intercalators,<sup>112</sup> the results of show that the pyridoacridines do not act by stabilizing cleavable complexes; thus, intercalator induced cytotoxicity involving topoII inhibition does not always involve cleavable complex formation. Therefore, in evaluating cytotoxic compounds that act as topoII poisons, neither inhibition of enzymatic activity, cytotoxic potency, or intercalative ability alone can be taken as suitable criteria for predicting mechanism of action or chemotherapeutic potential.

In view of its activity in the BIA, **23** is one of the more interesting pyridoacridines. Compound **23** intercalates efficiently into DNA as evidenced by its fluorescent properties in the absence and presence of DNA and by its ability to displace ethidium bromide from DNA. (See Figures 3.6 and 3.7.) Compound **23** was also reported to chelate a metal ion;<sup>90</sup> thus, like other phenanthroline compounds, **23** may cleave DNA by producing DNA-destructive hydroxyl radicals following intercalation.<sup>137,139,140</sup> Other pyridoacridines may be less capable of generating hydroxyl radicals due in part to their diminished capacities to chelate metal ions.

It is likely that the pyridoacridines as a class do not act by a single mechanism in causing cell death. By inhibiting topoII, the pyridoacridines can impair DNA synthesis, gene expression, chromosome segregation and ultimately cell proliferation. Evidence that topoII inhibition plays a part in pyridoacridine cytotoxicity has been provided. Despite the fact that many clinically useful anticancer drugs are intercalators, the mechanisms by which many of these compounds act are not well understood. It is known, for example, that not all intercalators give rise to topoII-mediated DNA breaks, despite binding to the same macromolecule ( i.e., DNA). The pyridoacridines, which have a reasonably well-defined mode of action, may be used in conjunction with other compounds, as tools for probing the mechanism of cell death in aberrant eukaryotic cells. With this enhanced understanding, we may be able to design better anticancer compounds.



### Review of Pyridoacridines

The pyridoacridines are among the growing number of DNA intercalating agents that contain a planar electron rich ring system. Some of these compounds, like dercitin (**17**), are tethered to a basic side-chain which may assist with DNA interaction via the phosphate backbone. Dercitin is the only pyridoacridine thus far reported to show in vivo activity (T/C of 170% at 5 mg/kg against P388 leukemia).<sup>73</sup> The structure of dercitin has been revised.<sup>125</sup> The pyridoacridines have been extensively reviewed in a recent publication.<sup>141</sup>

## CHAPTER 4

### THE CHEMISTRY OF THE ASCIDIAN *LISSOCLINUM*

#### *PATELLA*

##### *L. patella* from Singapore

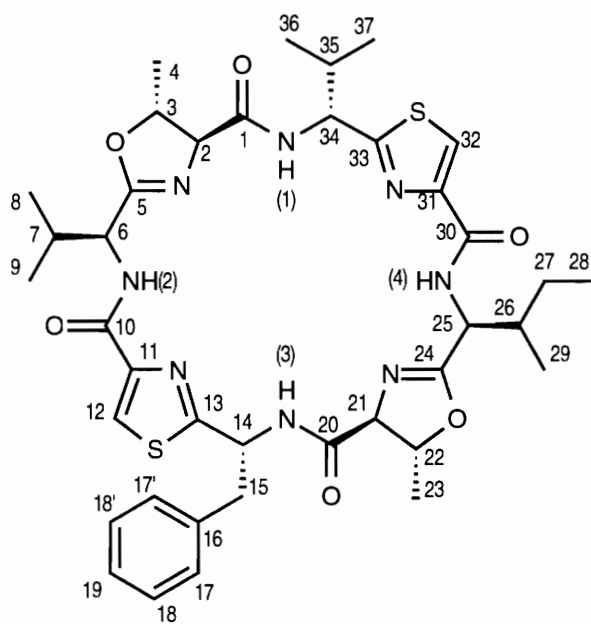
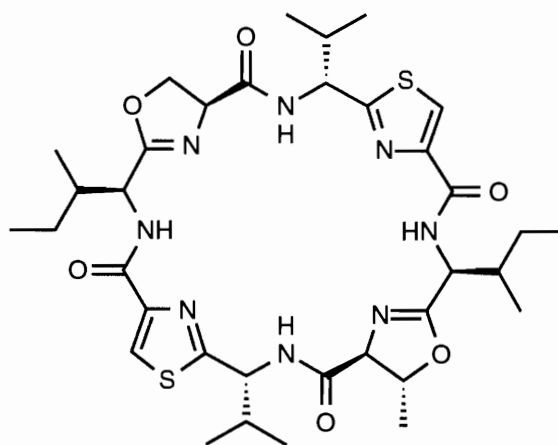
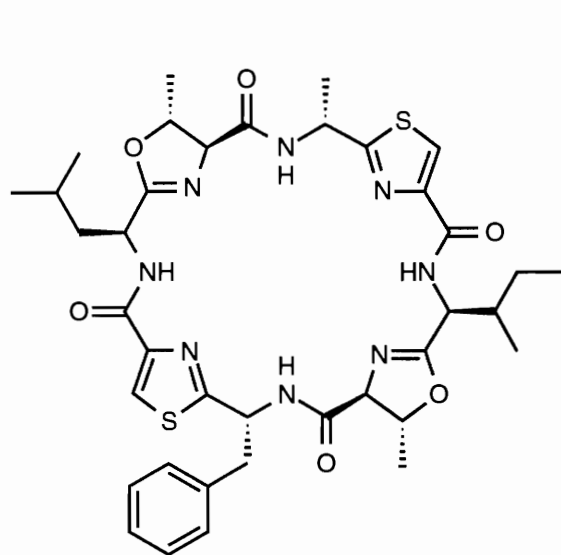
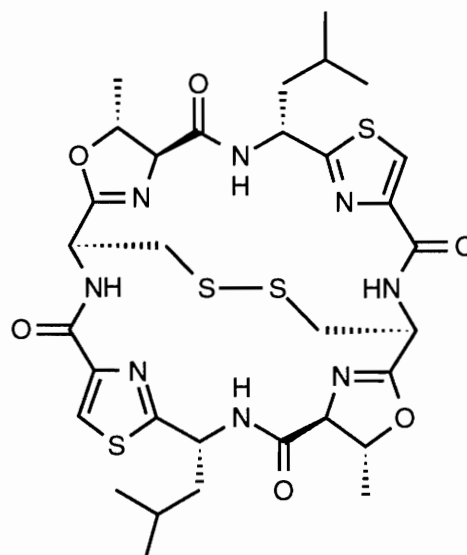
The first part of this chapter describes the isolation and characterization of a new cyclic peptide, patellamide E (**40**), which was isolated from *Lissoclinum patella* (Order: Aplousobranchia, Family: Didemnidae) collected at Pulau Salu, Singapore. Patellamide E is the newest member of a class of cyclic octapeptides possessing oxazoline and thiazole amino acids.<sup>142</sup>

##### Isolation of Patellamide E and Other Peptides

Purification of the CHCl<sub>3</sub> extract of *L. patella* using silica gel flash chromatography followed by silica gel HPLC led to patellamide E (**40**), patellamides A (**41**) and B (**42**),<sup>143,144</sup> and ulithiacyclamide (**43**).<sup>145</sup>

##### Structure Elucidation of Patellamide E

A molecular formula of C<sub>39</sub>H<sub>50</sub>N<sub>8</sub>O<sub>6</sub>S<sub>2</sub> for patellamide E (**40**) was provided by positive ion HR FAB mass spectral analysis. IR bands at 3371, 3326, 1666 and 1537 cm<sup>-1</sup> were indicative of amide NH and carbonyl stretches for peptides. The <sup>1</sup>H and <sup>13</sup>C NMR spectra (Appendix B) of **40** revealed striking similarities to the other patellamides (e.g., patellamide B (**42**)). A 14 mass unit difference between them suggested that **40** was a homolog of **42**. The <sup>13</sup>C NMR spectrum of **40** contained 37 resonances, including two corresponding to the degenerate phenyl carbons C17 & C17' (129.17 ppm) and C18 & C18' (128.55 ppm). This was in agreement with the molecular formula provided by mass

**40****41****42****43**

spectrometry. Table 4.1 contains the NMR assignments for **40**.

PS-DQF-COSY<sup>146</sup> data established a phenylalanine, an isoleucine, two methyl-oxazoline and two valine residues as constituents of **40**. Quaternary carbon atoms resonating at 168.09 (C5) and 168.21 (C24) supported the presence of two methyl-oxazoline rings. Broad proton singlet resonances at 7.46 and 7.52 ppm (H12 and H32,

Table 4.1

NMR<sup>a</sup> Assignments for Patellamide E in CDCl<sub>3</sub>

Atom no.	$\delta$ <sup>13</sup> C	(mult.) <sup>b</sup>	$\delta$ <sup>1</sup> H	(mult., <i>J</i> (Hz))	HMBC <sup>c</sup> correlations
1	172.97	(s)			
2	73.83	(d)	4.29	(d, 4.0)	C1, C5
3	82.21	(d)	4.88	(m)	C1, C5
4	21.52	(q)	1.40	(d, 6.5)	
5	168.09	(s)			
6	54.67	(d)	4.56	(dd, 8.0, 8.0)	C5, C10
7	28.74	(d)	2.17	(m)	C5
8	18.98	(q)	0.87	(d, 6.5)	
9	18.99	(q)	0.92	(d, 6.5)	
10	160.96	(s)			
11	147.77				
12	123.81	(d)	7.46	(bs)	C11, C13
13	170.20				
14	52.11	(d)	5.43	(ddd, 9.5, 9.5, 6.5)	C11, <sup>d</sup> C13, C16, C20
15	41.24	(t)	3.37	(dd, 14.0, 9.5)	C13, C16, C17
			3.20	(dd, 14.0, 6.5)	C13, C16, C17
16	136.18	(s)			
17	129.17	(d)	7.25	(m)	
18	128.55	(d)	7.25	(m)	
19	126.97	(d)	7.19	(m)	C16, C17, C18
20	172.57	(s)			
21	73.54	(d)	4.16	(d, 3.5)	C20, C24
22	82.11	(d)	4.86	(m)	C24
23	21.06	(q)	1.35	(d, 6.5)	
24	168.21	(s)			
25	53.00	(d)	4.66	(dd, 9.0, 8.0)	C24, C30
26	34.30	(d)	2.08	(m)	
27	24.90	(t)	1.46	(m)	
			1.26	(m)	
28	9.30	(q)	0.76	(t, 7.5)	
29	14.99	(q)	0.88	(d, 6.9) <sup>e</sup>	
30	161.37	(s)			
31	148.39	(s)			
32	123.03	(d)	7.52	(bs)	C31, C33
33	170.51	(s)			
34	55.68	(d)	5.14	(dd, 10.5, 4.5)	C1, C31, C33
35	32.23	(d)	2.26	(m)	C33
36	19.95	(q)	1.06	(d, 7.0)	
37	17.06	(q)	1.07	(d, 7.0)	
N1	—		7.20	(d, 10.5) <sup>e</sup>	
N2	—		7.69	(d, 8.0) <sup>e</sup>	
N3	—		7.65	(d, 9.5) <sup>e</sup>	C13, C14, C20
N4	—		7.64	(d, 9.0) <sup>e</sup>	C30

<sup>a</sup> Proton and carbon data were acquired at 500 and 125 MHz, respectively.

<sup>b</sup> From a DEPT experiment.

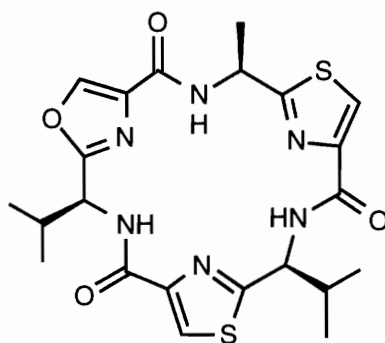
<sup>c</sup> The HMBC experiment was optimized to observe <sup>n</sup>J<sub>CH</sub> couplings of 8.5 Hz.

<sup>d</sup> Weak correlation.

<sup>e</sup> Obtained from a PS-DQF-COSY experiment because of severe overlap in the <sup>1</sup>H spectrum.

respectively) were suggestive of two thiazole rings, which were further supported by carbon resonances at 147.77 (C11), 123.81 (C12), and 170.20 (C13); 148.39 (C31), 123.03 (C32), and 170.51 (C33). The DEPT<sup>147</sup> experiment was used to establish the multiplicities of the carbon resonances while the HMQC<sup>148</sup> experiment permitted assignment of their attached protons. The structural units in Figure 4.1 accounted for all the mass of **40** except that required for four carbonyl groups. The partial structures in Figure 4.1 and the carbonyl groups accounted for all but one degree of unsaturation (the macrocyclic ring) required by the molecular formula.

Assignment of the quaternary carbon resonances using the HMBC<sup>131</sup> experiment resulted in the larger structural units **A** and **B** shown in Figure 4.2. Unfortunately, neither HMBC experiments, optimized for  ${}^nJ_{\text{CH}}$  of 2 to 15 Hz, nor similarly optimized selective INEPT<sup>149</sup> experiments were able to establish the C10-C11 or C30-C31 bonds. This apparently leaves two possible ways of connecting structural units **A** and **B**. However, the upfield chemical shifts of the C10 and C30 amide carbonyl resonances supported conjugation to the thiazole rings and allowed partial structures **A** and **B** to be connected in only one way to yield the structure shown for **40**. Foster et al. have recently shown, using proton  $T_1$  measurements, that the aromatic thiazole protons in the bistratamides (e.g., bistratamide C (**44**)) had longitudinal relaxation times in excess of 5 s and that an HMBC experiment optimized with a sufficiently long recycle time could detect the requisite three-bond correlations.<sup>150</sup>

**44**

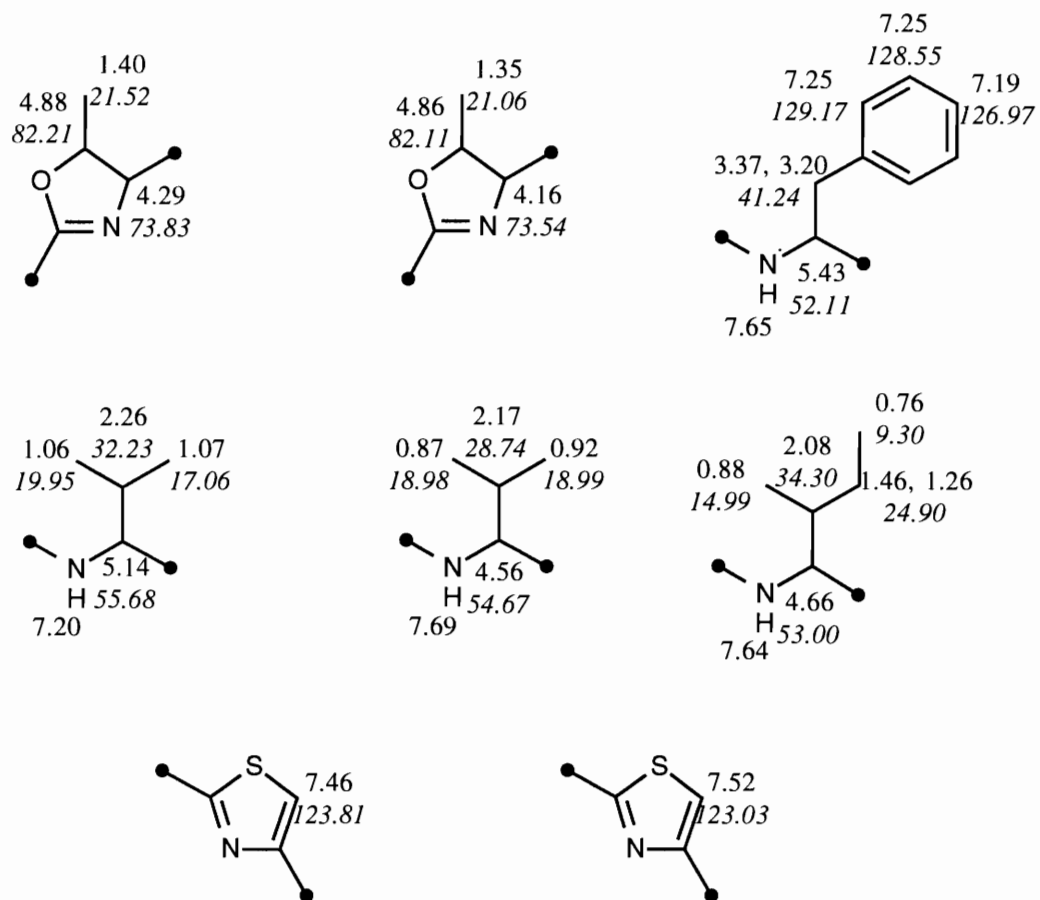


Figure 4.1. Proton and COSY derived amino acid spin networks for patellamide E.

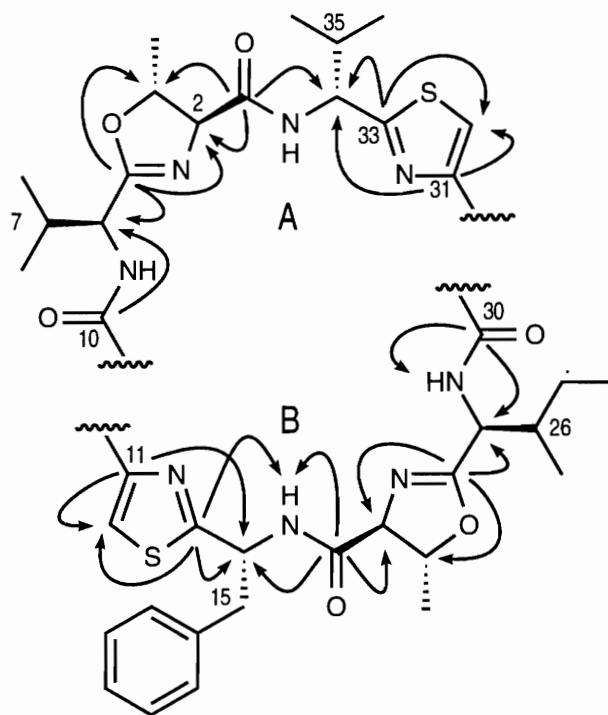


Figure 4.2. Partial structures and HMBC correlations for patellamide E.

#### Absolute Stereochemistry of Patellamide E

The absolute stereochemistry of **40** was established by comparing the amino acids obtained from acid hydrolysis with standard amino acids, both suitably derivatized for HPLC analysis.<sup>151</sup> The presence of L-threonine, L-valine, and L-isoleucine in the hydrolysate of **40** was established by this procedure. The absolute configurations of the thiazole amino acids were determined by a procedure greatly simplified from that previously published.<sup>152</sup> This procedure employed ozone in the destruction of the aromaticity of the thiazole in order to facilitate hydrolysis and prevent racemization. This procedure involves bubbling ozone through a solution of peptide, followed by acid hydrolysis, derivatization, and HPLC analysis. In addition to the previously identified amino acids, D-phenylalanine and D-valine were found in the hydrolysate of ozonized **40**, establishing the presence of (D-phenylalanine)-thiazole and (D-valine)-thiazole.

## Biological Activity of Patellamide E

Patellamide E was weakly cytotoxic (IC<sub>50</sub> 125 µg/mL) against HCT cells in vitro.

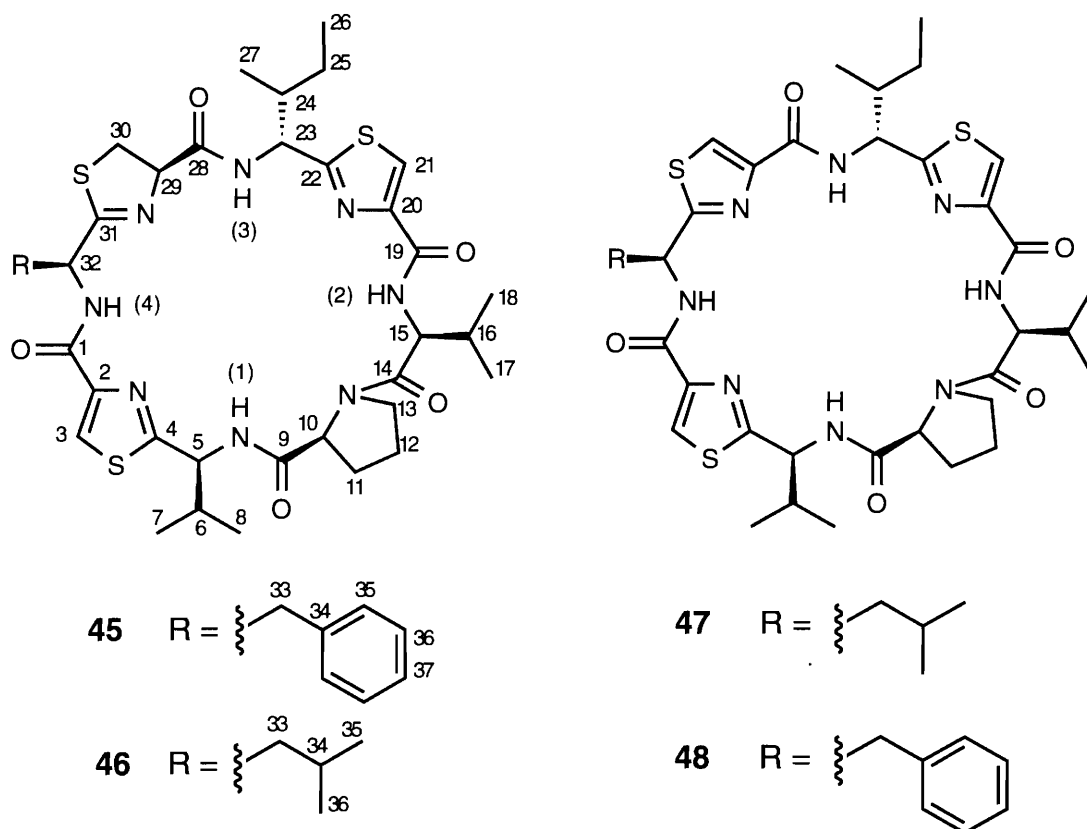
### *L. patella* from the Philippines

Continuing investigations of the chemistry of *L. patella*, have led to the isolation of tawicyclamides A and B (**45-46**), two new cyclic peptides from a Philippine collection of the ascidian. This section describes the structure determination of these peptides by a combination of NMR spectroscopy, oxidation studies, and tandem mass spectrometry (MS/MS). X-ray crystallography confirmed the structure of tawicyclamide B (**46**) and also furnished a three-dimensional conformation. This new family lacks the characteristic oxazoline rings normally present in lissoclinum peptides, but possesses a thiazoline ring and a proline (existing in the *cis* conformation) that facilitates an unusual three-dimensional conformation. A conformational reorganization occurring upon oxidation of the thiazoline ring to a thiazole prompted an investigation of the conformations of tawicyclamide B (**46**) and its oxidized analog, dehydrotawicyclamide B (**47**) by molecular modeling. These studies established the solution conformations of both **46** and **47**, and by analogy, also established the conformations of tawicyclamide A (**45**) and dehydrotawicyclamide A (**48**). The tawicyclamides assume a conformation in which the valine-proline peptide bonds are *cis* while the dehydrotawicyclamides assume an all-*trans* amide bond conformation.

### Isolation of Tawicyclamides A and B

The MeOH extract of *L. patella* was concentrated and partitioned between a series of solvents of increasing polarity. Repeated silica gel flash chromatography of the CHCl<sub>3</sub> soluble fraction, followed by reversed phase HPLC, yielded the new peptides tawicyclamides A (**45**) and B (**46**), and the known peptides patellamides A (**41**), and B<sup>143,144</sup> (**42**), and ulithiacyclamide<sup>145</sup> (**43**).





### Structure Elucidation of Tawicyclamide A

HR FAB mass spectral analysis showed a protonated molecular ion at  $m/z$  807.3135 for tawicyclamide A (**45**). In agreement with the molecular formula  $C_{39}H_{51}N_8O_5S_3$  ( $\Delta$  1.0 mmu), the  $^{13}C$  NMR spectrum of **45** contained 37 resonances, including signals for two degenerate phenyl carbons at 130.18 and 129.08 ppm. A DEPT<sup>147</sup> experiment established the multiplicities of the carbon resonances while an HMQC<sup>148</sup> experiment permitted assignment of the attached protons. Characteristic peptide resonances in the  $^1H$  NMR spectrum of **45** (Appendix B) included doublets at 7.41, 7.59, 8.00, and 8.34 ppm, attributable to amide NH protons, and doublets of doublets between 5.89 and 4.62 ppm corresponding to peptide  $\alpha$  protons. Further evidence establishing **45** as a peptide was provided by major stretches in the IR spectrum at  $3362\text{ cm}^{-1}$  (indicative of secondary amide NH stretching vibrations), amide I bands at  $1666$  and  $1641\text{ cm}^{-1}$  and amide II bands at  $1536$  and  $1514\text{ cm}^{-1}$ . The absence of IR bands corresponding to a carboxylate or

ammonium ion suggested that **45** was cyclic or had end terminal modifications that rendered it nonpolar. The former proved correct when the partial structures of **45**, as discussed below, accounted for all but one degree of unsaturation required by the molecular formula.

A singlet resonance at 7.02 ppm (H3) and a fine doublet at 7.42 ppm (H21;  $J = 0.8$  Hz) in the proton spectrum of **45** implied the presence of two thiazole rings. A PS-DQF-COSY<sup>146</sup> experiment established the presence of phenylalanine, isoleucine, proline and two valine residues. An additional spin network consisting of an  $\alpha$  proton (5.14 ppm; dd,  $J = 9.2, 1.3$  Hz;  $\delta$  13C = 77.94) coupled to geminal diastereotopic  $\beta$  protons (4.03 ppm, dd,  $J = 11.3, 1.3$  Hz and 3.05 ppm, dd,  $J = 11.3, 9.2$  Hz;  $\delta$  13C = 38.47) was attributed to a thiazoline ring, which was confirmed by nickel peroxide oxidation of **45** to form dehydrotawicyclamide A (**48**, Figure 4.3). Figure 4.4 contains the partial structures established from proton and COSY data.

Assignments of the quaternary carbon atoms of **45** were accomplished using the HMBC experiment (Figure 4.5). As evident from Figure 4.5, potential correlations that could establish the C19-C20 and the proline nitrogen-C14 bonds are not observed, thus, substructure **C** remains unconnected to the remainder of the molecule. A very strong ROESY correlation between H10 and H15 of the proline and valine, respectively, suggests that these residues are adjacent. Since tawicyclamide A is cyclic, there is only one way of combining the partial structures in Figure 4.5. Carbon atoms 14 and 19 are assigned based on their chemical shifts. Of the remaining unassigned carbonyl resonances, the upfield one (160.32 ppm) can be assigned to C19, which is adjacent to and in conjugation with the aromatic thiazole ring.

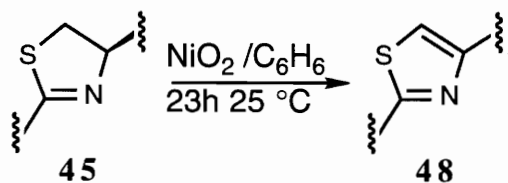


Figure 4.3. Nickel peroxide oxidation of tawicyclamide A.

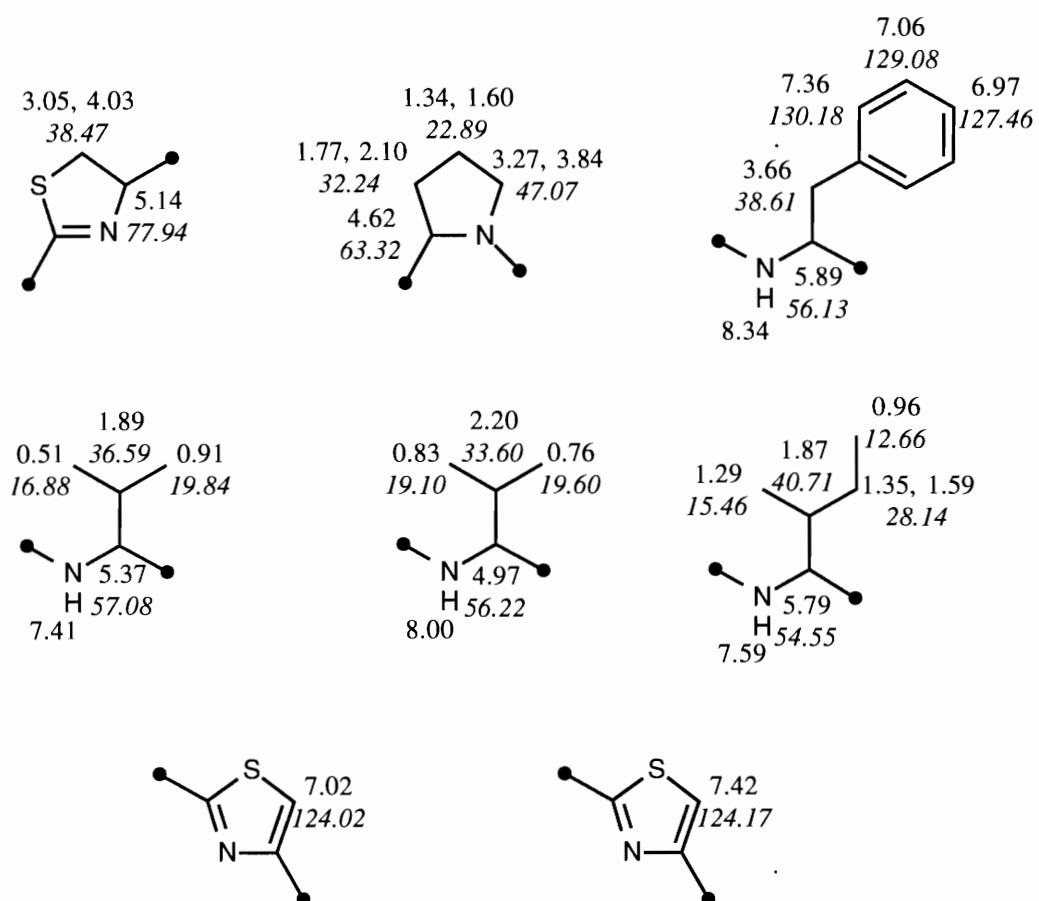


Figure 4.4. Proton and COSY derived amino acid spin networks for tawicyclamide A.

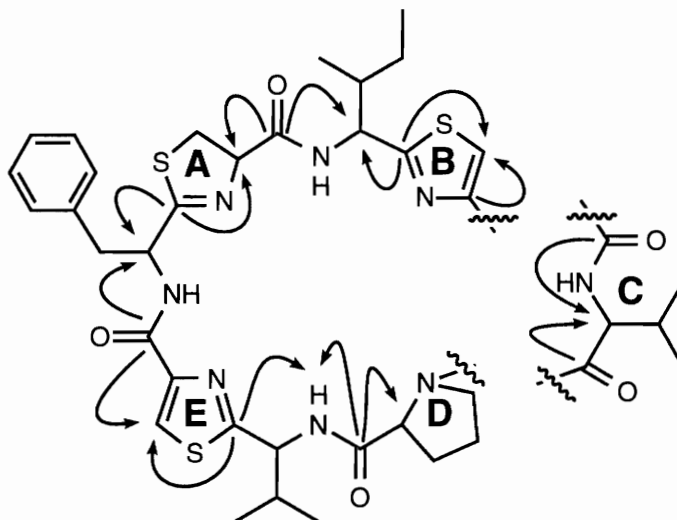


Figure 4.5. HMBC correlations for tawicyclamide A.

Complete NMR assignment of **45** based on COSY, HMQC, COLOC,<sup>153</sup> and HMBC<sup>131</sup> data are provided in Table 4.2. Despite abundant NMR data, the sequence of the amino acid residues in **45** remains not proven by direct spectroscopic evidence. Table 4.3 contains the NMR assignments for the oxidized analog dehydrotawicyclamide A (**48**).

#### Tandem Mass Spectrometry of Tawicyclamide A

With its constituent amino acids and tentative sequence in hand, tandem mass spectrometry (MS/MS) was used as an alternative sequencing method for definitively proving the structure of **45**. Fast atom bombardment (FAB) is a soft ionization technique that is particularly useful for generating protonated molecular ions of non-volatile compounds. In MS/MS the first mass spectrometer is used for mass separation and selection. Gas phase degradation resulting from collisional activation of the mass selected ion and scanning the second mass spectrometer result in a collision induced dissociation (CID) spectrum. The combination of FAB ionization and MS/MS can provide structural and sequence information that can be obtained by examining the CID spectra of structurally significant ions.<sup>154,155</sup>

Table 4.2

NMR<sup>a</sup> Assignments for Tawicyclamide A in C<sub>6</sub>D<sub>6</sub>

Atom no.	$\delta$ <sup>13</sup> C	(mult.) <sup>b</sup>	$\delta$ <sup>1</sup> H	(mult., <i>J</i> (Hz))	HMBC <sup>c</sup> correlations
1	161.57	(s)			
2	148.69	(s)			
3	124.02	(d)	7.02	(s)	C1, C2, C4
4	170.44	(s)			
5	57.08	(d)	5.37	(dd, 6.7, 3.3)	C9
6	36.59	(d)	1.89	(m)	C4
7	16.88	(q)	0.51	(d, 6.8)	
8	19.84	(q)	0.91	(d, 6.8)	
9	171.19	(s)			
10	63.32	(d)	4.62	(dd, 8.5, 2.1)	C9
11	32.24	(t)	1.77	(m)	C9
	—		2.10	(m)	C9
12	22.89	(t)	1.34	(m)	
	—		1.60	(m)	
13	47.07	(t)	3.27	(m)	
	—		3.84	(m)	
14	174.24	(s)			
15	56.22	(d)	4.97	(dd, 10.0, 8.5)	C14, C19
16	33.60	(d)	2.20	(m)	C14
17	19.10	(q)	0.83	(d, 6.8)	
18	19.60	(q)	0.76	(d, 6.8)	
19	160.32	(s)			
20	149.62	(s)			
21	124.17	(d)	7.42	(d, 0.8)	C20, C22
22	172.66	(s)			
23	54.55	(d)	5.79	(dd, 10.2, 2.8)	C20, C21, C22, C28
24	40.71	(d)	1.87	(m)	C22
25	28.14	(t)	1.35	(m)	
	—		1.59	(m)	
26	12.66	(q)	0.96	(t, 7.3)	
27	15.46	(q)	1.29	(d, 6.8)	
28	172.50	(s)			
29	77.94	(d)	5.14	(dd, 9.2, 1.3)	C28, C31
30	38.47	(t)	3.05	(dd, 11.3, 9.2)	C28
	—		4.03	(dd, 11.3, 1.3)	C28, C31
31	177.42	(s)			
32	56.13	(d)	5.89	(dd, 8.0, 8.0)	C1, C31
33	38.61	(t)	3.66	(m)	C31, C34
34	138.18	(s)			
35	130.18	(d)	7.36	(dd, 8.2, 1.3)	C35, C37
36	129.08	(d)	7.06	(ddd, 8.2, 7.5, 1.3)	C34, C36
37	127.46	(d)	6.97	(dt, 7.5, 1.3)	C35
N1	—		7.41	(d, 6.7)	C4, C9
N2	—		8.00	(d, 10.0)	C19
N3	—		7.59	(d, 10.2)	C28
N4	—		8.34	(d, 8.0)	C1

<sup>a</sup> Proton and carbon data were acquired at 500 and 125 MHz, respectively.

<sup>b</sup> From a DEPT experiment.

<sup>c</sup> The HMBC experiment was optimized to observe <sup>n</sup>J<sub>CH</sub> couplings of 8.5 Hz.

Table 4.3

NMR<sup>a</sup> Assignments for Dehydrotawicyclamide A in C<sub>6</sub>D<sub>6</sub>

Atom no.	$\delta$ <sup>13</sup> C	$\delta$ <sup>1</sup> H	(mult., <i>J</i> (Hz))	HMBC <sup>b</sup> correlations
1	160.46			
2	149.95			
3	123.30	7.43	(s)	C2, C4
4	167.90			
5	56.47	5.14	(dd, 7.9, 6.5)	C4, C9
6	34.83	2.19	(m)	C4
7	18.59	0.73	(d, 6.8)	
8	18.74	0.81	(d, 6.8)	
9	169.94			
10	60.78	4.42	(d, 7.9)	C9, C14
11	25.47	0.74	(m)	
	—	2.51	(dd, 12.3, 6.1)	C9
12	24.81	1.14	(m)	
	—	1.57	(m)	
13	47.69	2.93	(m)	
14	173.59			
15	55.69	5.00	(dd, 9.0, 6.7)	C14, C19
16	33.25	2.25	(m)	
17	18.13	1.20	(d, 6.8)	
18	19.99	1.15	(d, 6.8)	
19	160.79			
20	149.64			
21	123.46	7.73	(s)	C20, C22
22	169.35			
23	56.12	5.47	(dd, 7.9, 4.7)	C22, C28
24	41.54	1.97	(m)	
25	25.48	1.51	(m)	
26	11.75	0.62	(t, 7.3)	
27	15.10	0.72	(d, 6.8)	
28	160.48			
29	150.72			
30	124.11	7.77	(s)	C29, C31
31	170.59			
32	53.15	5.64	(ddd, 8.4, 7.4, 7.4)	C1, C31
33	41.37	3.35	(dd, 13.5, 7.4)	C31, C34
	—	3.44	(dd, 13.5, 8.4)	C31, C34
34	137.16			
35	129.34	6.99	(m)	C35, C37
36	128.69	6.93	(m)	C34, C36
37	127.03	6.90	(m)	C35
N1	—	8.55	(d, 7.9)	C4, C9
N2	—	8.70	(d, 9.0)	C14, C19
N3	—	8.86	(d, 7.9)	C22, C28
N4	—	8.26	(d, 7.4)	C1, C32, C33

<sup>a</sup> Proton and carbon data were acquired at 500 and 125 MHz, respectively.

<sup>b</sup> The HMBC experiment was optimized to observe <sup>n</sup>J<sub>CH</sub> couplings of 8.5 Hz.

The unambiguous structure of tawicyclamide A was established by interpreting the CID spectra of its protonated molecular ion and several fragment ions resulting from unimolecular dissociations. The CID spectrum of the protonated molecular ion of **45** ( $m/z$  807) was dominated by ions resulting from the fragmentation of the linear acylium ion depicted in Figure 4.6. This acylium ion resulted from protonation at the proline nitrogen followed by scission of the protonated N-acyl bond, and its fragmentation was the outcome of successive cleavages at the C-terminal. The more basic nature of the prolyl nitrogen –relative to the other amide nitrogen atoms– directed protonation, yielding a much simplified fragmentation pattern. The major fragmentation of the  $(M+H)^+$  ion of **45** involved loss of C-terminal fragments to produce  $m/z$  779, 708, 529, 512, 484, 399, and 297 ions (Figures 4.6, 4.7, and 4.8). Subsequent fragmentation of these ions results in the additional peaks in the CID spectrum.

Another dominant set of progeny ions can be seen in the CID spectra of both the  $m/z$  807 and 779 ions (Figures 4.7, 4.8, and Appendix C). These progeny ions result from decarbonylation of the  $m/z$  807 acylium ion to produce the  $m/z$  779 immonium ion, which ultimately loses the N-terminal proline residue to produce the  $m/z$  682 ion. Collision induced fragmentation of the  $m/z$  682 ion accounts for the progeny ions of this second series (Figure 4.9). Appendix C contains the CID spectra and structures of the  $m/z$  779, 611, 557, 529, 484, 399, 297, 285, 251, 223, 188, and 180 ions of **45**. Tandem mass spectral results are fully consistent with structure **45**.

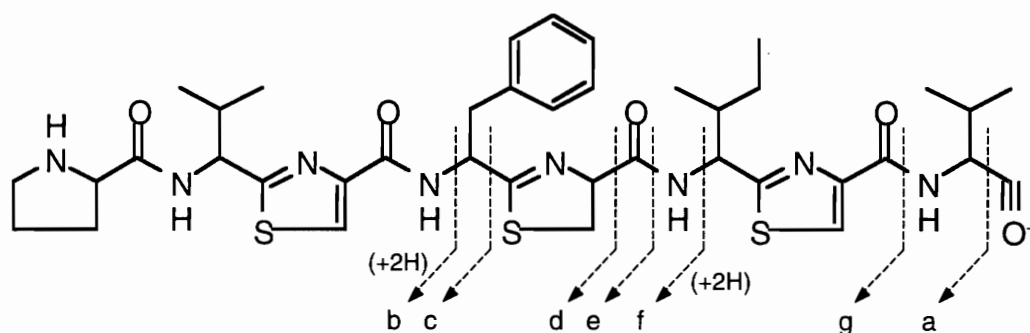


Figure 4.6. Linear acylium ion of tawicyclamide A resulting from scission of the proline N-CO bond.

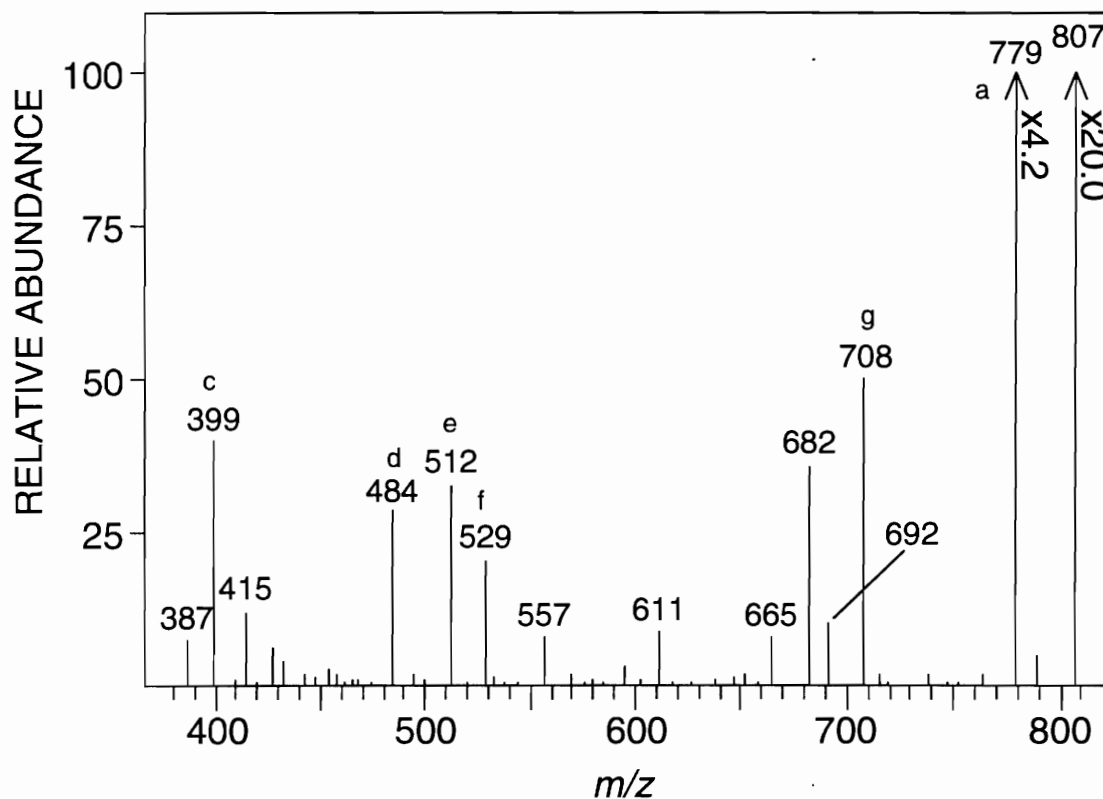


Figure 4.7. High mass region ( $m/z$  825-370) from the CID spectrum of the  $(M+H)^+$  ion of tawicyclamide A,  $m/z$  807. Letters correspond to the fragmentation depicted in Figure 4.6.



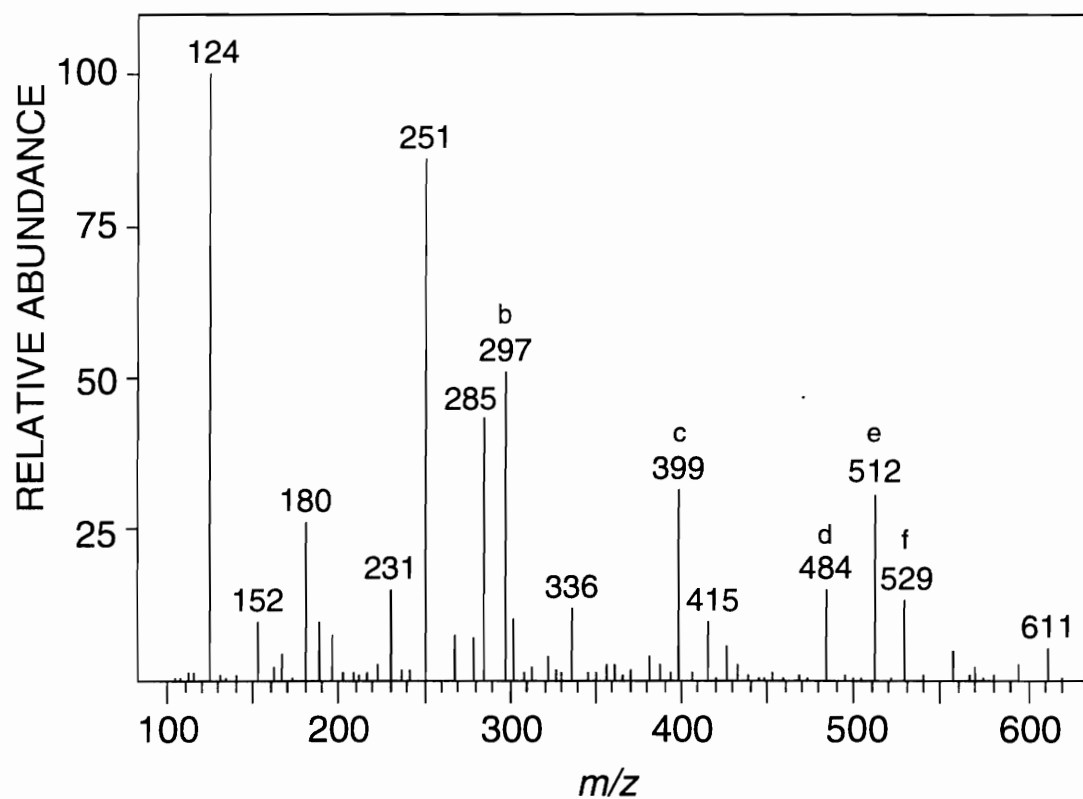


Figure 4.8. Low mass region ( $m/z$  625-80) from the CID spectrum of the  $(M+H)^+$  ion of tawicyclamide A,  $m/z$  807. Letters correspond to the fragmentation depicted in Figure 4.6.

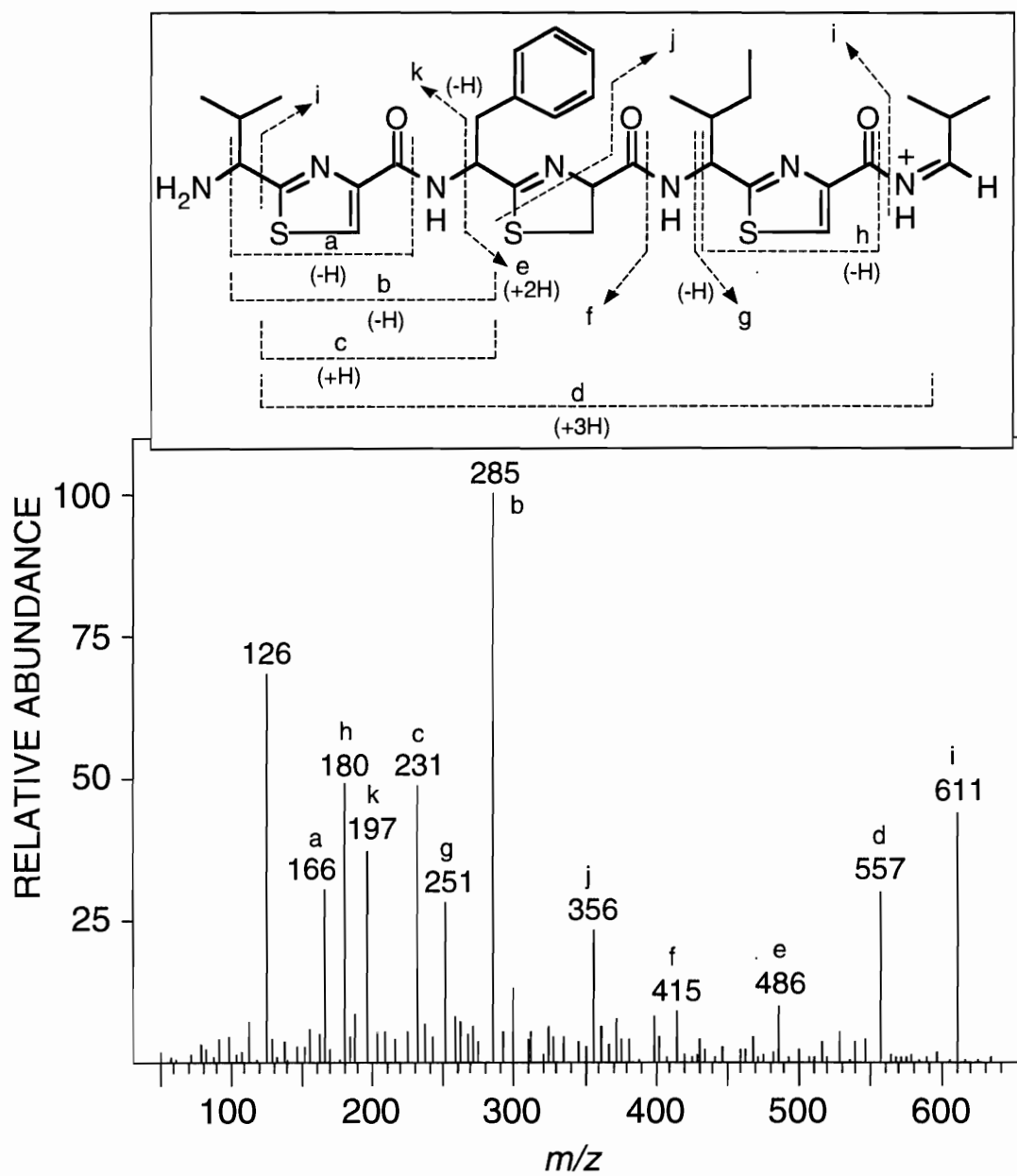


Figure 4.9. CID spectrum and structure of the  $m/z$  682 ion of tawicyclamide A.

Similar MS/MS analysis of the oxidized peptide, **48**, supported its proposed structure. The CID spectrum of  $m/z$  805, its protonated molecular ion, showed a fragmentation pattern virtually identical to that of **45** but with many fragments differing by two mass units.

#### Absolute Stereochemistry of Tawicyclamide A

The absolute stereochemistry of **45** was determined by comparing the 1-fluoro-2,4-dinitrophenyl-5-L-alanineamide (FDAA) derivatized amino acids from the acid hydrolysate of the peptide with similarly derivatized standard amino acids by HPLC according to the method of Marfey.<sup>151</sup> This procedure established L-proline, L-valine and L-phenylalanine as constituents of **45**. The absolute configurations of the thiazole amino acids were determined<sup>142,152</sup> to be (D-isoleucine)-thiazole and (L-valine)-thiazole.

#### Structure Elucidation of Tawicyclamide B

HR FAB MS provided an  $(M+H)^+$  at  $m/z$  773.3345 for tawicyclamide B (**46**), consistent with the molecular formula  $C_{36}H_{53}N_8O_5S_3$  ( $\Delta$  4.4 mmu). The  $^{13}C$  spectrum of **46** showed 36 unique resonances in agreement with this formula. Compound **46** showed remarkable spectral similarities to **45**; the most significant differences were the absence of phenylalanine resonances and the presence of two new methyl resonances (0.98 and 22.99; and 0.88 and 23.06 ppm in the  $^1H$  and  $^{13}C$  spectra, respectively (Appendix B)). Tables 4.4 and 4.5 contain the NMR assignments for the parent peptide, **46** and its oxidized analog, **47**, respectively.

These data, coupled with a 34 mass unit decrease in the molecular weight, allowed the conclusion that **46** differed from **45** by replacement of phenylalanine in **45** with leucine to form **46**. COSY data supported a leucine spin network with long range coupling to the thiazoline ring in **46** (Figure 4.10). This thiazoline ring was also confirmed by oxidation to a thiazole to give dehydrotawicyclamide B (**47**).

Table 4.4

NMR<sup>a</sup> Assignments for Tawicyclamide B in C<sub>6</sub>D<sub>6</sub>

Atom no.	$\delta$ <sup>13</sup> C	(mult.) <sup>b</sup>	$\delta$ <sup>1</sup> H	(mult., <i>J</i> (Hz))	HMBC <sup>c</sup> correlations
1	161.66	(s)			
2	149.01	(s)			
3	124.07	(d)	7.12	(s)	C1, C2, C4
4	170.68	(s)			
5	57.34	(d)	5.38	(dd, 6.5, 3.0)	C4
6	36.53	(d)	1.94	(m)	
7	17.05	(q)	0.54	(d, 6.5)	
8	19.84	(q)	0.91	(d, 6.5)	
9	171.29	(s)			
10	63.23	(d)	4.57	(dd, 8.5, 1.5)	C9
11	32.21	(t)	1.72	(m)	C9
	—		2.06	(m)	
12	22.80	(t)	1.30	(m)	
	—		1.58	(m)	
13	46.83	(t)	3.22	(m)	
	—		3.79	(m)	
14	174.06	(s)			
15	56.14	(d)	4.95	(dd, 10.0, 8.0)	C14, C19
16	33.60	(d)	2.12	(m)	C14
17	19.02	(q)	0.80	(d, 6.5)	
18	19.57	(q)	0.72	(d, 6.5)	
19	160.31	(s)			
20	149.69	(s)			
21	124.13	(d)	7.44	(s)	C19, C20, C22
22	172.73	(s)			
23	54.59	(d)	5.83	(dd, 10.5, 2.5)	C20, C22
24	40.82	(d)	1.90	(m)	C22
25	28.16	(t)	1.39	(m)	
	—		1.65	(m)	
26	12.67	(q)	1.00	(t, 7.3)	
27	15.48	(q)	1.32	(d, 7.0)	
28	172.61	(s)			
29	78.02	(d)	5.28	(dd, 9.3, 1.3)	C28, C31
30	38.39	(t)	3.12	(dd, 11.3, 9.3)	C28
	—		4.04	(dd, 11.3, 1.3)	C28, C29, C31
31	178.31	(s)			
32	53.20	(d)	5.73	(dd, 8.0, 8.0)	C1, C31
33	41.22	(t)	2.25	(m)	C31
34	25.87	(d)	1.83	(m)	
35	22.99	(q)	0.98	(d, 6.5)	
36	23.06	(q)	0.88	(d, 6.5)	
N1	—		7.43	(d, 6.5)	C4
N2	—		7.96	(d, 10.0)	C15, C19
N3	—		7.64	(d, 10.5)	C21, C22, C28
N4	—		8.26	(d, 8.0)	C1, C32, C33

<sup>a</sup> Proton and carbon data were acquired at 500 and 125 MHz, respectively.

<sup>b</sup> From a DEPT experiment.

<sup>c</sup> The HMBC experiment was optimized to observe <sup>1</sup>J<sub>CH</sub> couplings of 10.0 Hz.

Table 4.5

NMR<sup>a</sup> Assignments for Dehydrotawicyclamide B in C<sub>6</sub>D<sub>6</sub>

Atom no.	$\delta$ <sup>13</sup> C	$\delta$ <sup>1</sup> H	(mult., <i>J</i> (Hz))	HMBC <sup>b</sup> correlations
1	160.45			
2	150.20			
3	123.26	7.49	(s)	C2, C4
4	167.96			
5	56.45	5.15	(dd, 7.9, 6.6)	C4, C9
6	34.94	2.16	(m)	C4
7	18.52	0.71	(d, 6.8)	
8	18.73	0.79	(d, 6.8)	
9	170.05			
10	60.74	4.44	(d, 7.9)	C9, C14
11	25.49	0.72	(m)	
	—	2.51	(dd, 12.2, 6.4)	C9
12	24.77	1.18	(m)	
	—	1.53	(m)	
13	47.58	2.91	(m)	
14	173.36			
15	55.55	5.03	(dd, 8.8, 6.2)	C14, C19
16	33.15	2.25	(m)	C14
17	18.35	1.31	(d, 6.8)	
18	20.01	1.22	(d, 6.8)	
19	160.83			
20	149.52			
21	123.39	7.71	(s)	C20, C22
22	169.16			
23	56.20	5.39	(dd, 7.7, 4.6)	C22, C28
24	41.40	1.96	(m)	
25	25.35	1.52	(m)	
26	11.75	0.60	(t, 6.8)	
27	15.13	0.70	(d, 6.5)	
28	160.51			
29	150.97			
30	123.68	7.85	(s)	C28, C29, C31
31	171.16			
32	49.60	5.54	(ddd, 8.4, 7.4, 7.4)	C1, C31
33	43.93	1.95	(m)	C31
	—	2.04	(m)	C31
34	25.28	1.51	(m)	
35	22.08	0.74	(d, 6.6)	
36	22.35	0.69	(d, 6.6)	
N1	—	8.46	(d, 7.9)	C4, C9
N2	—	8.67	(d, 8.8)	C14, C19
N3	—	8.85	(d, 7.7)	C22, C28
N4	—	8.05	(d, 7.4)	C1, C32

<sup>a</sup> Proton and carbon data were acquired at 500 and 125 MHz, respectively.

<sup>b</sup> The HMBC experiment was optimized to observe <sup>n</sup>J<sub>CH</sub> couplings of 8.5 Hz.

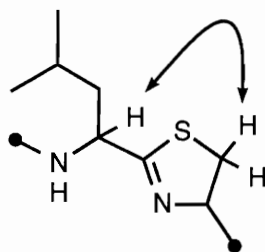


Figure 4.10. Partial structure of tawicyclamide B showing five bond correlation between leucine and thiazoline.

### Absolute Stereochemistry of Tawicyclamide B

HPLC analysis of the FDAA derivatized hydrolysate of **46** revealed the presence of L-proline, L-valine and L-leucine with a significant amount of D-leucine that resulted from partial racemization of the L-leucine from (L-leucine)-thiazoline. The L/D-leucine ratio was 1.38. The 16% ee of the L isomer did, however, support its presence in the natural product; and whereas partial racemization of L-leucine from (L-leucine)-thiazoline occurred upon acid hydrolysis of **46**, analysis of the hydrolysate of ozonized **46** revealed only L-leucine. A similar trend was observed for **45**.

### X-Ray Structure of Tawicyclamide B

Single crystal X-ray analysis was carried out on tawicyclamide B (**46**) in the laboratory of Prof. Jon Clardy. Since only the relative stereochemistry could be determined in the X-ray experiment, the absolute configuration shown in Figure 4.11 was set by the L-proline, L-valine, and L-leucine residues. The X-ray analysis confirmed the spectroscopically determined structure and also revealed the three-dimensional structure. The thiazole rings are essentially parallel and are separated by only 3.7 Å, a typical aromatic stacking distance. The resulting conformation has the hydrophobic side chains pointing away from the internal cavity; the isopropyl group of one valine points up, while the other valyl and leucyl side chains point down. This conformation also has a *cis*-valine-proline peptide bond. A weak intramolecular hydrogen bond from NH4 to O3 of 2.15 Å (148°) suggests that hydrogen bonding may also play a role in stabilizing the solid state conformation of **46**.

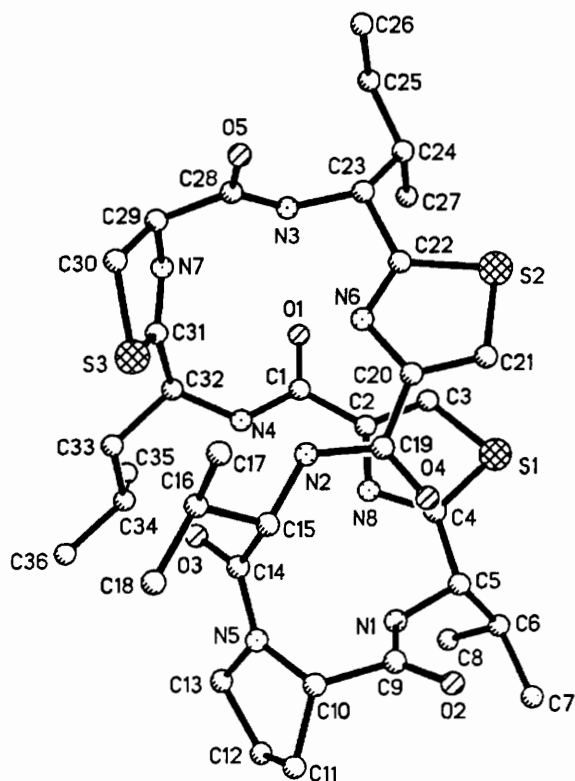


Figure 4.11. X-ray model of tawicyclamide B.

#### Molecular Modeling Studies on the Tawicyclamides

Nickel peroxide oxidation of the tawicyclamides appeared to result in conformational changes in remote parts of the molecules. For example, several pieces of NMR data suggested that, in  $C_6D_6$  solution, **47** adopted a drastically different conformation than its parent peptide, **46**. The dissimilarity between the ROESY<sup>129,130,156</sup> and  $^{13}C$  NMR data of these two peptides, especially data associated with the proline residue, indicated a significant change in the chemical environment of the atoms. These changes suggested isomerization of the valine-proline amide bond from *cis* to *trans* upon oxidation of the thiazoline to a thiazole. These observations prompted the investigation of the conformations of **46** and **47** by molecular modeling.

### Tawicyclamide B Molecular Modeling Studies

Compound **46** was modeled starting from the X-ray coordinates using a minimization-molecular dynamics-minimization (min-MD-min) procedure.<sup>157-159</sup> Initial energy minimization using the ABNR (Adopted Basis-set Newton-Raphson) technique was run to eliminate unfavorable constraints brought about by crystal packing forces and to locate the lowest energy conformer near the starting geometry. A MD simulation at 300 K was run using this low energy conformer. In order to evaluate the conformational space available to the molecule under experimental conditions, the effect of solvent was approximated by a constant dielectric ( $\epsilon$  2.284 for benzene @ 20 °C).

Minimization of several dynamics datasets resulted in convergence to an average structure practically identical to the starting low energy conformer and the crystal structure. Figure 4.12 shows the optimal conformation for **46**, which has a *cis*-valine-proline amide bond (C15-C14-N5-C10 dihedral =  $-10.3^\circ$ ), and an intramolecular hydrogen bond from NH4 to O3 of 2.05 Å ( $145^\circ$ ).

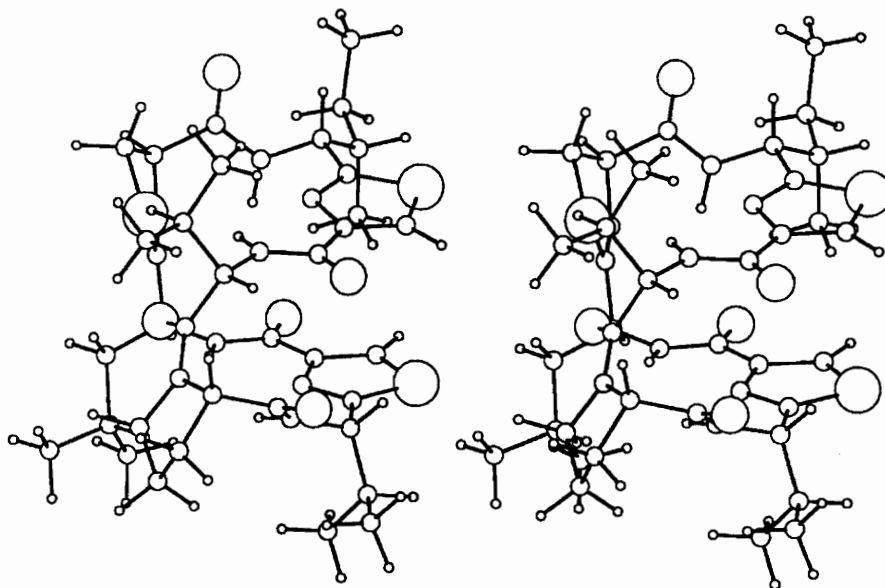


Figure 4.12. Stereo drawing of the solution structure of tawicyclamide B.



The stability of this conformation of **46** was illustrated by the fact that both stacking interaction and hydrogen bonding persisted throughout the min-MD-min procedure. Furthermore, proline allowed for the possibility of *cis-trans* isomerism, yet only one conformer appeared to be present in C<sub>6</sub>D<sub>6</sub> solution—as evidenced by a single set of NMR resonances. The activation energy barrier to rotation about the valine-proline amide bond was determined to be 14.9 kcal/mol, a value comparable to those reported for X-valine (X = any amino acid) rotation barriers.<sup>160</sup>

The solution structure of **46**, obtained from modeling studies, was in excellent agreement with NMR data. For example, a distance of 2.2 Å between H10 and H15 in this model was consistent with the very strong ROESY crosspeak observed between these two protons (Figure 4.13). This key nOe also implied a *cis* orientation about the valine-proline amide bond.

Figure 4.14 provides additional evidence for the proposed solution conformation of **46**. The figure shows that a strong nOe exists between one thiazole aromatic proton (H3) and the  $\gamma$ -methyl group of isoleucine (H27) which, in the model, are separated by 2.5 Å at closest approach. The relative downfield position of H27 is due primarily to anisotropic deshielding by the thiazole ring and is fully consistent with this model. Further evidence supporting the proposed solution conformer of **46** is provided by an nOe between one leucine  $\delta$  methyl group (H35) and the proline  $\delta$  protons (H13) which approach each other to within 2.4 Å.

A 10 ps MD simulation at 1000 K, carried out to escape local minimum energy wells, allowed for sampling of a larger conformational space and generated a reasonable number of structures for subsequent minimization. Following minimizations, convergence to an average structure similar to the starting conformer and to the crystal structure was again observed. The side chains were somewhat more flexible, showing larger rms deviations from the average structure, than the main chain atoms. The average energy of these minimized conformers was, however, 3.5 kcal/mole higher than the starting low energy

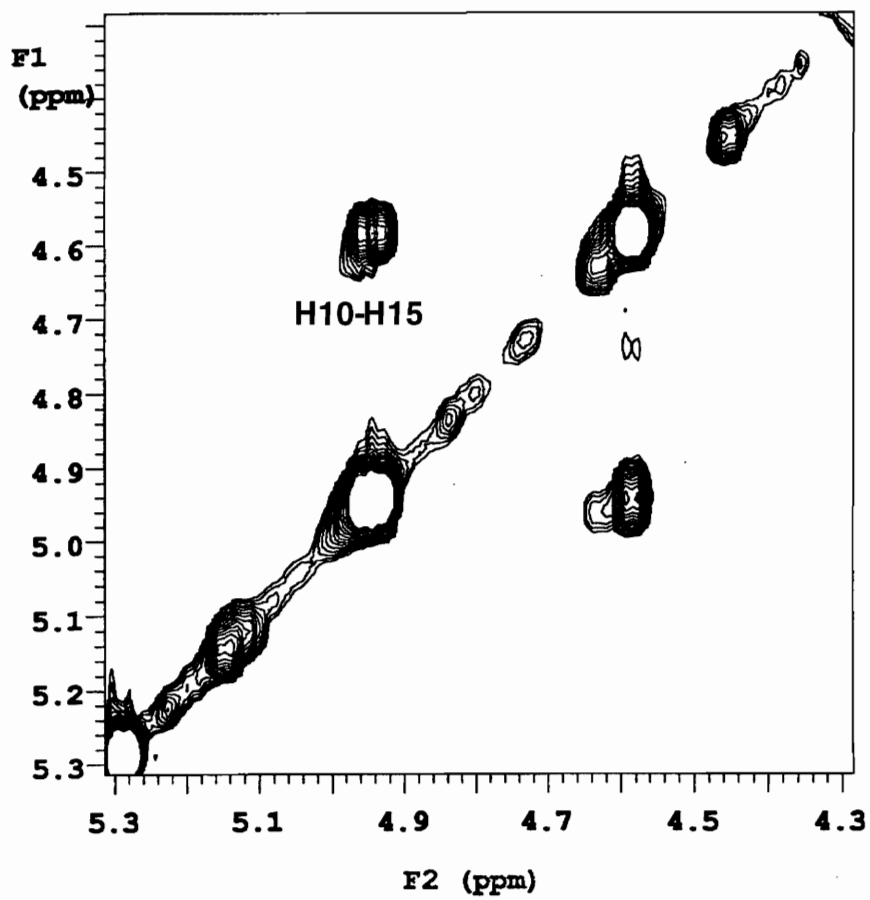


Figure 4.13. Region of a 300 ms ROESY spectrum of tawicyclamide B showing the H10-H15 crosspeak.

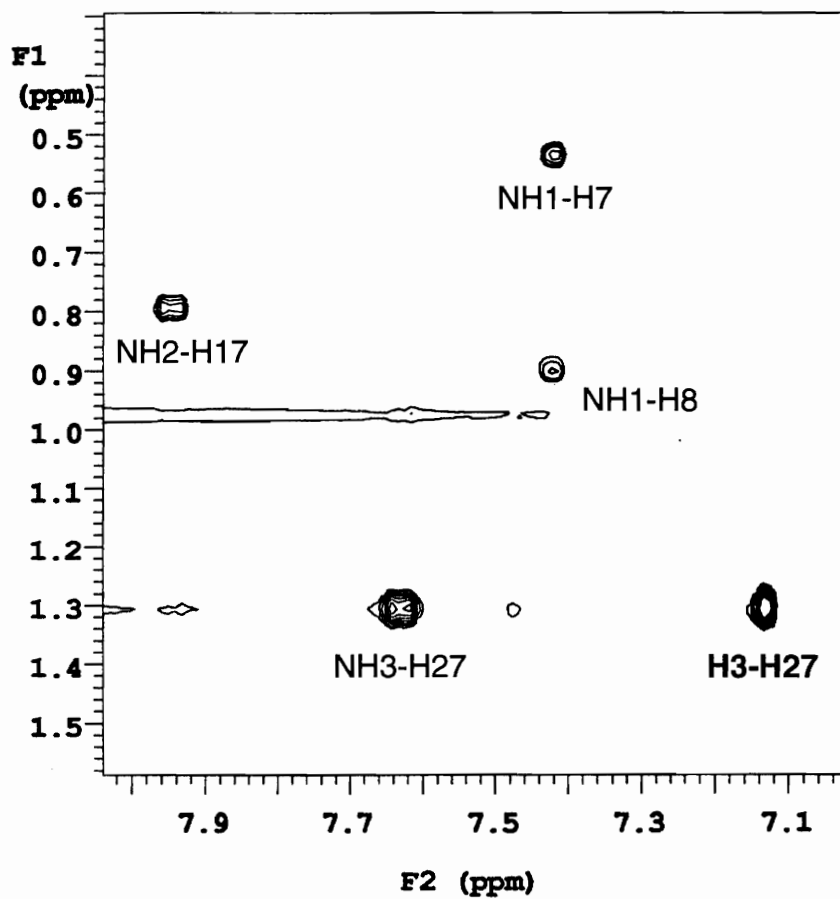


Figure 4.14. Region of a 300 ms ROESY spectrum of tawicyclamide B showing the H3-H27 crosspeak.

conformer as a result of large deviations of the amino acid side chains.

### Dehydrotawicyclamide B Molecular Modeling Studies

The starting model for **47** was taken from the x-ray structure of **46** by removal of two hydrogen atoms and explicit aromatization of the thiazoline ring. Modeling was again carried out using a constant dielectric corresponding to benzene. Energy minimizations were run to locate the lowest conformer near the starting geometry. This structure, not surprisingly, retained a *cis*-valine-proline amide bond after minimization with the ABNR technique. The molecule was first heated to 1000 K for 1.0 ps, allowed to equilibrate at this temperature for 1.0 ps, and finally simulated at 1000 K for 10 ps. Following minimizations of select structures throughout the trajectory, two populations of conformers were obtained: one was similar to the starting *cis* structure and the other was dissimilar, having a *trans*-valine-proline amide bonds. Interestingly, convergence to the *trans* structures occurred toward the end of the 10 ps simulation. Although this *trans* isomer appeared to fit the NMR data, its energy was higher, by 0.1 kcal/mole, than the *cis* isomer.

Since the calculations failed to give results energetically consistent with experimental data, another approach to find a starting conformation was taken. The valine-proline amide bond was constrained to 180° and subjected to an ABNR-MD-ABNR protocol. The dihedral constraint was removed after the first series of minimizations and the MD simulations were run to let the whole molecule relax. The molecule was heated to 300 K for 0.3 ps, equilibrated for 0.3 ps, and finally simulated at 300K for 3 ps. After minimization, the resulting structure contained the *trans* valine-proline amide bond and was very similar to that obtained from dynamics simulation starting from the *cis* dehydrotawicyclamide B conformer. Compared to the *cis*, this *trans* conformer of **47** was more stable by 0.9 kcal/mole. This result suggests that the final model obtained from the modeling protocol is sensitive to the starting geometry.

The lowest energy *trans* conformer of **47** is shown in Figure 4.15. The model shows that in **47**, the all *trans* peptide backbone forms a rectangle, with the three thiazole

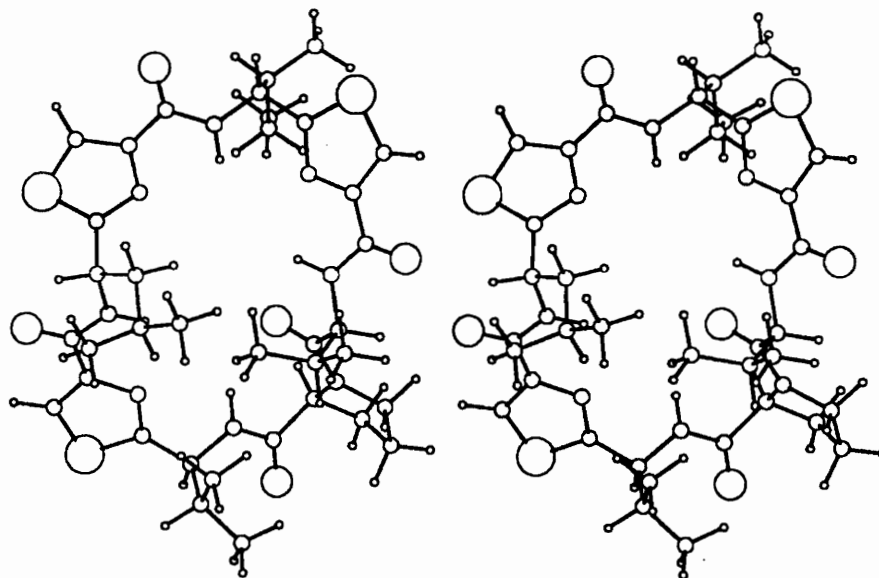
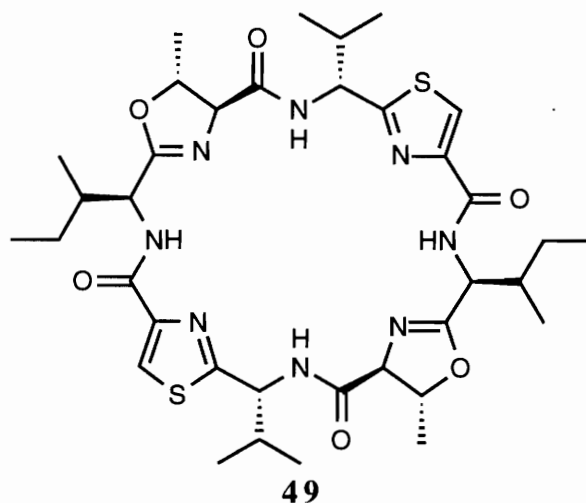


Figure 4.15. Stereo drawing of the solution structure of dehydrotawicyclamide B.

rings and the proline defining its corners. This shape is similar to that for ascidiacyclamide (49), although somewhat distorted from the “saddle” shape described.<sup>161-163</sup> The isoleucine side chain protrudes below the plane of the macrocyclic ring while the leucine and both valine side chains extend above the ring. An interesting feature of this conformer is that all the NH bonds point toward the center of the ring, away from the hydrophobic environment of the solvent.



The stacking of the thiazole rings and the stabilizing hydrogen bonding present in the parent peptide, **46** are not present in the dehydro isomer, **47**. The structure obtained from modeling studies agrees quite well with NMR data. For example, a strong ROESY crosspeak between both  $\delta$  proline protons (H13) and the  $\alpha$  valine proton (H15), supports this *trans* conformer (Figure 4.16). In the modeled structure, these protons are separated by 2.2 Å and 2.5 Å respectively. The model also shows that H10 and NH1 approach each other close enough (2.8 Å) to lead to the strong crosspeak observed in the ROESY spectrum (Figure 4.17). The absence of a crosspeak between H10 and H15 in the ROESY spectrum of **47** further supports the proposed *trans* conformer in which these hydrogen atoms are separated by 4.4 Å. These two hydrogen atoms were 2.2 Å apart in **46** and gave rise to a strong nOe as discussed earlier (see Figure 4.13).

Interestingly, upon changing the thiazoline ring to a thiazole, the resulting aromatization causes the adjacent carbonyl to come into resonance with the aromatic ring and become coplanar with the ring. This undoubtedly contributes to the drastic conformational changes observed upon oxidation.

Added proof of the proposed conformational changes come from the chemical shift differences between the proline  $\beta$  and  $\gamma$  carbons ( $\Delta\delta_{\beta\gamma}$ ), which supported the *cis* valine-proline amide bond configuration for the tawicyclamides and the *trans* configuration for the dehydrotawicyclamides. Siemion et al. had shown that for X-Pro (X = any amino acid), there was a linear dependence of the difference in the chemical shifts of the  $\beta$  and  $\gamma$  carbons of proline ( $\Delta\delta_{\beta\gamma}$ ) with dihedral angle  $\theta = (\psi - 60^\circ)$  according to the equation;  $\Delta\delta_{\beta\gamma} = 0.081|\theta| + 2.47$  for a *cis* orientation about the X-Pro amide bond, or  $\Delta\delta_{\beta\gamma} = 0.036|\theta| + 0.73$  for a *trans* orientation.<sup>164</sup> The observed  $\Delta\delta_{\beta\gamma}$  value of 9.5 for **46** placed it in the *cis*-X-Pro series. A  $\theta$  (O2-C9-C10-C11) angle of  $-79.7^\circ$  in the modeled *cis* conformer, predicted a  $\Delta\delta_{\beta\gamma}$  value of 8.9, whereas a  $\Delta\delta_{\beta\gamma}$  value of 0.7 placed **47** in the *trans*-X-Pro series. A  $\theta$  angle of  $-8.2^\circ$  in the *trans* conformer predicted a  $\Delta\delta_{\beta\gamma}$  value of 1.0. Similar values were obtained for tawicyclamide A (**45**) and dehydrotawicyclamide A (**48**).

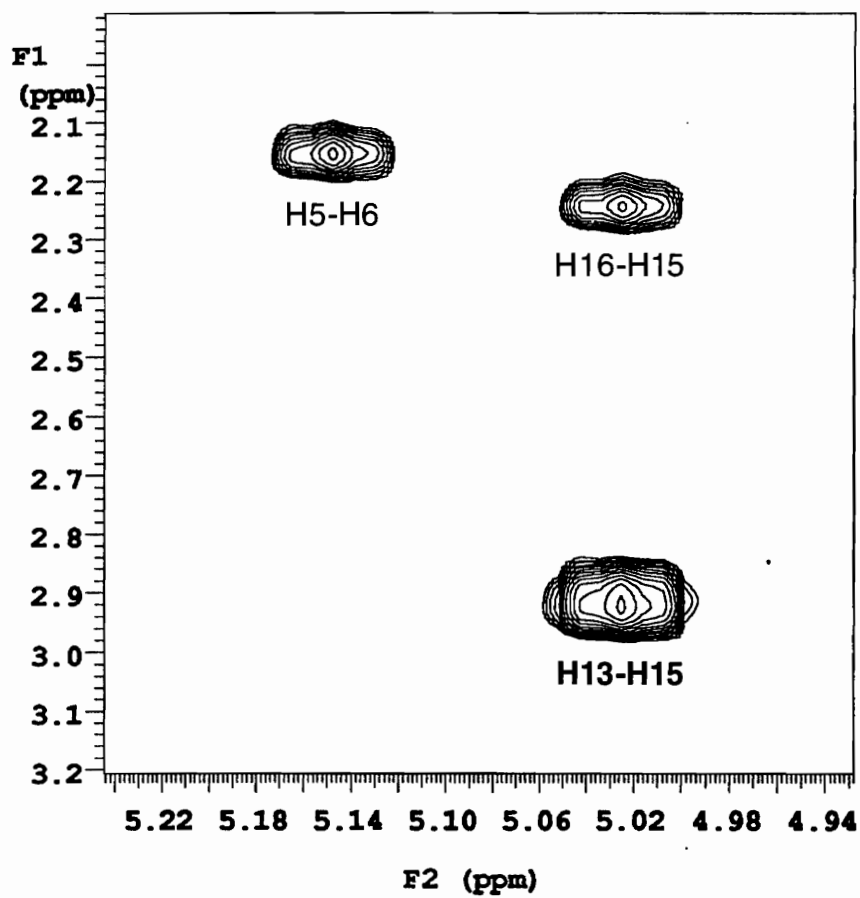


Figure 4.16. Region of a 300 ms ROESY spectrum of dehydrotawicyclamide B showing the H13-H15 crosspeak.

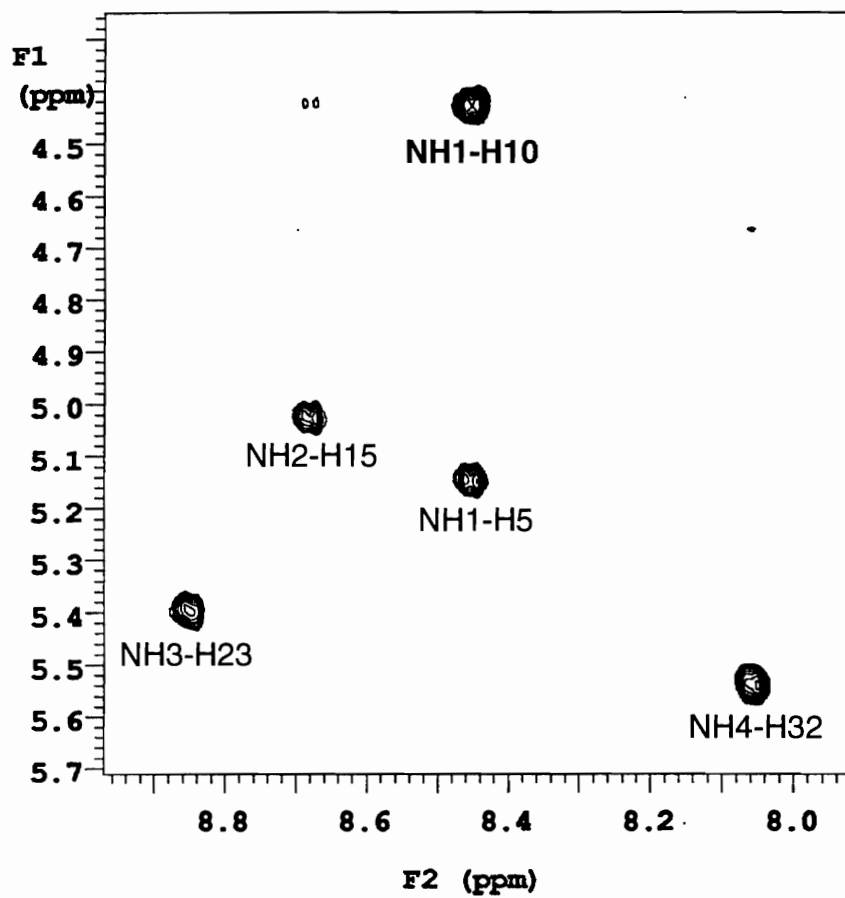


Figure 4.17. Region of a 300 ms ROESY spectrum of dehydrotawicyclamide B showing the NH1-H10 crosspeak.



The empirical observation that carbon atoms *syn* to the carbonyl oxygen of amides are shielded relative to those that are *anti*<sup>165</sup> is borne out by the NMR data. The proline  $\alpha$  carbon of the *trans* conformer **47** is shielded relative to the *cis* conformer **46**. Likewise, the proline  $\delta$  carbon atom of **46** is shielded relative to **47** as predicted.

### Biological Activity of the Tawicyclamides

The tawicyclamides (**45-46**) and their dehydro analogs, **47** and **48**, are weakly cytotoxic against human colon tumor cells, all with IC<sub>50</sub> values of 31  $\mu$ g/mL. These results are consistent with structure-activity studies that show that the oxazoline ring is essential for the cytotoxicity of this class of compounds.<sup>166</sup>

### Review of Cyclic Peptides

#### Cyclic Peptides from Ascidians

Ascidians have proven to be a rich source of bioactive amino acid-derived secondary metabolites.<sup>18,167</sup> The prolific Didemnidae family has produced several families of peptide metabolites such as the didemnins<sup>59</sup> and the lissoclinum peptides.<sup>142-144,150,168-175</sup> The lissoclinum peptides from *L. patella*, characterized by the presence of thiazole and oxazoline amino acids, fall into two general groups—the heptapeptide lissoclinamides and the octapeptide patellamides/ulithiacyclamides. These peptides exhibit in vitro cytotoxicity with the presence of the oxazoline ring proving important to their potency.<sup>166</sup>

Ulithiacyclamide is the most potent lissoclinum peptide. A large number of cyclic peptides have been isolated from ascidians.<sup>68,142-145,150,168-174,176-181</sup> These will not be explicitly reviewed here since amino acid derived metabolites from ascidians have been extensively reviewed in a recent publication.<sup>182</sup>

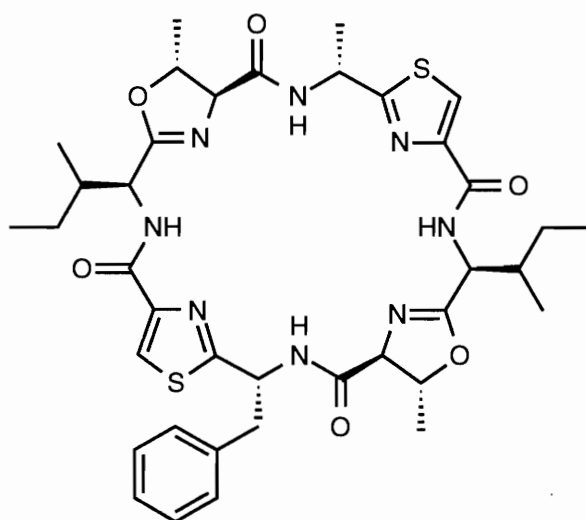
#### Three-Dimensional Structure of Cyclic Peptides from Ascidians

The three-dimensional structures of several ascidian derived cyclic peptides have been established. Some of the more intriguing conformations have been associated with the thiazole and oxazoline containing octapeptides from *L. patella*. The C<sub>2</sub>-symmetrical

ascidiacyclamide **49**, isolated from an unidentified ascidian, has been extensively studied.<sup>181</sup> X-ray crystallography established the three-dimensional structure of **49**, which exhibited a “saddle-shaped” conformation where the thiazole and oxazoline rings occupy the corners of a rectangle.<sup>161</sup> This is most similar to the all *trans* extended conformation of the dehydrotawicyclamides (Figure 4.15) where all the N-H bonds are directed toward the center of the ring. The same authors infer from NMR data that the solution structure is very similar to the solid-state structure.<sup>162</sup>

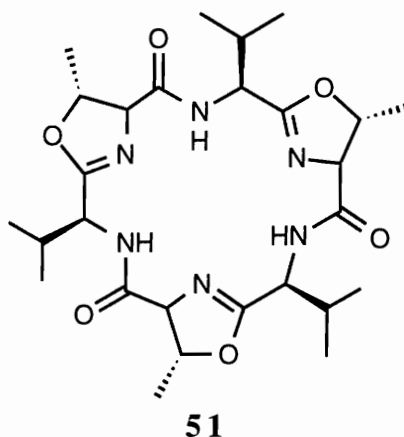
A related peptide from *L. patella*, patellamide D (**50**), assumes a dramatically different three-dimensional conformation.<sup>174</sup> Ishida et al. term this a type III conformation.<sup>163</sup> Although the alternating oxazoline rings of **50** is replaced by thiazoline and proline rings in the tawicyclamides, the conformation of the tawicyclamides may also be termed type III. Inspection of the X-ray structure of **50** (Figures 4 and 5 in reference<sup>174</sup>) reveals the same stacking interaction between the two thiazole rings as in **46**.

The three-dimensional structure of another lissoclinum peptide, ulithiacyclamide (**43**) was established by a combination of NMR and molecular modeling.<sup>183</sup> The molecule assumes different conformations depending on the solvent used for NMR studies. The conformation assumed in benzene and chloroform is most accurately described as type II.



**50**

The three-dimensional structure of the cyclic hexapeptide cyclohexazoline (**51**) from *L. bistratum* has been established by X-ray crystallography. Compound **51** assumes a planar conformation with no folding due to the small size of the macrocyclic ring.<sup>169</sup> This compound is identical to westiellamide (**51**), which was isolated from the blue-green alga *Westiellopsis prolifica*.<sup>184</sup>



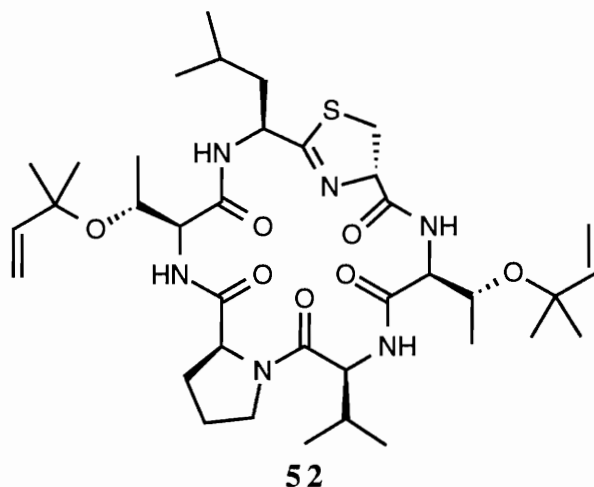
The related peptide bistratamide C (**44**), also from *L. bistratum*, was modeled and found to possess a conformation similar to **51**.<sup>150</sup>

#### *Cis-Trans* Proline Isomerization in Cyclic Peptides of Marine Origins

Proline, by allowing for two configurations, *cis* and *trans* via isomerization of the X-Pro amide bond (X = any amino acid), has profound effects on the three-dimensional structure of a molecule. The activation energy barrier for interconversion between *cis* and *trans* is fairly small (< 13 kcal/mol);<sup>160</sup> this amount of energy is readily available at room temperature. The energy required may be greater when the proline is constrained in a macrocyclic ring. Depending on the size of the macrocyclic ring the proline may be locked into one conformation or vacillate between the two conformations.

Molecular modeling studies have shown that some compounds, such as patellin 2 (**52**)—a proline containing cyclic peptide from *L. patella*, exists in multiple conformations in solution due to isomerization of the valine-proline amide bond. The *trans* isomer is

reported to predominate in high dielectric solvents.<sup>178</sup> Other compounds, like patellamide D, ascidiacyclamide, and the tawicyclamides and dehydrotawicyclamides, exist as single conformers.



In the absence of an X-ray structure or detailed molecular model, experimental NMR data can be used to determine the configuration of the X-Pro amide bond. For example, Siemion et al. have shown that the difference between the proline  $\beta$  and  $\gamma$   $^{13}\text{C}$  signals is greater for *cis*- than for *trans*-X-Pro as discussed above.<sup>164</sup> This empirical observation is a result of the shielding effect of the proline carbonyl group on the proline  $\beta$  carbon when it is *syn* to the carbonyl oxygen and lying in the carbonyl shielding cone. This observation is generally used to differentiate between *cis*- and *trans*-X-Pro amide bond configurations.<sup>168,170,177</sup> In addition to  $^{13}\text{C}$  chemical shifts, nOe correlations between X and Pro ( $\alpha$ - $\alpha$  for *cis* and  $\alpha$ - $\delta$  for *trans*), as illustrated in the discussion of **46** and **47**, may be used to distinguish *cis* from *trans*.

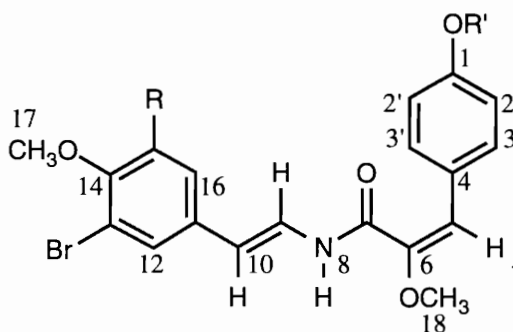
## CHAPTER 5

### THE CHEMISTRY OF THE ASCIDIAN *BOTRYLLUS* SP.

This chapter describes the structure determination of a series of bromotyrosine derivatives, the botryllamides, which were isolated from a *Botryllus* sp. (Order: Stolidobranchia, Family: Styelidae) ascidian. The identical series of compounds were also isolated from *Botryllus schlosseri* by Carroll, Coll and Bowden and are reported in a joint publication.<sup>185</sup> The botryllamides are structurally similar to the tunichromes.<sup>186-188</sup>

#### Isolation of the Botryllamides

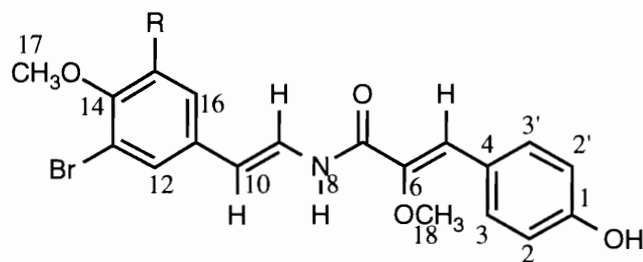
Botryllamide D (**53**) was initially isolated by Mr. J. Christopher Swersey but remained uncharacterized. A subsequent collection of the organism yielded botryllamides B (**54**), C (**55**), and A (**56**), in addition to **53**. Compound **57** was synthesized.



- 53:** R = H, R' = H  
**54:** R = Br, R' = H  
**57:** R = H, R' = Me

#### Structure Determination of Botryllamide D

The presence of a bromine atom in botryllamide D (**53**) was inferred by the 1:1 molecular ion doublet at  $m/z$  403 and 405 in the electron impact (EI) mass spectrum (Figure



**55:** R = H

**56:** R = Br

5.1) and supported by negative and positive ion FAB mass spectrometry which gave molecular ion doublets at  $m/z$  402&404 and 404&406 respectively. High resolution EI mass spectrometry provided a molecular mass which was consistent the molecular formula  $C_{19}H_{18}O_4N^79Br$ .

Fragment ion doublets in the EI mass spectrum at  $m/z$  212&214 and 226&228 corresponded to  $[C_9H_9OBr]^{*+}$  and  $[C_9H_{10}ONBr]^{*+}$ , respectively. These bromotyrosine fragment ions (and other spectroscopic data discussed below) were suggestive of the fragmentation shown in Figure 5.1, which apparently resulted from the cleavages indicated and subsequent ion-molecule reactions. The amide nitrogen contributed to the tendency of this molecule to form  $(M+1)^+$  and  $(m/z + 1)^+$  ions by ion-molecule reactions.<sup>189</sup> This is further illustrated by the nitrogen bearing  $m/z$  193 fragment  $[C_{10}H_{11}O_3N]^{*+}$  and the non-nitrogen bearing  $m/z$  177  $[C_{10}H_9O_3]^{*+}$  fragment. Structure **53** accounts for all major EI MS fragment ions in Figure 5.1.

The  $^{13}C$  spectrum (Appendix D) of **53** showed 17 resonances, including two for the degenerate aromatic carbons (C2, C2' and C3, C3') of the *para*-substituted phenyl ring. Examination of the  $^1H$  (Appendix D),  $^{13}C$ ,  $^1H$ - $^1H$  COSY,<sup>190</sup> TOCSY,<sup>191</sup> ROESY,<sup>129,130,156</sup> HMQC,<sup>148</sup> and HMBC<sup>131</sup> data acquired for botryllamide D in DMSO- $d_6$  enabled the establishment of the spin networks presented below and ultimately led to structure **53**. Table 5.1 contains the NMR assignments for **53**.

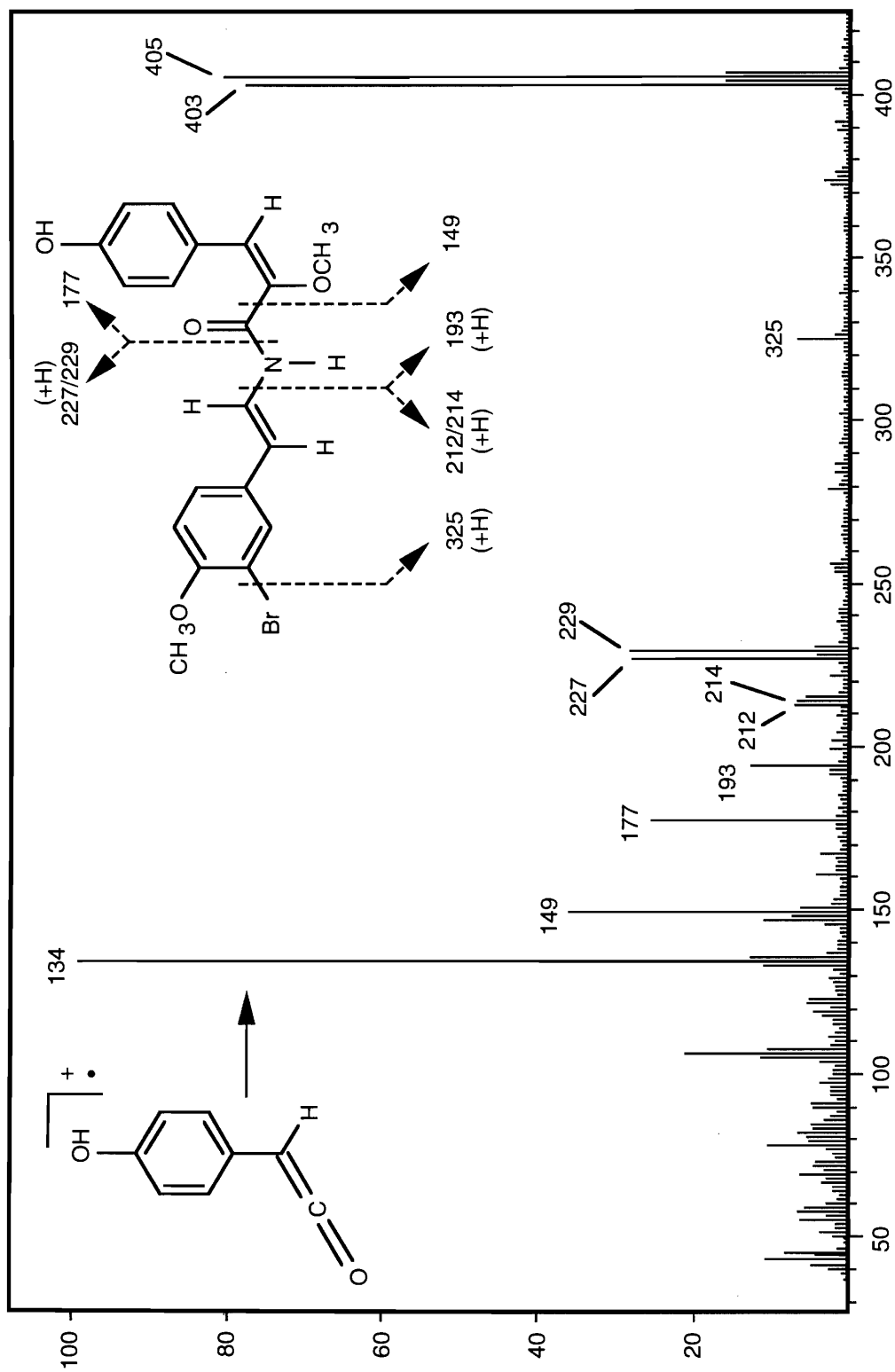


Figure 5.1. EI mass spectrum and fragmentation of botryllamide D.

Table 5.1

NMR<sup>a</sup> Assignments for Botryllamide D in DMSO-*d*<sub>6</sub>

Atom no.	$\delta$ <sup>13</sup> C	$\delta$ <sup>1</sup> H	(mult., <i>J</i> (Hz))	<sup>1</sup> <i>J</i> <sub>CH</sub> (Hz) <sup>b</sup>	HMBC <sup>c</sup> Correlations
1	156.02				
1-OH	—	9.38 <sup>d</sup>	(bs)		
2	114.88	6.64	(d, 8.5)	157	156.02, 124.86, 114.88
3	129.44	7.11	(d, 8.5)	153	156.02, 129.44, 114.88, 105.89
4	124.86				
5	105.89	5.93	(s)	151	161.65, 148.42, 129.44
6	148.42				
7	161.65				
8-NH	—	10.40 <sup>d</sup>	(d, 10.0)		161.65, 122.53, 111.76
9	122.53	7.34 <sup>e</sup>	(m)	171	161.65, 130.62, 111.76
10	111.76	6.21	(d, 14.8)	153	129.51, 125.71, 122.53
11	130.62				
12	129.51	7.55	(d, 2.0)	163	153.91, 125.71, 111.76, 111.03
13	111.03				
14	153.91				
15	112.90	7.01	(d, 8.7)	158	153.91, 130.62, 111.03
16	125.71	7.34 <sup>f</sup>	(m)	157	153.91, 130.62, 111.76
17	56.22	3.82	(s)	145	153.91
18	55.57	3.66	(s)	142	148.42

<sup>a</sup> Proton and carbon data were acquired at 500 and 125 MHz, respectively.

<sup>b</sup> Obtained from a coupled HMQC experiment.

<sup>c</sup> The HMBC experiment was optimized to observe <sup>n</sup>*J*<sub>CH</sub> couplings of 8.0 Hz.

<sup>d</sup> Exchangeable upon addition of D<sub>2</sub>O.

<sup>e</sup> 7.30 ppm, (d, *J* = 14.8 Hz) in DMSO-*d*<sub>6</sub> + D<sub>2</sub>O.

<sup>f</sup> 7.32 ppm, (dd, *J* = 8.7, 2.0 Hz) in DMSO-*d*<sub>6</sub> + D<sub>2</sub>O.



### *Trans*-Eneamide Substructure

The amide NH stretch was obscured in the IR spectrum of **53** by the strong OH stretch (see below), however, the presence of an amide group was suggested by the 10.40 ppm  $^1\text{H}$  resonance that exchanged on addition of  $\text{D}_2\text{O}$ . This resonance could be attributed to the amide NH proton (H8, d,  $J = 10.0$  Hz) of the *trans*-eneamide substructure. A 14.8 Hz doublet at 6.21 ppm (H10) coupling into a two proton multiplet at 7.34 ppm suggested that **53** contained a *trans*-disubstituted olefin. The 7.34 ppm proton further coupled to the exchangeable H8 proton. When H8 exchanged with deuterium in  $\text{D}_2\text{O}$ , the degenerate 7.34 ppm resonance collapsed into a one proton doublet at 7.30 ppm (H8,  $J = 14.8$  Hz) and a one proton doublet of doublet at 7.32 ppm (H16,  $J = 8.7, 2.0$  Hz). Coupled with a strong HMBC correlation from H8 to C7, these data established the *trans*-eneamide substructure ( $\text{CH}=\text{CHNHCO}$ ). This moiety is found in molecules such as the tunichromes,<sup>186,187,192</sup> clionamide,<sup>193,194</sup> and the celenamides.<sup>195</sup>

### Trisubstituted Olefin Substructure

The olefinic H5 proton at 5.93 ppm is a singlet but showed weak, homoallylic coupling to the H18 methoxy group at 3.66 ppm. Both H5 and H18 showed HMBC correlations to C6 (148.42 ppm). The upfield position of C5 (105.89), which bears the 5.93 ppm proton, suggested a polarized trisubstituted olefin where the methoxy group was borne by C6. The HMBC correlation between H5 and C7 (161.65) placed the olefin adjacent to the carbonyl of the *trans*-eneamide. Reciprocal HMBC (C3 to H5 and C5 to H3) and ROESY (H5 to H3) correlations established the trisubstituted olefin as one of the substituents of the *para*-substituted phenyl ring discussed below (Figure 5.2). The configuration about the C5-C6 double bond was established as (*E*) based on a ROESY correlation between H5 and H18 that indicated these protons were *cis* (Figure 5.3).

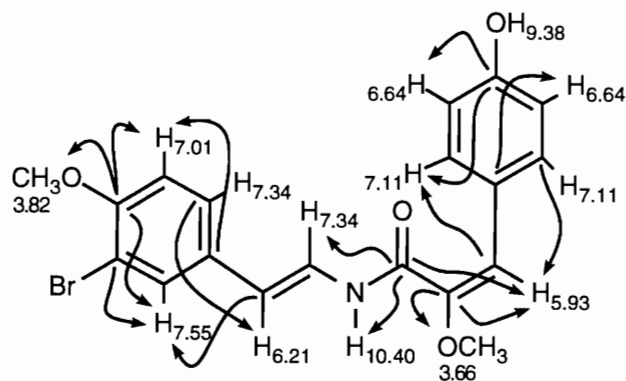


Figure 5.2. Select HMBC correlations for Botryllamide D.

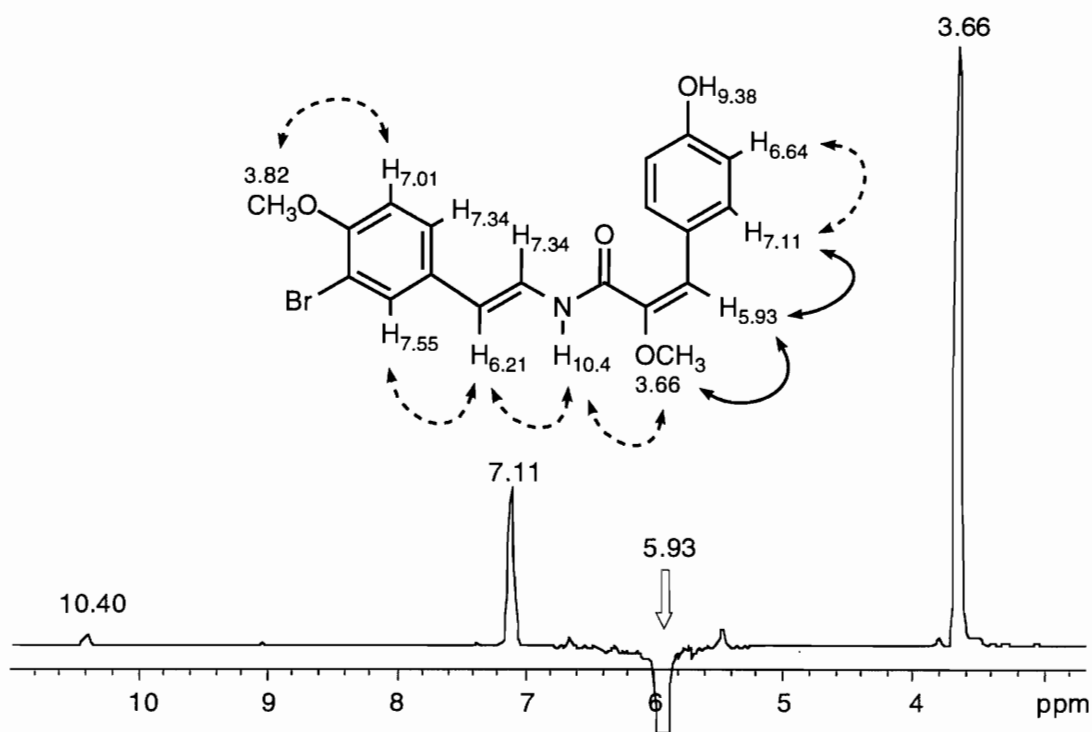


Figure 5.3. Botryllamide D ROESY correlations and slice through 400 ms ROESY spectrum showing correlations instrumental in establishing the configuration about the C5-C6 olefinic bond.

### *Para*-Disubstituted Benzene Ring Substructure

The NMR data defined another spin system consisting of mutually coupled 8.5 Hz doublets at 6.64 (H2, 2H) and 7.11 ppm (H3, 2H). The HMQC experiment revealed that the degenerate carbon atoms (C2 & C2') resonating at 114.88 ppm bore the 6.64 ppm protons, while the other degenerate carbon atoms (C3 & C3') at 129.44 ppm bore the 7.11 ppm protons. This was consistent with a *para*-disubstituted benzene ring. The broad IR band centered about 3250 cm<sup>-1</sup> was consistent with the presence of an OH group. A D<sub>2</sub>O exchange experiment revealed that the resonance at 9.38 (H1, bs) was exchangeable. The chemical shift of the exchangeable H1 proton was compatible with an aromatic OH group and was supported by the presence of an aromatic oxygen bearing carbon resonating at 156.02 ppm (C1). HMBC correlations from C1 to H2 and H3 established the hydroxyl group as the other substituent of the *para*-substituted benzene ring while methylation of **53** with diazomethane yielded a single product with one additional methoxy group but without the 9.38 ppm (H1) exchangeable proton. The proton data for 1-methoxybotryllamide D (**57**) are given in the experimental section while the proton spectrum is shown in Appendix D.

### 1, 2, 4-Trisubstituted Benzene Ring Substructure

NMR data delineated a final spin network consisting of coupled aromatic protons H15 (7.01 ppm, d,  $J = 8.7$  Hz) and H16 (7.34 ppm, m) with *meta* coupling from H16 to H12 (7.55 ppm, d,  $J = 2.0$  Hz). HMBC and ROESY data were used to establish the positions of the substituents. A strong ROESY correlation between H15 and the 3.82 ppm methoxy group (H17, s) implied that this substituent was attached to C14. An HMBC correlation between H17 and C14 (153.91 ppm) confirmed this as the methoxy bearing phenyl carbon. Correlations from C14 to all three aromatic protons (H12, H15, and H16) suggested that they were two or three bonds away from the methoxy bearing C14 carbon. Additionally, an HMBC correlation between C11 (130.62 ppm) and H15 assigned the *ipso*

carbon and established the position of a second substituent. HMBC correlations between C12, C16 and H10 firmly established this substituent as the *trans* enamide moiety. HMBC correlation from the upfield quaternary aromatic carbon C13 (111.03) to H12 and H15 placed this carbon between C12 and C14 and suggested that it bore the final substituent of the trisubstituted aromatic ring, a bromine atom.

These data led to the proposal of structure **53** for botryllamide, a modified dipeptide consisting of a methylated bromotyrosine residue and a methoxylated tyrosine residue. The additional ROESY correlations (dashed lines) depicted in Figure 5.3 are in complete accord with this structure.

#### Structure Determination of Botryllamides B, C, and A

Table 5.2 contains the proton NMR data for botryllamides D, B, C, and A. The proton and COSY spectra for compounds **53-57** are shown in Appendix D. Botryllamide B (**54**) has a bromine atom attached to C15 and differed from **53** only in that respect. Figure 5.4 shows a strong ROESY correlation between H5 (5.95 ppm) and H18 (3.66 ppm) supporting the same (*E*) configuration about the C5-C6 olefinic bond in **54** as in **53**. Botryllamide C (**55**) differs from **53** by the configuration about the C5-C6 olefinic bond. As shown in Figure 5.4, the absence of substantial nOe between H5 (6.83 ppm) and H18 (3.61 ppm) supports the opposite stereochemistry. Botryllamide A (**56**) has the same (*Z*) configuration about the C5-C6 olefinic bond as **55** but has a second bromine atom attached at C15.

#### Biology

Botryllamide D showed only marginal activity (IC<sub>50</sub>, 42 μM; 17 μg/mL) when tested in vitro against human colon tumor cells and was inactive when tested in vivo in the P388 mouse leukemia model (T/C of 110 at 27 mg/kg, the highest dose tested).

Table 5.2  
Proton NMR Assignments for Botryllamides D, B, C, and A in DMSO-*d*<sub>6</sub>

Atom no.	botryllamide D, $\delta$ <sup>1</sup> H (mult., <i>J</i> (Hz))	botryllamide B, $\delta$ <sup>1</sup> H (mult., <i>J</i> (Hz))	botryllamide C, $\delta$ <sup>1</sup> H (mult., <i>J</i> (Hz))	botryllamide A, $\delta$ <sup>1</sup> H (mult., <i>J</i> (Hz))
1-OH	9.38 (bs)	9.37 (s)	9.87 (bs)	9.86 (bs)
2	6.64 (d, 8.5)	6.64 (d, 8.6)	6.81 (d, 8.7)	6.81 (d, 8.7)
3	7.11 (d, 8.5)	7.11 (d, 8.6)	7.59 (d, 8.7)	7.59 (d, 8.7)
5	5.93 (s)	5.95 (s)	6.82 (s)	6.83 (s)
8-NH	10.40 (d, 10.0)	10.51 (d, 10.1)	10.28 (d, 10.1)	10.41 (d, 10.1)
9	7.34 (m)	7.47 (dd, 14.5, 10.1)	7.42 (dd, 14.6, 10.1)	7.53 (dd, 14.5, 10.1)
10	6.21 (d, 14.8)	6.20 (d, 14.6)	6.44 (d, 14.6)	6.41 (d, 14.5)
12	7.55 (d, 2.0)	7.66 (s)	7.55 (d, 2.2)	7.63 (s)
15	7.01 (d, 8.7)	—	7.02 (d, 8.7)	—
16	7.34 (m)	7.66 (s)	7.34 (dd, 8.7, 2.2)	7.63 (s)
17	3.82 (s)	3.76 (s)	3.82 (s)	3.76 (s)
18	3.66 (s)	3.66 (s)	3.61 (s)	3.61 (s)

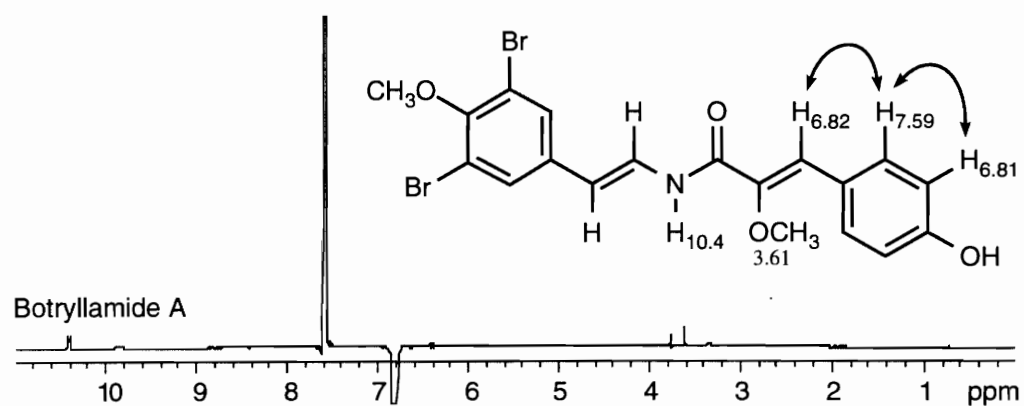
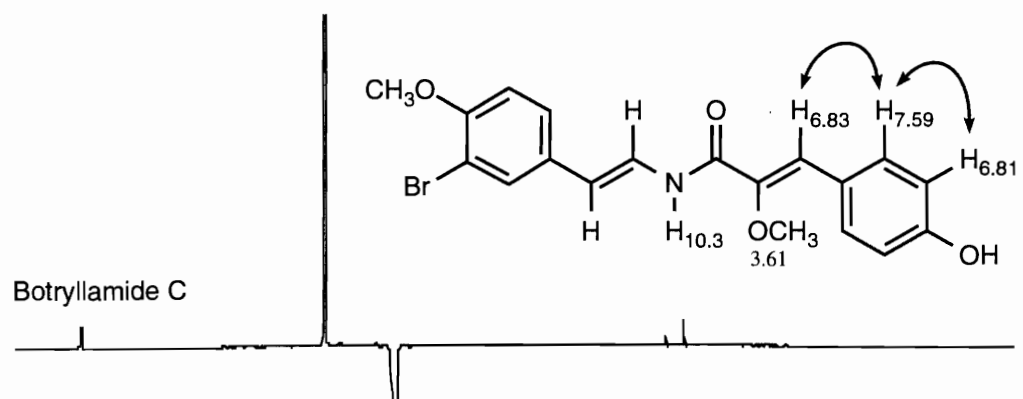
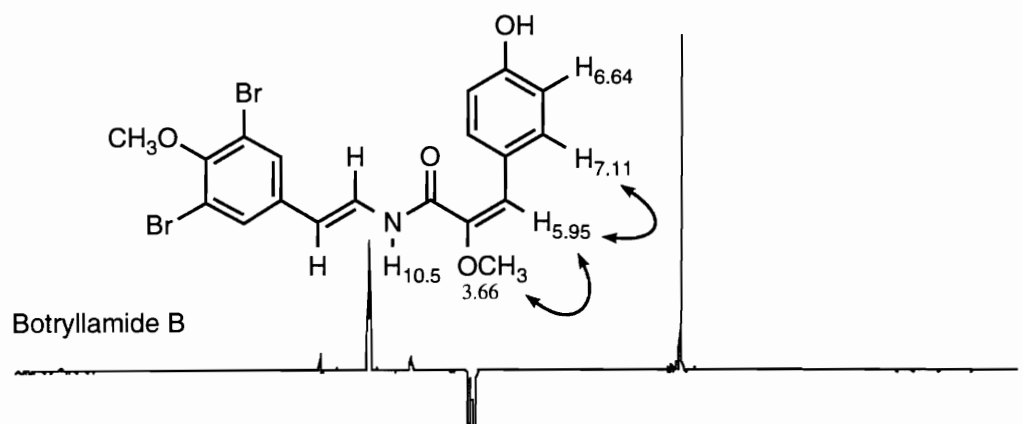
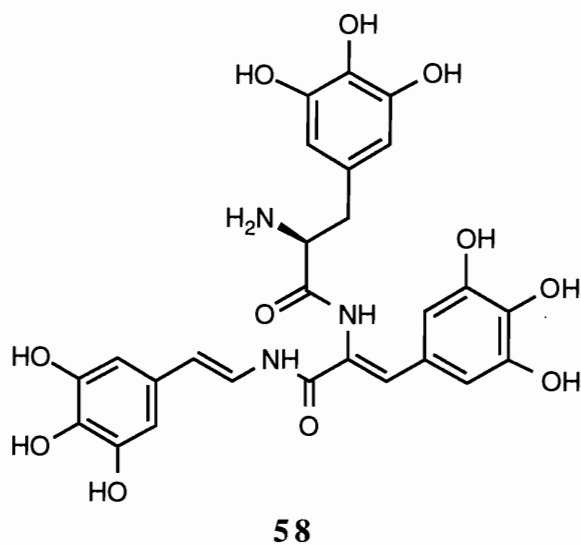


Figure 5.4. Slices from 400 ms ROESY spectra used to establish the configuration about the C5-C6 olefinic bond in botryllamides B, C, and A, respectively.

### Review of Linear Peptide Alkaloids from Ascidians

Ascidians produce an array of linear and cyclic amino acid derived metabolites.<sup>18,167</sup> Several linear peptide alkaloids have been recently described from sponges and ascidians.<sup>186,187,193-195</sup> The tunichromes (e.g., tunichrome An-1 (**58**)) were initially isolated from the ascidian *Ascidia nigra* and are considered biological reducing agents.<sup>186-188</sup> These compounds are believed to play roles in tunicate hematology, serving both as reductants of vanadium (V(V)) and complexing agents for the reduced vanadium (V(III)). These properties of the tunichromes are believed to stabilize V(III) in the ascidians vanadophore blood cells.<sup>188</sup> An-1 and several other tunichromes have been synthesized.<sup>192,196</sup> The amino acid phenylalanine serves as a precursor in the biosynthesis of tunichromes in the ascidian *Ascidia ceratodes*. This was demonstrated by the incorporation of radiolabeled phenylalanine into tunichrome An-1.<sup>197</sup>



## CHAPTER 6

### EXPERIMENTAL

#### Chemicals, Reagents, and Organisms

The isolation and chemical characterization of the new compounds discussed in this dissertation are described below. The purity of these compounds were assessed by chromatographic and NMR analysis. Reagent grade solvents were distilled prior to use. NMR solvents were purchased from Aldrich (Milwaukee, WI), Cambridge Isotope (Woburn, MA), or Isotec Inc. (Miamisburg, OH).

Bleomycin sulfate, ethidium bromide, Fast Blue RR (4-benzoylamino-2,5-dimethoxybenzenediazonium chloride hemi[zinc chloride]) salt, 6-bromo-2-naphthyl- $\beta$ -D-galactopyranoside, tris(hydroxymethyl)aminomethane (trizma base), FDAA reagent, amino acid standards, and calf thymus DNA were purchased from Sigma Chemical Co. (St. Louis, MO.). Bacteriological agar was purchased from SCOTT Laboratories, Inc. (Fiskerville, RI.). Bacteriological media for BIA (peptone, yeast extract, glucose, tryptone, etc.) were purchased from Difco Laboratories (Detroit, MI.). Inorganic salts were purchased from Aldrich Chemical Company, Inc. (Milwaukee, WI.). *Escherichia coli* strain BR513-84 was a generous gift from Lederle Laboratories (Pearl River, NY.).

#### General Experimental Procedures

##### Nuclear Magnetic Resonance (NMR) Spectroscopy

NMR data were obtained on a Varian Unity 500 spectrometer operating at 500 and 125 MHz for proton and carbon, respectively. Proton chemical shifts are reported in ppm relative to the residual protiated solvent resonance (7.15 ppm for C<sub>6</sub>D<sub>6</sub>; 7.24 ppm for



CDCl<sub>3</sub>; 3.30 ppm for MeOH-*d*<sub>4</sub>; and 2.49 ppm for DMSO-*d*<sub>6</sub>). Carbon-13 chemical shifts are reported in ppm relative to the solvent resonance (128.0 ppm for C<sub>6</sub>D<sub>6</sub>; 77.0 ppm for CDCl<sub>3</sub>; 49.0 ppm for MeOH-*d*<sub>4</sub>; and 39.5 ppm for DMSO-*d*<sub>6</sub>). The COLOC experiment was acquired on an IBM AF 200 spectrometer operating at 200 and 50 MHz for carbon and proton, respectively.

#### Infrared (IR) Spectroscopy, Ultraviolet (UV) Spectroscopy, and Polarimetry

IR spectra were recorded on a Perkin-Elmer 1600 Fourier Transform spectrophotometer using a thin film of compound on sodium chloride plates. UV spectra were obtained on a Beckman DU-8 or Hewlett-Packard HP8452A spectrophotometer. Optical rotations were measured with a Jasco DIP-370 polarimeter in a 10 mm or 100 mm cell.

#### Mass Spectrometry (MS)

High and low resolution mass measurements (FAB, EI, CI) were made on a Varian MAT-731 or on a Finnigan MAT 95 mass spectrometer. Electrospray mass measurements were made on a VG Fisons Trio quadruple mass spectrometer.

#### The Chemistry of *Cystodytes* sp.

##### Collection, Extraction, and Isolation

The encrusting ascidian, *Cystodytes* sp.,<sup>128</sup> was collected by SCUBA (-10 m) near Waya Island, Fiji, and was kept frozen until extracted. The freeze dried animal (182 g) was homogenized and extracted with MeOH-CHCl<sub>3</sub> (1:1, 5 x 900 mL) to give 2.8 g of crude solid. A portion of the crude extract was partitioned according to the Kupchan scheme.<sup>198</sup> The CCl<sub>4</sub> soluble partition fraction was chromatographed on silica gel using a step gradient from 25% EtOAc in hexane to 100% EtOAc then continuing to 50% MeOH in EtOAc in steps of ~5%.

The mixture of compounds eluting from the silica column with 100% EtOAc was separated by HPLC using a 10 mm I.D. x 250 mm long DYNAMAX column with 60 Å, 8 µm Amino support. Using a mobile phase of 2.5% MeOH in CH<sub>2</sub>Cl<sub>2</sub> and a flow rate of 3.0 mL/min, HPLC yielded shermilamines C (**34**, 12.6 mg) and B<sup>123</sup> (**38**, 8.4 mg).

Fractions eluting from the silica gel column with 10 to 30% MeOH in EtOAc contained a mixture of compounds which was ultimately resolved into dehydrokuanoniamine B (**33**, 3.7 mg), kuanoniamine D<sup>122</sup> (**37**, 10.5 mg) and, eilatin<sup>90</sup> (**23**, 4 mg) by HPLC on Amino support using 4% MeOH in CH<sub>2</sub>Cl<sub>2</sub> as the mobile phase. BIA bioautography<sup>108</sup> on silica gel was used to guide the isolation of **23**.

The CHCl<sub>3</sub> soluble Kupchan partition fraction was chromatographed on silica gel using the step gradient discussed above. The fraction eluting with 100% EtOAc containing crude cystodytin A was further purified by HPLC (DYNAMAX-100 Å 5 µm Silica, 4.6 mm I.D. x 250 mm long column; 5% MeOH in CHCl<sub>3</sub>; 1.0 mL/min) to yield cystodytin A<sup>121</sup> (**36**, 3.5 mg). The fraction eluting from the silica gel column with 10% MeOH in EtOAc was further purified by silica gel HPLC as described above to yield cystodytin J (**35**, 4.2 mg).

#### Physical and Spectral Properties of Dehydrokuanoniamine B, Shermilamine C, and Cystodytin J

##### Dehydrokuanoniamine B (**33**)

Orange solid; IR (film):  $\nu_{\max}$  3284, 3186, 3151, 3129, 3071, 3058, 3036, 3026, 2921, 2851, 1641, 1632, 1567, 1452 cm<sup>-1</sup>; UV(MeOH):  $\lambda_{\max}$  ( $\epsilon$ ) 237 (50967), 261 (30120), 344 (16413), 359 (16953), 452 (6047); UV(MeOH, TFA):  $\lambda_{\max}$  ( $\epsilon$ ) 277 (43640), 267 (20720), 306 (40333), 359 (11447), 527 (5940); LR FAB MS (glycerol):  $m/z$  401 (M+H)<sup>+</sup>, 302, 288; HR FAB MS (glycerol):  $m/z$  401.1429 (M+H)<sup>+</sup>, C<sub>23</sub>H<sub>21</sub>N<sub>4</sub>OS requires 401.1436; NMR data contained in Table 3.1.

Shermilamine C (34)

Orange solid; IR (film):  $\nu_{\max}$  3285, 3203, 3052, 2925, 2854, 1634, 1433  $\text{cm}^{-1}$ ;  
 UV(MeOH):  $\lambda_{\max}$  ( $\epsilon$ ) 231 (9185), 279 (6669), 296 (5693), 350 (2683), 390 (1896), 463  
 (1664); UV(MeOH, TFA):  $\lambda_{\max}$  ( $\epsilon$ ) 218 (12414), 277 (6033), 300 (7491), 318 (8123),  
 359 (1703), 382 (1716), 538 (1423); LR FAB MS (glycerol):  $m/z$  431 (M+H)<sup>+</sup>, 332, 318;  
 HR FAB MS (glycerol):  $m/z$  431.1529 (M+H)<sup>+</sup>, C<sub>24</sub>H<sub>23</sub>N<sub>4</sub>O<sub>2</sub>S requires 431.1542; NMR  
 data contained in Table 3.2.

Cystodytin J (35)

Yellow solid; LR FAB MS (3-Nitrobenzyl Alcohol):  $m/z$  318 (M+H)<sup>+</sup>, 247; LR FAB  
 MS (glycerol):  $m/z$  320 ((M+2)+H)<sup>+</sup>, 247; HR FAB MS (glycerol):  $m/z$  320.1390  
 ((M+2)+H)<sup>+</sup>, C<sub>19</sub>H<sub>18</sub>N<sub>3</sub>O<sub>2</sub> requires 320.1399; NMR data contained in Table 3.3.

Preparation of TFA Salts of Dehydrokuanoniamine B and  
 Shermilamine C

The compounds were dissolved in MeOH containing 0.05% TFA. Removal of the  
 solvent under reduced pressure yielded the magenta trifluoroacetate salts.

Fluorescence Spectroscopy

Fluorescence measurements were made on an PC1 spectrofluorometer equipped with  
 a thermostated cuvette compartment and interfaced with an IBM computer. Ethidium  
 bromide displacement fluorescence studies were carried out with excitation at 530 nm and  
 emission at 600 nm (or from 550 to 700 nm with 8 nm resolution). Eilatin's fluorescence  
 studies were carried out with excitation at 520 nm and emission from 480 to 580 nm with  
 resolution of 8 nm. All spectra were corrected for background fluorescence.

Biochemical Induction Assay (BIA)

The BIA test was a modification of the procedure reported by Elespuru and White.<sup>108</sup>  
 Briefly, the overnight culture of BR513-84 was diluted to an A<sub>600</sub> of 5.7 and used to

inoculate agar that was placed on a bioassay plate prepared with a nutrient containing basal layer. Test compounds were applied to Difco, 1/4" sterile paper disks and placed on the bioassay plate which was then incubated for 3 h at 37 °C.  $\beta$ -Galactosidase production is a measure of the induction taking place during incubation. After removing and discarding the disks, BNG (6-bromo-2-naphthyl- $\beta$ -D-galactopyranoside) substrate (**28**) and Fast Blue RR salt (**29**) are applied to the plate in an agar suspension overlay. The BNG substrate is cleaved by  $\beta$ -galactosidase into a bromonaphthol product (**31**) which couples with the diazonium salt (**29**), Fast Blue RR, to give a reddish azo dye (**32**).

#### Other Assays

Cytotoxicity assays, K<sup>+</sup>-SDS protein-DNA coprecipitation assay, assay for DNA topoII catalytic activity, and macromolecule synthesis inhibition assay were performed in the laboratory of Prof. Louis R. Barrows and are described elsewhere.<sup>74</sup>

#### The Chemistry of *Lissoclinum patella* (Singapore)

##### Collection, Extraction, and Isolation

Specimens of *L. patella* were collected by SCUBA off Pulau Salu, Singapore. The CHCl<sub>3</sub> extract of 22.6 g freeze dried ascidian (1.094g) was purified by flash chromatography on silica gel (75:25 EtOAc/hexane) to yield a 191 mg fraction which was further purified by HPLC (Rainin DYNAMAX silica; 10 x 250 mm; 30:70 acetone/hexane; 5.0 mL/min; detection by refractive index) to yield 120 mg (0.53 % dry weight) patellamide E (**40**). The other peptides were isolated in a similar manner.

##### Physical and Spectral Properties of Patellamide E

White amorphous solid; IR (film):  $\nu_{\max}$  3371, 3326, 2966, 2931, 2875, 1666, 1537, 1513, 1484 cm<sup>-1</sup>;  $[\alpha]^{25}_{\text{D}}$  48.6° (c = 0.58, CHCl<sub>3</sub>); UV(MeOH):  $\lambda_{\max}$  235 nm ( $\epsilon$  12305); LR FAB MS (glycerol) *m/z* 791 (M+H)<sup>+</sup>, 763, 748, 700, 285, 214; HR FAB MS (glycerol) *m/z* 791.3359 (M+H)<sup>+</sup>, C<sub>39</sub>H<sub>51</sub>N<sub>8</sub>O<sub>6</sub>S<sub>2</sub> ( $\Delta$  = 1.7 mmu); NMR data contained in Table 4.1.

### General Hydrolysis and Derivatization

Hydrolysis of the peptides were carried out in ~4 mL 6N HCl under a nitrogen atmosphere in a sealed bomb at 104 °C for 23 h. After removing traces of HCl by repeated evaporation in vacuo, the residual hydrolysate was suspended in 300  $\mu$ L H<sub>2</sub>O and derivatized with 1-fluoro-2,4-dinitrophenyl-5-L-alanineamide (FDAA).<sup>151</sup> HPLC analysis (Waters NOVAPAK C<sub>18</sub>; 4.6 x 100 mm column; linear gradient elution, triethylammonium phosphate (50 mM, pH 3.0)/acetonitrile, 90:10 to 60:40 in 45 min; 1.5 mL/min; UV detection at 340 nm) of the FDAA derivatized hydrolysate in conjunction with similarly derivatized amino acid standards established the stereochemistry of the constituent amino acids.

### Ozonolysis of Patellamide E

A slow stream of O<sub>3</sub> was bubbled into a 10 mL CH<sub>2</sub>Cl<sub>2</sub> solution of **40** (1.7 mg; 2.15x10<sup>-3</sup> mmole) in a threaded bomb at 25 °C for approximately 8 min. Upon removal of the solvent under a stream of N<sub>2</sub>, the residue was subjected to hydrolysis and derivatization as described above.

### Stereochemistry of Patellamide E

Hydrolysis of **40** (1.7 mg; 2.15x10<sup>-3</sup> mmole) was carried out in 5 mL 6N HCl under N<sub>2</sub> atmosphere in a sealed bomb at 110 °C for 18 h. Analyses established the presence of L-threonine, L-valine and L-isoleucine in the hydrolysate of **40**. Similar analyses established D-valine and D-phenylalanine in addition to confirming the previously identified amino acids in the acid hydrolysate of ozonized **40**.

## The Chemistry of *Lissoclinum patella* (Philippines)

### Collection, Extraction, and Isolation

Specimens of *L. patella* were collected by SCUBA off Tawitawi Island in the Southern Philippines. The MeOH extract of 118.4 g of freeze dried ascidian was concentrated in vacuo to a volume of 200 mL and partitioned according to a modified

Kupchan scheme.<sup>198</sup> Briefly, a 10% aqueous MeOH solution was partitioned with hexane (5 x 110 mL). Increasing the aqueous content of the lower phase to 26% and partitioning with CHCl<sub>3</sub> (3 x 110 mL) afforded a combined CHCl<sub>3</sub> layer which was concentrated in vacuo to yield 4.9 g (4.1%) of a crude solid. Vacuum flash chromatography (60 mL sintered glass funnel; 20 g silica gel G; step gradient elution from 0 to 10% MeOH-CHCl<sub>3</sub>), carried out on a 2.77 g portion of this residue, yielded a fraction (505 mg; eluting with 2.5% MeOH/CHCl<sub>3</sub>) which showed <sup>1</sup>H NMR resonances characteristic of peptides. TLC of this fraction (silica gel; 100% ethyl acetate) revealed a series of spots (*R<sub>f</sub>* = 0.20 - 0.40) visible with 254 nm UV light and giving positive responses to chlorine-tolidine for nitrogen containing compounds.<sup>199</sup> Further silica gel chromatography using hexane-acetone mixtures followed by reversed phase HPLC using acetonitrile-water mixtures yielded 8 mg ulithiacyclamide<sup>145</sup> (**43**), 24 mg patellamide A<sup>143,144</sup> (**41**), 100 mg patellamide B<sup>143,144</sup> (**42**), tawicyclamide A (**45**) and tawicyclamide B (**46**).

#### Physical and Spectral Properties of Tawicyclamides A and B

##### Tawicyclamide A (**45**)

Clear colorless solid; 63 mg (0.10% dry weight); IR (film):  $\nu_{\max}$  3362, 3332, 2963, 2930, 2874, 1666, 1641, 1609, 1536, 1514, 1484, 1428 cm<sup>-1</sup>; [ $\alpha$ ]<sub>D</sub><sup>25</sup> -15.0° (c = 0.427, CHCl<sub>3</sub>); UV(MeOH):  $\lambda_{\max}$  249.7 nm ( $\epsilon$  16530); LR FAB MS (glycerol): *m/z* 807 (M+H)<sup>+</sup>, 779, 682, 529, 484, 399, 297, 251, 197, 180; HR FAB MS (glycerol) *m/z* 807.3135 (M+H)<sup>+</sup>, C<sub>39</sub>H<sub>51</sub>N<sub>8</sub>O<sub>5</sub>S<sub>3</sub> requires 807.3145; NMR Data contained in Table 4.2.

##### Tawicyclamide B (**46**)

Clear colorless solid; 69 mg (0.10% dry weight); IR (film):  $\nu_{\max}$  3360, 3332, 2960, 2927, 2872, 1667, 1642, 1537, 1514 cm<sup>-1</sup>; [ $\alpha$ ]<sub>D</sub><sup>25</sup> +2.1° (c = 0.347, CHCl<sub>3</sub>); UV(MeOH):  $\lambda_{\max}$  249.7 nm ( $\epsilon$  15029); LR FAB MS (glycerol): *m/z* 773 (M+H)<sup>+</sup>, 745, 297, 251, 197, 180; HR FAB MS *m/z* 773.3345 (M+H)<sup>+</sup>, C<sub>36</sub>H<sub>53</sub>N<sub>8</sub>O<sub>5</sub>S<sub>3</sub> requires 773.3301; NMR Data contained in Table 4.4.

### Tandem Mass Spectrometry (MS/MS) on Tawicyclamide A and Dehydrotawicyclamide A

Tandem mass spectra (Dr. Dennis R. Phillips) were obtained with a VG 70-SEQ (EBqQ geometry) spectrometer. Samples were dissolved in glycerol/3-nitrobenzyl alcohol (1:1) and 1  $\mu$ L placed on the tip of a direct insertion FAB probe. The samples were ionized by FAB using a 7-8 keV xenon beam. The CID mass spectra were obtained by selecting the precursor ion with MS-I followed by collisional activation with krypton gas (reducing the primary beam by 50%) and scanning MS-II. The precursor ion translational energy was 42 electron volts.

### General Oxidation Procedure

Nickel peroxide was prepared<sup>200</sup> and available oxygen was determined by titration of iodine liberated from potassium iodide solution. The peptides were dissolved in benzene and treated with nickel peroxide for 23 h at room temperature. TLC (silica gel; 100% ethyl acetate) indicated complete conversion of the starting materials to single products. Filtration of the reaction mixture through Celite and concentration of the filtrate afforded the pure oxidized peptides.

### Preparation, Physical, and Spectral Properties of Dehydrotawicyclamide B

NiO<sub>2</sub> (722 mg; 65.2  $\mu$ moles available O<sub>2</sub>) was stirred with **46** (12.3 mg; 15.9  $\mu$ moles) in 6 mL C<sub>6</sub>H<sub>6</sub> for 23 h at 25 °C to yield oxidation product **47** (3.7 mg, 30% recovery) as a clear colorless solid. LR FAB MS (glycerol): *m/z* 771 (M+H)<sup>+</sup>, 743, 672, 493, 483, 297; HR FAB MS (glycerol): *m/z* 771.3153 (M+H)<sup>+</sup>, C<sub>36</sub>H<sub>51</sub>N<sub>8</sub>O<sub>5</sub>S<sub>3</sub> requires 771.3145; NMR Data contained in Table 4.5.

### Preparation, Chemical, and Physical Properties of Dehydrotawicyclamide A

Compound **45** (9.8 mg; 12.2  $\mu$ moles) in 6 mL C<sub>6</sub>H<sub>6</sub> was stirred with 751 mg (67.8  $\mu$ moles available O<sub>2</sub>) NiO<sub>2</sub> for 23 h at 25 °C yielded oxidation product **48** (2.5 mg; 26%

recovered) as a clear colorless solid. LR FAB MS (glycerol):  $m/z$  805 (M+H)<sup>+</sup>, 777, 680, 527, 484, 399, 297; HR FAB MS (glycerol):  $m/z$  805.3017 (M+H)<sup>+</sup>, C<sub>39</sub>H<sub>49</sub>N<sub>8</sub>O<sub>5</sub>S<sub>3</sub> requires 805.2988; NMR Data contained in Table 4.3.

#### Ozonolysis of Tawicyclamide A

A slow stream of O<sub>3</sub> was bubbled into a 10 mL CH<sub>2</sub>Cl<sub>2</sub> solution of **45** (1.5 μmoles) placed in a threaded bomb at 25 °C for approximately 15 min. Upon removal of the solvent under a stream of N<sub>2</sub>, the residue was subjected to hydrolysis and derivatization as described below.

#### Stereochemistry of Tawicyclamide A

Coinjection with standard amino acid derivatives established the presence of L-proline, L-valine and L-phenylalanine in the hydrolysate of **45**. One additional equivalence of L-valine and D-isoleucine were further discovered in the hydrolysate of ozonized **45**.

#### Stereochemistry of Tawicyclamide B

HPLC analysis of the FDAA derivatized hydrolysate of **46** revealed the presence of L-proline, L-valine and L-leucine.

#### Molecular Modeling Studies on Tawicyclamide B and Dehydrotawicyclamide B

Molecular modeling studies were carried out using QUANTA/CHARMm<sup>201,202</sup> version 3.2.3 implementation of a molecular mechanics force field. The effect of solvent was approximated by using a constant dielectric of 2.284 (benzene), and all energy terms were calculated. Modeling involved a minimization-molecular dynamics-minimization protocol. The structures were subjected to Adopted-Basis-set Newton-Raphson energy minimization which was terminated when the energy value gradient between cycles was less than 0.001 kcal/mol.. The nonbonded interactions were switched off between 6.5 and 7.5 Å with atom pairs up to 8 Å included in the nonbonded list. The time step of integration was 1 fs



and the nonbonded integration list was updated every 25 fs. Bond lengths involving hydrogen atoms were kept fixed using the SHAKE<sup>203</sup> algorithm. Typical molecular dynamics simulations involved a 1 ps heating period during which time the system was heated to 300 K or 1000 K followed by a 1 ps equilibration period then 10 ps of dynamics simulation at the appropriate elevated temperature. Energy barrier to rotation was calculated by constraining the valine-proline dihedral to  $-90^\circ$  and minimizing. The energy of this structure without constraints less the energy of the unconstrained energy minimized *cis* structure is taken as the barrier to rotation.

### The Chemistry of *Botryllus* sp.

#### Collection, Extraction, and Isolation of Botryllamide D

The encrusting colonial Styelidae ascidian belonging to the genus *Botryllus*<sup>128</sup> was collected by SCUBA (-10 m) in April 1991 near Siquijor Island, Philippines and was kept frozen until extracted. This specimen was collected as part of an NCDDG<sup>204</sup> program. The frozen animals (10 g) were repeatedly extracted with MeOH to give 1.01g of a yellow residue after evaporation of solvent. Flash chromatography, employing a step gradient with increasing percentages of MeOH in water, yielded crude botryllamide D in a fraction eluting with 70% MeOH from a reversed phase C18 column. Reversed phase HPLC (Rainin Dynamax-Microsorb C18, 4.6 x 250 mm, 70:30 MeOH/H<sub>2</sub>O, 3.0 mL/min) yielded pure botryllamide D (**53**).

#### Physical and Spectral Properties of Botryllamide D

Yellow oil (7.1 mg, 0.07% yield based on wet weight); IR (film):  $\nu_{\max}$  3250 (br), 3072, 3008, 2932, 2836, 1672, 1602, 1513, 1493, 1486, 1257, 1236, 1163, 1051, and 1020  $\text{cm}^{-1}$ ; UV(MeOH):  $\lambda_{\max}$  225 nm (sh)  $\epsilon = 10514$ , 306.4 nm (br),  $\epsilon = 13229$ ; LR FAB MS (Positive ion, glycerol):  $m/z$  404&406 (~1:1, (M+H)<sup>+</sup>), 225, 177, 149, 134 (base), and 133; LR FAB MS (Negative ion, glycerol):  $m/z$  402&404 (~1:1, (M-H)<sup>-</sup>), 325; LR EI MS:  $m/z$  403&405 (~1:1, M<sup>+</sup>), 325, 227&229, 212&214, 193, 177, 149, and 134 (see

Figure 5.1); HR EI MS:  $m/z$  403.0439 ( $M^+$ ),  $C_{19}H_{18}O_4N^{79}Br$  requires 403.0420; NMR data contained in Table 5.1.

#### Preparation of 1-Methoxybotryllamide D

Compound **53** (1.7 mg,  $4.2 \times 10^{-6}$  moles) was dissolved in 400  $\mu$ L acetone to which 1.2 mL glyme containing  $CH_2N_2$  was added. The solution was stirred at 24 °C for 21 h. TLC on C18 support (80:20 MeOH/H<sub>2</sub>O) showed quantitative conversion to a slower moving product characterized as 1-methoxybotryllamide D (**57**).

#### Physical Properties of 1-Methoxybotryllamide D

Proton NMR data for 1-methoxybotryllamide D (**57**) in DMSO- $d_6$ : 3.79 (1-OMe, s); 6.99 (H2, d,  $J = 8.8$  Hz); 7.70 (H3, d,  $J = 8.8$  Hz); 6.64 (H5, s); 10.53 (H8, d,  $J = 9.6$  Hz); 7.41 (H9, dd,  $J = 14.7, 9.6$  Hz); 6.44 (H10, d,  $J = 14.7$  Hz); 7.56 (H12, d,  $J = 2.1$  Hz); 7.04 (H15, d,  $J = 8.6$  Hz); 7.36 (H16, dd,  $J = 8.6, 2.1$  Hz); 3.83 (H17, s); 3.62 (H18, s).

#### Collection and Isolation of Botryllamides B, C, and A

A second collection of the ascidian (69 g wet wt, 6 g dry wt) that was made in July, 1993 yielded in addition to botryllamide D, three new botryllamides. The specimen was soaked in MeOH and yielded a rich yellow solution which was concentrated to a residue. The residue was chromatographed on C18 support using a step gradient comprised of water with increasing amounts of MeOH. The fraction eluting from C18 with 60:40 MeOH/H<sub>2</sub>O was further purified by flash chromatography on C18 using a mobile phase of 70:30 MeOH/H<sub>2</sub>O to yield 9.5 mg **53**. Another fraction eluting from C18 with 70:30 MeOH/H<sub>2</sub>O was also purified by flash chromatography on C18 using a mobile phase of 70:30 MeOH/H<sub>2</sub>O to yield 20.5 mg additional **53**, 55.5 mg botryllamide C (**55**), and 15.8 mg botryllamide B (**54**). The fraction eluting from C18 with 80:20 MeOH/H<sub>2</sub>O was

further purified by flash chromatography on C18 using a mobile phase of 70:30 MeOH/H<sub>2</sub>O to yield 120 mg Botryllamide A (**56**).

#### Physical and Spectral Properties of Botryllamides B, C, and A

The botryllamide D (**53**, 30.0 mg, 0.04% yield based on wet weight) isolated from the second collection of the ascidian showed spectroscopic properties identical to those reported above.

#### Botryllamide B (**54**)

Yellow powder (15.8 mg, 0.02% yield based on wet weight); LR EI MS: *m/z* 481&483&485 (~1:2:1, M<sup>+</sup>), 177, 149, and 134 (base); C<sub>19</sub>H<sub>17</sub>O<sub>4</sub>N<sup>79</sup>Br<sub>2</sub> requires 480.9524; Proton NMR data contained in Table 5.2.

#### Botryllamide C (**55**)

Yellow powder (55.5 mg, 0.08% yield based on wet weight); LR EI MS: *m/z* 403&405 (~1:1, M<sup>+</sup>), 325, 227&229, 212&214, 177, 149, and 134 (base); C<sub>19</sub>H<sub>18</sub>O<sub>4</sub>N<sup>79</sup>Br requires 403.0420; Proton NMR data contained in Table 5.2.

#### Botryllamide A (**56**)

Yellow powder (120.0 mg, 0.17% yield based on wet weight); LR EI MS: *m/z* 481&483&485 (~1:2:1, M<sup>+</sup>), 177, 149, and 134 (base); C<sub>19</sub>H<sub>17</sub>O<sub>4</sub>N<sup>79</sup>Br<sub>2</sub> requires 480.9524; Proton NMR data contained in Table 5.2.

APPENDIX A

NMR SPECTRA OF COMPOUNDS FROM *CYSTODYTES* SP.

Dehydrokuanoniamine B Proton Spectrum

exp1 pulse sequence: s2pul

SAMPLE	DEC. & VT	
date	May 24 91	cn H1
solvent	dmso	dof 0
file	/disk4/mc~	cn nnn
donald/kuanoniamin~	dmf	cn c
e/63-6Aproton	dmf	200
ACQUISITION	temp	20.0
sfrq	499.843	PROCESSING
tn	H1	fn 65536
at	2.653	math f
np	32000	
sw	6031.4	warr wft
fb	3400	warp
pw	9.2	wbs
pw	9.2	wnt
tpwr	62	DISPLAY
dl	1.500	sp 23.7
tof	539.7	wp 6031.4
nt	64	vs 230
ct	64	sc 15
alock	n	wc 150
gain	20	hzmm 40.21
FLAGS	is	244.56
il	n	rfl 1220.9
in	n	rfp 1244.6
dp	y	th 120
hs	nn	ins 27.000
	ai	cdc ph

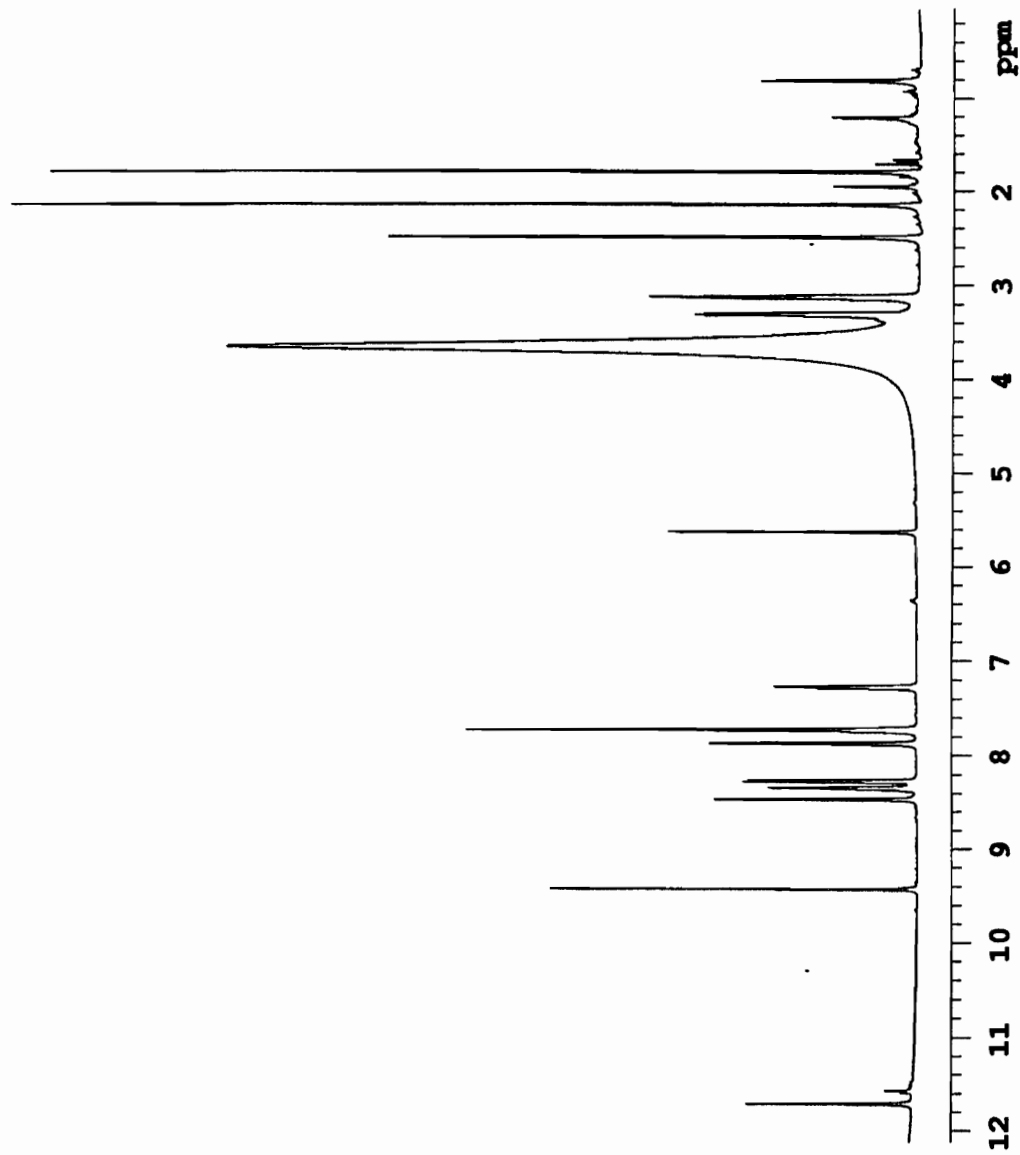


Figure A1. 500 MHz proton spectrum of dehydrokuanoniamine B

Dehydrokuanoniamine B Carbon Spectrum

exp1 pulse sequence: s2pul

SAMPLE	DEC. & VT	
date	May 30 91	dn R1
solvent	DMSO	dof 539.7
file	/disk4/sc~ dn	Y
donald/Kuanoniamin- dnm		W
e/63-6Acarbon dmf		12200
ACQUISITION	dpwz	52
sfrq	125.697	temp 25.0
tn	C13	PROCESSING
st	1.179	lb 1.00
np	59264	fn 65536
sw	25125.6	math f
fb	13900	
bs	16	werr
pw	8.0	wexp
pw	8.0	wbs
tpwz	62	wnt
di	10.000	DISPLAY
tof	750.3	sp 38.7
nt	20000	wp 25125.6
ct	4658	vs 3303
alock	n	sc 15
gain	not used	wc 150
FLAGS	hzm	167.50
il	n	is 500.00
in	n	rfl 4926.3
cp	Y	rff 4965.0
hs	nn	th 120
	ins	1.000
	nm	cdc
	ph	

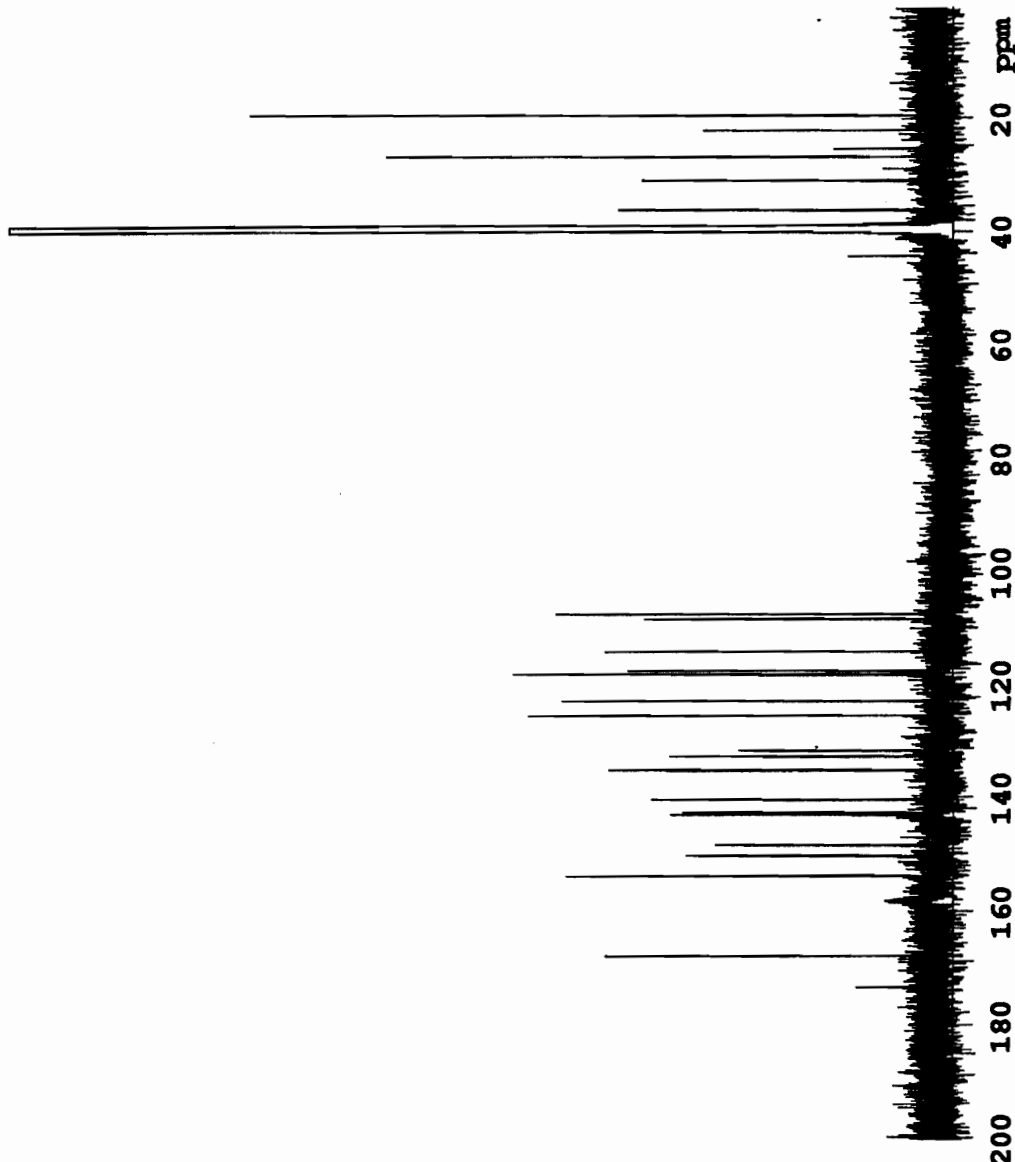
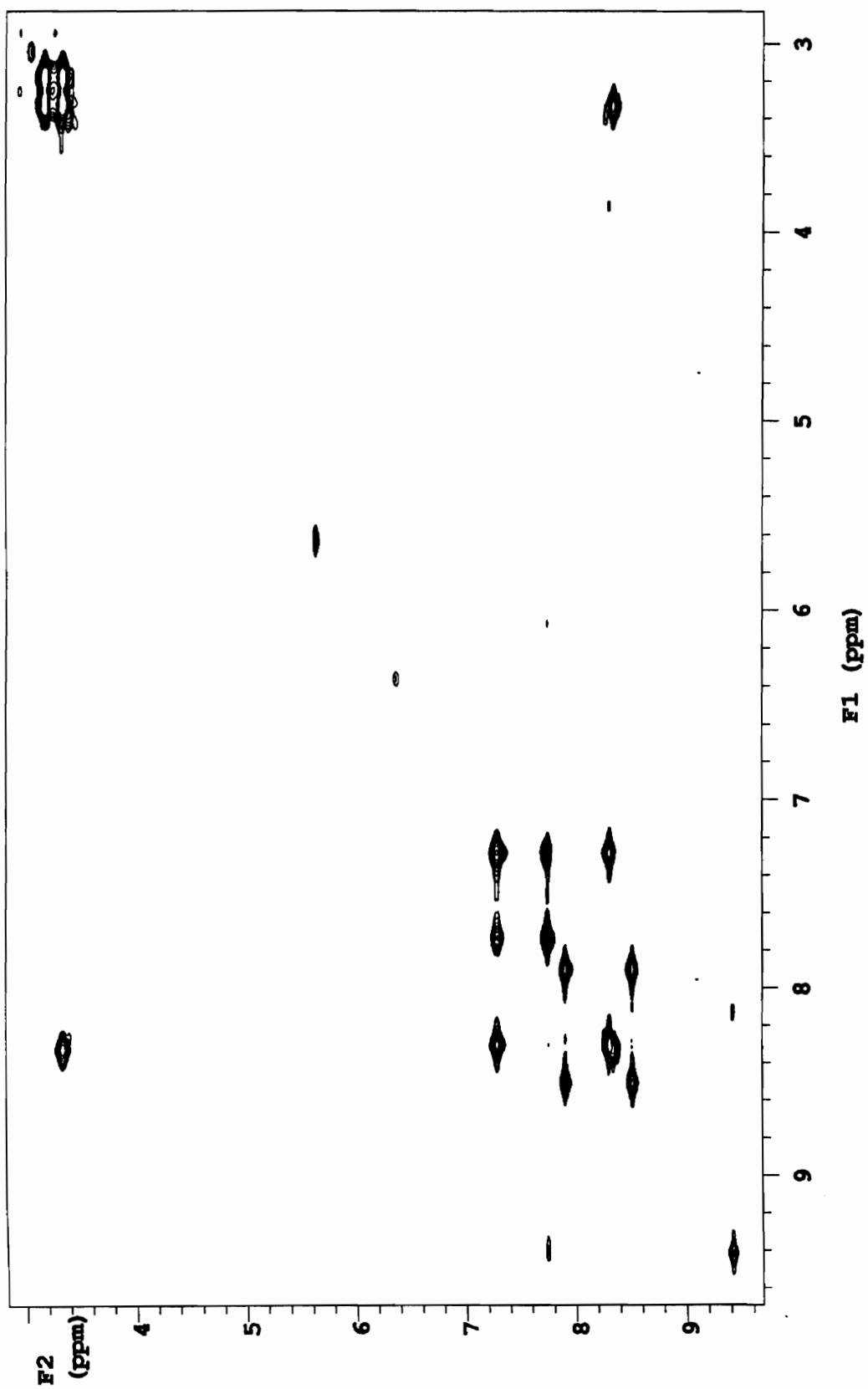


Figure A2. 125 MHz carbon spectrum of dehydrokawicyclamide B.



## Dehydrokuanoniamine B COSY Spectrum

exp5 pulse sequence: dqcosy

SAMPLE		DEC. & VT		ACQUISITION ARRAYS	
date	May 15 91	dn		H1	
solvent	DMSO	dof		0	
file	/disk4/mc~	dm		nnn	
donaId/Kuanoniamin~		dmm		c	phase
e/dehydro_cosy		dmf		200	1
ACQUISITION		temp		27.0	2
sfrq	499.843		PROCESSING		
tn		H1	gf	0.071	
at	0.170		gfs	not used	
np	2048		wtfile		
sw	6031.4		proc	ft	
fb	3400		fn	2048	
bs	16		math	f	
ss	8				
tpwr	62		werr		
pw	9.2		wexp		
d1	1.500		wbs		
presat	0		wnt		
tof	539.7		2D PROCESSING		
nt	16		gfl	0.021	
ct	16		gfl	not used	
alock		n	wtfile1		
gain	25		procl	ft	
	FLAGS		fnl	2048	
il		n	DISPLAY		
in		n	sp	1415.1	
dp		y	wp	3425.4	
hs		nn	vs	286	
sspul		y	sc	20	
	2D ACQUISITION		wc	205	
sw1	6031.4		hzmm	16.71	
ni	300		is	500.00	
phase	arrayed		rfl	1220.9	
	2D DISPLAY		rfl	1244.6	
sp1	1415.1		th	3	
wp1	3425.4		ins	1.000	
sc2	18		ai cdc av		
wc2	120				
rfl1	1220.9				
rfl1	1220.9				
rfl1	1220.9				
rfl1	1220.9				
rfl1	1220.9				
rfl1	1220.9				
rfl1	1220.9				
rfl1	1220.9				
rfl1	1220.9				

Figure A4. Parameter set for 500 MHz COSY spectrum of dehydrokuanoniamine B.



Shermilamine C Proton Spectrum

exp1 pulse sequence: s2pul

SAMPLE	Jun 12 91	dn	H1
date	Jun 12 91	dn	H1
solvent	dmso	dof	0
file	/disk4/mc-dm	dm	nnn
donald/temp/shermi-	dm	dm	c
lamines/sherm-c-pr-	dmf	dmf	200
oton temp	25.0		
DEC. & VT			
ACQUISITION	499.843	fn	65536
tn	H1	math	f
at	5.356		
np	65024	warr	
sw	6069.8	warp	wft
fb	3400	wbs	
pw	9.1	wnt	
pw	9.1	DISPLAY	
tpwr	62	sp	-54.9
dl	1.500	wp	6069.8
tof	481.3	vs	91
nt	32	sc	15
ct	32	wc	150
alock	n	hzmm	40.47
gain	20	is	244.56
FLAGS	rfl		1299.5
il	n	rfp	1244.6
in	n	th	120
dp	y	ins	27.000
hs	nn	ai	oda
			ph

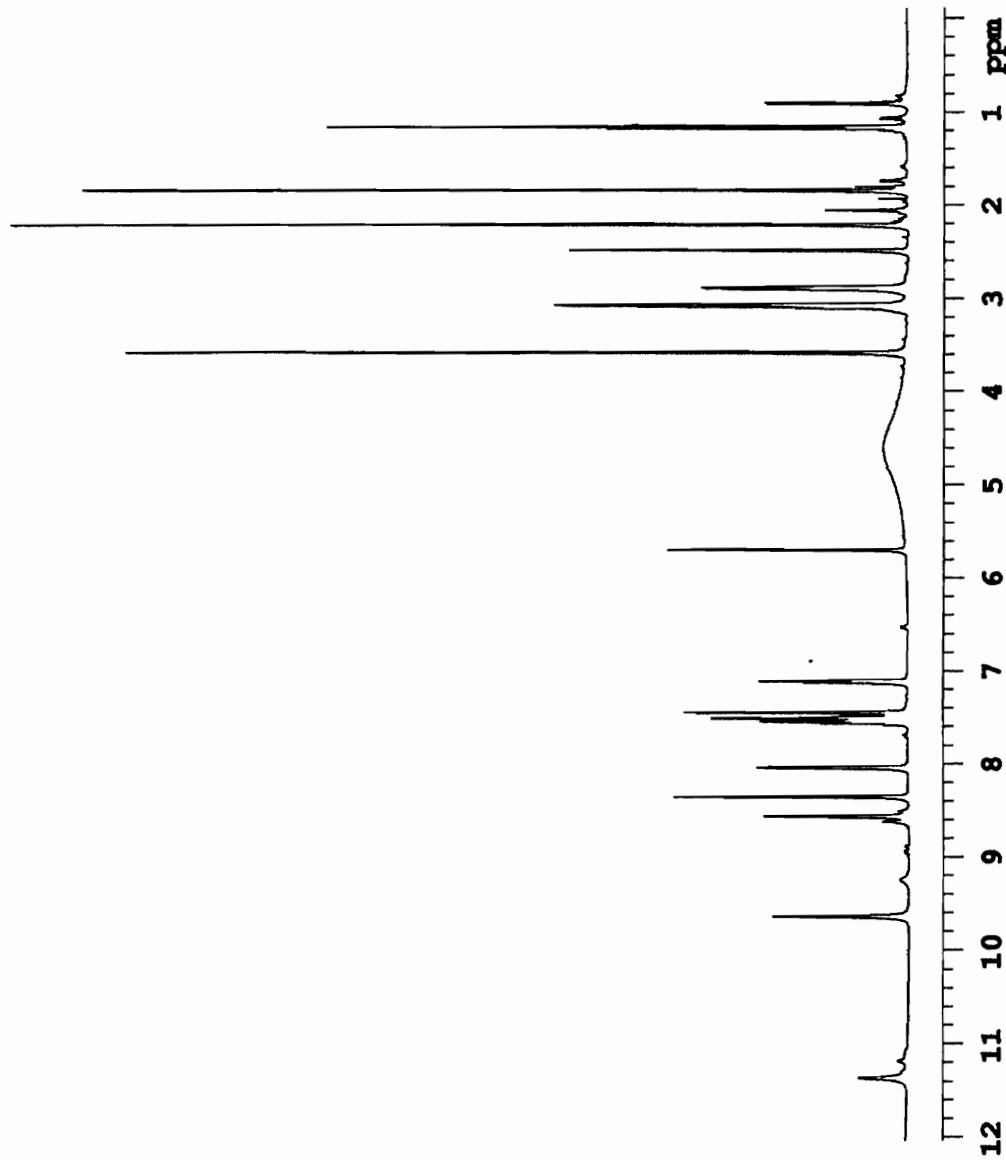


Figure A5. 500 MHz proton spectrum of shermilamine C.

Shermilamine C Carbon Spectrum

exp1 pulse sequence: s2pul

SAMPLE	DEC. & VT	
date	Jun 14 91	dn H1
solvent	DMSO	dof 481.3
file	/disk4/mc~ dn	y w
donald/temp/shermi~ dnm		12200
lamines/sherm-c-ca~ dmf		52
rbon dpwr		25.0
ACQUISITION	temp	25.0
sfreq	125.697	PROCESSING
tn	C13	lb 1.00
at	1.284	fn 65536
np	68096	math f
sw	26507.6	
fb	14600	werr
bs	16	wexp
pw	8.0	wbs wft
pw	8.0	wnt
tpwr	62	DISPLAY
dl	5.000	sp -9.0
tof	1392.5	wp 26507.6
nt	100000	vs 2183
ct	2449	sc 15
alock	n	wc 150
gain	not used	hzmm 176.72
FLAGS		is 500.00
il	n	rfl 4974.0
in	n	rfp 4965.0
dp	y	th 120
bs	nn	ins 1.000
	nm	cdc ph

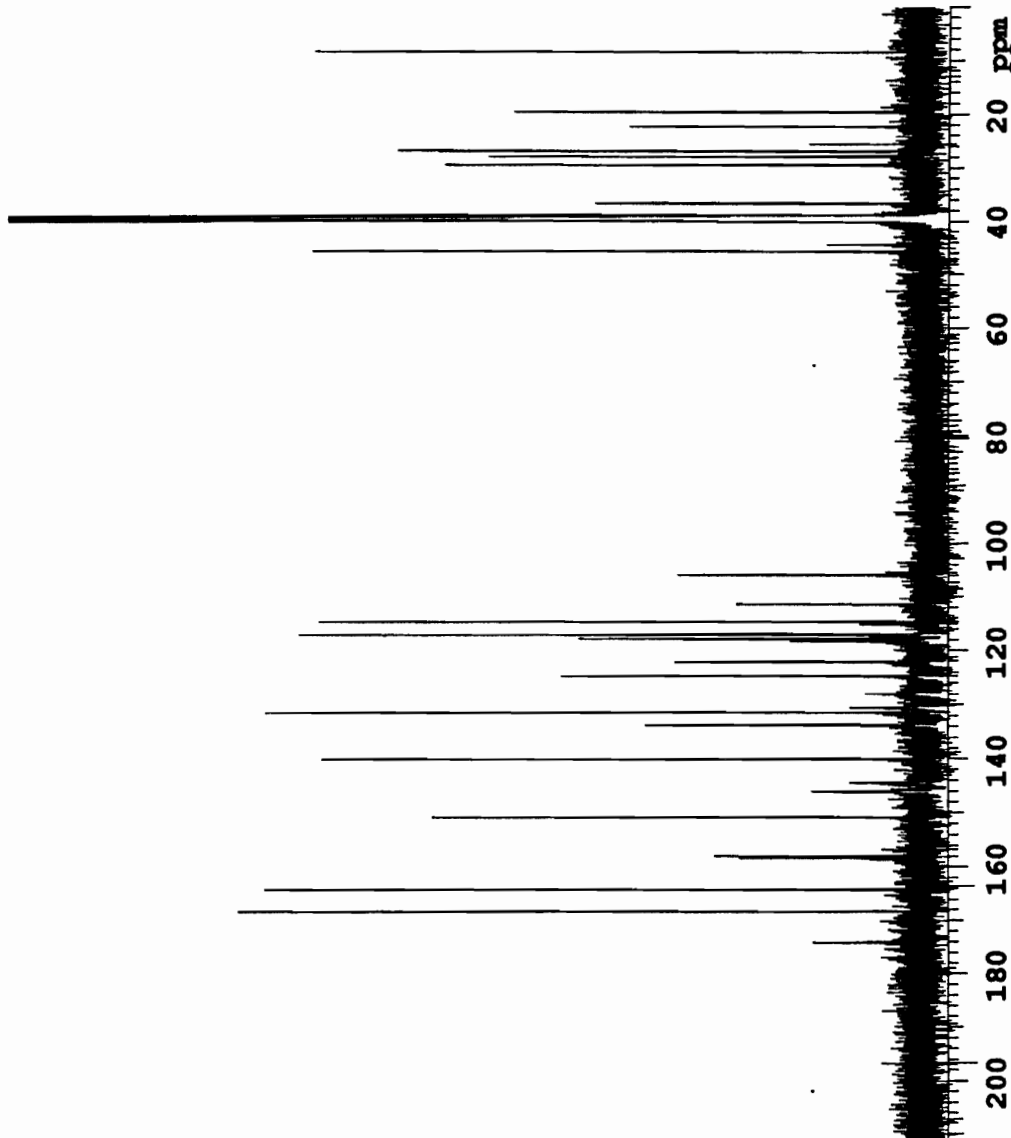
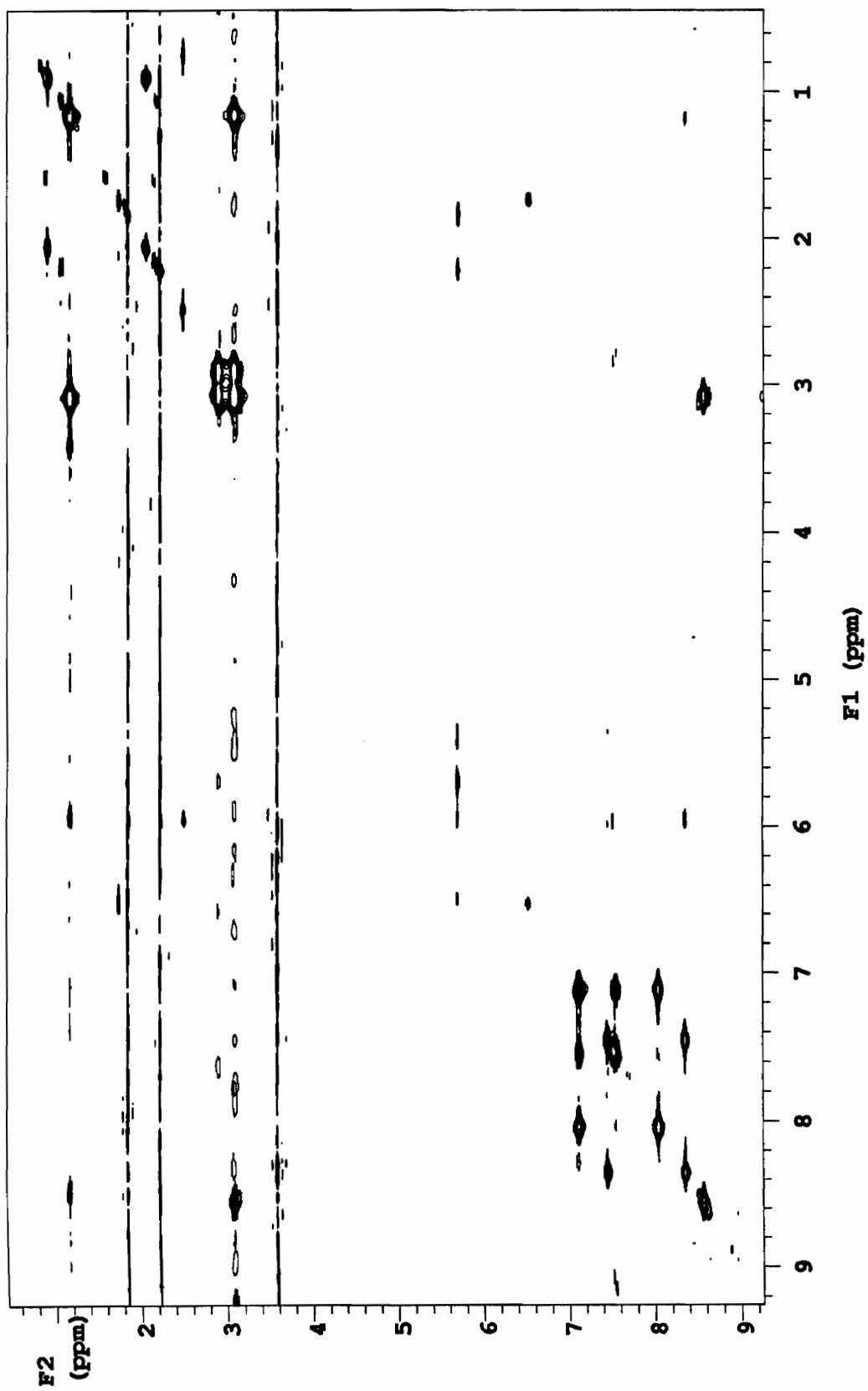


Figure A6. 125 MHz carbon spectrum of shermilamine C.



## Shermilamine C COSY Spectrum

expl pulse sequence: dqcosy

SAMPLE		DEC. & VT		ACQUISITION ARRAYS	
date	Jun 12 91	dn	H1	array	phase
solvent	DMSO	dof	0	arraydim	600
file	/disk4/mc~	dm	nnn		
donald/temp/shermi~	dmm	c	1	phase	
lamines/sherm-c-dq~	dmf	200	1	1	
	cosy	temp	25.0	2	2
ACQUISITION		PROCESSING			
sfrq	499.843	gf	0.138		
tn	H1	gfs	not used		
at	0.337	wtfile			
np	4096	proc	ft		
sw	6069.8	fn	4096		
fb	3400	math	f		
bs	8				
ss	8	werr			
tpwr	62	wexp			
pw	9.1	wbs			
dl	1.500	wnt			
presat	0	2D PROCESSING			
tof	481.3	gfl	0.021		
nt	8	gfl	not used		
ct	8	wtfile1			
alock	n	procl	ft		
gain	15	fnl	2048		
FLAGS		DISPLAY			
il	n	sp	223.9		
in	n	wp	4400.4		
dp	y	vs	115		
hs	nn	sc	20		
sspul	y	wc	205		
2D ACQUISITION		hzmm	21.48		
sw1	6069.8	is	500.00		
ni	300	rfl	1299.5		
phase	arrayed	rfp	1244.6		
2D DISPLAY		th	2		
sp1	224.0	ins	1.000		
wp1	4402.5	ai cdc av			
sc2	18				
wc2	120				
rf11	1299.5				
rfp1	1244.6				

Figure A8. Parameter set for 500 MHz COSY spectrum of shermilamine C.

Cystodytin J Proton Spectrum

exp1 pulse sequence: s2pul

SAMPLE	DEC. & VT	
date Jun 15 91	dn H1	
solvent cdcl3	dof 0	
file /disk4/mc~ dm	nnn	
donald/cystodytin~~ dnm	c	
D/cysto-D-proton dmf	200	
ACQUISITION temp	25.0	
sfreq 499.843	PROCESSING	
tn H1	fn 65536	
at 7.548	math f	
rp 65024		
sw 4307.1	weir	wft
fb 2400	wexp	
pw 9.2	wbs	
pw 9.2	wnt	
tpwz 62	DISPLAY	
dl 0	sp 327.1	
tof -5.0	wp 4307.1	
nt 32	vs 43	
ct 32	sc 15	
alock n	wc 150	
gain 30	hzmm 28.71	
FLAGS	is 500.00	
il n	rfl 3291.8	
in n	rfp 3618.9	
cp y	th 120	
hs nn	ins 1.000	
	ai cdc ph	

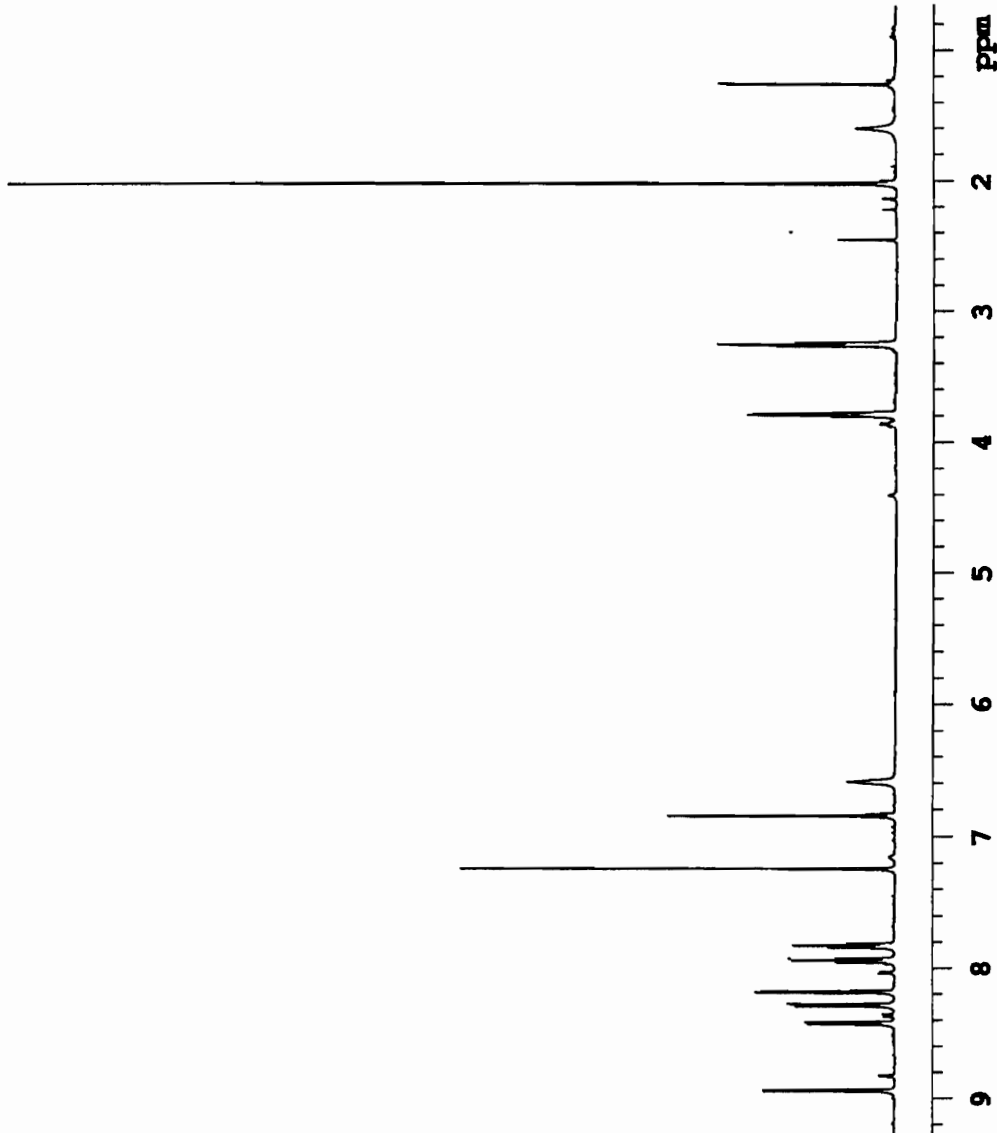


Figure A9. 500 MHz proton spectrum of cystodytin J.

Cystodytin J Carbon Spectrum

exp1 pulse sequence: s2pul

SAMPLE	DEC. & VT	
date	Jun 14 91	dn H1
solvent	CDCL3	dof 127.0
file	/disk4/mc~ dm	Y
donald/cystodytin-- dnm		W
D/cysto-D-carbon dmf	12200	
ACQUISITION	dpwr 52	
sfreq	125.697	temp 25.0
tn	CL3	PROCESSING
at	1.285	lb 2.00
np	64000	fn 65536
sw	24906.6	math f
fb	13700	
bs	16	werr
pw	8.0	wexp
pw	8.0	wbs
tpwr	62	wnt
dl	5.000	DISPLAY
tof	644.7	sp 104.3
nt	1e+06	wp 24906.6
ct	5488	vs 540
alock	n	sc 15
gain	not used	wc 150
FLAGS	hmm	166.04
il	n	is 500.00
in	n	rfl 9574.4
dp	Y	rfp 9678.7
hs	nn	th 120
	ins	1.000
	nm	cdc ph

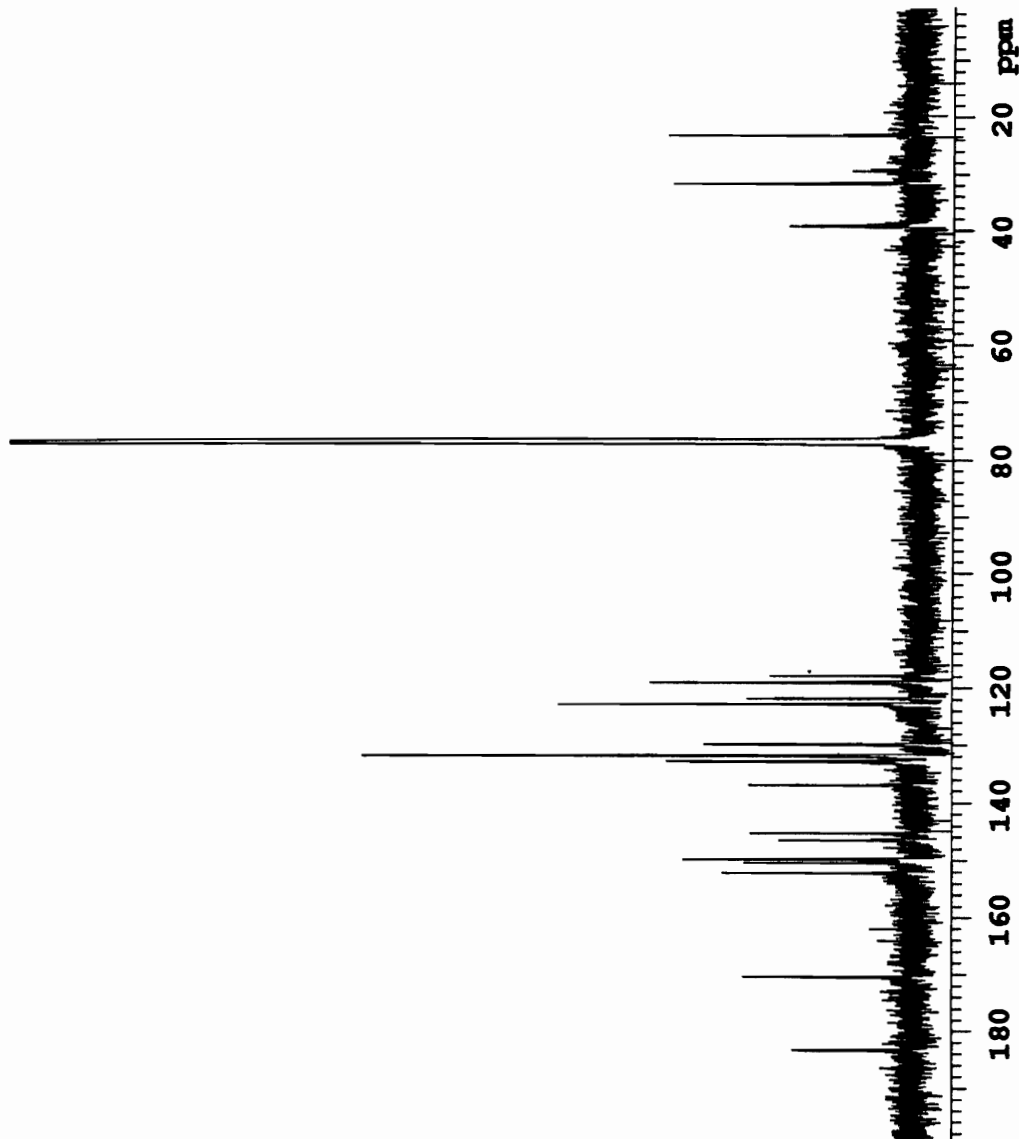


Figure A10. 125 MHz carbon spectrum of cystodytin J.

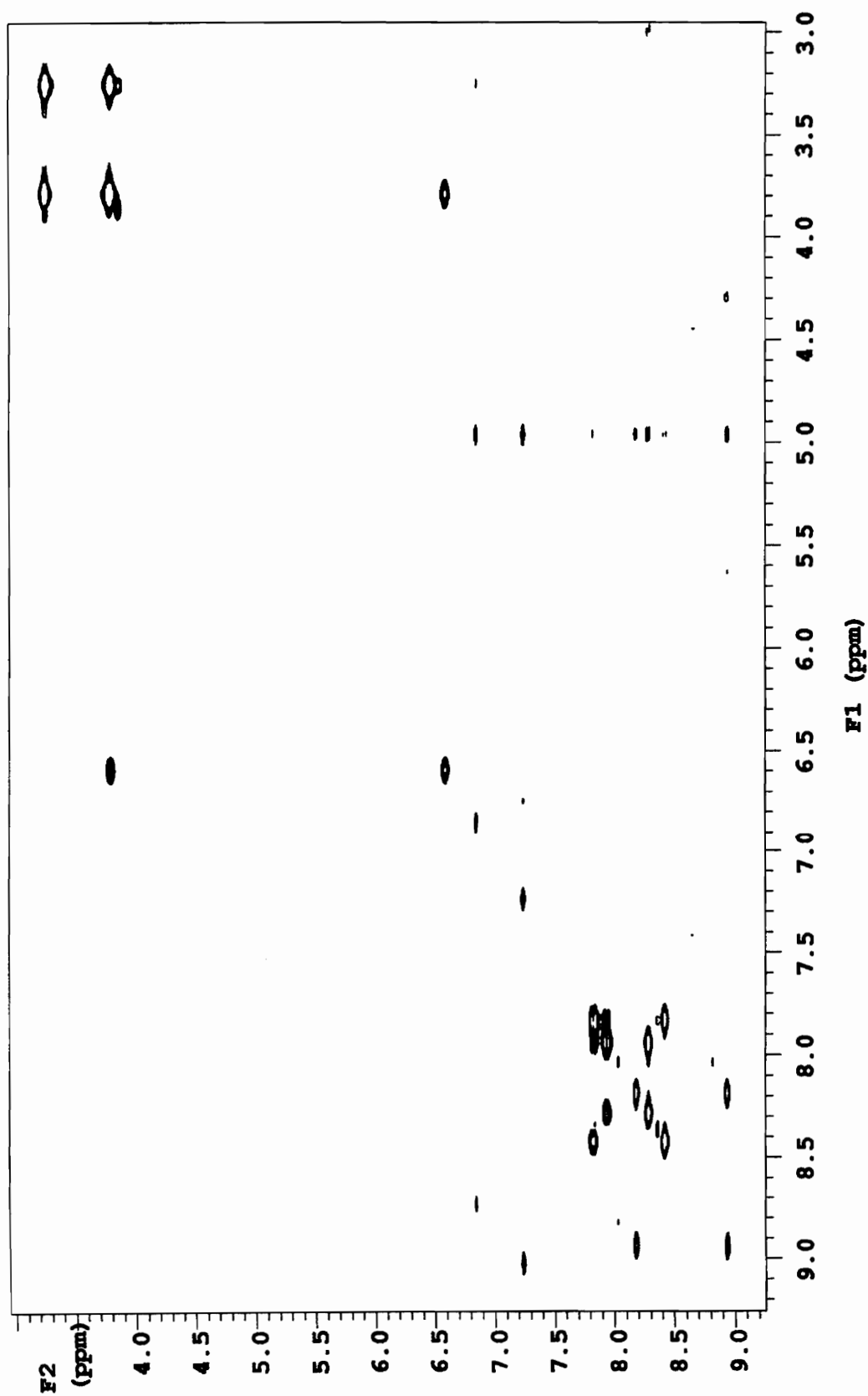


Figure A11. 500 MHz COSY spectrum of cystodytin J.

## Cystodytin J COSY Spectrum

exp7 pulse sequence: dqcosy

SAMPLE		DEC. & VT		ACQUISITION ARRAYS	
date	Jun 15 91	dn	H1	array	phase
solvent	cdcl3	dof	0	arraydim	512
file	/disk4/mc~	dm	nnn		
donald/temp/tapel/~	dmm	c		i	phase
cystodytin-D/cysto~	dmf	200		1	1
	J_cosy	temp	25.0	2	2
ACQUISITION		PROCESSING			
sfrq	499.843	gf	0.097		
tn	H1	gfs	not used		
at	0.238	wtfile			
np	2048	proc	ft		
sw	4307.1	fn	2048		
fb	2400	math	f		
bs	16				
ss	8	warr			
tpwr	62	wexp			
pw	9.2	wbs			
dl	1.500	wnt			
presat	0	2D PROCESSING			
tof	-5.0	gfl	0.024		
nt	16	gfs1	not used		
ct	16	wtfile1			
alock	n	procl	ft		
gain	25	fn1	2048		
FLAGS		DISPLAY			
il	n	sp	1476.5		
in	a	wp	3149.3		
cp	y	vs	300		
hs	n	sc	20		
sspul	n	wc	205		
2D ACQUISITION		hzmm	15.36		
sw1	4307.1	is	500.00		
ni	256	rfl	3291.8		
phase	arrayed	rfp	3618.9		
2D DISPLAY		th	5		
sp1	1476.5	ins	1.000		
wp1	3149.3	ai cdc av			
sc2	18				
wc2	120				
rfl1	3291.8				
rfl1	3618.9				

Figure A12. Parameter set for 500 MHz COSY spectrum of cystodytin J.



APPENDIX B

NMR SPECTRA OF COMPOUNDS FROM *LISSOCLINUM*

*PATELLA*

Patellamide E Proton Spectrum

exp1 pulse sequence: s2pul

SAMPLE	DEC. & VT	
date	Oct 25 90	dn H1
solvent	cdcl3	dof 0
file	/disk4/mc- dm	nnn
donald/patellamide- dmm		c
-E/pate-proton dmf		200
ACQUISITION	PROCESSING	
sfrq	499.843	lb not used
tn	H1	gf not used
at	3.704	gfs not used
np	28480	fn 65536
sw	3844.7	math f
fb	2200	
pw	10.2	verz
pw	10.2	verp wft
tpwr	60	wbs
dl	0	wnt
tof	-326.0	DISPLAY
nt	64	sp 236.6
ct	64	wp 3844.7
alock	n	vs 480
gain	8	sc 15
FLAGS	wc 150	
il	n	hzmm 25.63
in	n	is 500.00
dp	y	rfl 3382.3
hs	nn	rfp 3618.9
	th	120
	ins	1.000
	ai	cdc ph

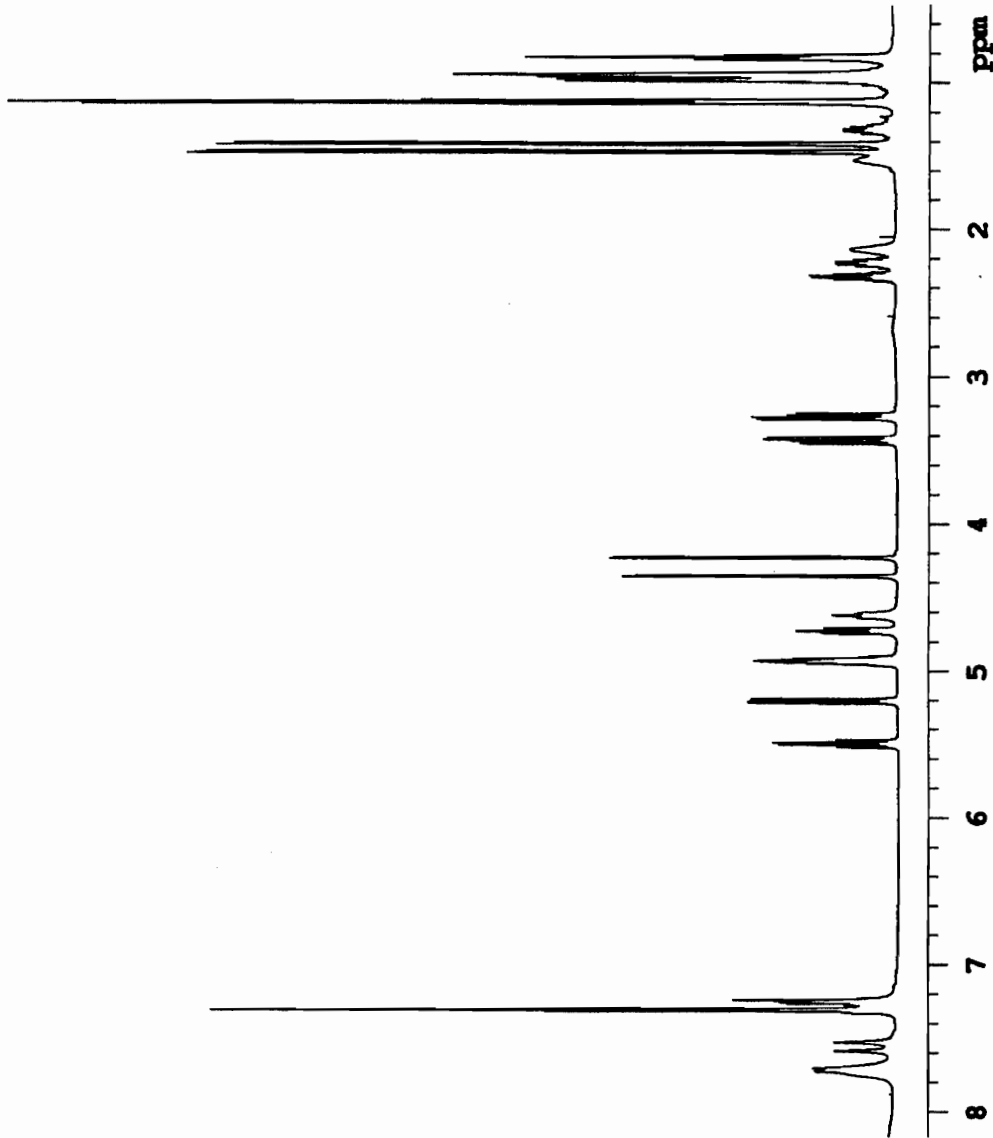


Figure B1. 500 MHz proton spectrum of patellamide E.

Patellamide E Carbon Spectrum

expl pulse sequence: s2pul

SAMPLE	DEC. & VT		
date	Dec 26 90	dn	H1
solvent	cdcl3	dof	-326.0
file	/disk4/mc~	dn	Y
donald/patellamide~	dnm	w	
-E/patE-carbon	dmf		12200
ACQUISITION	cpwr		52
sfrq	125.697	temp	26.0
tn	C13	PROCESSING	
at	0.706	lb	0.50
np	32000	fn	65536
sw	22662.9	math	f
fb	12500		
bs	16	warr	
pw	8.0	wexp	
pw	8.0	wbs	wft
tpwr	62	wnt	
dl	2.000	DISPLAY	
tof	-586.7	sp	-21.5
nt	1024	vp	22662.9
ct	1024	vs	117
alock	n	sc	15
gain	25	wc	150
FLAGS		hnm	151.09
il	n	is	500.00
in	n	rfl	9700.2
cp	Y	rfp	9678.7
hs	nn	th	23
	ins		1.000

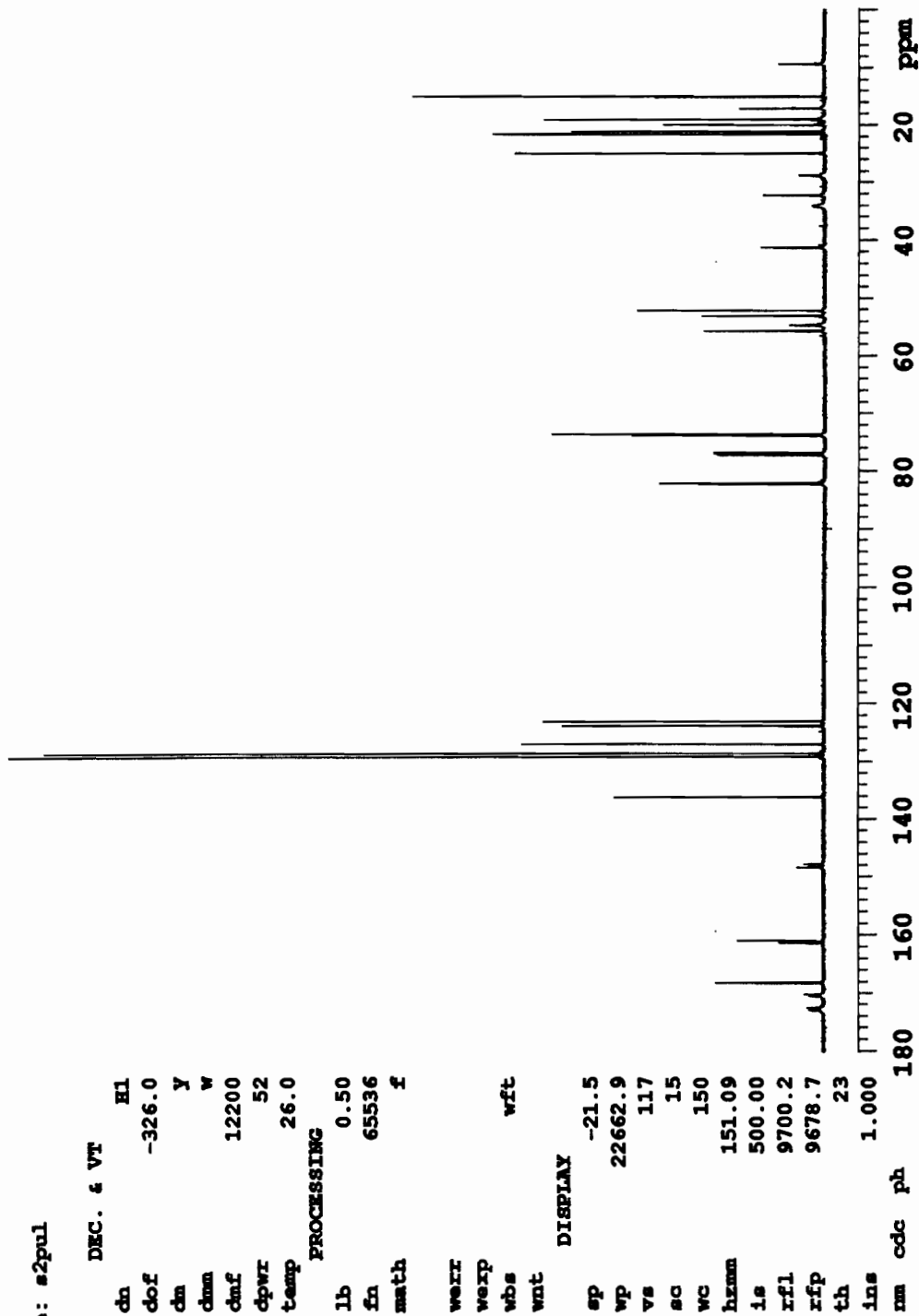


Figure B2. 125 MHz carbon spectrum of patellamide E.

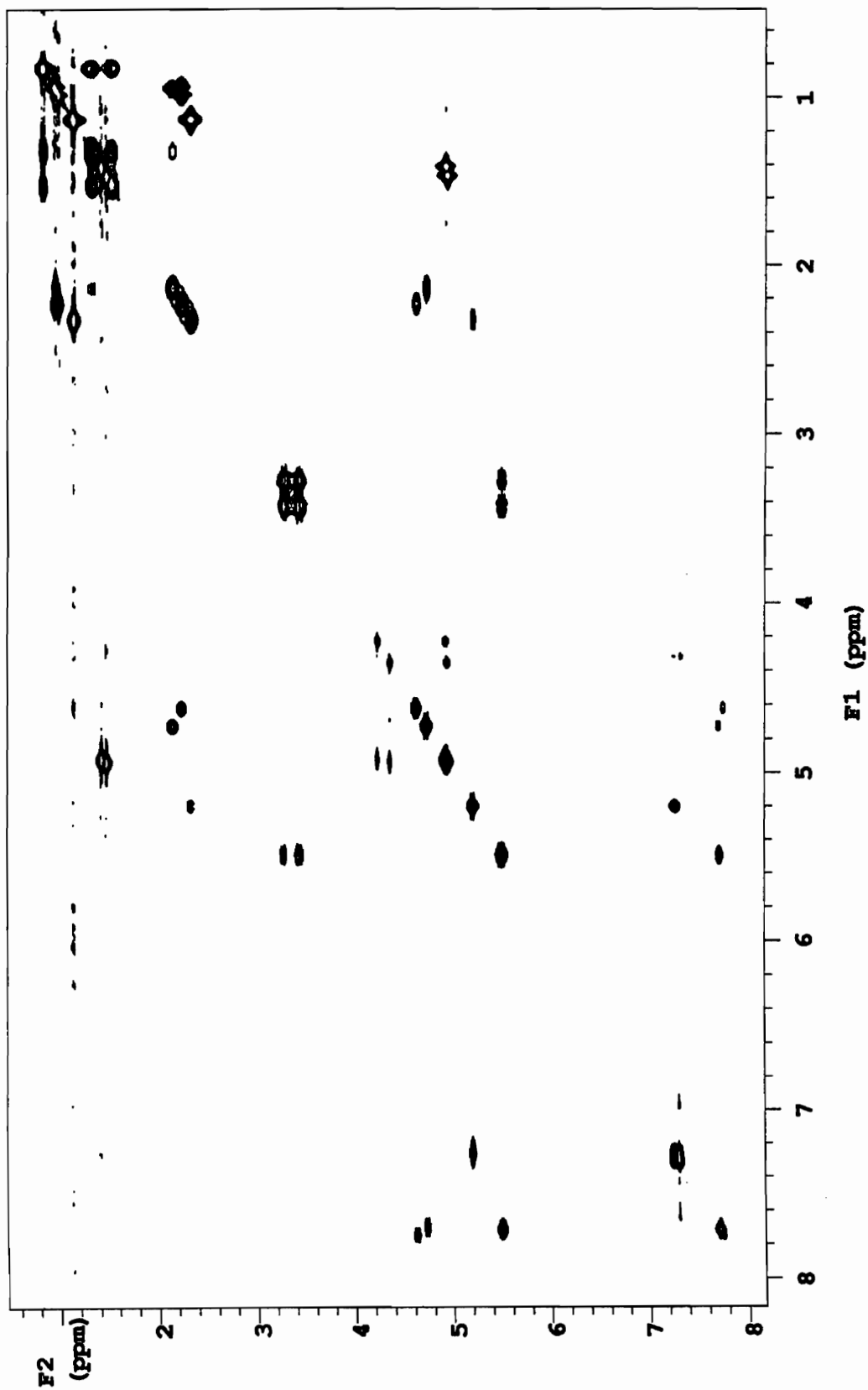


Figure B3. 500 MHz COSY spectrum of patellamide E.

## Patellamide E COSY Spectrum

expl pulse sequence: dqcosy

SAMPLE		DEC. & VT		ACQUISITION ARRAYS	
date	Oct 25 90	dn	H1	array	phase
solvent	cdcl3	dof	0	arraydim	1024
file	/disk4/mc~	dm	nnn		
donald/patellamide~	dmm	c		1	phase
-E/patE-cosy	dmf	200		1	1
ACQUISITION		PROCESSING		2	2
sfrq	499.843	gf	0.230		
tn	H1	gfs	not used		
at	0.533	wtfile			
np	4096	proc	ft		
sw	3844.7	fn	4096		
fb	2200	math	f		
ss	8				
tpwr	60	werr			
pw	10.3	wexp			
d1	1.000	wbs			
presat	0	wnt			
tof	-326.0	2D PROCESSING			
nt	8	gfl	0.058		
ct	8	gfsl	not used		
alock	n	wtfile1			
gain	8	procl	ft		
FLAGS		fnl	2048		
il	n	DISPLAY			
in	n	sp	236.6		
dp	y	wp	3844.7		
hs	yn	vs	297		
sspul	y	sc	20		
2D ACQUISITION		wc	205		
sw1	3844.7	hzmm	18.75		
ni	512	is	500.00		
phase	arrayed	zfl	3382.3		
2D DISPLAY		rfl	3618.9		
sp1	236.6	th	3		
wp1	3844.7	ins	1.000		
sc2	18	ai cdc av			
wc2	120				
rfl1	3382.3				
rfl1	3618.9				

Figure B4. Parameter set for 500 MHz COSY spectrum of patellamide E.

Tawicyclamide A Proton Spectrum

expl pulse sequence: s2pul

SAMPLE	DEC. & VT	
date	Sep 8 90	dn H1
solvent	cdcl3	dof 0
file	/disk5/mc~	dm nnn
donald/tawicyclami~	dmn	c
de-A/tawi-A-proton	dmf	200
ACQUISITION	PROCESSING	
sfrq	499.843	fn 65536
tn	H1	math f
at	3.707	
np	32000	verr
sw	4315.9	wexp wft
fb	2400	wbs
pw	10.2	wnt
pw	10.2	DISPLAY
tpwz	60	sp 53.4
dl	0	wp 4315.9
tof	-257.9	vs 365
nt	16	sc 15
ct	16	wc 150
alock	n	hzmm 28.77
gain	8	ls 500.00
FLACS	rfl	3521.6
il	n	rfp 3575.0
in	n	th 120
cp	y	ins 1.000
hs	nn	al cdc ph

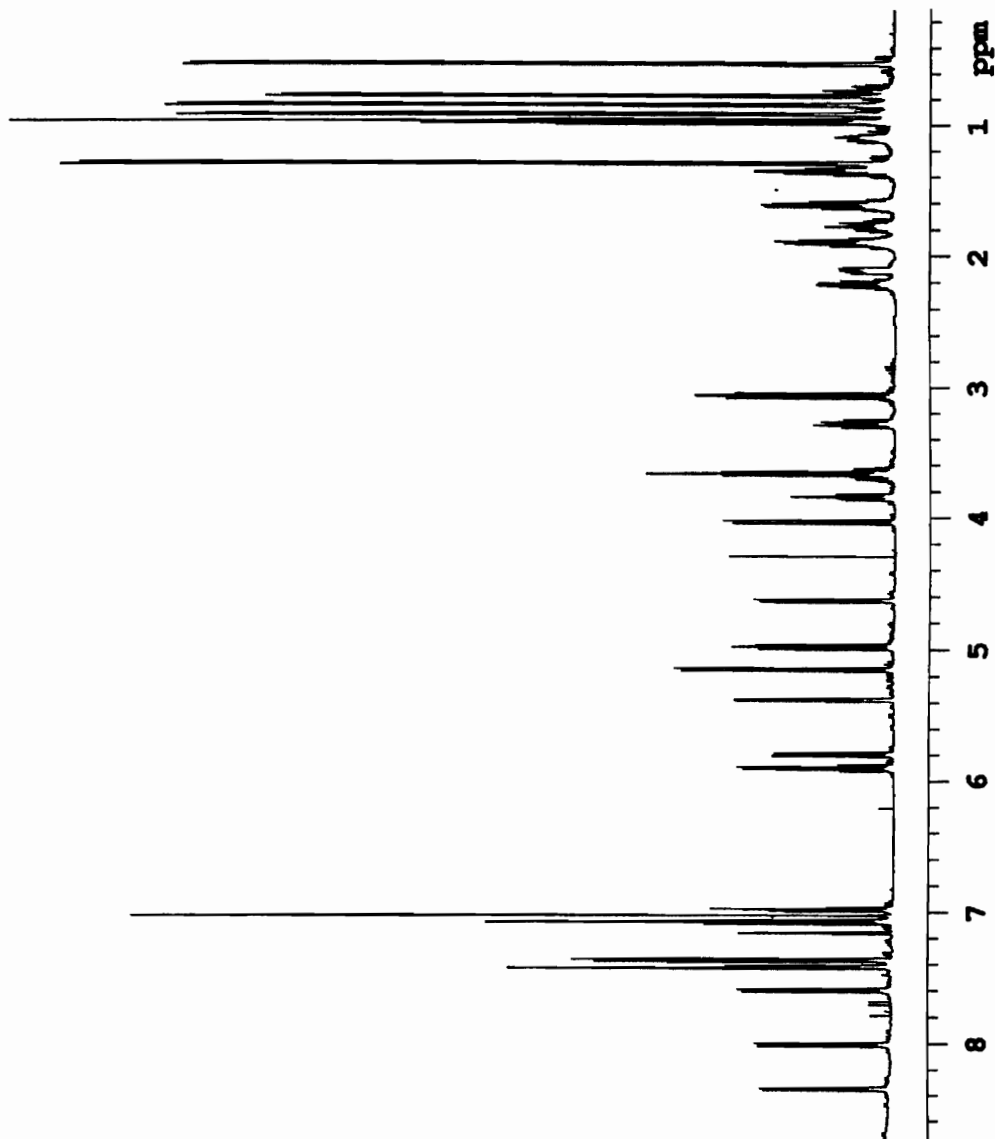


Figure B5. 500 MHz proton spectrum of tawicyclamide B.

## Tawicyclamide A Carbon Spectrum

exp1 pulse sequence: s2pul

date	Nov 8 90	dn	H1
solvent	c6d6	dof	-346.7
file	/disk5/mc~	dm	YYY
donald/tawicyclami~	chmn	s	
de-A/tawi-A-carbon	dmf	12200	
ACQUISITION	dpwr	52	
sfrq	125.697	temp	26.0
tn	C13	PROCESSING	
at	1.228	lb	1.00
np	65536	fn	not used
sv	26684.5	math	f
fb	14700		
bs	16	warz	
pw	8.0	wexp	
pw	8.0	wbs	sa
tpwr	58	wnt	
dl	2.000	DISPLAY	
tof	963.3	sp	-359.3
nt	2048	wp	26684.5
ct	749	vs	352
alock	n	sc	15
gain	45	wc	150
FLAGS		hrmn	177.90
il	n	is	0.12
in	n	rfl	16511.3
dp	y	rfp	16152.1
hs	nn	th	120
	ins		1.000
	nm	cdc	ph

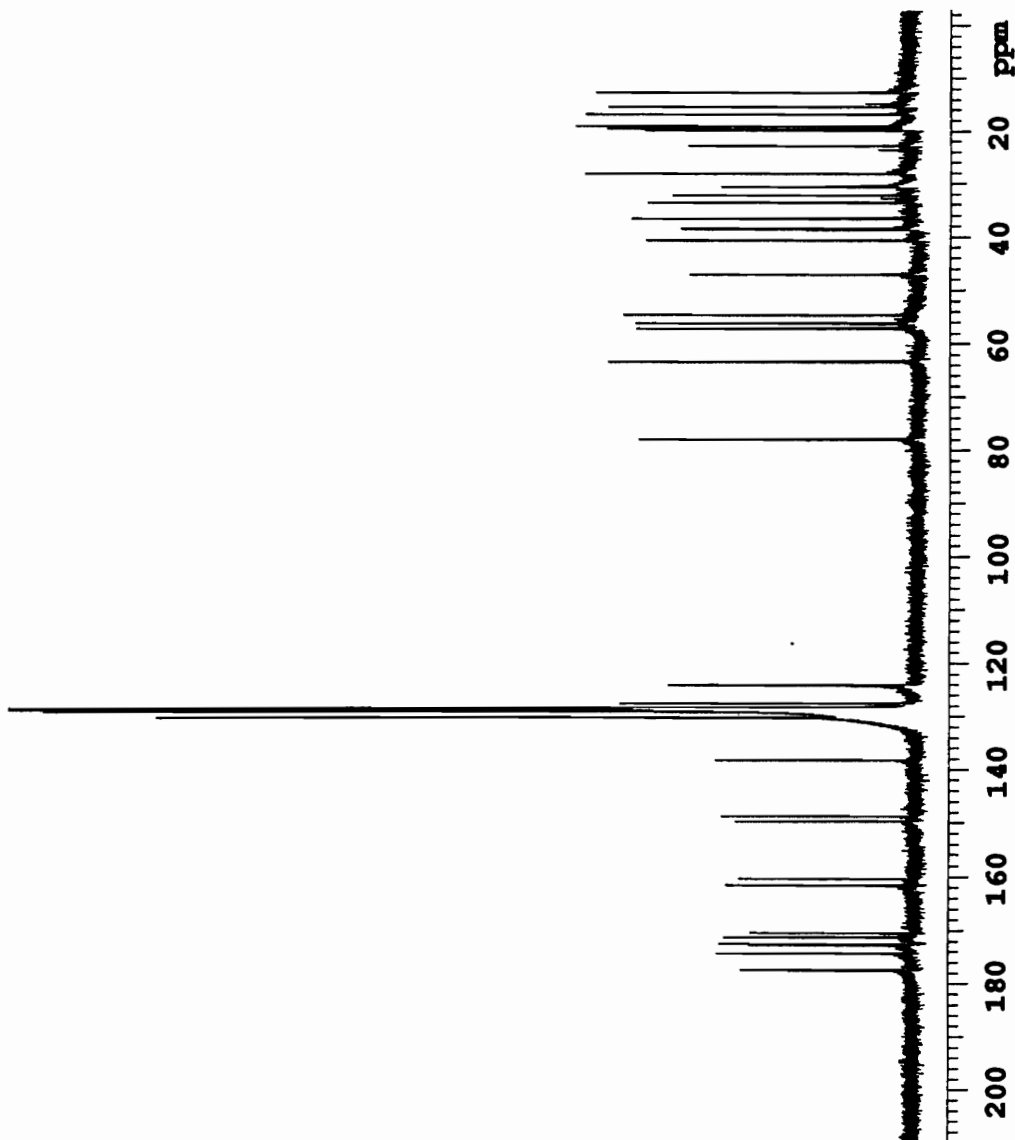


Figure B6. 125 MHz carbon spectrum of tawicyclamide A.

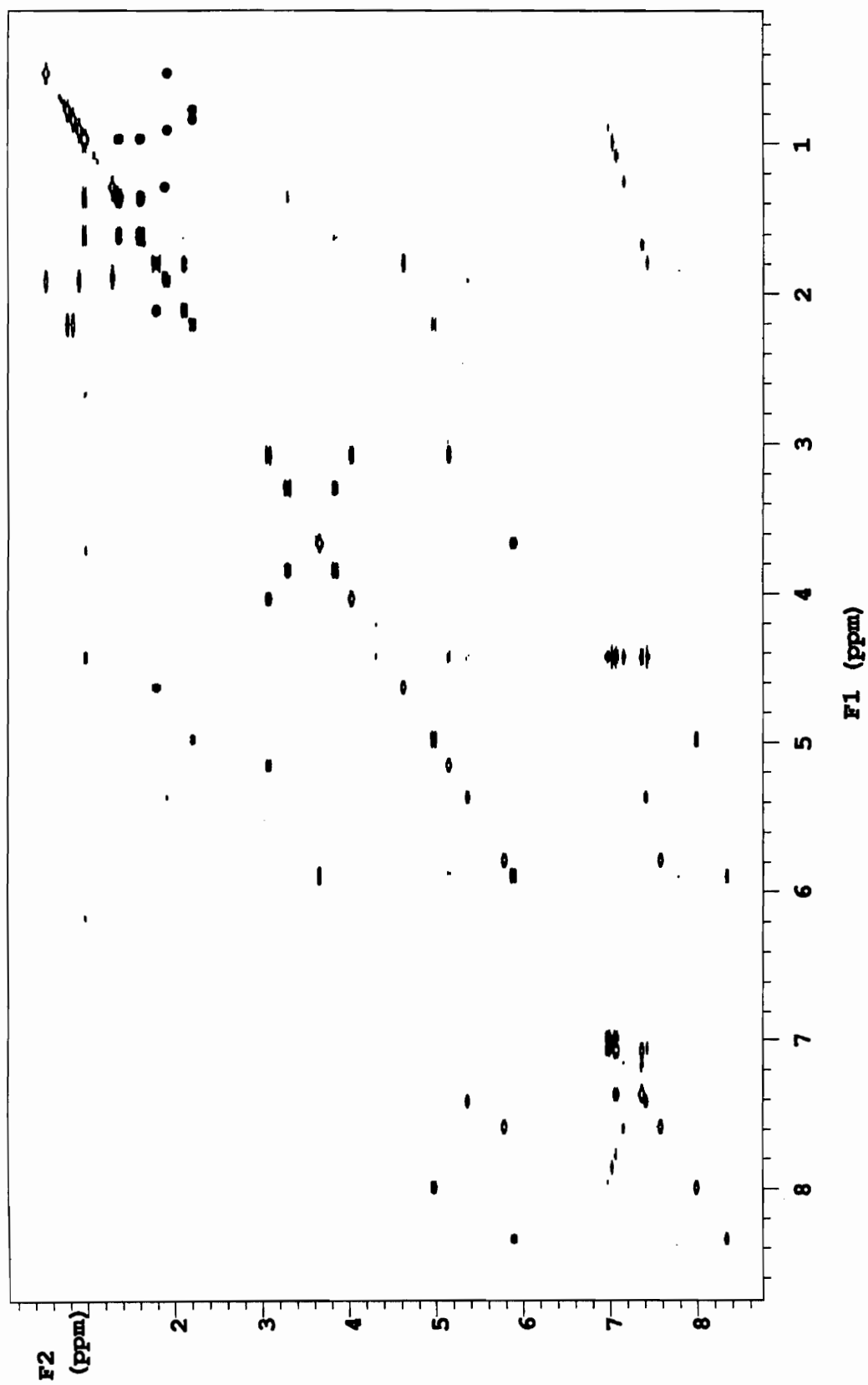


Figure B7. 500 MHz COSY spectrum of tawicyclamide A.



## Tawicyclamide A COSY Spectrum

expl pulse sequence: dqcozy

SAMPLE		DEC. & VT		ACQUISITION ARRAYS	
date	Sep 8 90	dn	H1	array	phase
solvent	cdcl3	dof	0	arraydim	1024
file	/disk5/mc-	dm	nnn		
donald/tawicyclami-	dmm	c	1	phase	
de-A/tawi-A-cosy	dmf	200	1	1	
ACQUISITION	temp	25.0	2	2	
sfrq	499.843	PROCESSING			
tn	H1	gf	0.190		
at	0.475	gfs	not used		
np	4096	wtfile			
sw	4315.9	proc	ft		
fb	2400	fn	4096		
ss	8	math	f		
tpwr	60				
pw	10.0	werr			
dl	2.000	wexp			
presat	0	wbs			
tof	-257.9	wnt			
nt	8	2D PROCESSING			
ct	8	gfl	0.053		
alock	n	gfs1	not used		
gain	8	wtfile1			
FLAGS		procl	ft		
il	n	fn1	2048		
in	n	DISPLAY			
dp	y	sp	53.4		
hs	n	wp	4315.9		
sspul	n	vs	67		
2D ACQUISITION		sc	6		
sw1	4315.9	wc	225		
ni	512	hzmm	20.47		
phase	arrayed	is	500.00		
2D DISPLAY		rfl	3521.6		
sp1	53.4	rfp	3575.0		
wp1	4315.9	th	2		
sc2	0	ins	1.000		
wc2	130	ai cdc av			
rfl1	3521.6				
rfl1	3575.0				

Figure B8. Parameter set for 500 MHz COSY spectrum of tawicyclamide A.

Tawicyclamide B Proton Spectrum

exp1 pulse sequence: s2pul

SAMPLE	DEC. & VT	
date	Sep 21 90	dn H1
solvent	cdcl3	dof 0
file	/disk5/mc- dm	nm
donald/tawicyclami-	dm	c
da-B/tawi-B-proton	dmf	200
ACQUISITION PROCESSING		
sfrq	499.843	fn 65536
tn	H1	math f
at	3.707	
np	32000	weir
sw	4315.9	wezp wft
fb	2400	wbs
pw	10.2	wnt
pw	10.2	DISPLAY
tpwr	60	sp 51.0
dl	0	vp 4315.9
tof	-257.9	vs 339
nt	16	sc 15
ct	16	wc 150
alock	n	hrmm 28.77
gain	8	is 500.00
FLAGS		
il	rfl	3522.9
in	rfp	3573.9
cp	n	th 120
hs	y	ins 1.000
	nn	al cdc ph

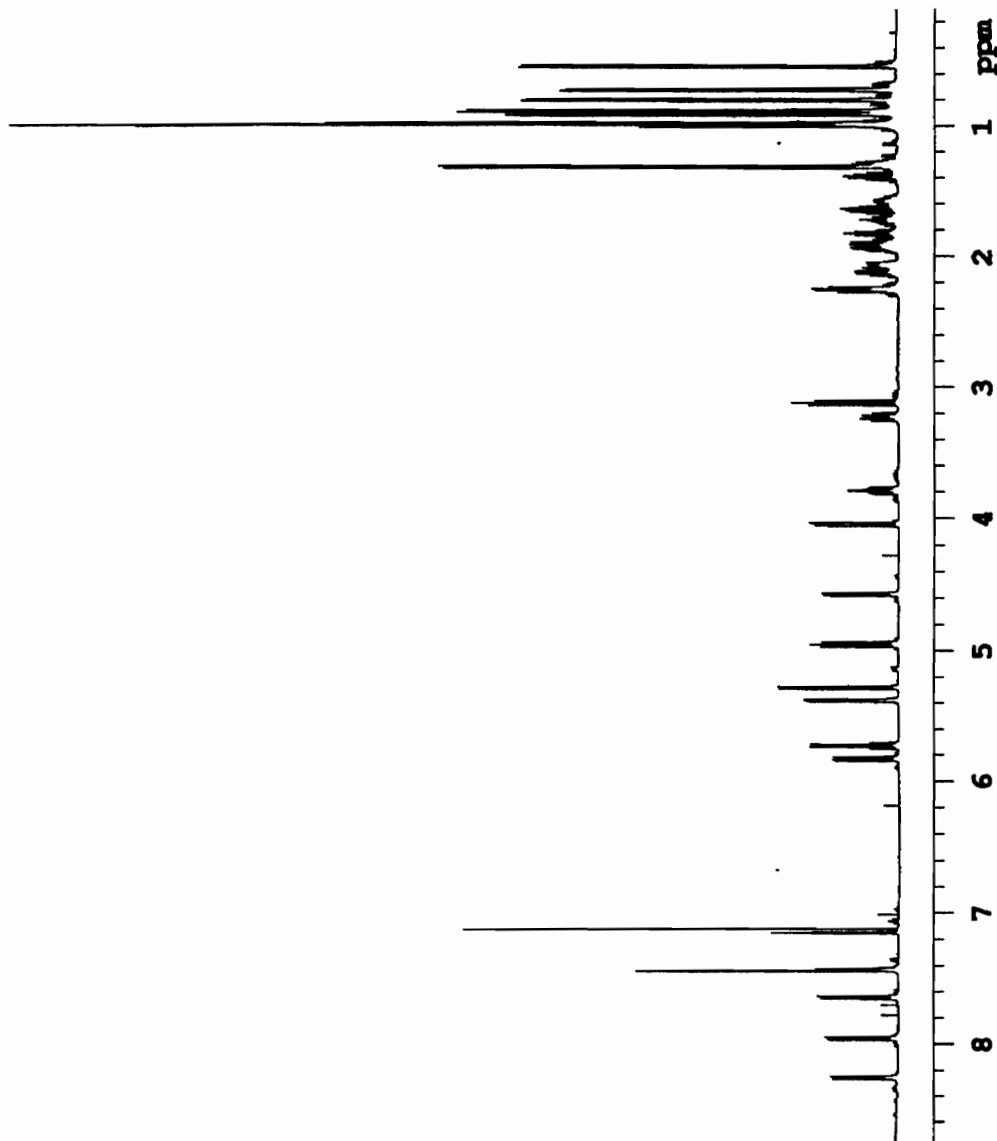


Figure B9. 500 MHz proton spectrum of tawicyclamide B.

Tawicyclamide B Carbon Spectrum

expl pulse sequence: s2pul

SAMPLE	DEC. & VT		
date	Nov 8 90	dn	H1
solvent	c6d6	dof	-346.7
file	/disk5/mc- dn	YYY	
donald/tawicyclami- dnm		s	
de-B/tawi-B-carbon dmf		12200	
ACQUISITION	dpwr	52	
sfrq	125.697	temp	26.0
tn	C13	PROCESSING	
at	1.228	lb	1.00
np	65536	fn	not used
sw	26684.5	math	f
fb	14700		
bs	16	werr	
pw	8.0	wexp	
pw	8.0	wbs	ea
tpwr	58	wnt	
dl	2.000	DISPLAY	
tof	963.3	sp	-359.3
nt	100000	wp	26684.5
ct	4391	vs	2401
alock	n	sc	15
gain	45	wc	150
FLAGS		hrmm	177.90
il	n	is	0.12
in	n	rfl	16511.3
cp	y	rfp	16152.1
hs	nn	th	120
		ins	1.000
	nm	cdc	ph

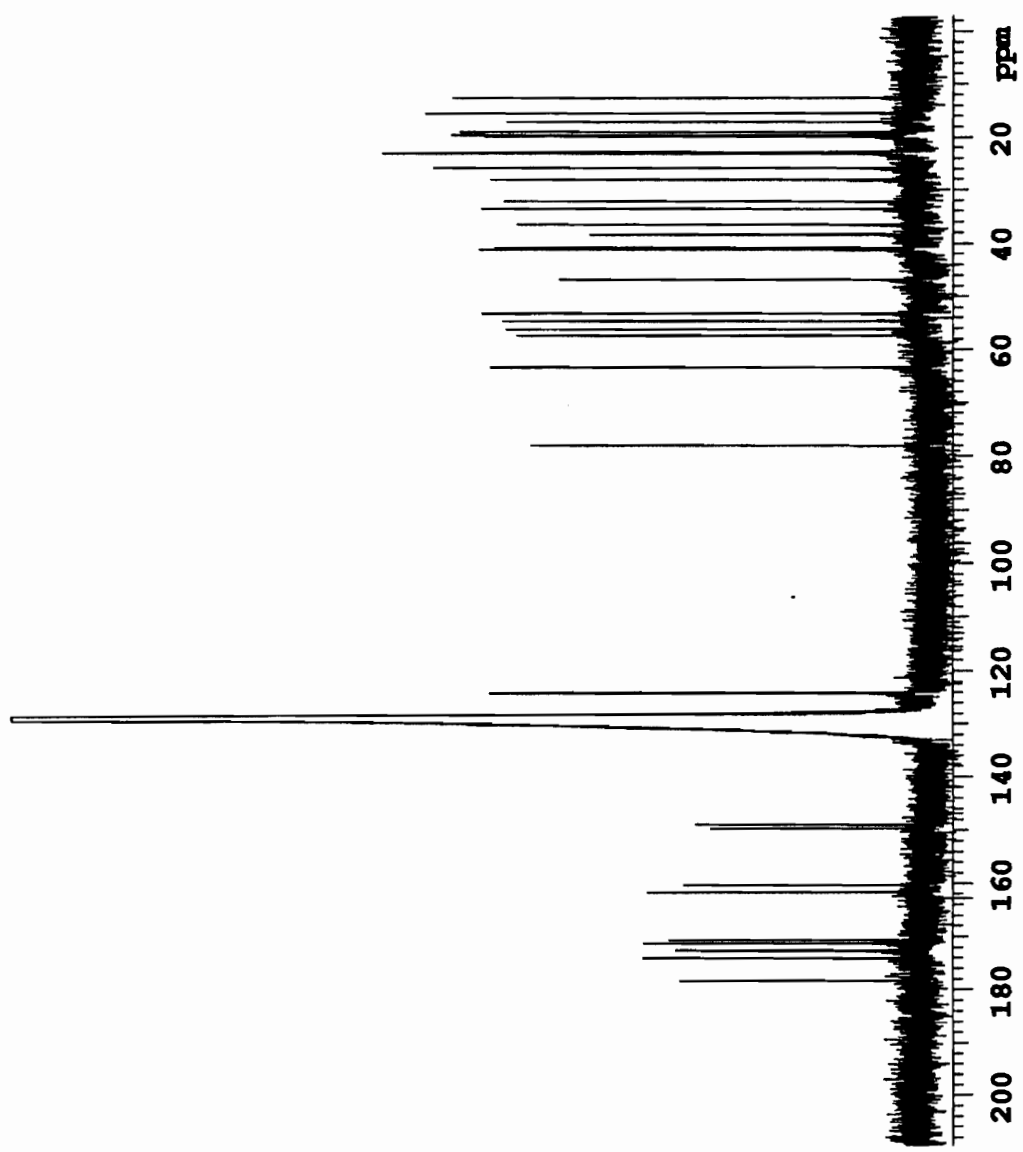


Figure B10. 125 MHz carbon spectrum of tawicyclamide B.

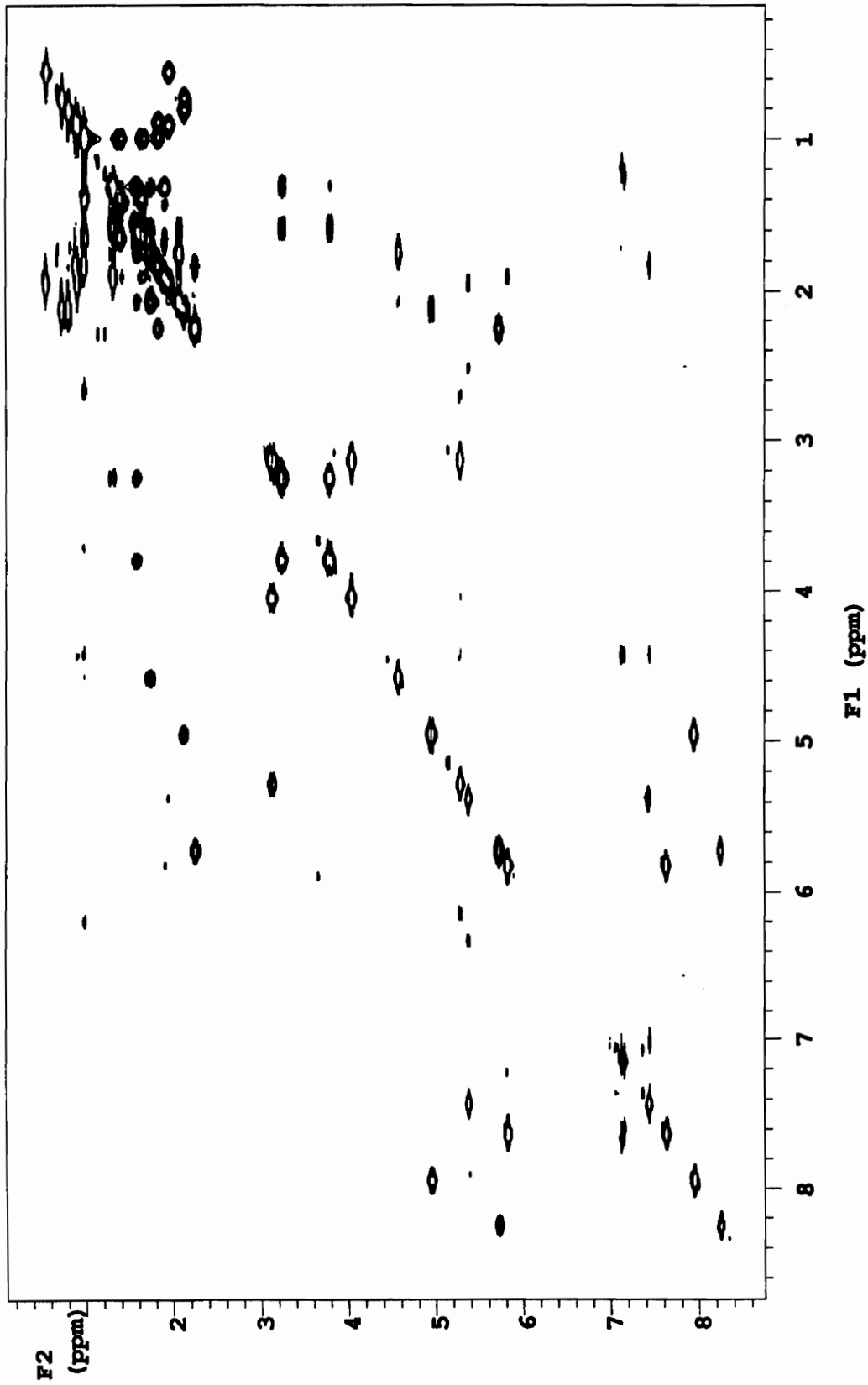


Figure B11. 500 MHz COSY spectrum of tawicyclamide B.

## Tawicyclamide B COSY Spectrum

expl pulse sequence: dqcosy

SAMPLE		DEC. & VT		ACQUISITION ARRAYS	
date	Sep 21 90	dm	H1	array	phase
solvent	cdcl3	dof	0	arraydim	512
file	/disk5/mc-	dm	nnn		
	donald/tawicyclami-	dmm	c	1	phase
	de-B/tawi-B-cosy	dmf	200	1	1
	ACQUISITION	temp	25.0	2	2
sfrq	499.843	PROCESSING			
tn	H1	gf	0.103		
at	0.237	gfs	not used		
np	2048	wtfile			
sw	4315.9	proc	ft		
fb	2400	fn	2048		
ss	8	math	f		
tpwr	60				
pw	11.1	werr			
d1	2.000	wexp			
presat	0	wbs			
tof	-257.9	wnt			
nt	8	2D PROCESSING			
ct	8	gf1	0.027		
alock	n	gfs1	not used		
gain	8	wtfile1			
	FLAGS	procl	ft		
il	n	fn1	2048		
in	n	DISPLAY			
dp	y	sp	53.4		
hs	yn	wp	4315.9		
sspul	y	vs	571		
	2D ACQUISITION	sc	20		
sw1	4315.9	wc	205		
ni	256	hzmm	21.05		
phase	arrayed	is	500.00		
	2D DISPLAY	rfl	3521.6		
sp1	53.4	rfp	3575.0		
wp1	4315.9	th	3		
sc2	18	ins	1.000		
wc2	120	ai cdc av			
rfl1	3521.6				
rfl1	3575.0				

Figure B12. Parameter set for 500 MHz COSY spectrum of tawicyclamide B.

Dehydrotawicyclamide B Proton Spectrum

exp2 pulse sequence: s2pul

SAMPLE	DEC. & VT
date Mar 9 91	dn H1
solvent c6d6	dof 0
file /disk5/mc~	dm nnn
donald/oxytawicycl~	chm c
amide-B/oxytawib-p~	dmf 200
roton	PROCESSING
ACQUISITION	gf not used
sfrq 499.843	gfs not used
tn H1	fn 65536
at 3.199	math f
np 29184	
sw 4561.5	werr wft
fb 2500	wexp
pw 9.1	wbs
pw 9.1	wnt
tpwr 62	DISPLAY
dl 0	sp 5.9
tof -227.2	vp 4561.5
nt 16	vs 308
ct 16	sc 15
alock n	wc 150
gain 25	hzmm 30.41
FLAGS	is 500.00
il n	rfl 3568.0
in n	rfp 3573.9
cp y	th 120
hs nn	ins 1.000
	al cdc ph

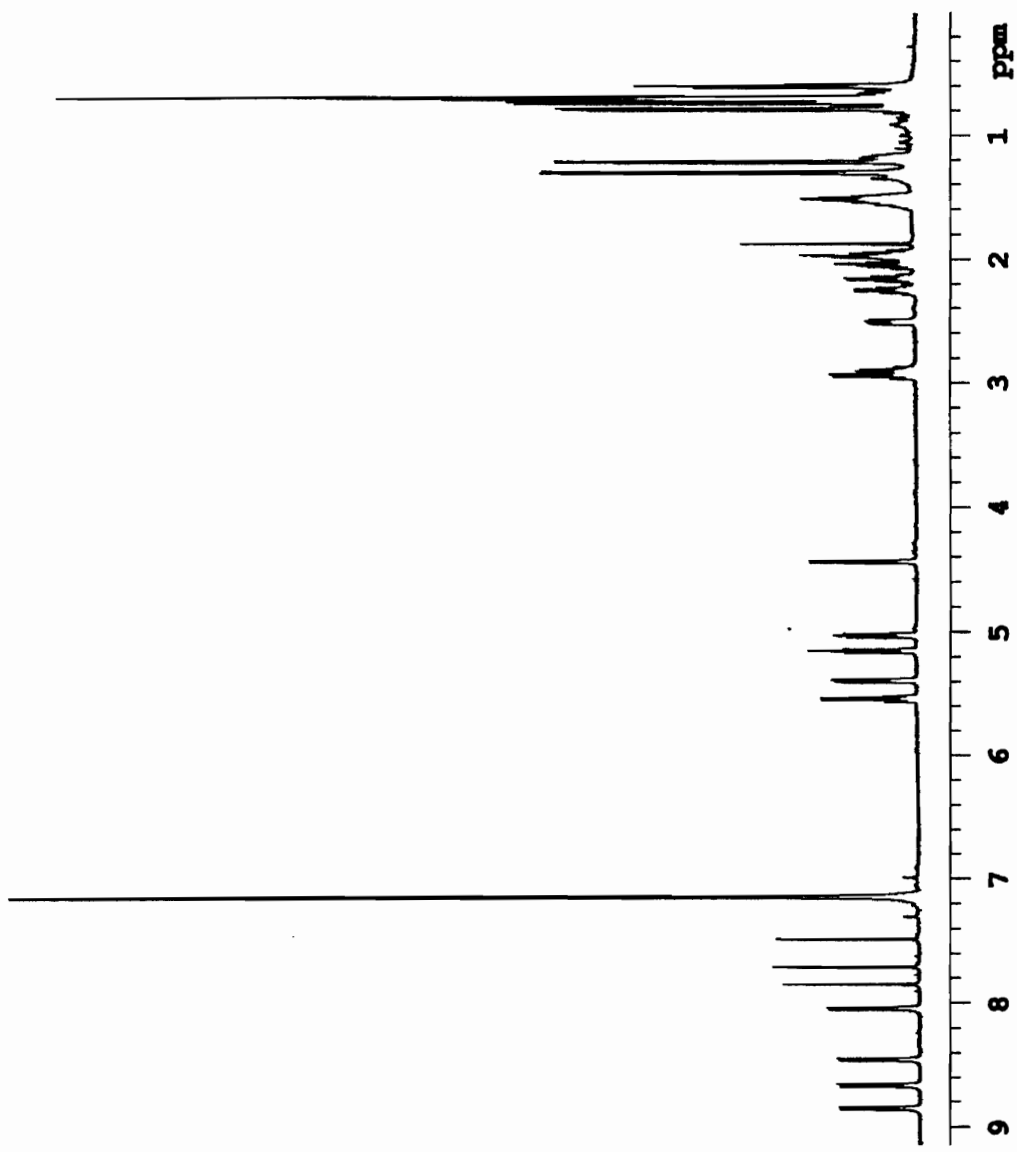


Figure B13. 500 MHz proton spectrum of dehydrotawicyclamide B.

Dehydrotawicyclamide B Carbon Spectrum

exp2 pulse sequence: s2pul

SAMPLE	DEC. & VT
date Mar 1 91 dn	H1
solvent cdcl3 dof	-178.7
file /disk5/mc~ dn	Y
donald/oxytawicycl~ dmn	W
amide-B/oxytawib-C~ dmf	12200
carbon dpwr	52
temp	26.0
ACQUISITION	PROCESSING
sfrq 125.697	1.00
tn Cl3 lb	65536
at 0.705 fn	f
np 35584 math	
sw 25220.7	
fb 13900 weix	
bs 16 wexp	
pw 8.0 wbs	wft
pw 8.0 wnt	
tpwr 62	DISPLAY
d1 2.000 sp	-27.5
tof 638.6 wp	25220.7
nt 90000 vs	5352
ct 15324 sc	15
alock n wc	150
gain 45 hrmm	168.14
FLAGS	is 500.00
ll n rfl	16116.7
ln n rfp	16089.2
cp y th	120
bs nn lns	1.000

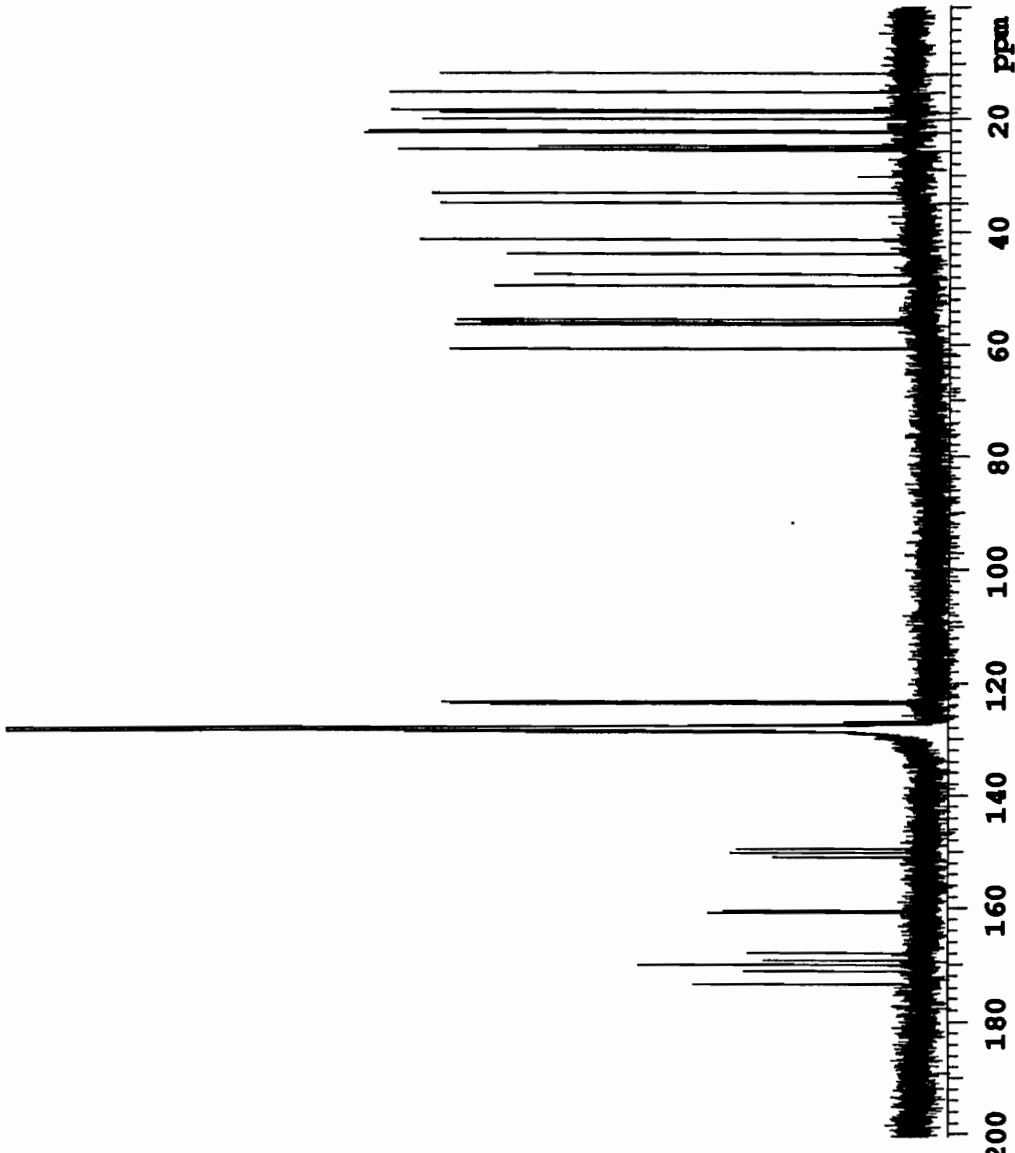


Figure B14. 125 MHz carbon spectrum of dehydrotawicyclamide B.

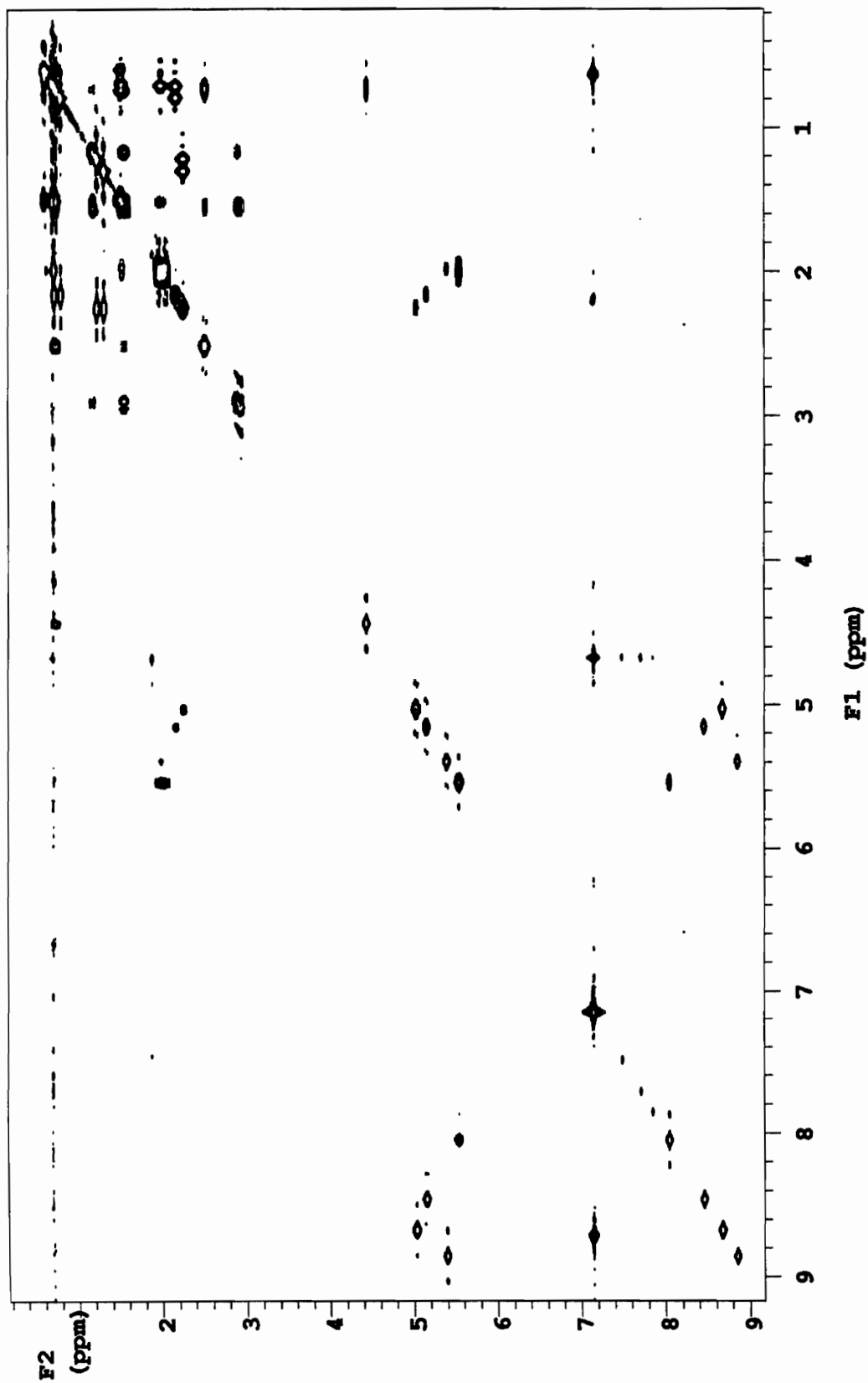


Figure B15. 500 MHz COSY spectrum of dehydrotawicyclamide B.



## Dehydrotawicyclamide B COSY Spectrum

expl pulse sequence: dqcosy

SAMPLE		DEC. & VT		ACQUISITION ARRAYS	
date	Mar 1 91	dn		H1	array
solvent	c6d6	dof		0	phase
file	/disk5/mc~	dm		nnn	arraydim 1024
donald/oxytawicycl~	dmm	c		i	phase
amide-B/oxytawiB-c~	dmf	200		1	1
osy				2	2
ACQUISITION		gf	0.098		
sfrq	499.843	gfs	not used		
tn	H1	wtfile			
at	0.228	proc	ft		
np	2048	fn	2048		
sw	4493.9	math	f		
fb	2500				
bs	8	werr			
ss	8	wexp			
tpwr	62	wbs			
pw	8.7	wnt			
dl	1.000	2D PROCESSING			
presat	0	gfl	0.050		
tof	-178.7	gfs1	not used		
nt	8	wtfile1			
ct	8	procl	ft		
alock	n	fn1	2048		
gain	25	DISPLAY			
FLAGS		sp	87.8		
il	n	wp	4493.9		
in	n	vs	310		
dp	y	sc	20		
hs	n	wc	205		
sspul	y	hzmm	21.92		
2D ACQUISITION		is	500.00		
sw1	4493.9	rfl	3486.1		
ni	512	rfp	3573.9		
phase	arrayed	th	4		
2D DISPLAY		ins	1.000		
sp1	87.8	ai	cdc	av	
wp1	4493.9				
sc2	18				
wc2	120				
rfl1	3486.1				
rfl1	3573.9				

Figure B16. Parameter set for 500 MHz COSY spectrum of dehydrotawicyclamide B.

Dehydrotawicyclamide A Proton Spectrum

exp1 pulse sequence: s2pul

SAMPLE	Mar 8 91	dn	H1
date	Mar 8 91	dn	H1
solvent	c6d6	dof	0
file	/disk5/mc--	dm	nnn
donald/orytawicycl-	dmn	c	
amide-A/orytawia-p--	dmf	200	
rotor			
PROCESSING			
ACQUISITION	gf	not used	
sfrq	499.843	gfs	not used
tn	H1	fn	65536
at	3.199	math	f
np	29184		
sw	4561.5	warr	wft
fb	2500	wexp	
pw	9.1	wbs	
pw	9.1	wnt	
tpwr	62	DISPLAY	
d1	0	sp	3.8
tof	-227.2	wp	4561.5
nt	16	vs	379
ct	16	sc	15
alock	n	wc	150
gain	25	hzmm	30.41
FLAGS		ls	500.00
il	n	rfl	3570.1
in	n	rfp	3573.9
cp	y	th	120
hs	nn	ins	1.000
	ai	odc	ph

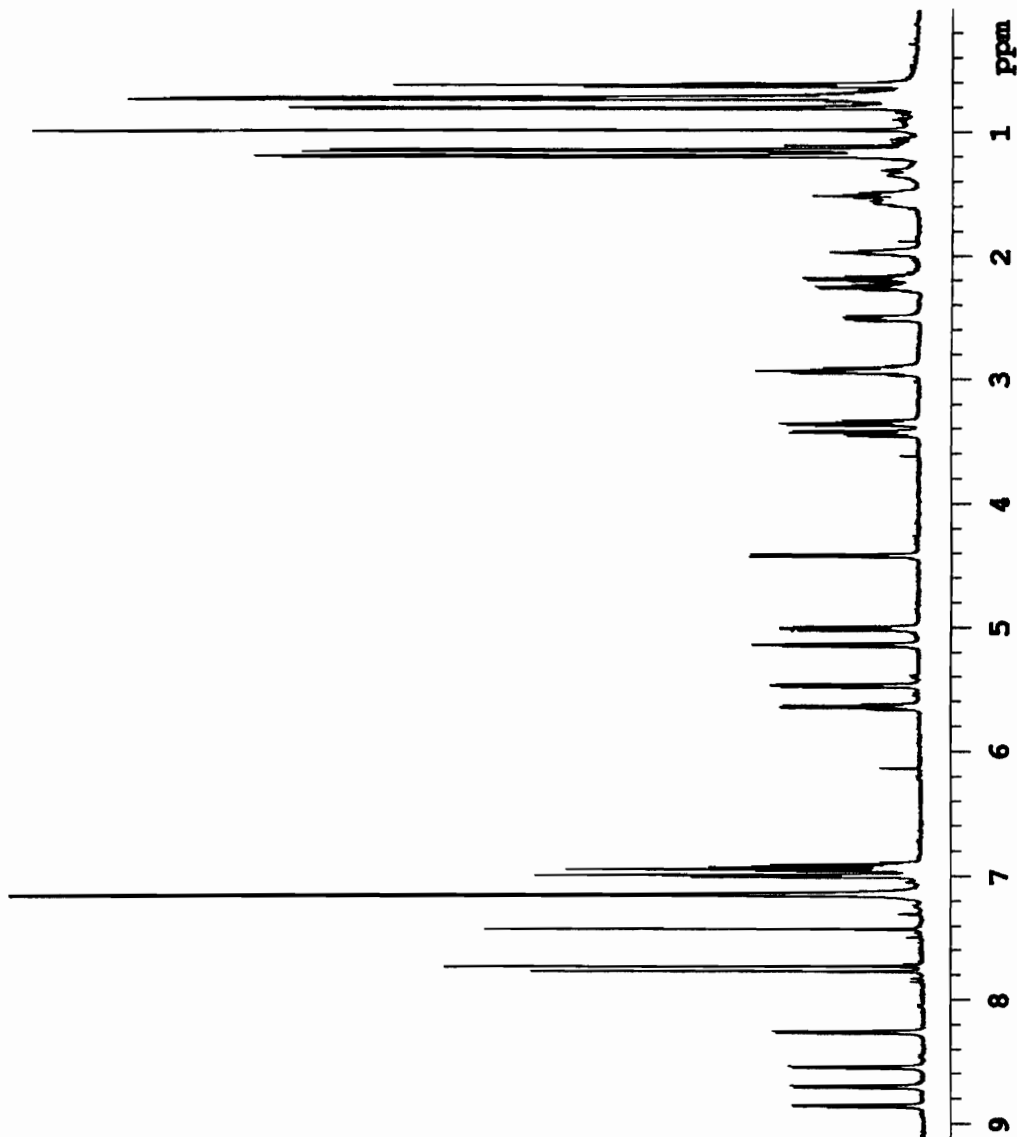


Figure B17. 500 MHz proton spectrum of dehydrotawicyclamide A.

Dehydrotawicyclamide A Carbon Spectrum

exp1 pulse sequence: s2pul

SAMPLE	DEC. & VT	
date	Mar 16 91	dn H1
solvent	c6d6	dof -178.7
file	/disk5/mc~	dn Y
donald/oxytawicycl~	dm	z
amide-A/oxytawia-c~	dmf	12200
carbon	dpwr	52
temp	20.0	
ACQUISITION	PROCESSING	
sfrq	125.697	
tn	C13	lb 1.00
at	0.705	fn 65536
mp	35584	math f
sw	25220.7	
fb	13900	werr
bs	16	wexp
pw	8.0	wbs
pw	8.0	wnt
tpwr	62	DISPLAY
d1	1.500	sp -15.9
tof	638.6	wp 25220.7
nt	100000	vs 2523
ct	3392	sc 15
alock	Y	wc 150
gain	45	hzmm 168.14
FLAGS		is 500.00
il	n	rfl 16105.2
in	n	rpf 16089.2
dp	Y	th 120
hs	nn	ins 1.000
	nm	cdc ph

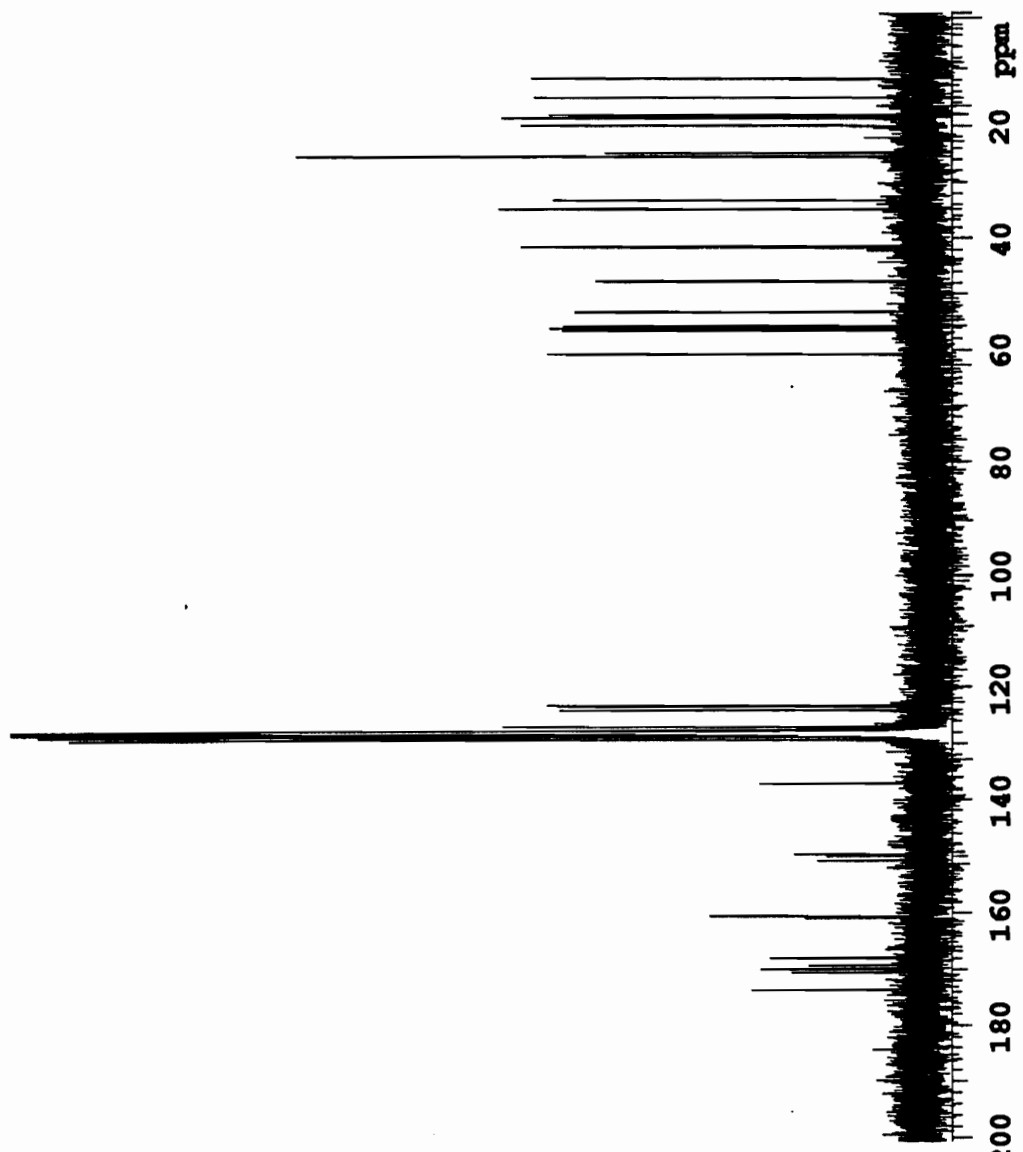


Figure B18. 125 MHz carbon spectrum of dehydrotawicyclamide A.

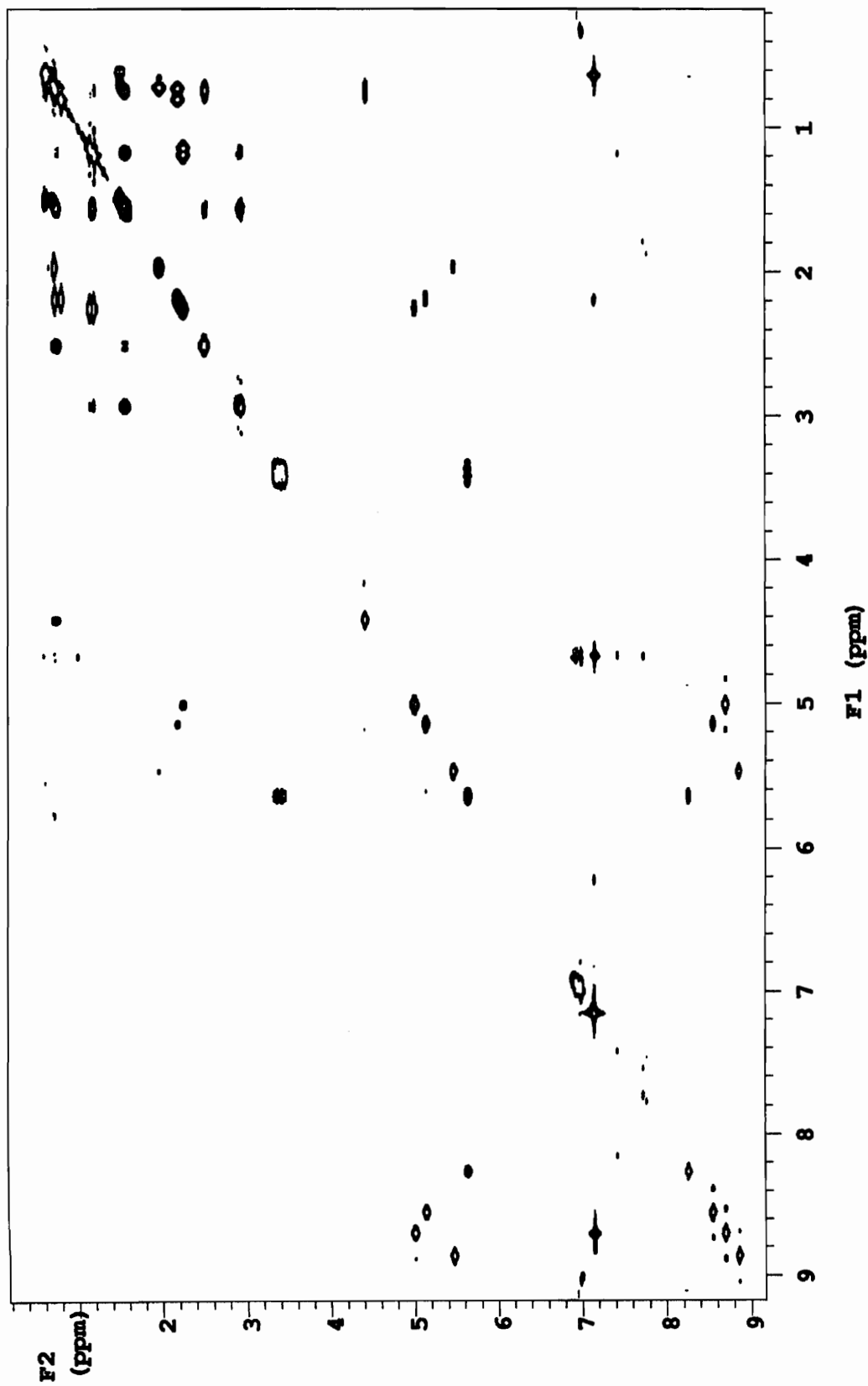


Figure B19. 500 MHz COSY spectrum of dehydrotawicyclamide A.

## Dehydrotawicyclamide A COSY Spectrum

expl pulse sequence: dqcosy

SAMPLE		DEC. & VT		ACQUISITION ARRAYS	
date	Mar 1 91	dn		H1	array
solvent	c6d6	dof		0	arraydim
file	/disk5/mc~	dm		nnn	phase
donald/oxytawicycl~	dmm	c		i	phase
amide-A/oxytawia-c~	dmf	200		1	1
	osy			2	2
ACQUISITION		PROCESSING			
		gf	0.098		
sfrq	499.843	gfs	not used		
tn		H1	wtfile		
at	0.228	proc	ft		
np	2048	fn	2048		
sw	4493.9	math	f		
fb	2500				
bs	8	werr			
ss	8	wexp			
tpwr	60	wbs			
pw	8.7	wnt			
dl	1.000	2D PROCESSING			
presat	0	gfl	0.047		
tof	-178.7	gfs1	not used		
nt	8	wtfile1			
ct	8	procl	ft		
alock	n	fn1	2048		
gain	8	DISPLAY			
	FLAGS	sp	87.8		
il	n	wp	4493.9		
in	n	vs	918		
dp	y	sc	20		
hs	n	wc	205		
sspul	y	hzmm	21.92		
2D ACQUISITION		is	500.00		
sw1	4493.9	rfl	3486.1		
ni	512	rfp	3573.9		
phase	arrayed	th	3		
2D DISPLAY		ins	1.000		
sp1	87.8	ai	cdc	av	
wp1	4493.9				
sc2	18				
wc2	120				
rfl1	3486.1				
rfl1	3573.9				

Figure B20. Parameter set for 500 MHz COSY spectrum of dehydrotawicyclamide A.

## APPENDIX C

### CID SPECTRA OF TAWICYCLAMIDE A

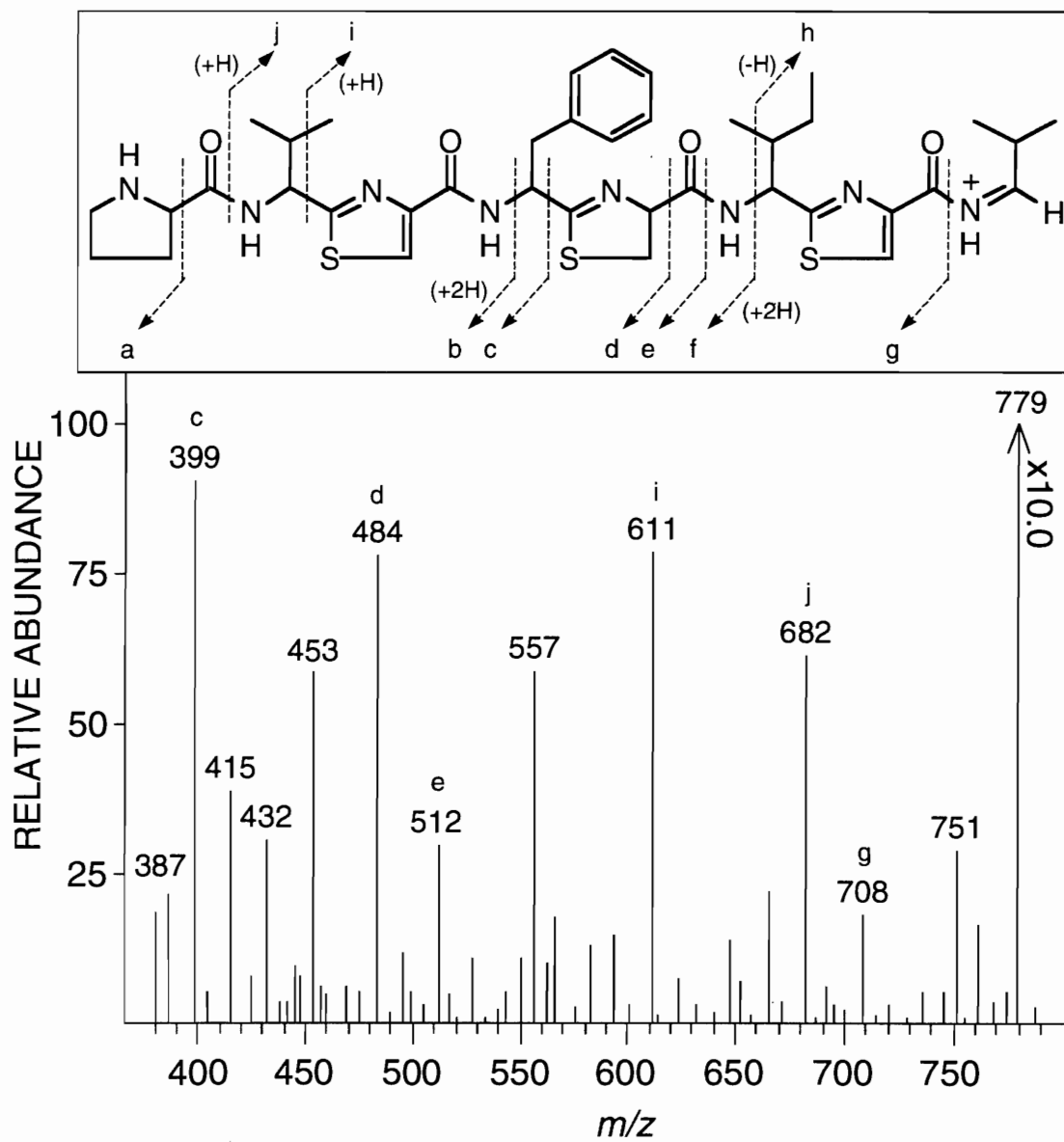


Figure C1. CID spectrum (high mass region) and structure of the  $m/z$  779 ion of tawicyclamide A.

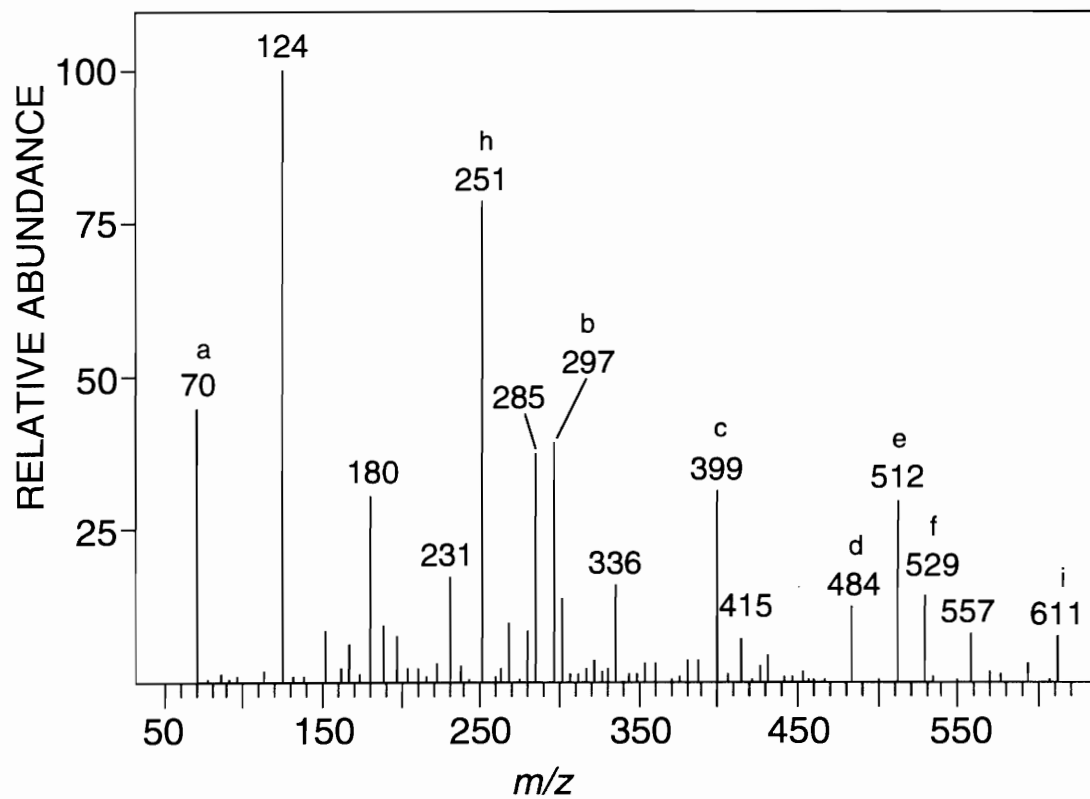


Figure C2. Low mass region from the CID spectrum of the  $m/z$  779 ion of tawicyclamide A.



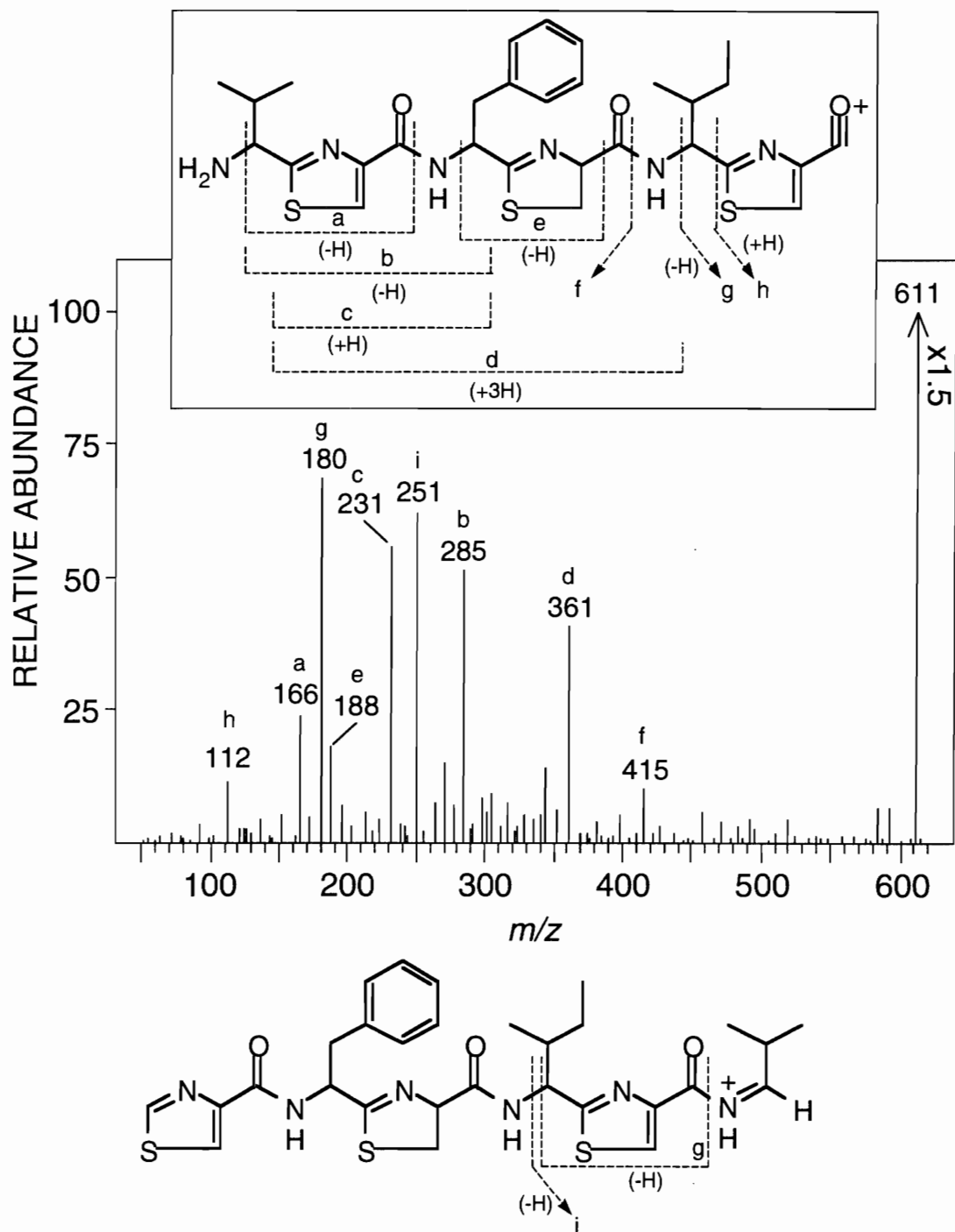


Figure C3. CID spectrum and structure of the  $m/z$  611 ion of tawicyclamide A.

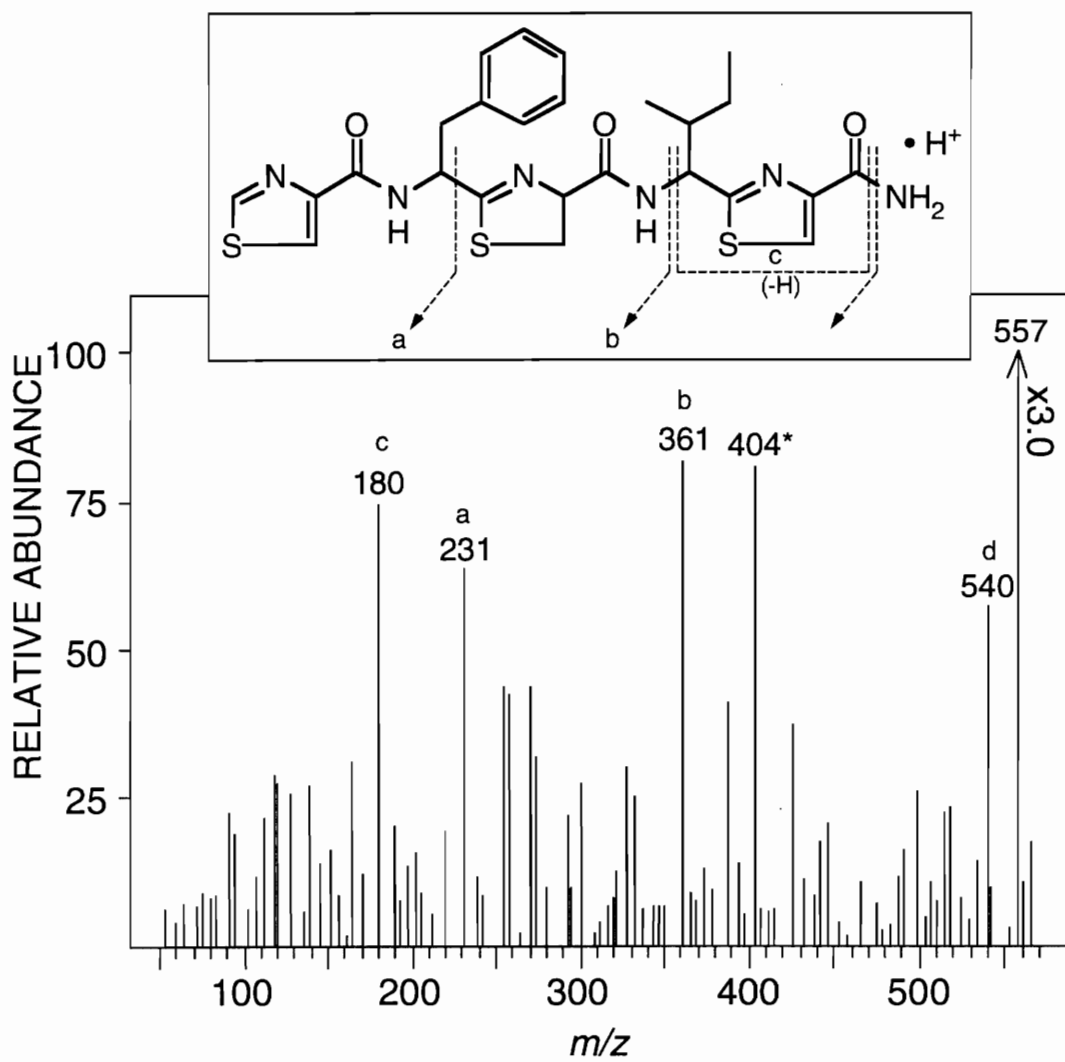


Figure C4. CID spectrum and structure of the  $m/z$  557 ion of tawicyclamide A. (\*Matrix ion)

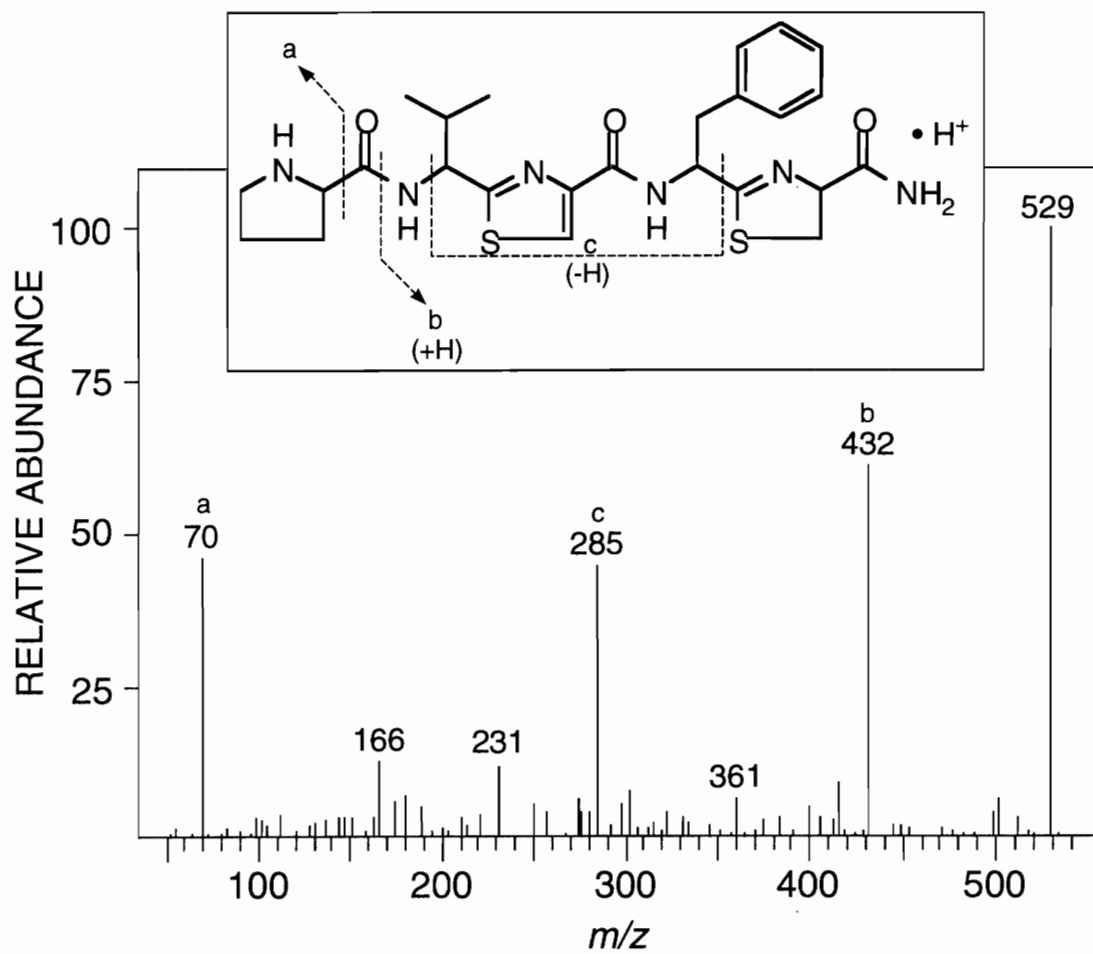


Figure C5. CID spectrum and structure of the  $m/z$  529 ion of tawicyclamide A.

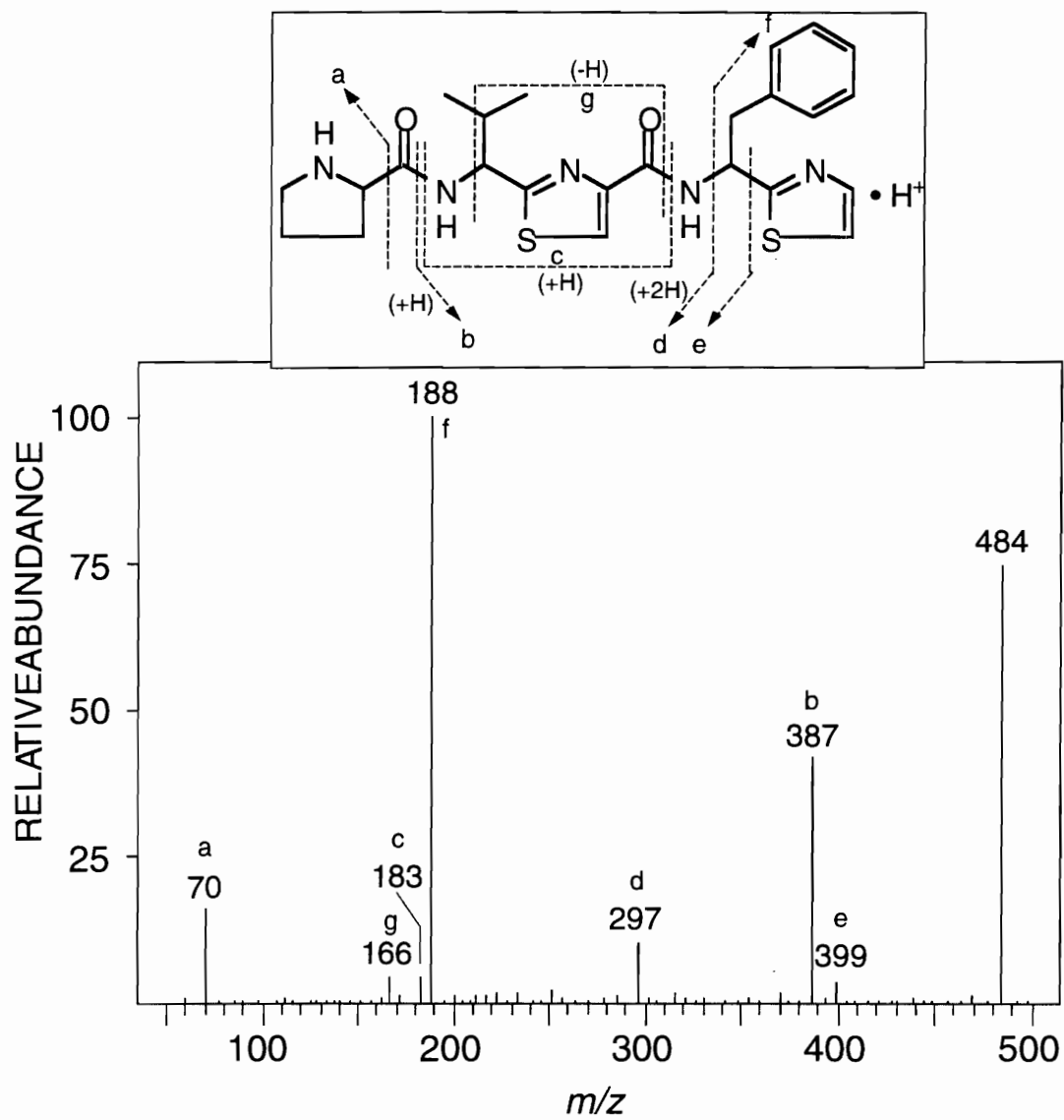


Figure C6. CID spectrum and structure of the  $m/z$  484 ion of tawicyclamide A.

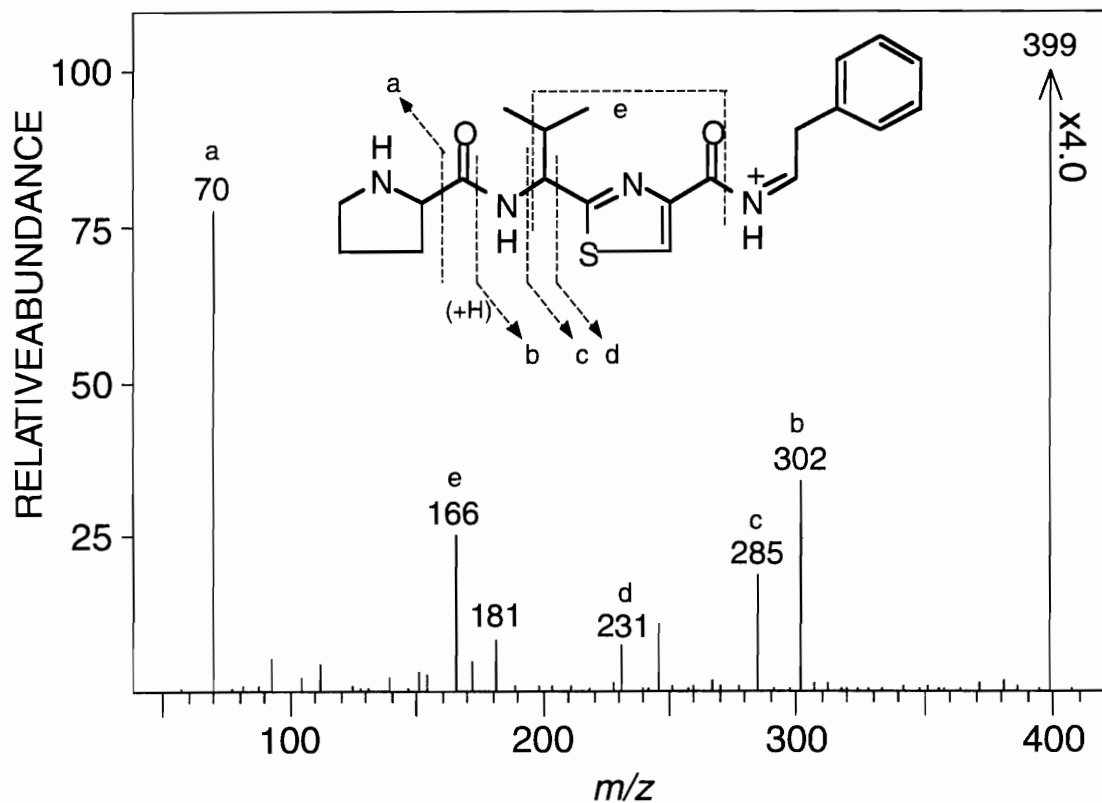


Figure C7. CID spectrum and structure of the  $m/z$  399 ion of tawicyclamide A.

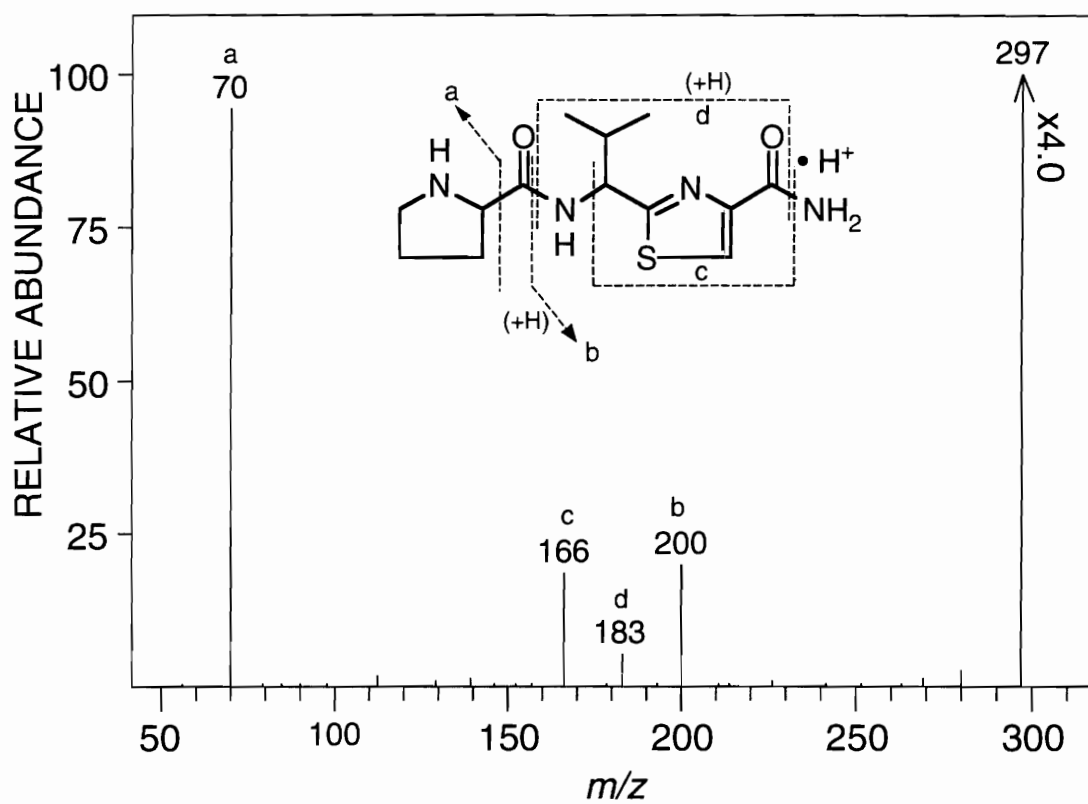


Figure C8. CID spectrum and structure of the  $m/z$  297 ion of tawicyclamide A.

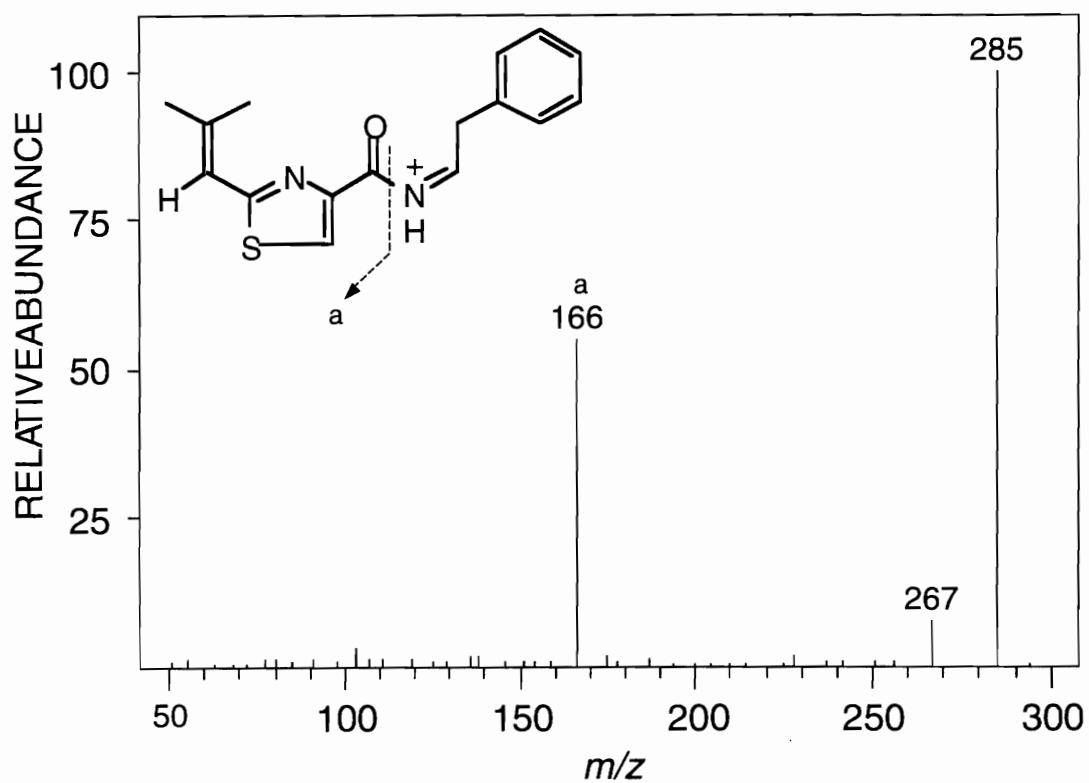


Figure C9. CID spectrum and structure of the  $m/z$  285 ion of tawicyclamide A.

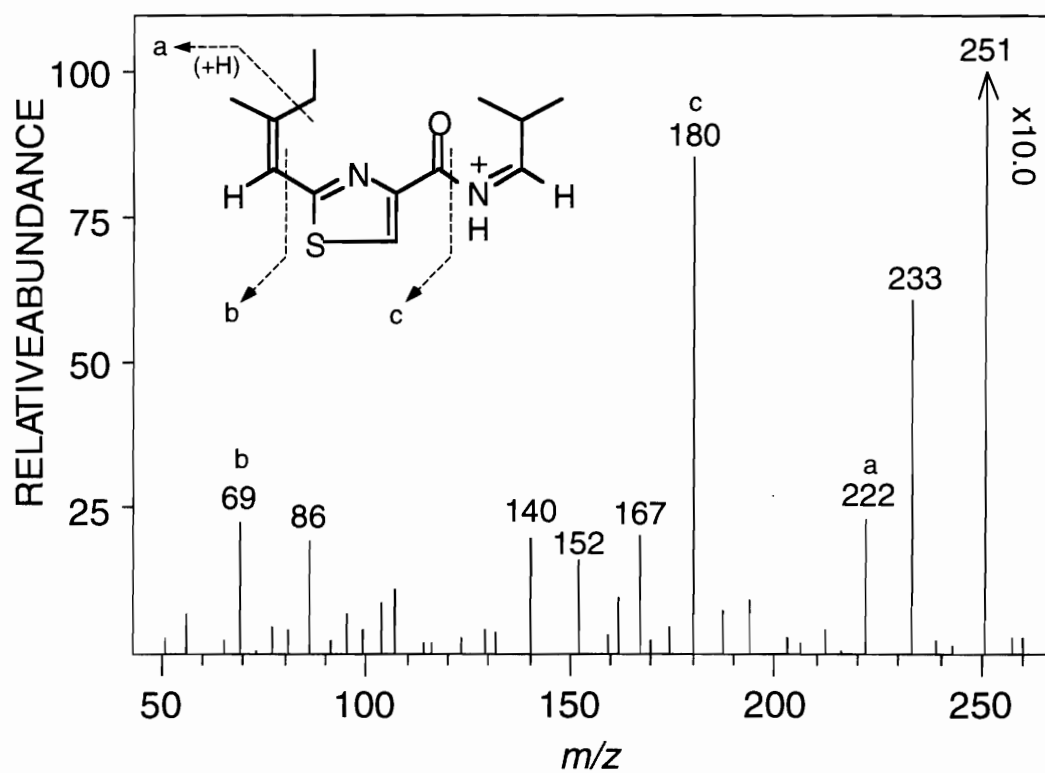


Figure C10. CID spectrum and structure of the  $m/z$  251 ion of tawicyclamide A.



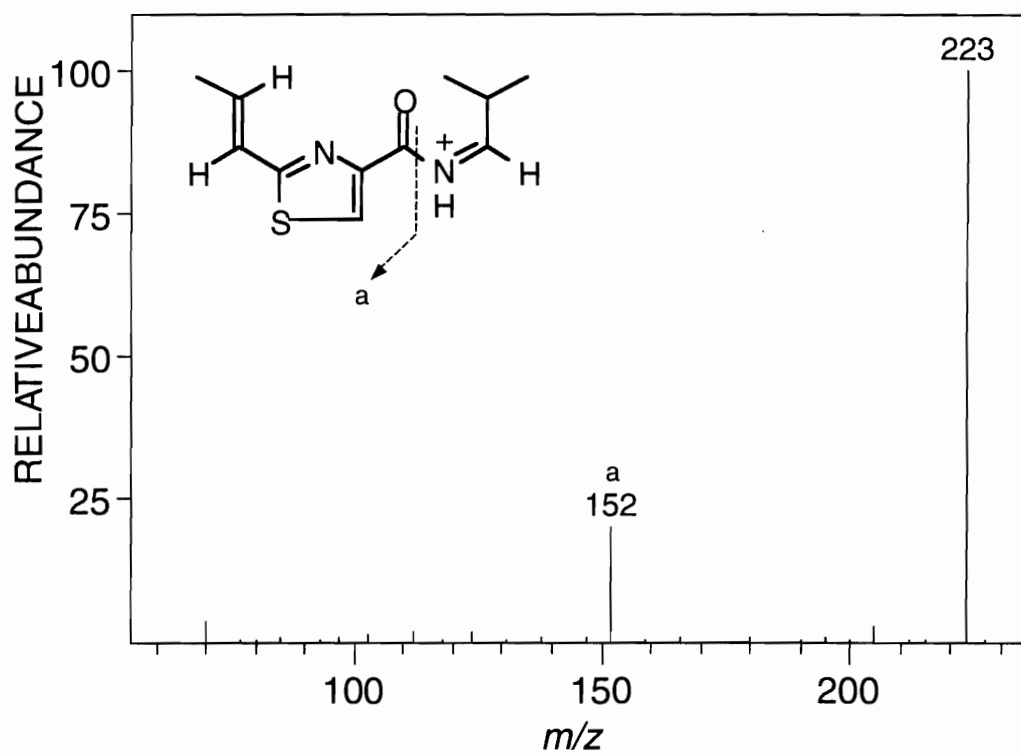


Figure C11. CID spectrum and structure of the  $m/z$  223 ion of tawicyclamide A.

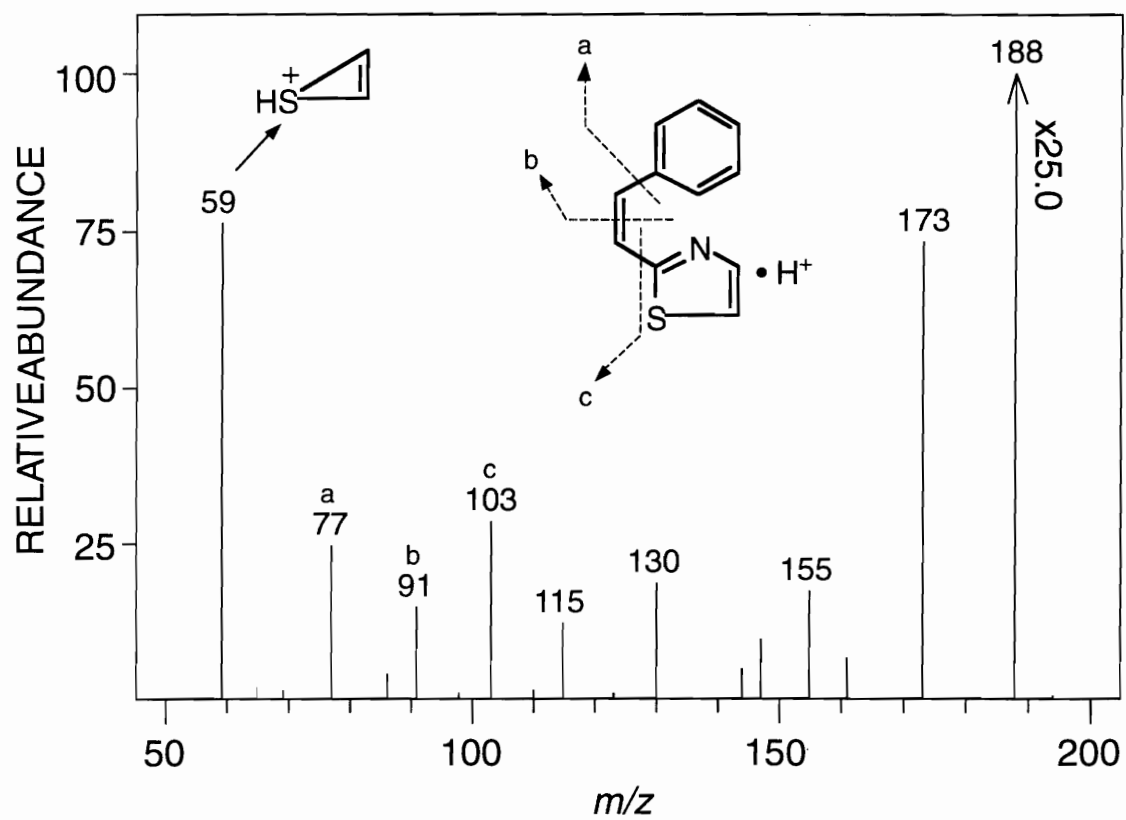


Figure C12. CID spectrum and structure of the  $m/z$  188 ion of tawicyclamide A.

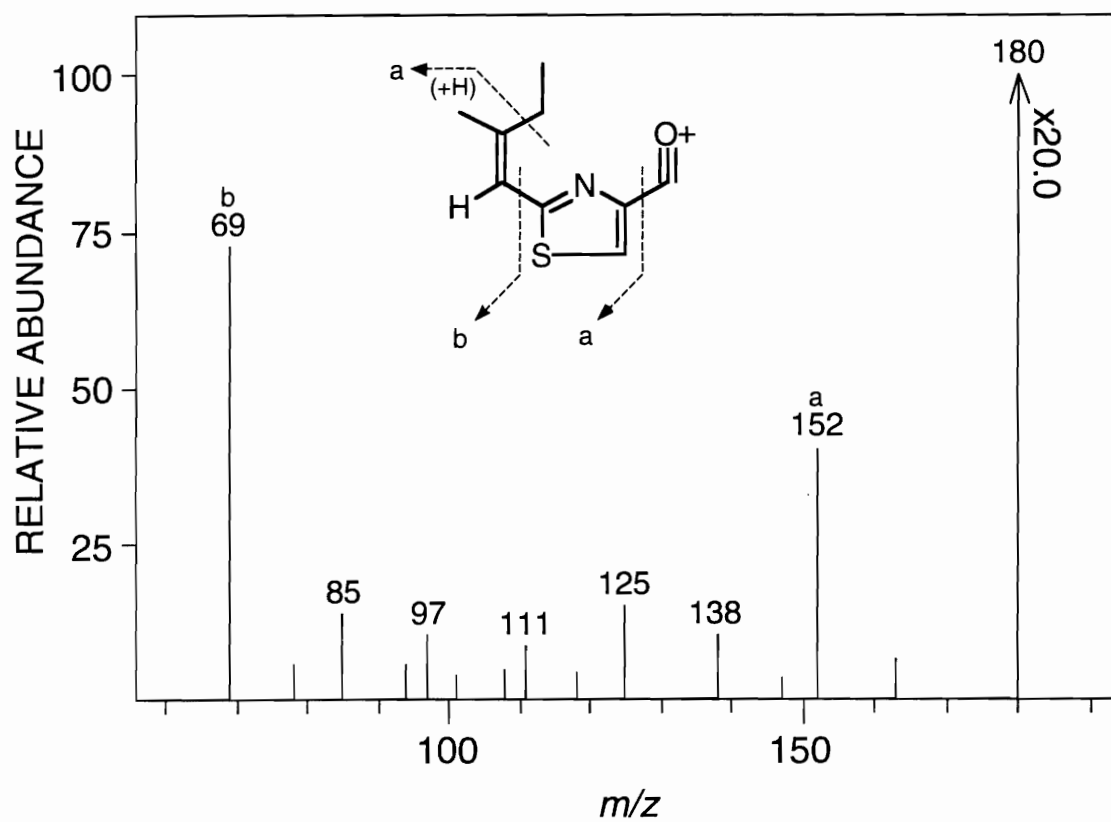


Figure C13. CID spectrum and structure of the  $m/z$  180 ion of tawicyclamide A.

APPENDIX D

NMR SPECTRA OF COMPOUNDS FROM *BOTRYLLUS* SP.

## Botryllamide D Proton Spectrum

exp1 pulse sequence: s2pul

SAMPLE		DEC. & VT	
date	Mar 18 92	dn	H1
solvent	DMSO	dof	0
file	/disk4/mc~	dm	nnn
donald/nci798/swer~	dmn	c	
zey-proton	dmf	200	
	dpwr	30	
ACQUISITION			
sfrq	499.843	PROCESSING	
tn	H1	wtfile	
at	3.798	proc	ft
np	40960	fn	not used
sw	5393.0	math	f
fb	3000		
bs	32	weax	
ss	2	wexp	
tpwr	62	wbs	
pw	5.5	wnt	wft
d1	1.500	DISPLAY	
tof	349.8	sp	155.2
nt	8	wp	5393.0
ct	8	vs	118
alock	n	sc	15
gain	not used	wc	150
	FLAGS	hzmm	35.95
il	n	is	819.56
in	n	rfl	1089.4
dp	y	rfp	1244.6
hs	nn	th	120
	ins		6.000
	nm	cdc	ph

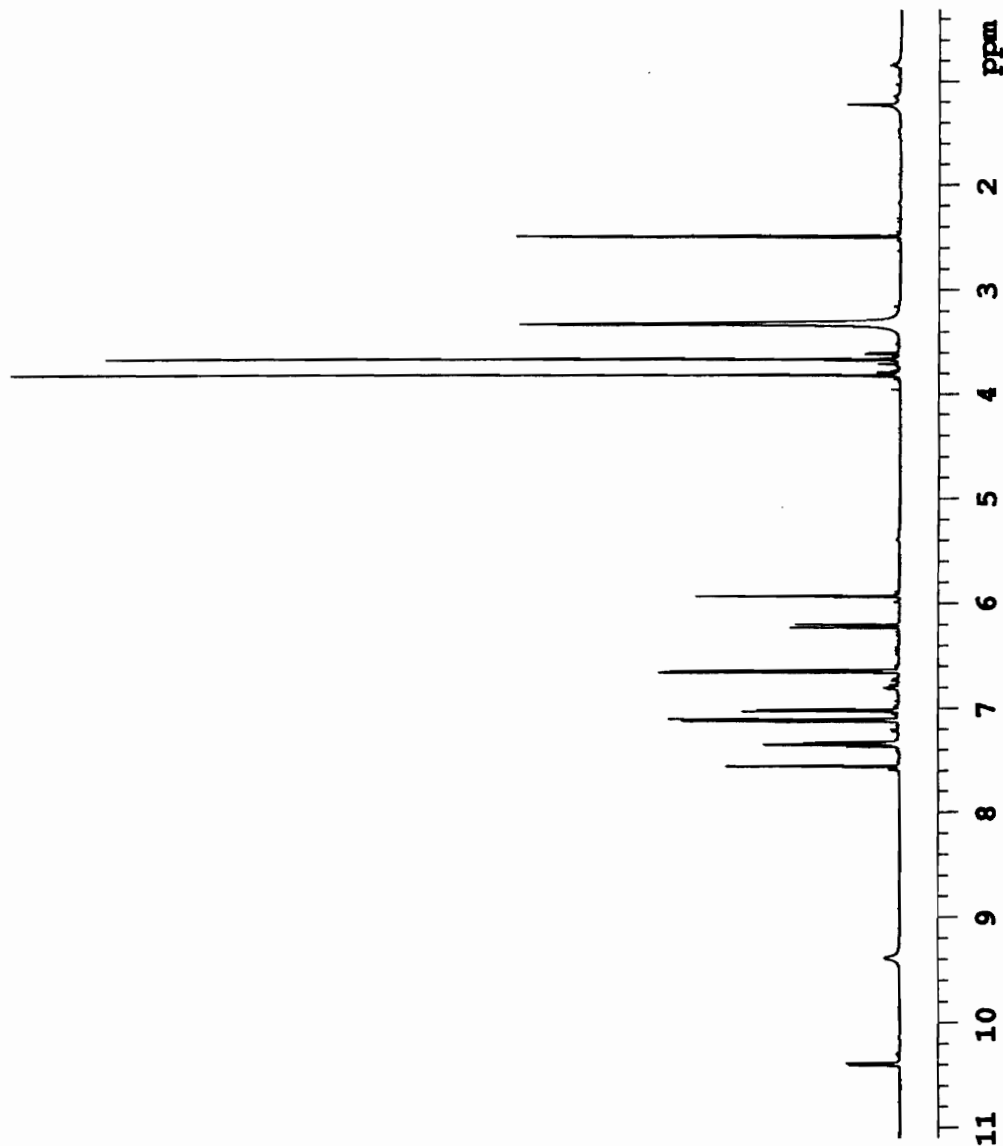


Figure D1. 500 MHz proton spectrum of botryllamide D.

Botryllamide D: DMSO + D2O

exp1 pulse sequence: s2pul

SAMPLE	DEC. & VI		
date	Jun 1 92	dn	H1
solvent	DMSO	dof	0
file	/disk4/mc~ dn	nmn	
donald/nci798/prot~ dnm		c	
on-D2O-ex dmf		200	
cpwr		30	
ACQUISITION			
sfrq	499.843	PROCESSING	
tn	H1	wtfile	
at	1.483	proc	ft
rp	16000	fn	not used
sw	5393.0	math	f
fb	3000		
bs	32	verr	
ss	2	wexp	
tpwr	63	wbs	
pw	9.5	wnt	wft
d1	2.000	DISPLAY	
tof	349.8	sp	151.3
nt	16	wp	5393.0
ct	16	vs	172
alock	n	sc	15
gain	not used	wc	150
FLAGS		hzmm	35.95
il	n	is	7.8125e+0~
in	n		6
cp	y	rfl	1093.3
hs	nn	rfp	1244.6
		th	120
		ins	6.000
		ai	cdc
		ph	

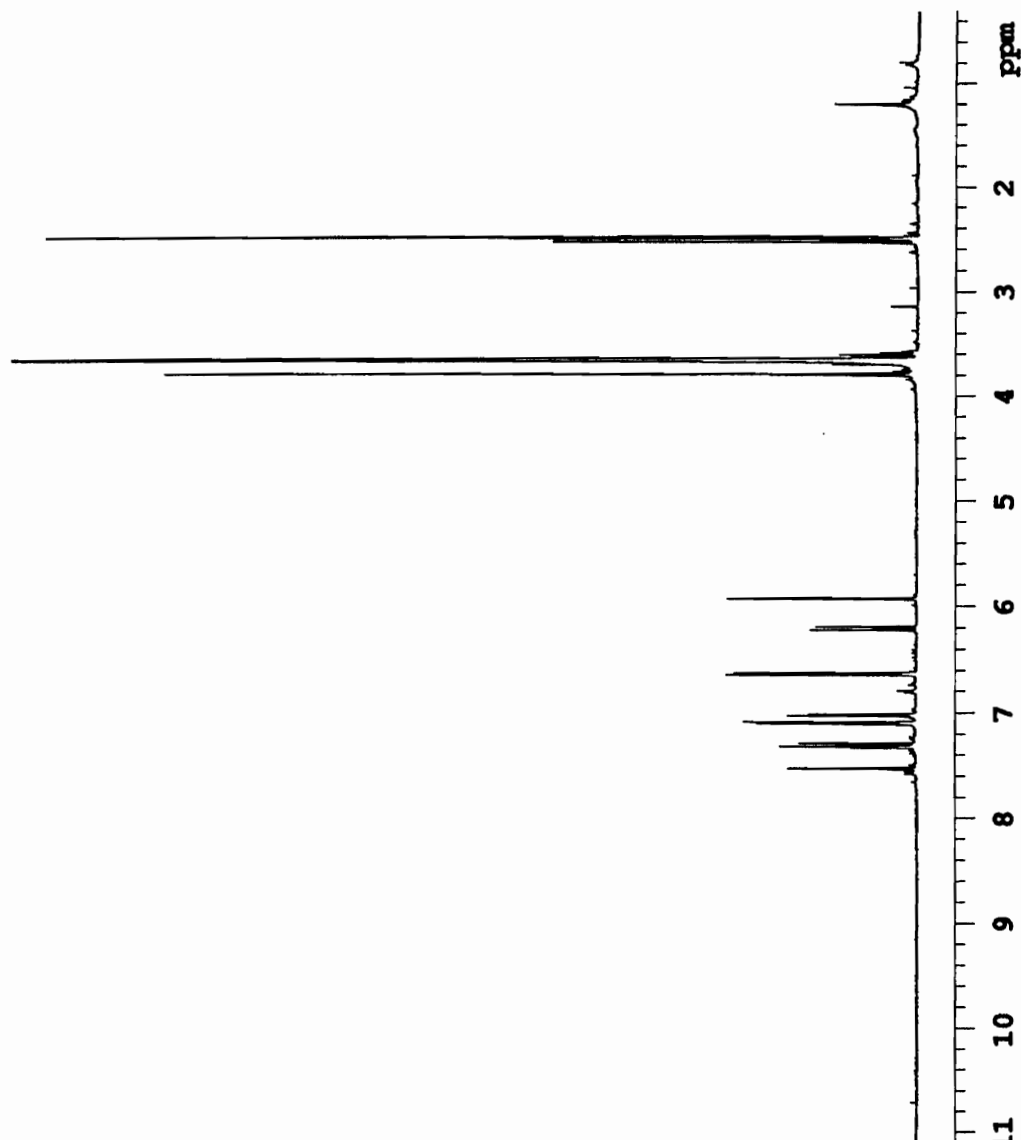


Figure D2. 500 MHz proton spectrum of botryllamide D (deuterium exchanged).

## Botryllamide D Carbon Spectrum

expl pulse sequence: s2pul

SAMPLE	DEC. & VT	
date	Mar 18 92	dn H1
solvent	DMSO	dof 349.8
file	/disk4/mc~ dn	YYY
donald/nci798/swer~ dnm		s
zey-carbon dmf		17632
ACQUISITION	cpwr	58
sfrq	125.697	PROCESSING
tn	C13	lb 1.50
at	1.300	wtfile
np	65024	proc ft
sw	25000.0	fn not used
fb	13800	math f
bs	16	
ss	2	werr
tpwr	62	wexp
pw	10.2	wbs wft
d1	2.000	wnt
tof	0	DISPLAY
nt	10000	sp -648.0
ct	3824	wp 25000.0
alock	n	vs 353
gain	not used	sc 15
FLAGS	wc	150
il	n	hzmm 166.67
in	n	ls 500.00
dp	y	rfl 5613.0
hs	nn	rffp 4965.0
	th	120
	ins	1.000
	nm	cdc
	ph	

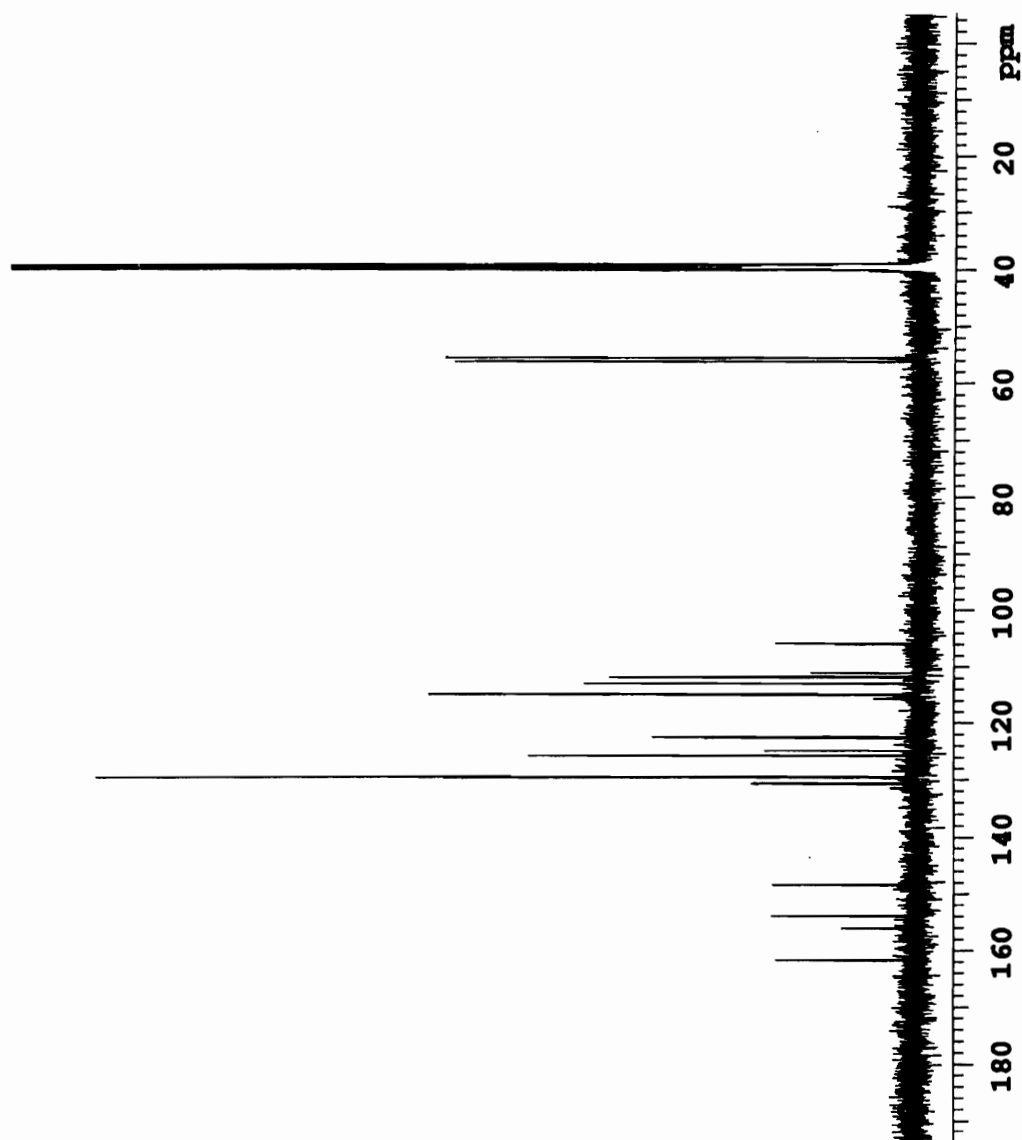


Figure D3. 125 MHz carbon spectrum of botryllamide D.

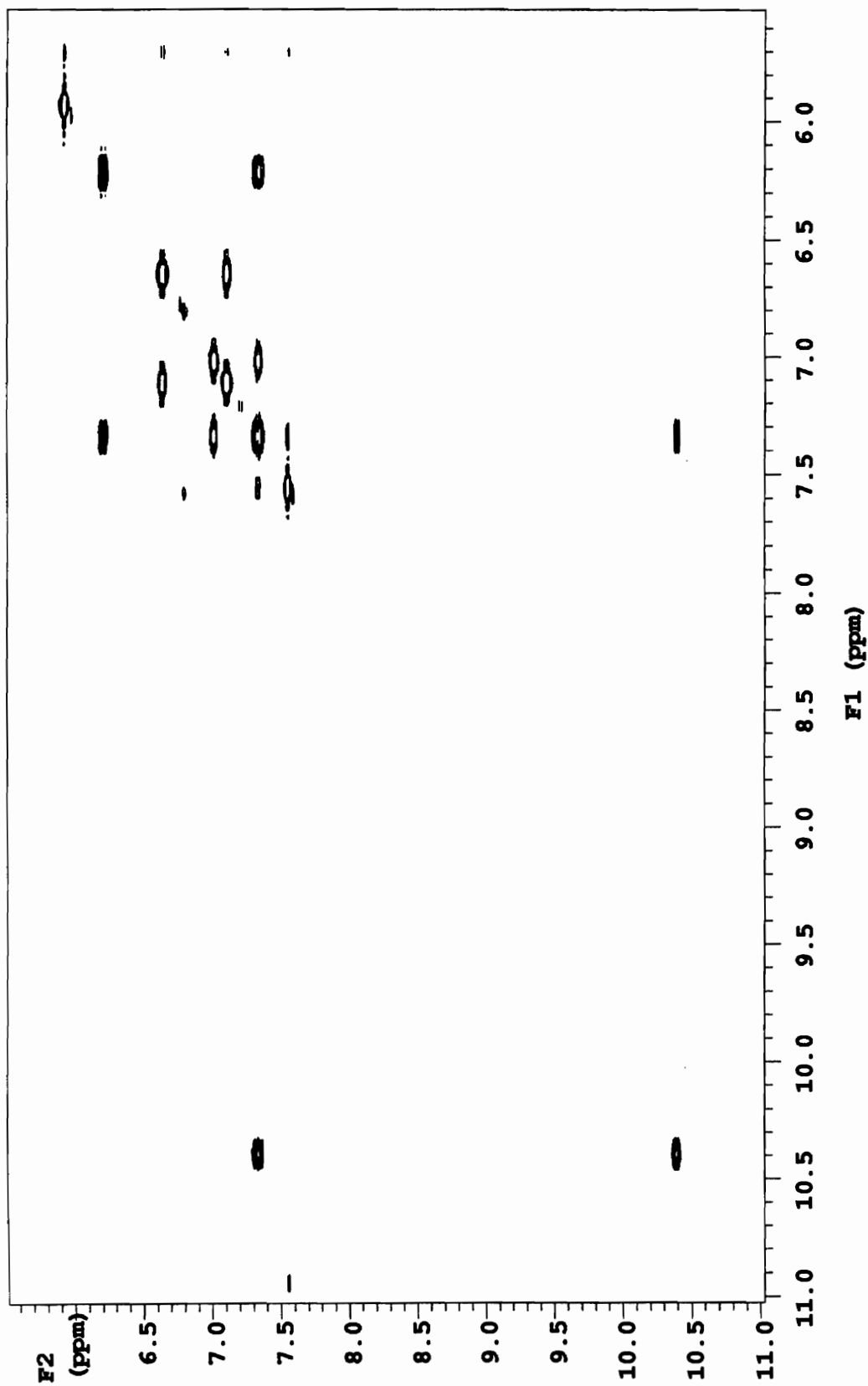


Figure D4. 500 MHz COSY spectrum of botryllamide D.



## Botryllamide D COSY Spectrum

expl pulse sequence: cosyys

SAMPLE		DEC. & VT		ACQUISITION ARRAYS	
date	Mar 18 92	dn	H1	array	phase
solvent	DMSO	dof	0	arraydim	512
file	/disk4/mc-	dm	nnn		
	donald/nci798/swer-	dmm	c	1	phase
	zey-PScosy	dof	200	1	1
	ACQUISITION	dpwr	30	2	2
sfrq	499.843	PROCESSING			
tn	H1	gf	0.087		
at	0.190	gfs	not used		
mp	2048	wtfile			
sw	5393.0	proc	ft		
fb	3000	fn	2048		
bs	32	math	f		
ss	8				
tpwr	62	werr			
pw	11.1	wexp			
p1	11.1	wbs			
d1	0.495	wnt			
presat	0	2D PROCESSING			
tof	349.8	gf1	0.011		
nt	8	gfs1	not used		
ct	8	wtfile1			
alock	n	procl	ft		
gain	27	fn1	2048		
FLAGS		DISPLAY			
il	n	sp	155.2		
in	n	wp	5393.0		
dp	y	vs	5762		
hs	nn	sc	6		
2D ACQUISITION		wc	130		
sw1	5393.0	hzmm	41.48		
ni	256	is	819.56		
phase	arrayed	rfl	1089.4		
2D DISPLAY		rfp	1244.6		
sp1	155.2	th	2		
wp1	5393.0	ins	6.000		
sc2	0	ai cdc ph			
wc2	130				
rfl1	1089.4				
rfp1	1244.6				

Figure D5. Parameter set for 500 MHz COSY spectrum of botryllamide D.

Botryllamide B Proton Spectrum

exp1 pulse sequence: s2pul

SAMPLE	DEC. & VT	
date	Aug 9 93	dn H1
solvent	DMSO	dof 0
file	/disk4/mc-dm	nnn
donaId/temp/r798/2~	chmm	c
1-9_proton	dmf	200
ACQUISITION	dpwr	30
sfrq	499.843	temp 25.0
tn	H1	PROCESSING
at	2.980	lb not used
np	32768	wtfile
sw	5498.3	proc ft
fb	3100	fn 65536
bs	8	math f
tpwr	62	
pw	3.0	warr
dl	2.000	wexp
tof	250.5	wbs
nt	16	wnt wft
ct	16	DISPLAY
alock	s	sp 0.0
gain	0	wp 5498.3
FLAGS	vs	119
il	n	sc 15
in	n	wc 150
dp	y	hrrmm 36.66
hs	nn	is 6746.22
		rfl 1244.6
		rfp 1244.6
		th 120 11
		ins 10.200

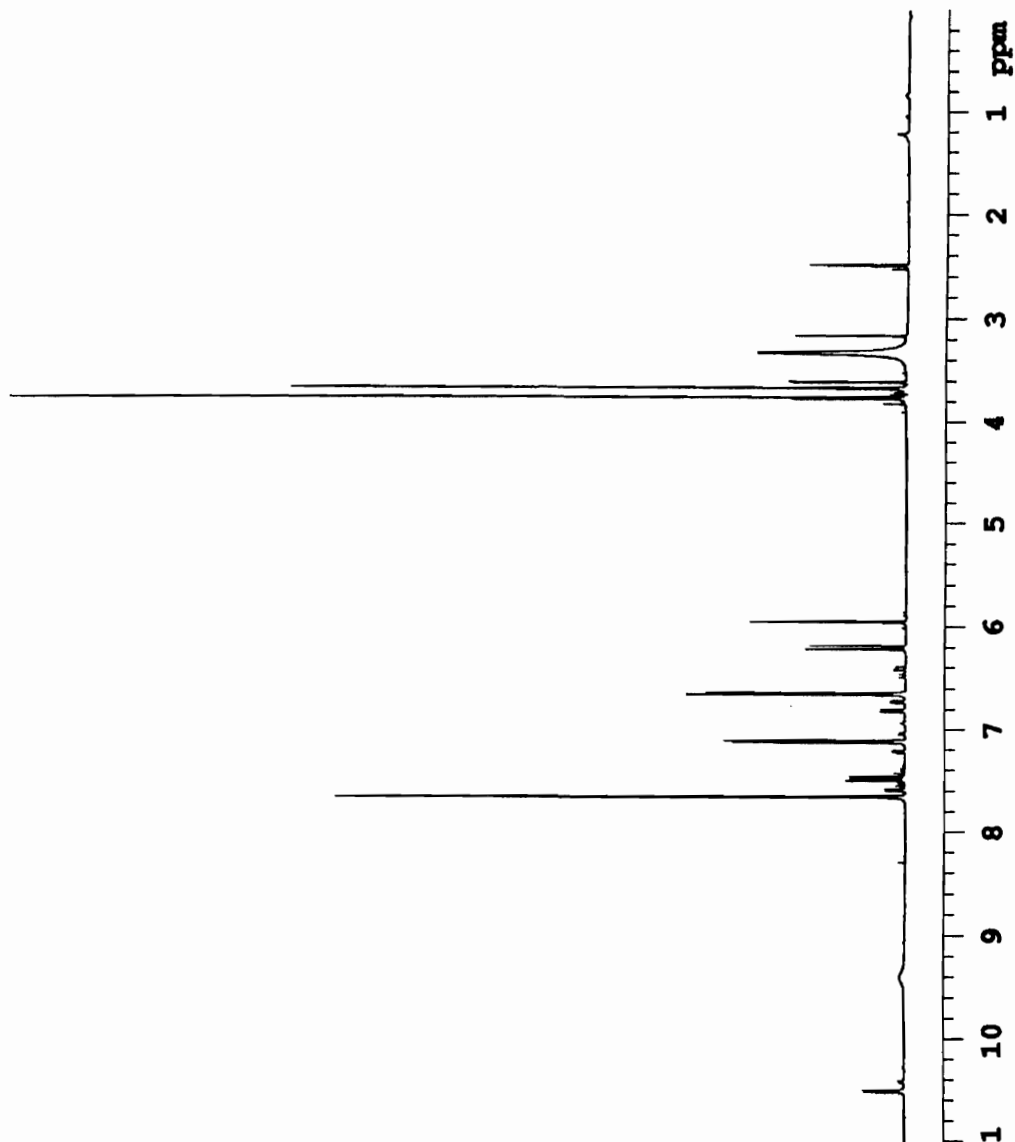


Figure D6. 500 MHz proton spectrum of botryllamide B.

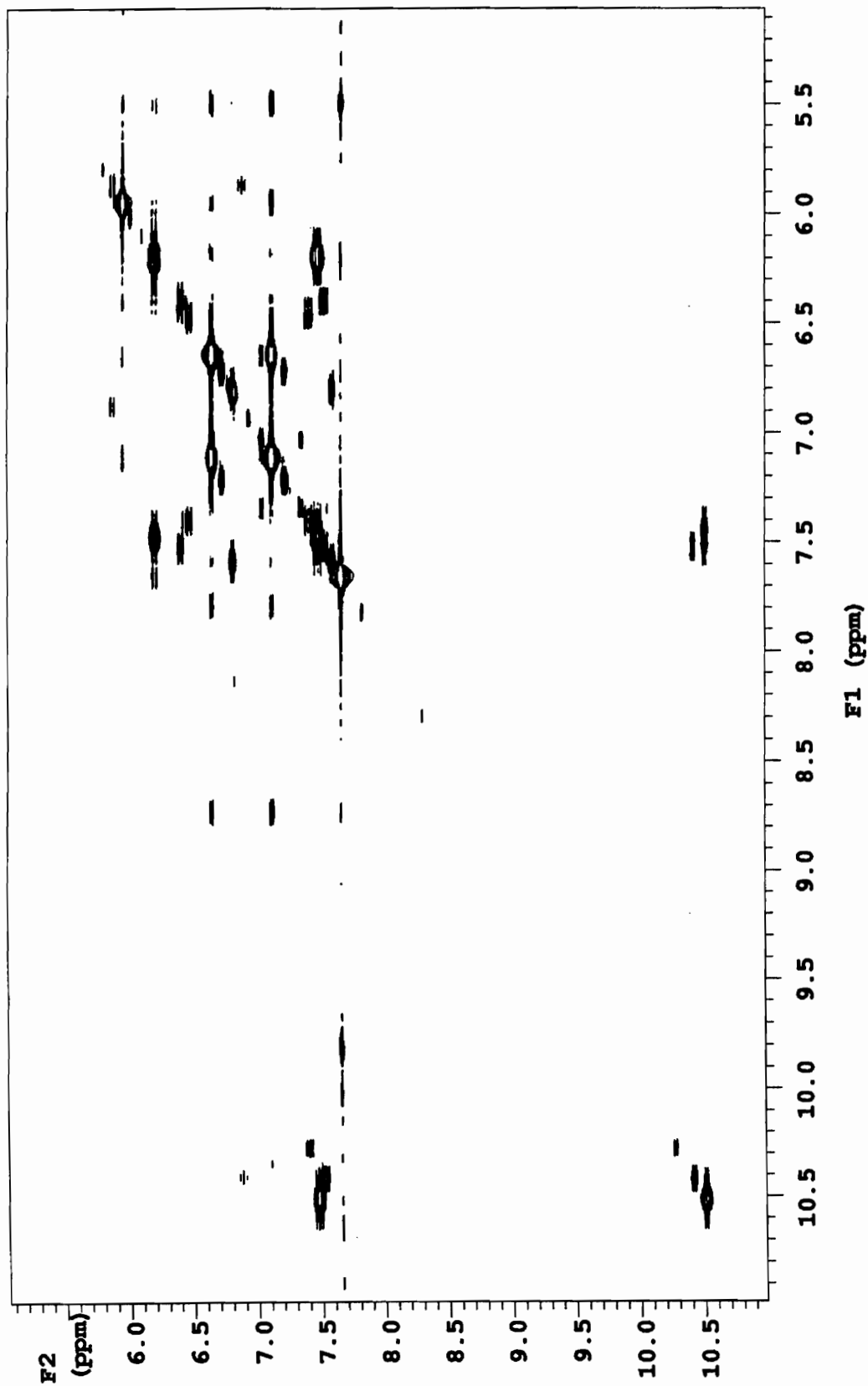


Figure D7. 500 MHz COSY spectrum of botryllamide B.

## Botryllamide B COSY Spectrum

expl pulse sequence: relayh

SAMPLE		DEC. & VT	
date	Aug 9 93	dn	H1
solvent	DMSO	dof	0
file	/disk4/mc~	dm	nnn
donald/temp/r798/B~		dmm	c
otryllamide_B_cosy		dmf	200
ACQUISITION		dpwr	30
sfrq	499.843	temp	25.0
tn	H1	PROCESSING	
at	0.372	sb	0.185
np	4096	abs	not used
sw	5498.3	wtfile	
fb	3100	proc	ft
bs	4	fn	4096
ss	8	math	f
tpwr	62		
pw	12.2	werr	
pl	12.2	wexp	
dl	2.000	wbs	
phase	0	wnt	
tof	250.5	2D PROCESSING	
nt	12	sbl	0.027
ct	4	absl	not used
alock	s	wtfile1	
gain	20	procl	ft
FLAGS		fnl	1024
il	y	DISPLAY	
in	n	sp	2527.6
dp	y	wp	2957.3
hs	nn	vs	4180
2D ACQUISITION		sc	20
sw1	5498.3	wc	205
ni	300	hzmm	14.43
2D DISPLAY		is	33.57
sp1	2528.6	rfl	1244.6
wp1	2959.0	rfp	1244.6
sc2	18	th	8
wc2	120	ins	1.000
rfl1	1244.6	ai	cdc av
rfp1	1244.6		

Figure D8. Parameter set for 500 MHz COSY spectrum of botryllamide B.

Botryllamide C Proton Spectrum

exp1 pulse sequence: s2pul

SAMPLE	DEC. & VT	
date Aug 8 93	dn H1	
solvent DMSO	dof 0	
file /disk4/mc~ da	nnn	
donald/temp/x798/2~ dnm	c	
1-8_proton dmf	200	
ACQUISITION	cpwr 30	
sfreq 499.843	temp 25.0	
tn H1	PROCESSING	
at 2.980	wtfile	
np 32768	proc	ft
sw 5498.3	fn	32768
fb 3100	math	f
bs 8		
tpwr 62	werr	
pw 3.0	wexp	
dl 2.000	wbs	
tof 250.5	wnt	wft
nt 16	DISPLAY	
ct 16	sp	0.0
alock s	vp	5498.3
gain 0	vs	117
FLAGS	sc	15
il n	wc	150
in n	hzmm	36.66
dp y	is	1004.62
hs nn	rfl	1244.6
	rfp	1244.6
	th	120
	ins	5.200 11
	nm	cdc ph

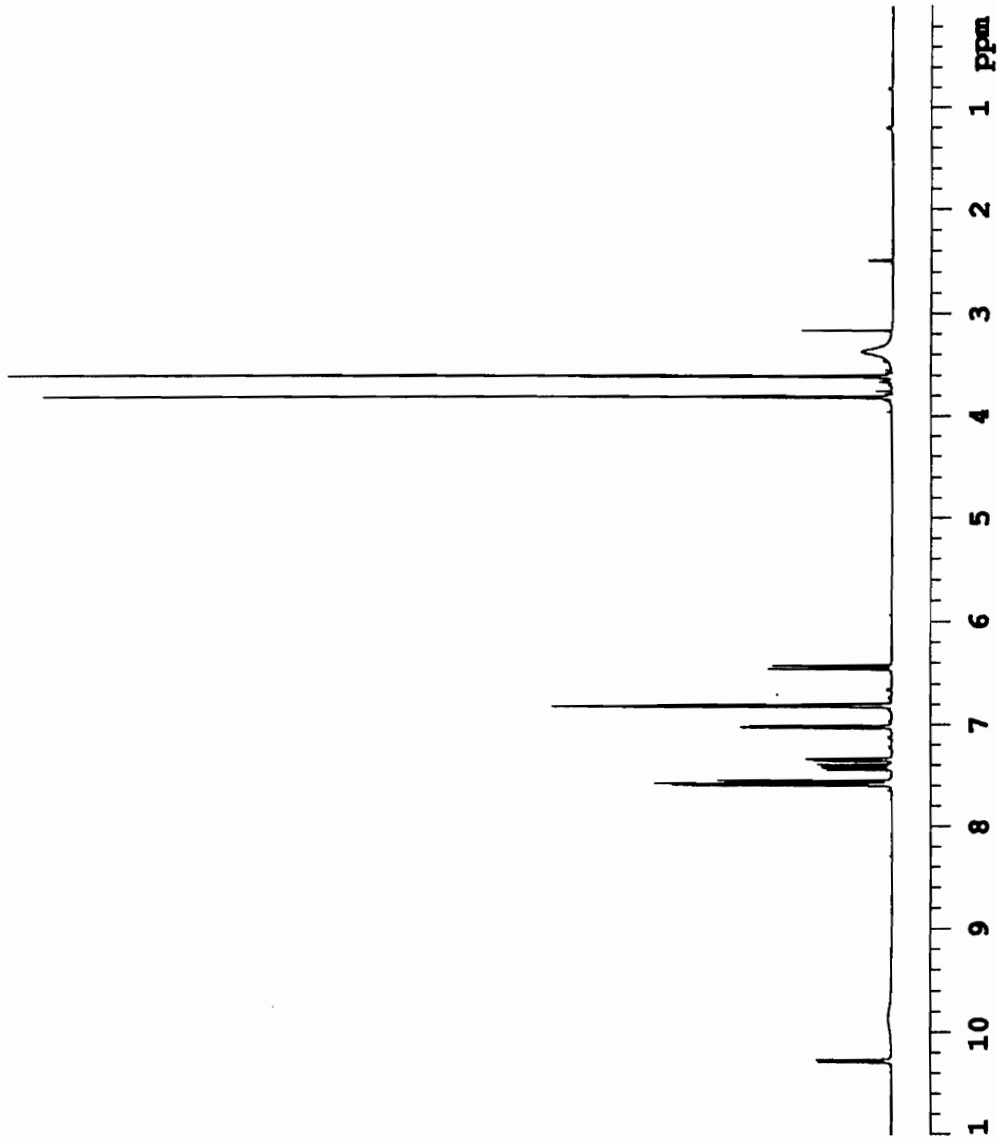


Figure D9. 500 MHz proton spectrum of botryllamide C.

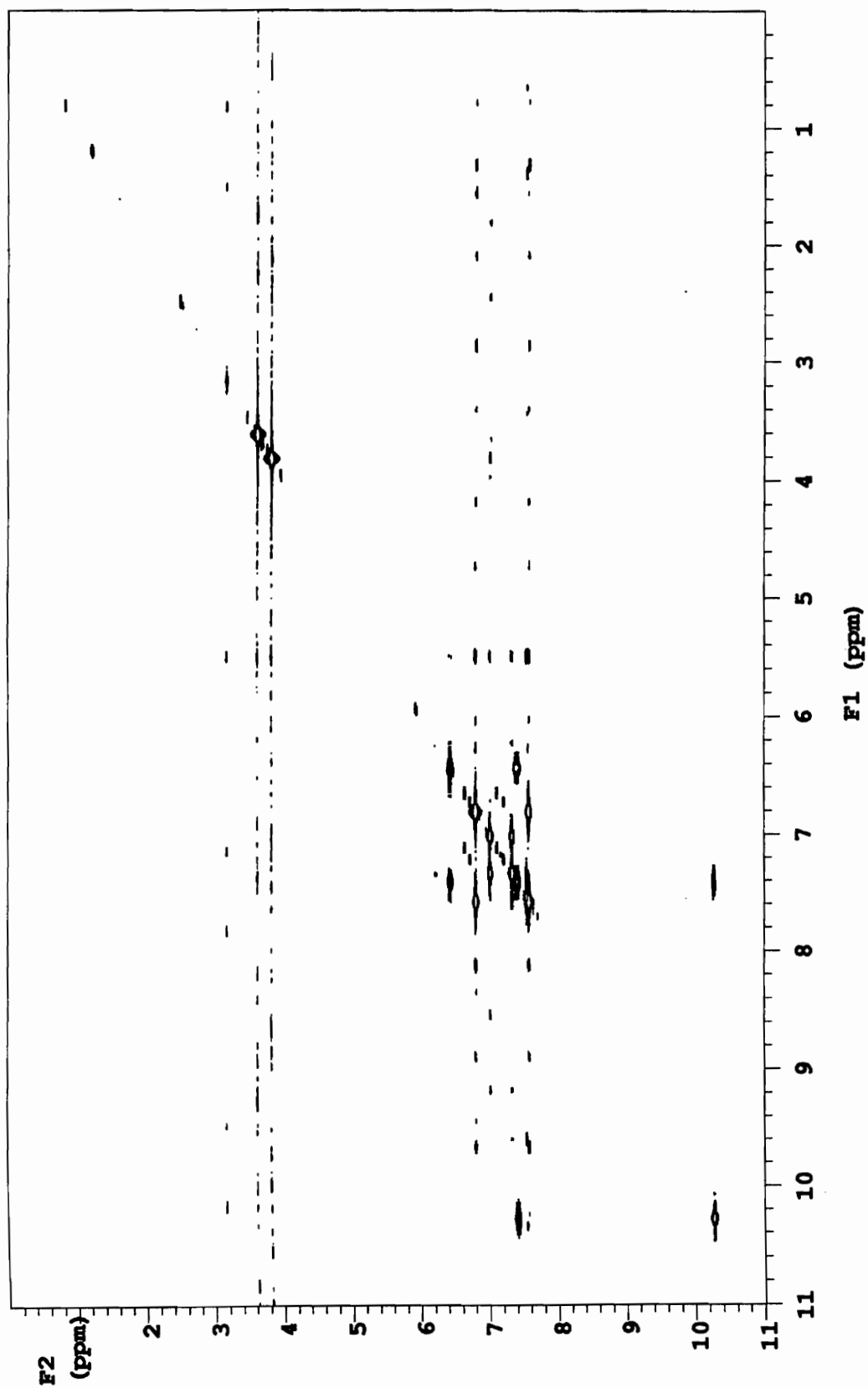


Figure D10. 500 MHz COSY spectrum of botryllamide C.

## Botryllamide C COSY Spectrum

expl pulse sequence: relayh

```

      SAMPLE          DEC. & VT
date   Aug  8 93  dn          H1
solvent DMSO  dof           0
file   /disk4/mc~ dm          nnn
donald/temp/r798/B~ dmm       c
otryllamide_C_cosy dmf       200
      ACQUISITION    dpwr      30
sfrq   499.843  temp        25.0
tn      H1          PROCESSING
at      0.372  ab          0.185
np      4096  abs         not used
sw      5498.3  wtfile
fb      3100  proc         ft
bs      4      fn          4096
ss      8      math        f
tpwr   62
pw      11.4  verr
pl      11.4  wexp
dl      2.000  wbs
phase  0      wnt
tof     250.5  2D PROCESSING
nt      8      sb1         0.027
ct      8      sbs1        not used
alock  s      wtfile1
gain   0      procl        ft
      FLAGS          fn1          1024
il      y          DISPLAY
in      n      sp          0.0
cp      y      wp          5498.3
hs      nn     vs          1000
      2D ACQUISITION  sc          20
sw1     5498.3  wc          205
ni      300    hzmm        13.33
      2D DISPLAY      is          33.57
sp1     0.0    rfl          1244.6
wp1     5498.3  rfp          1244.6
sc2     18     th          5
wc2     120    ins         1.000
rfl1    1244.6  ai cdc av
rfpl    1244.6

```

Figure D11. Parameter set for 500 MHz COSY spectrum of botryllamide C.

## Botryllamide A Proton Spectrum

exr1 pulse sequence: s2pul

```

SAMPLE          DEC. & VT
date    Aug 8 93   dn    H1
solvent  DMSO     dof    0
file    /disk4/mc-  dm   nnn
donald/r798/22-8_p-  dm   c
        roton     daf    200
        ACQUISITION dpwr   30
sfrq    499.843   temp  25.0
        H1        PROCESSING
tn       2.049   wtfile
at       22528  proc
np       5498.3 fn    32768   ft
sw       3100   math
fb       8
bs
tpwr    62   weir
pw      4.0   wezp
d1      2.000 wbs
tof     250.5 wnt
nt      16
ct      16   sp    0.0
alock   s   wp    5498.3
gain    0   vs    115
        FLAGS    sc    15
il      n   wc    150
in      n   hzmm  36.66
cp      y   is    33.57
hs      nn  rfl   1244.6
        th      rfp   1244.6
        ins    1.000 11
        nm    cdc   ph

```

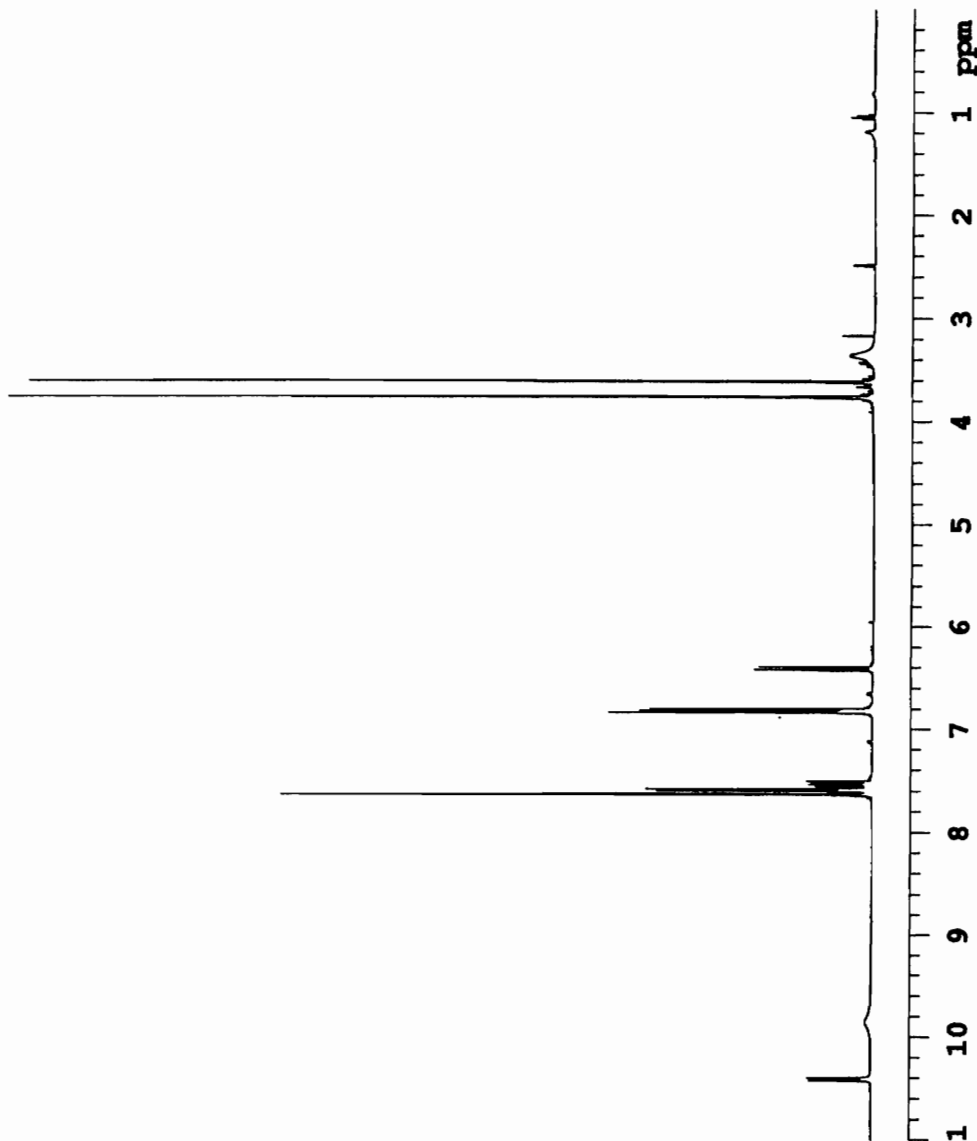


Figure D12. 500 MHz proton spectrum of botryllamide A.



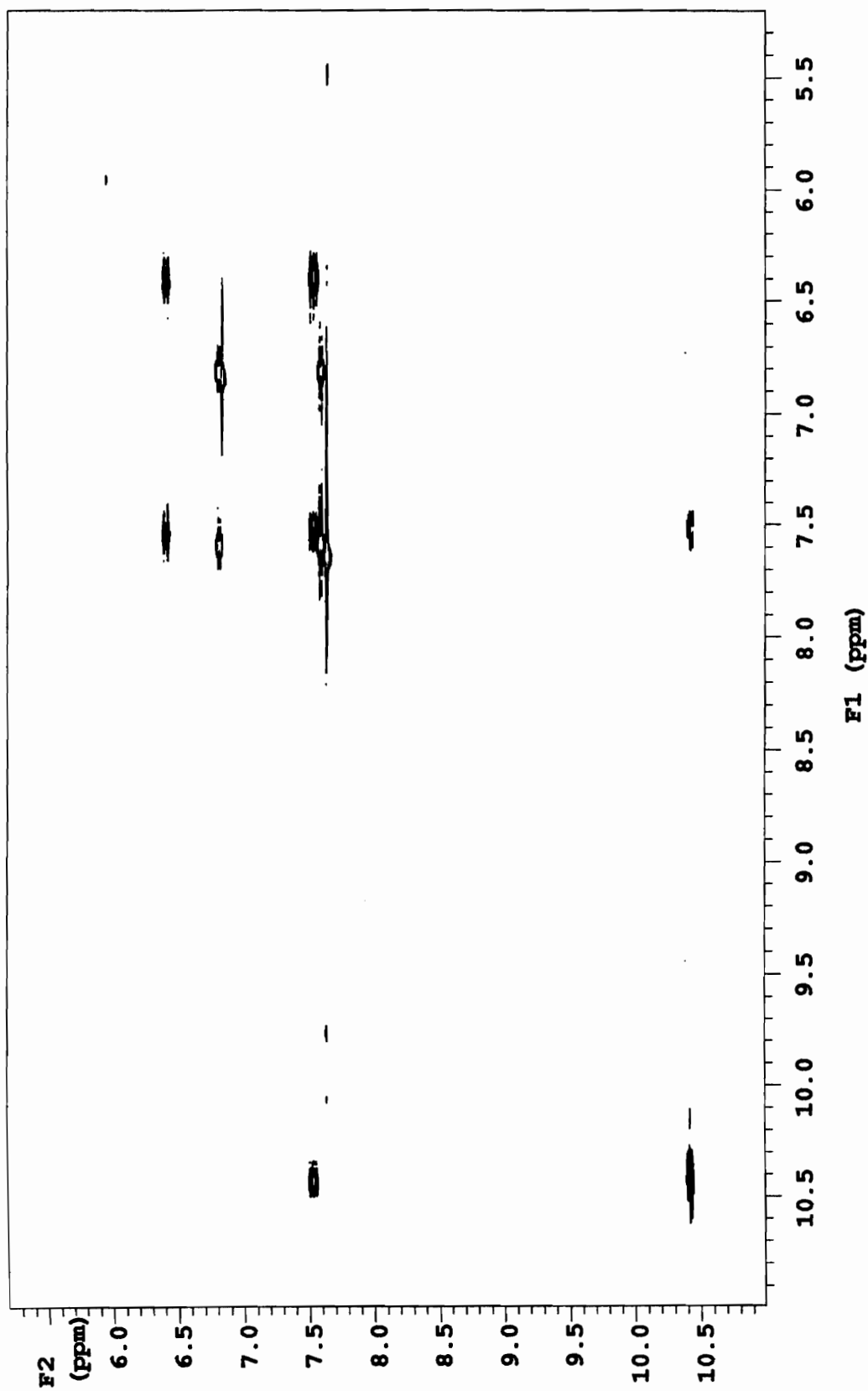


Figure D13. 500 MHz COSY spectrum of botryllamide A.

## Botryllamide A COSY Spectrum

expl pulse sequence: relayh

SAMPLE		DEC. & VT	
date	Aug 8 93	dn	H1
solvent	DMSO	dof	0
file	/disk4/mc~	dm	nnn
	donald/r798/22-8_r~	dmm	c
	elayh	dmf	200
ACQUISITION		dpwr	30
sfrq	499.843	temp	25.0
tn	H1	PROCESSING	
at	0.372	sb	0.185
np	4096	sbs	not used
sw	5498.3	wtfile	
fb	3100	proc	ft
bs	8	fn	4096
ss	8	math	f
tpwr	62		
pw	11.5	werr	
pl	11.5	wexp	
dl	2.000	wbs	
phase	0	wnt	
tof	250.5	2D PROCESSING	
nt	16	sbl	0.023
ct	8	sbs1	not used
alock	a	wtfile1	
gain	0	procl	ft
FLAGS		fn1	1024
il	y	DISPLAY	
in	n	sp	3158.8
dp	y	wp	717.2
hs	nn	vs	16000
2D ACQUISITION		sc	6
sw1	5498.3	wc	225
ni	300	hzmm	42.29
2D DISPLAY		is	33.57
sp1	2959.0	rfl	1244.6
wp1	1226.6	rfp	1244.6
sc2	0	th	12
wc2	130	ins	1.000
rfl1	1244.6	ai cdc av	
rfp1	1244.6		

Figure D14. Parameter set for 500 MHz COSY spectrum of botryllamide A.

APPENDIX E

ISOLATION FLOW DIAGRAMS

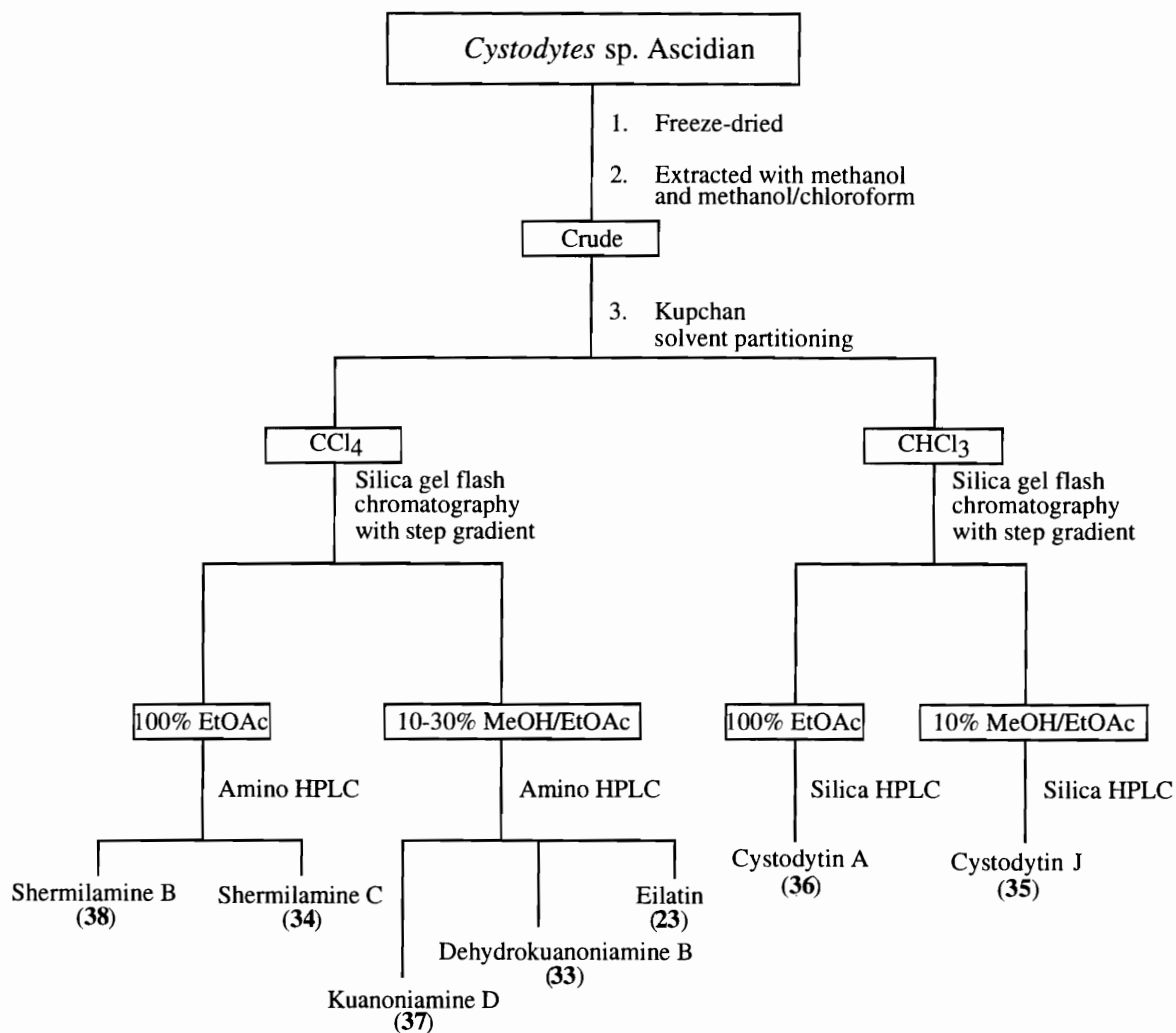


Figure E1. Isolation flow diagram for the pyridoacridines from the ascidian *Cystodytes* sp.

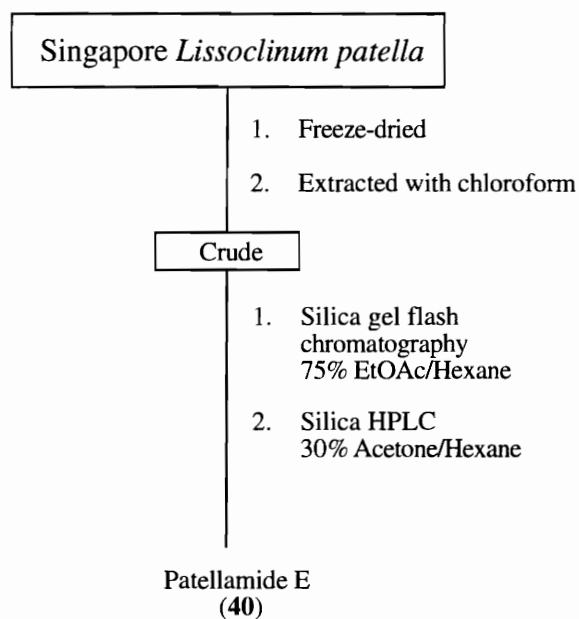


Figure E2. Isolation flow diagram for patellamide E from the ascidian *Lissoclinum patella* (Singapore)

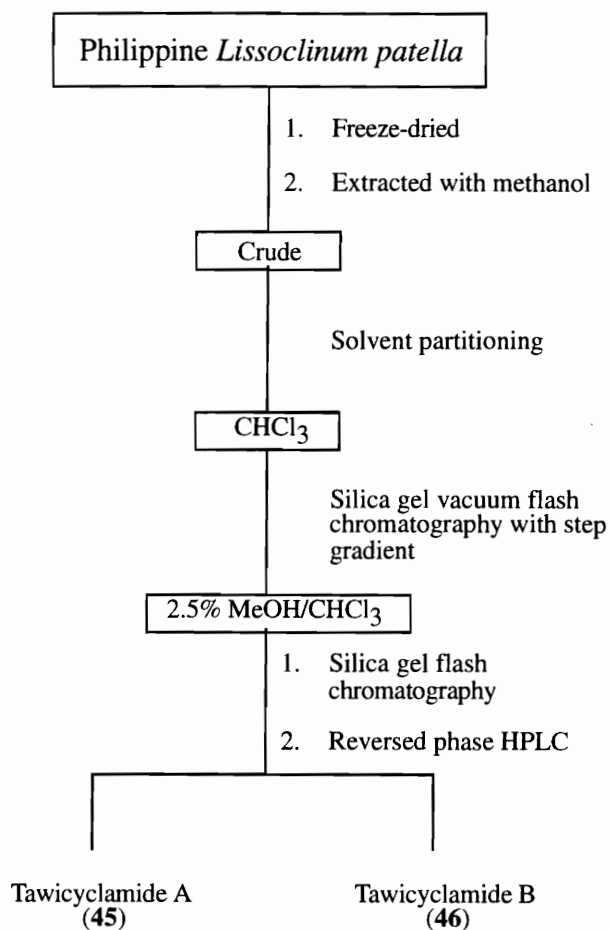


Figure E3. Isolation flow diagram for the tawicyclamides from the ascidian *Lissoclinum patella* (Philippine).

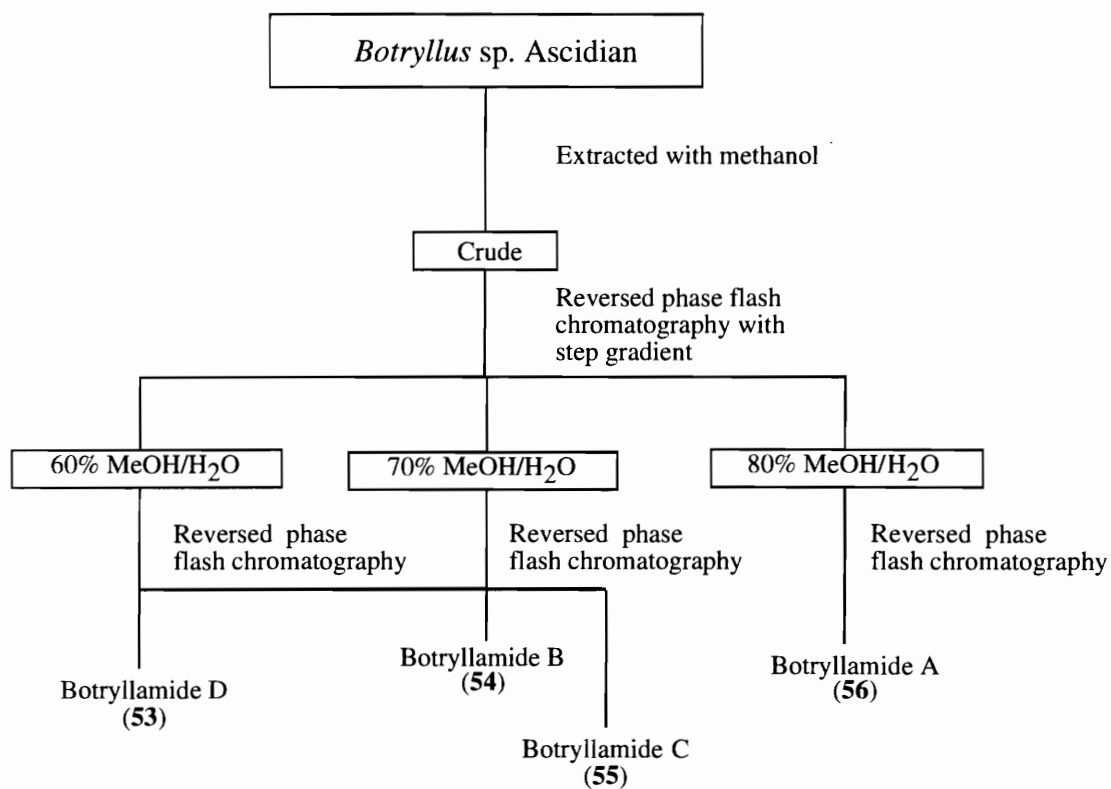


Figure E4. Isolation flow diagram for the botryllamides from the ascidian *Botryllus sp.*

## REFERENCES

1. Barth, R. H.; Broshears, R. E. *The Invertebrate World*; CBS College Publishing: New York, NY, 1982, pp 646.
2. George, J. D.; George, J. J. *Marine Life*; Wiley-Interscience: New York, NY, 1979, pp 288.
3. Pomponi, S. A. In *Biomedical Importance of Marine Organisms*; D. G. Fautin, Ed.; California Academy of Sciences: San Francisco, 1988; Vol. 13; pp 7.
4. Suganuma, M.; Fujiki, H.; Suguri, H.; Yoshizawa, S.; Hirota, M.; Nakayasu, M.; Ojika, M.; Wakamatsu, K.; Yamada, K.; Sugimura, T. *Proc. Natl. Acad. Sci. USA* **1988**, *85*, 1768.
5. Ireland, C. M.; Copp, B. R.; Foster, M. P.; McDonald, L. A.; Radisky, D. C.; Swersey, J. C. In *Marine Biotechnology*; D. H. Attaway and O. R. Zaborsky, Ed.; Plenum Press: New York, 1993; Vol. 1: Pharmaceutical and Bioactive Natural Products; pp 1.
6. Attaway, D. H.; Zaborsky, O. R. *Marine Biotechnology*; Plenum Press: New York, NY, 1993; Vol. 1: Pharmaceutical and Bioactive Natural Products, pp 500.
7. Faulkner, D. J. *Nat. Prod. Rep.* **1984**, *1*, 252.
8. Faulkner, D. J. *Nat. Prod. Rep.* **1984**, *1*, 551.
9. Faulkner, D. J. *Nat. Prod. Rep.* **1986**, *3*, 1.
10. Faulkner, D. J. *Nat. Prod. Rep.* **1987**, *4*, 539.
11. Faulkner, D. J. *Nat. Prod. Rep.* **1988**, *5*, 613.
12. Faulkner, D. J. *Nat. Prod. Rep.* **1990**, *7*, 269.
13. Faulkner, D. J. *Nat. Prod. Rep.* **1991**, *8*, 97.
14. Faulkner, D. J. *Nat. Prod. Rep.* **1992**, *9*, 323.
15. Pawlik, J. R. *Chem. Rev.* **1993**, *93*, 1911.
16. Paul, V. J.; Fenical, W. In *Bioorganic Marine Chemistry*; P. J. Scheuer, Ed.; Springer-Verlag: Berlin, 1987; Vol. 1; pp 1.
17. Scheuer, P. J. *Science* **1990**, *248*, 173.



18. Ireland, C. M.; Roll, D. M.; Molinski, T. F.; McKee, T. C.; Zabriskie, T. M.; Swersey, J. C. In *Biomedical Importance of Marine Organisms*; D. G. Fautin, Ed.; California Academy of Sciences: San Francisco, 1988; Vol. 13; pp 41.
19. Negrelli, R. F. *Ann. N. Y. Acad. Sci.* **1960**, *90*, 615.
20. Hashimoto, Y. *Marine Toxins and Other Bioactive Marine Metabolites*; Japan Scientific Societies Press: Tokyo, 1979, pp 369.
21. Narahashi, T. In *Handbook of Natural Toxins*; A. T. Tu, Ed.; Marcel Dekker, Inc.: New York, NY, 1988; Vol. 3: Marine Toxins and Vemoms; pp 185.
22. Yasumoto, T.; Murata, M. *Chem. Rev.* **1993**, *93*, 1897.
23. Lee, W. W.; Benitez, A.; Goodman, L.; Baker, B. R. *J. Am. Chem. Soc.* **1960**, *82*, 2648.
24. Evans, J. S.; Musser, E. A.; Mengel, G. D.; Forsblad, K. R.; Hunter, J. H. *Proc. Soc. Exp. Biol. Med.* **1961**, *106*, 350.
25. Bergmann, W.; Feeney, R. J. *J. Org. Chem.* **1951**, *16*, 981.
26. Bergmann, W.; Burke, D. C. *J. Org. Chem.* **1955**, *20*, 1501.
27. Hashimoto, Y.; Okaichi, T. *Ann. N. Y. Acad. Sci.* **1960**, *90*, 667.
28. Boyd, M. R.; Shoemaker, R. H.; Cragg, G. M.; Suffness, M. In *Pharmaceuticals and the Sea*; C. W. Jefford, K. L. Rinehart and L. S. Shield, Ed.; Technomic Publishing Company: Landcaster, PA, 1988.
29. Geller, R. B.; Saral, R.; Karp, J. E.; Santos, G. W.; Burke, P. J. *Leukemia* **1990**, *4*, 313.
30. Whitley, R. J.; Soong, S. J.; Dolin, R.; Galasso, G.; Ch'ien, L. T.; Alford, C. A. *N. Engl. J. Med.* **1977**, *297*, 289.
31. Cohen, S. S. *Cancer* **1977**, *40*, 509.
32. Krebs, H. C. *Fortschr. Chem. Org. Naturst.* **1986**, *49*, 151.
33. Fusetani, N. In *Bioorganic Marine Chemistry*; P. J. Scheuer, Ed.; Springer-Verlag: Berlin, 1987; Vol. 1; pp 62.
34. Kato, Y.; Fusetani, N.; Matsunaga, S.; Hashimoto, K. *J. Am. Chem. Soc.* **1986**, *108*, 2780.
35. Suganuma, M.; Fujiki, H.; Furuya-Suguri, H.; Yoshizawa, S.; Yasumoto, S.; Kato, Y.; Fusetani, N.; Sugimura, T. *Cancer Res.* **1990**, *50*, 3521.
36. Ishihara, H.; Martin, B. L.; Brautigan, D. L.; Karaki, H.; Ozaki, H.; Kato, Y.; Fusetani, N.; Watabe, S.; Hashimoto, K.; Uemura, D.; Hartshorne, D. J. *Biochem. Biophys. Res. Commun.* **1989**, 871.
37. Gerwick, W. H.; Fenical, W.; Fritsch, N.; Clardy, J. *Tetrahedron Lett.* **1979**, 145.

38. Gerwick, W. H.; Fenical, W. *J. Org. Chem.* **1981**, *46*, 22.
39. O'Brien, E. T.; Jacobs, R. S.; Wilson, L. *Mol. Pharmacol.* **1983**, *24*, 493.
40. O'Brien, E. T.; Asai, D. J.; Groweill, A.; Lipshutz, B. H.; Fenical, W.; Jacobs, R. S.; Wilson, L. *J. Med. Chem.* **1986**, *29*, 1851.
41. Kashman, Y.; Groweiss, A.; Shmueli, U. *Tetrahedron Lett.* **1980**, *21*, 3629.
42. Longley, R. E.; McConnell, O. J.; Essich, E.; Harmody, D. *J. Nat. Prod.* **1993**, *56*, 915.
43. Coue, M.; Brenner, S. L.; Spector, I.; Korn, E. D. *FEBS Lett.* **1987**, *213*, 316.
44. Spector, I.; Shochet, N. R. *Science* **1983**, *219*, 493.
45. Spector, I.; Shochet, N. R.; Blasberger, D.; Kashman, Y. *Cell Motil. Cytoskel.* **1989**, *13*, 127.
46. Schatten, G.; Schatten, H.; Spector, H.; Cline, C.; Paweletz, N.; Simerly, C.; Petzelt, C. *Exp. Cell Res.* **1986**, *166*, 191.
47. Suffness, M.; Newman, D. J.; Snader, K. In *Bioorganic Marine Chemistry*; P. J. Scheuer, Ed.; Springer-Verlag: Berlin, 1989; Vol. 3; pp 131.
48. Sigel, M. M.; Wellham, L. L.; Lichter, W.; Dudek, L. E.; Gargus, J. L.; Lucas, A. H. In *Food-Drugs from the Sea: Proceedings*; H. W. Y. Jr, Ed.; Mar Tech Soc: Washington, DC, 1969; pp 281.
49. Wright, A. E.; Forelo, D. A.; Gunawardana, G. P.; Gunasekera, S. P.; Koehn, F. E.; McConnell, O. J. *J. Org. Chem.* **1990**, *55*, 4508.
50. Rinehart, K. L.; Holt, T. G.; Fregeau, N. L.; Stroh, J. G.; Keifer, P. A.; Sun, F.; Li, L. H.; Martin, D. G. *J. Org. Chem.* **1990**, *55*, 4512.
51. Rinehart, K. L.; Holt, T. G.; Fregeau, N. L.; Stroh, J. G.; Keifer, P. A.; Sun, F.; Li, L. H.; Martin, D. G. *J. Org. Chem.* **1991**, *56*, 1676.
52. Rinehart, K. L. *Pure & Appl. Chem.* **1989**, *61*, 525.
53. Pettit, G. R.; Day, J. F.; Hartwell, J. L.; Wood, H. B. *Nature (London)* **1970**, *227*, 962.
54. Pettit, G. R.; Herald, C. L.; Doubek, D. L.; Herald, D. L. *J. Am. Chem. Soc.* **1982**, *104*, 6846.
55. Hennings, H.; Blumberg, P. M.; Pettit, G. R.; Herald, C. L.; Shores, R.; Yuspa, S. H. *Carcinogenesis* **1987**, *8*, 1343.
56. Munro, M. H. G.; Blunt, J. W.; Barns, G.; Battershill, C. N.; Lake, R. J.; Perry, N. B. *Pure Appl. Chem.* **1989**, *61*, 529.

57. Schmitz, F. J.; Bowden, B. F.; Toth, S. I. In *Marine Biotechnology*; D. H. Attaway and O. R. Zaborsky, Ed.; Plenum Press: New York, 1993; Vol. 1: Pharmaceutical and Bioactive Natural Products; pp 197.
58. Rinehart, K. L.; Shaw, P. D.; Shield, L. S.; Gloer, J. B.; Harbour, G. C.; Koker, M. E. S.; Samain, D.; Schwartz, R. E.; Tymiak, A. A.; Weller, D. L.; Carter, G. T.; Munro, M. H. G.; Hughes, R. G.; Renis, H. E.; Swyneberg, E. B.; Stringfellow, D. A.; Vavra, J. J.; H., C. J.; Zurenko, G. E.; Kuentzel, S. L.; Li, L. H.; Bakus, G. J.; Brusca, R. C.; Craft, L. L.; Young, D. N.; Conner, J. L. *Pure Appl. Chem.* **1981**, *53*, 795.
59. Rinehart, K. L.; Gloer, J. B.; Cook, J. C.; Mizensak, S. A.; Scahill, T. A. *J. Am. Chem. Soc.* **1981**, *103*, 1857.
60. Rinehart, K. L.; Gloer, J. B.; Hughes, R. G.; Renis, H. E.; McGovren, J. P.; Swynenberg, E. B.; Stringfellow, D. A.; Kuentzel, S. L.; Li, L. H. *Science* **1981**, *212*, 933.
61. Dorr, F. A.; Kuhn, J. G.; Phillips, J.; von Hoff, D. D. *Eur. J. Cancer Clin. Oncol.* **1988**, *24*, 1699.
62. Stewart, J. A.; Tong, W. P.; Hartshorn, J. N.; McCormack, J. J. *Proc. Am. Soc. Clin. Oncol.* **1986**, *5*, 33.
63. Chun, H. G.; Davies, B.; Hoth, D.; Suffness, M.; Plowman, J.; Flora, K.; Grieshaber, C.; Leyland-Jones, B. *Invest. New Drugs* **1986**, *4*, 279.
64. Dorr, A.; Schwartz, R.; Kuhn, J.; Bayne, J.; von Hoff, D. D. *Proc. Am. Assoc. Cancer Res.* **1986**, *5*, 39.
65. Canonico, P. G.; Pannier, W. L.; Huggins, J. W.; Rinehart, K. L. *Antimicro. Ag. Chemother.* **1982**, *22*, 696.
66. Montgomery, D. W.; Zukoski, C. F. *Transplantation* **1985**, *40*, 49.
67. Montgomery, D. W.; Celniker, A.; Zukoski, C. F. *Transplantation Proc.* **1987**, *19*, 1295.
68. Pettit, G. R.; Kamano, Y.; Herald, C. L.; Tuinman, A. A.; Boettner, F. E.; Kizu, H.; Schmidt, J. M.; Baczynskyj, L.; Tomer, K. B.; Bontems, R. J. *J. Am. Chem. Soc.* **1987**, *109*,
69. Bai, R.; Pettit, G. R.; Hamel, E. *Biochem. Pharmacol.* **1990**, *39*, 1941.
70. Bai, R.; Pettit, G. R.; Hamel, E. *Biochem. Pharmac.* **1990**, *40*, 1859.
71. Bai, R.; Pettit, G. R.; Hamel, E. *J. Biol. Chem.* **1990**, *265*, 17141.
72. Gunawardana, G. P.; Kohmoto, S.; Gunasakera, S. P.; McConnell, O. J.; Koehn, F. E. *J. Am. Chem. Soc.* **1988**, *110*, 4856.
73. Burren, N. S.; Sazesh, S.; Gunawardana, G. P.; Clement, J. J. *Cancer Res.* **1989**, *49*, 5267.

74. McDonald, L. A.; Eldredge, G. S.; Barrows, L. R.; Ireland, C. M. *Submitted for publication.*
75. Tachibana, K.; Scheuer, P. J.; Tsukitani, Y.; Kikuchi, H.; van Engen, D.; Clardy, J.; Gopichand, Y.; Schmitz, F. J. *J. Am. Chem. Soc.* **1981**, *103*, 2469.
76. Murakami, Y.; Oshima, Y.; Yasumoto, T. *Bull. Jpn. Soc. Sci. Fish.* **1982**, *48*, 69.
77. Hirata, Y.; Uemura, D. *Pure Appl. Chem.* **1986**, *58*, 701.
78. Bai, R.; Paull, K. D.; Herald, C. L.; Malspeis, L.; Pettit, G. R.; Hamel, E. *J. Biol. Chem.* **1991**, *266*, 15882.
79. Gerwick, W. H.; Proteau, P. J.; Nagle, D. G.; Hamil, E.; Blokhin, A.; Slate, D. L. *J. Org. Chem.* **1994**, *59*, 1243.
80. Radisky, D. C.; Radisky, E. S.; Barrows, L. R.; Copp, B. R.; Kramer, R. A.; Ireland, C. M. *J. Am. Chem. Soc.* **1992**, *115*, 1632.
81. Barrows, L. R.; Radisky, D. C.; Copp, B. R.; Swaffar, D. S.; Kramer, R. A.; Warters, R. L.; Ireland, C. M. *Anti-Cancer Drug Design* **1993**, *8*, 331.
82. Copp, B. R.; Ireland, C. M. *J. Org. Chem.* **1991**, *56*, 4596.
83. Swaffar, D. S.; Ireland, C. M.; Barrows, L. R. *Anti-Cancer Drugs* **1994**, *5*, 15.
84. Williams, D. H.; Stone, M. J.; Hauck, P. R.; Rahman, S. K. *J. Nat. Prod.* **1989**, *52*, 1189.
85. Schmitz, F. J.; DeGuzman, F. S.; Hossain, M. B.; van der Helm, D. *J. Org. Chem.* **1991**, *56*, 804.
86. Zhang, H.; D'Arpa, P.; Liu, L. F. *Cancer Cells* **1990**, *2*, 23.
87. Slichenmeyer, W. J.; Rowinsky, E. K.; Donehower, R. C.; Kaufmann, S. H. *J. Natl. Cancer Inst.* **1993**, *85*, 271.
88. Hamel, E. *Pharmac. Ther.* **1992**, *55*, 31.
89. Shochet, N. R.; Rudi, A.; Kashman, Y.; Hod, Y.; El-Maghrami, M. R.; Spector, I. *J. Cell. Physiol.* **1993**, *157*, 481.
90. Rudi, A.; Benayahu, Y.; Goldberg, I.; Kashman, Y. *Tetrahedron Lett.* **1988**, *29*, 6655.
91. Cohen, P.; Holmes, C. F. B.; Tsukitani, Y. *Trends Biochem. Sci.* **1990**, *15*, 98.
92. 12-O-Tetradecanoylphorbol-13-acetate.
93. Haystead, T. A. J.; Sim, A. T. R.; Carling, D.; Honner, R. C.; Tsukitani, Y.; Cohen, P.; Hardie, D. G. *Nature* **1989**, *337*, 78.
94. Sassa, T.; Richter, W. W.; Uda, N.; Suganuma, M.; Suguri, H.; Yoshizawa, S.; Horita, M.; Fujiki, H. *Biochem. Biophys. Res. Commun.* **1989**, *159*, 939.

95. de Silva, E. D.; Williams, D. E.; Andersen, R. J.; Klix, H.; Holmes, F. B.; Allen, T. M. *Tetrahedron Letters* **1992**, *33*, 1561.
96. Nishiwaki-Matsushima, R.; Ohta, T.; Nishiwaki, S.; Suganuma, M.; Kohyama, K.; Ishikawa, T.; Carmichael, W. W.; Fujiki, H. *J. Cancer Res. Clin. Oncol.* **1992**, *118*, 420.
97. Mosmann, T. *J. Immunol. Methods* **1983**, *65*, 55.
98. Denizot, F.; Lang, R. *J. Immunol. Methods* **1986**, *89*, 271.
99. Carmichael, J.; DeGraff, W. G.; Gazdar, A. F.; Minna, J. D.; Mitchell, J. B. *Cancer Res.* **1987**, *47*, 936.
100. Barrows, L. R.; Borchers, A. H.; Paxton, M. B. *Carcinogenesis* **1987**, *8*, 1853.
101. Jeggo, P. A.; Caldecott, K.; Pidsley, S.; Banks, G. R. *Cancer Res.* **1989**, *49*, 7057.
102. Caldecott, K.; Banks, G.; Jeggo, P. *Cancer Res.* **1990**, *50*, 5778.
103. Kemp, L. M.; Sedgwick, S. G.; Jeggo, P. A. *Mutation Res.* **1984**, *132*, 189.
104. 1,3-bis(2-chloroethyl)-1-nitrosourea
105. Herrlich, P.; Mallick, U.; Ponta, H.; Pahmsdorm, H. *J. Hum. Genet.* **1984**, *67*, 360.
106. Alberts, B.; Bray, D.; Lewis, J.; Raff, M.; Roberts, K.; Watson, J. D. *Molecular Biology of the Cell*; Second ed.; Garland Publishing: New York, 1989, pp 1219.
107. Stryer, L. *Biochemistry*; Third ed.; W. H. Freeman and Company: New York, 1988, pp 1089.
108. Elespuru, R. K.; White, R. *J. Cancer Res.* **1983**, *48*, 2819.
109. Chen, G. L.; Liu, L. F. In *Annual Reports in Medicinal Chemistry*; D. M. Bailey, Ed.; Academic Press, Inc.: Orlando, Fl, 1986; Vol. 21; pp 257.
110. Wang, J. C. *Biochemica et Biophysica Acta.* **1987**, *909*, 1.
111. Glisson, B. S.; Ross, W. E. *Pharmac. Ther.* **1987**, *32*, 89.
112. Liu, L. F. *Annu. Rev. Biochem.* **1989**, *58*, 351.
113. Osheroff, N. *Pharmac. Ther.* **1989**, *41*, 223.
114. Osheroff, N.; Zechiedrich, E. L.; Gale, K. C. *BioEssays* **1991**, *13*, 269.
115. Gilman, A. G.; Rall, T. W.; Nies, A. S.; Taylor, P. *The Pharmacological Basis of Therapeutics*; Eighth ed.; Pergamon Press: New York, 1990, pp 1811.
116. Pommier, Y.; Schwartz, R. E.; Zwellung, L. A.; Kohn, K. W. *Biochemistry* **1985**, *24*, 6406.

117. Pommier, Y.; Minfore, J. K.; Schwartz, R. E.; Zwelling, L. A.; Kohn, K. W. *Biochemistry* **1985**, *24*, 6410.
118. Muller, M. T.; Helal, K.; Soisson, S.; Spitzer, J. R. *Nucl. Acids Res.* **1989**, *17*, 9499.
119. Jaxel, C.; Wani, K.; Wall, M. E.; Pommier, Y. *Cancer Res.* **1989**, *49*, 1465.
120. LePecq, J.; Paoletti, C. *J. Mol. Biol.* **1967**, *27*, 87.
121. Kobayashi, J.; Cheng, J.; Wälchli, M. R.; Nakamura, H.; Hirata, Y.; Sasaki, T.; Ohizumi, Y. *J. Org. Chem.* **1988**, *53*, 1800.
122. Carroll, A. R.; Scheuer, P. J. *J. Org. Chem.* **1990**, *55*, 4426.
123. Carroll, A. R.; Cooray, N. M.; Poiner, A.; Scheuer, P. J. *J. Org. Chem.* **1989**, *54*, 4231.
124. Charyulu, G. A.; McKee, T. C.; Ireland, C. M. *Tetrahedron Lett.* **1989**, *32*, 4201.
125. Gunawardana, G. P.; Koehn, F. E.; Lee, A. Y.; Clardy, J.; He, H.; Faulkner, D. J. *J. Org. Chem.* **1992**, *57*, 1523.
126. Taraporewala, I. B.; Cessac, J. W.; Chanh, T. C.; Delgado, A. V.; Schinazi, R. F. *J. Med. Chem.* **1992**, *35*, 2744.
127. The ascidian was collected by SCUBA (-10 m) near Waya Island, Fiji.
128. The ascidian was identified by Dr. Françoise Monniot, Muséum National d'Histoire Naturelle, Paris, France.
129. Bothner-By, A. A.; Stephens, R. L.; Lee, J.-M.; Warren, C. D.; Jeanloz, R. W. *J. Am. Chem. Soc.* **1984**, *106*, 811.
130. Bax, A.; Davis, D. G. *J. Magn. Reson.* **1985**, *63*, 207.
131. Bax, A.; Summers, M. F. *J. Am. Chem. Soc.* **1986**, *108*, 2093.
132. Cooray, N. M.; Scheuer, P. J. *J. Org. Chem.* **1988**, *53*, 4619.
133. Kobayashi, J.; Tsuda, M.; Tanabe, A.; Ishibashi, M.; Cheng, J.; Yamamura, S.; Sasaki, T. *J. Nat. Prod.* **1991**, *54*, 1634.
134. Burres, N. S.; Frigo, A.; Rasmussen, R. R.; McAlpine, J. B. *J. Nat. Prod.* **1992**, *55*, 1582.
135. Michael, J. P.; Pattenden, G. *Angew. Chem. Int. Ed. Engl.* **1993**, *32*, 1.
136. Sigman, D. S.; Chen, C.-h. B. *Annu. Rev. Biochem.* **1990**, *59*, 207.
137. Barton, J. K. *Science* **1986**, *233*, 727.

138. IC<sub>90</sub> is the concentration at which 90% of monomer-length kDNA production is inhibited.
139. Sigman, D. S.; Graham, D. R.; D'Aurora, B.; Stern, A. M. *J. Biol. Chem.* **1979**, *254*, 12269.
140. Kuwabara, M.; Yoon, C.; Goyne, T.; Thederahn, T.; Sigman, D. S. *Biochemistry* **1986**, *25*, 7401.
141. Molinski, T. F. *Chem. Rev.* **1993**, *93*, 1825.
142. McDonald, L. A.; Ireland, C. M. *J. Nat. Prod.* **1992**, *55*, 376.
143. Ireland, C. M.; Durso Jr., A. R.; Newman, R. A.; Hacker, M. P. *J. Org. Chem.* **1982**, *47*, 1807.
144. Sesin, D. F.; Gaskell, S. J.; Ireland, C. M. *Bull. Soc. Chim. Belg.* **1986**, *95*, 853.
145. Ireland, C. M.; Scheuer, P. J. *J. Am. Chem. Soc.* **1980**, *102*, 5688.
146. Rance, M.; Sørensen, O. W.; Bodenhausen, G.; Wagner, G.; Ernst, R. R.; Wüthrich, K. *Biochem. Biophys. Res. Commun.* **1983**, *117*, 479.
147. Dodrell, D. M.; Pegg, D. T.; Bendal, M. R. *J. Magn. Reson.* **1982**, *48*, 323.
148. Summers, M. F.; Marzilli, L. G.; Bax, A. *J. Am. Chem. Soc.* **1986**, *108*, 4285.
149. Bax, A. *J. Magn. Reson.* **1984**, *57*, 314.
150. Foster, M. P.; Concepción, G. P.; Caraan, G. B.; Ireland, C. M. *J. Org. Chem.* **1992**, *57*, 6672.
151. Marfey, P. *Carlsberg Res. Commun.* **1984**, *49*, 591.
152. Biskupiak, J. E.; Ireland, C. M. *J. Org. Chem.* **1983**, *48*, 2302.
153. Kessler, H.; Griesinger, C.; Zarbock, J.; Loosli, H. R. *J. Magn. Reson.* **1984**, *57*, 331.
154. Eckart, K.; Schwartz, H.; Tomer, K. B.; Gross, M. L. *J. Am. Chem. Soc.* **1985**, *107*, 6765.
155. Biemann, K. *Methods Enzymol.* **1990**, *193*, 455.
156. Kessler, H.; Griesinger, C.; Kressebaum, R.; Wagner, K.; Ernst, R. R. *J. Am. Chem. Soc.* **1987**, *109*, 607.
157. Brown, F. K.; Hempel, J. C.; Dixon, J. S.; Amato, S.; Mueller, L.; Jeffs, P. W. *J. Am. Chem. Soc.* **1989**, *111*, 7328.
158. Howard, A. E.; Kollman, P. A. *J. Med. Chem.* **1988**, *31*, 1669.
159. Foster, M. P. Ph.D. Thesis, University of Utah, 1993.

160. MacArthur, M. W.; Thornton, J. M. *J. Mol. Biol.* **1991**, *218*, 397.
161. Ishida, T.; Inoue, M.; Hamada, Y.; Kato, S.; Shioiri, T. *J. Chem. Soc., Chem. Commun.* **1987**, 370.
162. Ishida, T.; Tanaka, M.; Nabae, M.; Inoue, M.; Kato, S.; Hamada, Y.; Shioiri, T. *J. Org. Chem.* **1988**, *53*, 107.
163. Ishida, T.; In, Y.; Doi, M.; Inoue, M.; Hamada, Y.; Shioiri, T. *Biopolymers* **1992**, *32*, 131.
164. Siemion, I. Z.; Wieland, T.; Pook, K. H. *Angew. Chem., Int. Ed. Eng.* **1975**, *14*, 702.
165. Dorman, D. E.; Bovey, F. A. *J. Org. Chem.* **1973**, *38*, 2379.
166. Shioiri, T.; Hamada, Y.; Kato, S.; Shibata, M.; Kondo, Y.; Nakagawa, H.; Kohda, K. *Biochem. Pharmacol.* **1987**, *36*, 4181.
167. Ireland, C. M.; Molinski, T. F.; Roll, D. M.; Zabriskie, T. M.; McKee, T. C.; Swersey, J. C.; Foster, M. P. In *Bioorganic Marine Chemistry*; P. J. Scheuer, Ed.; Springer-Verlag: Berlin, 1989; Vol. 3; pp 1.
168. Foster, M. P.; Ireland, C. M. *Tetrahedron Lett.* **1993**, *34*, 2871.
169. Hambley, T. W.; Hawkins, C. J.; Lavin, M. F.; van den Brenk, A.; Watters, D. J. *Tetrahedron* **1992**, *48*, 341.
170. McDonald, L. A.; Foster, M. P.; Phillips, D. R.; Ireland, C. M. *J. Org. Chem.* **1992**, *57*, 4616.
171. Hawkins, C. J.; Lavin, M. F.; Marshall, K. A.; van den Brenk, A. L.; Watters, D. J. *J. Med. Chem.* **1990**, *33*, 1634.
172. Degnan, B. M.; Hawkins, C. J.; Lavin, M. F.; McCaffrey, E. J.; Parry, D. L.; van den Brenk, A. L.; Watters, D. J. *J. Med. Chem.* **1989**, *32*, 1349.
173. Williams, D. E.; Moore, R. E.; Paul, V. J. *J. Nat. Prod.* **1989**, *52*, 732.
174. Schmitz, F. J.; Ksebati, M. B.; Chang, J. S.; Wang, J. L.; Hossain, M. B.; van der Helm, D.; Engel, M. H.; Serban, A.; Silfer, J. A. *J. Org. Chem.* **1989**, *54*, 3463.
175. Wasylyk, J. M.; Biskupiak, J. E.; Costello, C. E.; Ireland, C. M. *J. Org. Chem.* **1983**, *48*, 4445.
176. Lindquist, N. L.; Fenical, W.; van Duyne, G. D.; Clardy, J. *J. Am. Chem. Soc.* **1991**, *113*, 2033.
177. Aracil, J.; Badre, A.; Fadli, M.; Jeanty, G.; Banaigs, B.; Francisco, C.; Lafargue, F.; Heitz, A.; Anmelas, A. *Tetrahedron Lett.* **1991**, *23*, 2609.
178. Zabriskie, T. M.; Foster, M. P.; Stout, T. J.; Clardy, J.; Ireland, C. M. *J. Am. Chem. Soc.* **1990**, *112*, 8080.



179. Degnan, B. M.; Hawkins, C. J.; Lavin, M. F.; McCaffrey, E. J.; Parry, D. L.; Watters, D. J. *J. Med. Chem.* **1989**, *32*, 1354.
180. Helms, G. L.; Moore, R. E.; Niemczura, W. P.; Patterson, G. M. L.; Tomer, K. B.; Gross, M. L. *J. Org. Chem.* **1988**, *53*, 1298.
181. Hamamoto, Y.; Endo, M.; Nakagawa, M.; Nakanishi, T.; Mizukawa, K. *J. Chem. Soc., Chem. Commun.* **1983**, 323.
182. Davidson, B. S. *Chem. Rev.* **1993**, *93*, 1771.
183. Ishida, T.; Ohishi, H.; Inoue, M.; Kamigauchi, M.; Sugiura, M.; Takao, N.; Kato, S.; Shioiri, T. *J. Org. Chem.* **1989**, *54*, 5337.
184. Prinsep, M. R.; Moore, R. E.; Levine, I. A.; Patterson, G. M. L. *J. Nat. Prod.* **1992**, *55*, 140.
185. McDonald, L. A.; Swersey, J. C.; Ireland, C. M.; Carroll, A. R.; Coll, J. C.; Bowden, B. F. *Submitted for publication.*
186. Bruening, R. C.; Oltz, E. M.; Furukawa, J.; Nakanishi, K. *J. Am. Chem. Soc.* **1985**, *107*, 5298.
187. Bruening, R. C.; Oltz, E. M.; Furukawa, J.; Nakanishi, K.; Kustin, K. *J. Nat. Prod.* **1986**, *49*, 193.
188. Oltz, E. M.; Bruening, R. C.; Smith, M. J.; Kustin, K.; Nakanishi, K. *J. Am. Chem. Soc.* **1988**, *110*, 6162.
189. McLafferty, F. W. *Interpretation of Mass Spectra*; Third ed.; University Science Books: Mill Valley, California, 1980, pp 223.
190. Martin, G. E.; Zektzer, A. S. *Two-Dimensional NMR Methods for Establishing Molecular Connectivity A Chemist's Guide to Experiment Selection, Performance, and Interpretation*; VCH Publishers, Inc.: New York, 1988, pp 58.
191. Braunschweiler, L.; Ernst, R. R. *J. Magn. Reson.* **1983**, *53*, 521.
192. Kim, D.; Li, Y.; Horenstein, B. A.; Nakanishi, K. *Tetrahedron Lett.* **1990**, *31*, 7119.
193. Anderson, R. J. *Tetrahedron Lett.* **1978**, *29*, 2541.
194. Anderson, R. J.; Stonard, R. J. *Can. J. Chem.* **1979**, *57*, 2325.
195. Stonard, R. J.; Anderson, R. J. *Can. J. Chem.* **1980**, *58*, 2121.
196. Horenstein, B. A.; Nakanishi, K. *J. Am. Chem. Soc.* **1989**, *111*, 6242.
197. He, X.; Kustin, K.; Parry, D. L.; Robinson, W. E.; Ruberto, G.; Nakanishi, K. *Experientia* **1992**, *48*, 367.
198. Kupchan, S. M.; Britton, R. W.; Ziegler, M. F.; Siegel, C. W. *J. Org. Chem.* **1973**, *38*, 178.

199. Krebs, K. G.; Heusser, D.; Wimmer, H. In *Thin Layer Chromatography*; E. Stahl, Ed.; Springer-Verlag: Berlin, 1969; pp 862.
200. Nakagawa, K.; Konaka, R.; Nakata, T. *J. Org. Chem.* **1962**, *27*, 1597.
201. Brooks, B. R.; Bruccoleri, R. E.; Olafson, B. D.; States, D. J.; Swaminathan, S.; Karplus, M. *J. Comput. Chem.* **1983**, *4*, 187.
202. Polygen Corp. 200 Fifth Ave., Waltham, MA 02254.
203. Ryckaert, J. P.; Cicotti, G.; Berendsen, H. J. C. *J. Comput. Phys.* **1977**, *23*, 327.
204. The National Cooperative Drug Discovery Group (NCDDG) is comprised of the National Cancer Institute (NCI), Bristol-Myers Squibb (BMS) and several academic groups including ours.